Assessment of ERA5-Land Lake Ice Related Variables from Satellite Observations

by

Ariana Mansingh

A thesis

presented to the University of Waterloo

in fulfillment of the

thesis requirement for the degree of

Master of Science

in

Geography

Waterloo, Ontario, Canada, 2025

© Ariana Mansingh 2025

Author's Declaration

I hereby declare that I am the sole author of this thesis. This is a true copy of the thesis, including any required final revisions, as accepted by my examiners.

I understand that my thesis may be made electronically available to the public.

Abstract

Lake ice is an important climatic indicator because it responds to and alters surface energy fluxes, which in turn influence weather and climate (e.g., precipitation, air temperature). Therefore, accurately representing lake-atmosphere interactions within climate and weather models has been shown to reduce forecast errors. Despite the recognized importance of lake ice processes within models, few studies have evaluated the quality of the lake ice-related variables available from ERA5-Land, a widely used reanalysis product. To address this gap, this thesis evaluates ERA5-Land's lake ice estimates against satellite-derived observations from NOAA, CIS, IMS and MODIS. It assesses biases in lake ice fraction, timing and surface temperature across seven Canadian lakes over 20 years (2004-2023). The study lakes are grouped into northern lakes (Great Bear, Great Slave, Athabasca and Winnipeg) and the Laurentian Great Lakes (Superior, Huron and Erie). The biases were quantified using mean bias error (MBE) and mean absolute error (MAE), with ERA5-Land treated as "predicted" values and satellite-derived products as "observed" values.

This thesis provides one of the first spatial and temporally extensive evaluations of ERA5-Land's lake ice estimates. The overall findings show that ERA5-Land consistently overestimated lake ice fraction during freeze-up and break-up. Across all lakes, ERA5-Land generally produced earlier freeze-up timing, earlier break-up start, and later break-up end than observations. While timing bias followed similar patterns across lakes, distinct patterns emerged between the northern lakes and the Laurentian Great Lakes. These patterns indicate broader weaknesses of ERA5-Land, which uses the Freshwater Lake model (FLake) as its lake parameterization scheme, notably the omission of snow cover over lake ice and the tendency of the product to form a full ice cover on the Laurentian Great Lakes, which typically experience 40-80% ice fraction at winter maximum. As a result, high MAE was observed during both freeze-up (max=47%) and break-up (max=62%). Consequently, this overestimation of ice cover in ERA5-Land typically led to a daytime cold bias in surface temperatures during the ice-covered period. Additionally, it contributed to ice timing biases, notably the freeze-up end (~22 days earlier on average) and the break-up start (~25-28 days later on average).

The lack of consideration of snow cover on ice in FLake/ERA5-Land prevents accounting for its effects on ice growth, heat absorption, and surface temperature. It is well known that snow slows ice growth by reducing downward heat transfer. Thus, ERA5-Land overestimates lake ice thickness across all lakes, which in turn contributes to the delay in break-up start. The early break-up end

timing is likely linked to ERA5-Land neglecting the cooling effect of snow's high albedo, which would otherwise slow melt by reflecting solar radiation. Additionally, during months of high snowfall, ERA5-Land produced a larger warm surface temperature bias, most notable among the northern lakes.

Overall, this thesis quantified the biases arising from two notable weaknesses in ERA5-Land's parameterization: the omission of snow cover on ice and the inability to account for partial ice coverage in the large lakes examined in this research. The quantification of biases provides insight into how these weaknesses skew ERA5-Land estimates. This thesis provides new insights into the limitations of ERA5-Land regarding lake ice, which should be considered leading to for future product releases.

Keywords: ERA5-Land, lake ice, FLake, reanalysis model, satellite

Acknowledgements

I would like to first express my gratitude to my supervisor, Dr. Claude Duguay, for his expert insight, advice, patience and support. His guidance over these years has been instrumental in this research journey, which has greatly contributed to my academic and professional development.

I would also like to extend my thanks to my committee members, Dr. Richard Kelly and Dr. Grant Gunn, for their time and guidance.

Special thanks to the Cryo-cluster for being such a profound and invaluable network of support. I would like to extend special thanks to several individuals. To my first and closest friend, Connor McRae-Pharo, who was always willing to support me in any way he could, even from British Columbia. To Jaya Sree Mugunthan for also showing me unwavering support, even when it meant staying late at the office to help me. To Owen Nowitsky and Peter Wray for their support in fostering a productive writing environment and had a meaningful impact on my writing process. Last but certainly not least, to Tyler Herrington, who worked on a different aspect of ERA5-Land and offered thoughtful conversations and insights.

Dedication

To my partner, Satindra Deonarain, for his unwavering support and for showing me patience and understanding, even when I had no patience for myself. For helping me in every way, from scheduling cafe dates and being a silent and motivating presence in my work to helping me with anything he could, no matter how menial. For always being there for me in every way.

To my parents, Nevita Singh and Chris Mansingh, for supporting me in every way they could. For being a monumental influence and guiding me down this path. For having high hopes in me without any doubts that I'll reach them. For being willing victims in listening to my mock presentations and scientific rambles, no matter how confusing.

Most of all, in loving memory of my puppy, Rufus, for unconditional love and equal parts sass. Forever loved and remembered.

Table of Contents

Author's Declaration ii

Abstract iii

Acknowledgements v

Dedication vi

List of Figures xi

List of Tables xii

List of Abbreviations xiv

List of Symbols xvi

Chapter 1 General Introduction 1

1.1 Motivation 1

1.2 Research Objectives 2

1.3 Thesis outline 2

Chapter 2 Background 3

2.1 Introduction 3

2.2 Lake ice phenology 3

2.2.1 Controls of ice phenology 3

2.2.2 Freeze-up 8

2.2.3 Ice growth 9

2.2.4 Break-up 11

2.2.5 Summary 13

2.3 Lake and lake ice inclusion in weather-climate modelling 13

2.3.1 European Centre for Medium-Range Weather Forecasts Fifth generation of European ReAnalysis 15

2.3.2 Previous Assessments of FLake 21
Chapter 3 Methodology 23
3.1 Study areas 23
3.1.1 Great Bear Lake 26
3.1.2 Great Slave Lake 28
3.1.3 Lake Athabasca 30
3.1.4 Lake Winnipeg 32
3.1.6 Lake Superior 34
3.1.7 Lake Huron 36
3.1.8 Lake Erie 38
3.2 Satellite-Derived Products: General Description 40
3.2.1 Interactive Multisensor Snow and Ice Mapping System Daily Northern Hemisphere Snow and Ice Analysis at 1 km, 4 km, and 24 km Resolutions, Version 1 40
3.2.2 Canadian Ice Service Lake Ice Product 43
3.2.3 National Oceanic and Atmospheric Administration Lake Ice Product 43
3.2.4 MODIS Land Surface Temperature and Emissivity 43
3.3 Datasets: Variables of Interest and Preprocessing Procedure 45
3.3.1 ERA5-Land 45
3.3.2 IMS Daily Ice Cover 47
3.3.3 CIS Weekly Ice Cover 47
3.3.4 NOAA Daily Ice Charts 48
3.3.5 MOD11C1 48
3.4 Assessments 51
3.4.1 Lake Ice Fraction and Timing 53

3.4.2 Lake ice surface temperature assessment 56
Chapter 4 Results and Discussion 58
4.1 Introduction 58
4.2 Freeze-up Differences 59
4.2.1 Lake Ice Fraction 59
4.2.2 Lake Ice Timing 62
4.2.3 Discussion 67
4.3 Break-up Differences 70
4.3.1 Lake Ice Fraction 70
4.3.2 Lake Ice Timing 72
4.3.3 Discussion 79
4.4 Lake Ice Temperature Differences during Ice-covered Period 83
4.4.1 Discussion 87
Chapter 5 Conclusion 92
5.1 Summary of Findings 92
5.2 Limitations 94
5.3 Future Work 95
References 97
Appendix A - Missing and Filtered Data 114
Appendix B – Supplementary Lake Ice Fraction Figures and Tables 116
Appendix C – MOD11C1 Monthly boxplots 123
C.1 Great Bear Lake 123
C.2 Great Slave Lake 143
C.3 Lake Athabasca 163

C.4 Lake Winnipeg 183
C.5 Lake Superior 203
C.6 Lake Huron 223
C.7 Lake Erie 243

List of Figures

Figure 1: HTESSEL lake schematic (adapted from ECMWF, 2018) 16
Figure 2: Diagram of self-similarity (Betts et al., 2020) 17
Figure 3: Climate zone map of study sites and key rivers (Data source: CEC, 2020) 23
Figure 4: Overall flowchart of the methodology 52
Figure 5: Average (2004-2023) ice fraction (%) for all lakes of this study during freeze-up 61
Figure 6: Average (2004-2023) ice to water transition agreement (%) during freeze-up between ERA5-Land and IMS for Great Bear Lake, Great Slave Lake and Lake Athabasca 64
Figure 7: Average (2004-2023) ice to water transition agreement (%) during freeze-up between ERA5-Land and IMS for Lake Erie, Lake Superior and Lake Winnipeg 65
Figure 8: Average (2004-2023) ice to water transition agreement (%) during freeze-up between ERA5-Land and IMS for Lake Huron 66
Figure 9: Average (2004-2023) ice fraction (%) for all lakes of this study during break-up 71
Figure 10: Ice–water agreement (%) between ERA5-Land and IMS during break-up (2004–2023) .. 75
Figure 11: Average (2004-2023) ice to water transition agreement (%) during break-up between ERA5-Land and IMS for Great Bear Lake, Great Slave Lake and Lake Athabasca 76
Figure 12: Average (2004-2023) ice to water transition agreement (%) during break-up between ERA5-Land and IMS for Lake Erie, Lake Superior and Lake Winnipeg 77
Figure 13: Average (2004-2023) ice to water transition agreement (%) during break-up between ERA5-Land and IMS for Lake Huron 78
Figure 14: Break-up evolution of ERA5-Land ice fraction and albedo for Great Slave Lake (left) and Great Bear Lake (right) for the years 2004, 2009, and 2015 81
Figure 15: Average lake-wide surface temperature of MOD11C1 and ERA5-Land during daytime .. 84
Figure 16: Average lake-wide surface temperature of MOD11C1 and ERA5-Land during nighttime 86

List of Tables

Table 1: Climate zones (Adapted from Beck et al., 2018; CEC, 2020) 24
Table 2: Characteristics of study sites (Geological Survey of Canada, 1967; International Lake Environment Committee Foundation, n.d.; Lakepedia, n.d.; Peel et al., 2007; Statistics Canada, Environment, Energy and Transportation Statistics Division, 2009) 25
Table 3: Climate normal (1991-2020) for Great Bear Lake (ECCC, 2023) 27
Table 4: Climate normal (1991-2020) for Great Slave Lake (ECCC, 2023) 29
Table 5: Climate normal for Lake Athabasca (ECCC, 2023) 31
Table 6: Climate normal (1991-2020) for Lake Winnipeg (ECCC, 2023) 33
Table 7: Climate normal (1991-2020) for Lake Superior (ECCC, 2023; Palecki et al., 2021) 35
Table 8: Climate normal (1991-2020) for Lake Huron (ECCC, 2023; Palecki et al., 2021) 37
Table 9: Climate normal (1991-2020) for Lake Erie (ECCC, 2023) 39
Table 10: Data sources of IMS (UNIC, 2008) 41
Table 11: Variables of IMS surface type maps (UNIC, 2008) 42
Table 12: Variables of interest within MOD11C1. (Institute for Computational Earth System Sciences, n.d.) 44
Table 13: MOD11C1 algorithms (information from Wan et al. 2002) 44
Table 14: Lake variables provided in ERA5-Land with the selected variables highlighted in blue (Muñoz et al., 2019) 46
Table 15: MOD11C1 quality assurance (Institute for Computational Earth System Sciences, n.d.) 50
Table 16: Agreement of IMS and ERA5-Land via Comparison Codes 56
Table 17: Characteristics of selected satellite products and their associated assessment 59
Table 18: Direction and magnitude of bias in lake ice fraction (%) during freeze-up per lake 62
Table 19: Difference in freeze-up dates of ERA5-Land to satellite-derived products 63
Table 20: Direction and magnitude of bias in lake ice fraction (%) during break-up per lake 72
Table 21: Difference in break-up dates of ERA5-Land to satellite-derived products 73
Table 22: Daytime biases (MBE and MAE) during ERA5-Land's ice-covered period 85
Table 23: Nighttime biases (MBE and MAE) during ERA5-Land's ice-covered period 85
Table 24: Snowfall climate normal for all lakes of this study during the ice-covered period (FUE-BUS) (Environment Climate Change Canada, 2023) 89

Table 25: Air temperature climate normal for all lakes of this study during the ice-covered period (FUE-BUS) (Environment Climate Change Canada, 2023) 90
Table 26: Rainfall climate normal for all lakes of this study during the ice-covered period (FUE-BUS) (Environment Climate Change Canada, 2023)..... 91

List of Abbreviations

AVHRR	Advanced Very High-Resolution Radiometer
BU	Break-Up
BUE	Break-Up End
BUS	Break-Up Start
CEC	Commission for Environmental Cooperation
CIS	Canadian Ice Service
ECCC	Environment and Climate Change Canada
ECMWF	European Centre for Medium-Range Weather Forecasts
ECV	Essential Climate Variable
ERA5-Land	Fifth Generation of European Reanalysis
FLake	Freshwater Lake Model
FU	Freeze-Up
FUE	Freeze-Up End
FUS	Freeze-Up Start
GBL	Great Bear Lake
GCOS	Global Climate Observing System
GLERL	Great Lakes Environment Research Laboratory
GSL	Great Slave Lake
HTESSEL	Hydrology Tiled ECMWF Scheme of Surface Exchanges Over Land
IMS	Interactive Multisensor Snow and Ice Mapping System
LAADS DAAC	Level-1 and Atmosphere Archive and Distribution System Distributed Active Archive Center

LIC	Lake Ice Cover
LIP	Lake Ice Phenology
LIST	Lake Ice Surface Temperature
LST	Land Surface Temperature
LSWT	Lake Surface Water Temperature
MAE	Mean Absolute Error
MBE	Mean Bias Error
MODIS	Moderate Resolution Spectroradiometer
NOAA	National Oceanic and Atmospheric Administration
NWT	Northwest Territories
SAR	Radar-1 Synthetic Aperture Radar
SEB	Surface Energy Balance
USNIC	U.S. National Ice Center
YD	Year Date

List of Symbols

d_l	Lake Depth
d_{ice}	Lake Ice Depth
d_{ML}	Upper Mixed Layer of Depth
$\frac{d}{dt}$	Time Derivative
G_w	Heat Flux in the Near-Surface Water Layer Just Beneath the Ice
κ_{ice}	Thermal Conductivity of Ice ($2.29\ J\ m^{-1}\ s^{-1}\ K^{-1}$)
L_f	Latent Heat of Fusion ($3.3\ \cdot\ 10^5\ J\ kg^{-1}$)
ϕ_{ice}	Dimensionless Universal Function of Dimensionless Depth
ϕ'_{ice}	Dimensionless Temperature Gradient
Φ_{T_l}	Dimensionless Function of Dimensionless Depth
p_{ice}	Ice Mean Property for Density ($9.1\ 10^2\ kg\ m^{-3}$)
T_{BL}	Temperature At the Bottom of the Water Body ($z = d_l$)
T_f	Freshwater Freezing Point (273.15 K)
T_{ML}	Temperature Of the Upper Mixed Layer of Depth (d_{ML})
$T_{sk,i}$	Temperature at the Upper Ice Surface
T_{ice}	Ice Temperature
$T_l(z)$	Temperature at Depth Function (Z)
z	Function of Depth
ζ_i	Dimensionless Depth

Chapter 1
General Introduction

1.1 Motivation

Lakes are recognized as an essential component of the climate system since they respond to and play a role in climate and weather (ACIA, 2004; Adrian et al., 2009; Rosenzweig et al., 2007). Lakes are recognized as an Essential Climate Variable (ECV) by the Global Climate Observing System (GCOS) due to their sensitivity to climate change (Belward et al., 2016; Global Climate Observing System, 2022). Lake surface water temperature (LSWT) and lake ice cover (LIC), from which ice phenology can be derived, are two thematic variables of lakes as an ECV known to be strongly modulated by changes and variability in air temperature (Adrian et al., 2009; Woolway et al., 2020); whereas changes in LSWT, as well as the extent of lake ice cover, modify the timing and magnitude of heat and moisture transfers to the overlaying atmosphere (Brown & Duguay, 2010; Kheyrollah Pour et al., 2012).

Within northern regions, lakes are an especially important component of land-atmosphere interactions since they can occupy a significant fraction of the landscape (Prowse et al., 2011). Thus, improving our understanding of lake-atmosphere interactions and processes allows for better climate modelling and weather prediction (Eerola et al., 2009; Kheyrollah Pour et al., 2012). In situ measurements of LSWT, LIC, and other lake variables, such as albedo, are limited spatially for that purpose; they are usually point measurements that represent a limited area and are therefore not spatially representative of the entire lake surface. The solution to this challenge is to utilize remote sensing and lake modelling to fill the gap regarding lake variables, such as LIC (Brown, 2012). However, lake modelling also poses its own challenges, notably in the difficulty of accounting for all interrelated limnological and meteorological variables (Adrian et al., 2009; Christensen et al., 2006; Yan et al., 2008). For example, the albedo of ice cover is difficult to parameterize as it changes both daily and seasonally with changing snow and ice conditions (old snow would have a lower albedo than fresh snow, and the water content of the snow varies, which alters albedo) (Brown & Duguay, 2010). Another modelling challenge is that many lakes tend to occupy an area smaller than the spatial resolution of climate and weather forecasting models, consequently occupying a subarea of a grid, which makes inclusion of lakes in these models challenging (Brown & Duguay, 2010; Mironov, 2005). Therefore, there is a need to improve the implementation of lakes and lake ice into models to fully capture lake-atmosphere interactions. To address the need for improved lake ice modelling, for

example, existing models should be evaluated for accuracy and bias of lake ice timing and extent, as these influence other atmospheric variables such as cloud cover, precipitation and air temperature (Changnon & Jones, 1972; Rouse et al., 2005; Woolway et al., 2020).

Currently, a few studies have evaluated lake ice estimates of the widely used European Centre for Medium-Range Weather Forecasts (ECMWF) Fifth generation of European ReAnalysis (ERA5/ERA5-Land) products (Betts et al., 2020; Muñoz Sabater, 2019; Siles & Leconte, 2023). However, there is yet to be a comprehensive study over a large spatial and temporal scales. Thus, the thesis addresses this gap by evaluating ERA5-Land's lake variables for seven lakes over a 20-year period. Specifically, it evaluates ERA5-Land's estimate of lake ice cover, phenology (timing derived from ice cover) and lake surface temperature against satellite-derived products.

1.2 Research Objectives

The research aims to evaluate ERA5-Land's proficiency at estimating lake ice fraction, timing, and surface temperature. ERA5-Land estimates are assessed against satellite-derived products. This evaluation allows for an assessment of ERA5-Land's ability to capture different ice regimes by evaluating several lakes along a latitudinal gradient. The goal of the project is to provide insight into biases/errors within the FLake's lake ice parameterization, which can inform potential improvements in future releases of reanalysis products (e.g. ERA6). More specifically, the objectives of the research are:

1. To quantify biases/errors in ERA5-Land lake ice fraction, timing and temperature.
2. To assess ERA5-Land's ability to capture the spatial patterns of lake ice fraction and timing.

1.3 Thesis outline

This thesis is organized into five chapters, including the introduction chapter. Chapter 2 serves as the literature review to provide background of lake ice processes, their responses and influences on climate and weather. This chapter concludes with emphasizing the importance of lake ice incorporation for accurate climate and weather modelling. Chapter 3 outlines the methodology, including description of study areas, datasets and assessments conducted. Chapter 4 presents the results and discussion for each period (freeze-up, break-up and ice-covered season) where the corresponding assessment (lake ice fraction, timing and surface temperature) is provided. Finally, Chapter 5 summarizes key findings, limitations and recommendations for future work.

Chapter 2
Background

2.1 Introduction

Given this study's aim to evaluate ERA5-Land's performance regarding lake ice estimates. This chapter is organized into three sections. It begins with an overview of lake ice phenology, specifically, its drivers, climatic relevance and the physical processes of ice formation and melting. The second section discusses the integration of lakes within climate models with particular attention to ERA5-Land's lake parameterization and previous assessments of its lake component known as FLake. The last section details the satellite products used, in particular, how these products estimate lake ice timing, fraction and surface temperature.

2.2 Lake ice phenology

Lake ice phenology refers to the stages and timing of ice formation and melt (Hewitt et al., 2018), also known as freeze-up (FU) and break-up (BU), respectively. BU and FU can be further broken down into freeze-up start (FUS), freeze-up end (FUE), break-up start (BUS) and break-up end (BUE). FUS refers to the date of initial ice formation, while FUE refers to the date of complete ice coverage to represent the period of ice formation. BUS and BUE follow the same logic, but regarding the timing of melt (Brown & Duguay, 2012; Duguay et al., 2006). While these ice date definitions seem to follow a simple linear cycle since each event follows the previous, this, however, is not always the case. Melt and refreeze events can interrupt the cycle which complicates ice formation and melt (Bernhardt et al., 2012; Kirillin et al., 2012). Thus, ice formation and melt do not consistently follow linear growth or decrease.

2.2.1 Controls of ice phenology

Lake ice phenology (LIP) and lake surface water temperature (LSWT) are both governed by the surface energy balance (SEB), which integrates radiative, turbulent, and conductive fluxes to determine energy surplus or deficit at the lake surface (Liston & Hall, 1995; Prowse et al., 2011; Williams, 1965). Furthermore, the energy surplus and deficit at the lake surface determines ice formation, growth and melt (Brown & Duguay, 2010). As a result, freeze-up and break-up act as an integrated indicator of net heat gain and loss (notably through radiative and turbulent fluxes) (Liston

& Hall, 1995). Meanwhile, LSWT represents the net energy fluxes of the SEB, thus acting as a sensitive indicator of SEB. Warmer LSWT indicates an energy surplus, whereas a colder LSWT indicates an energy deficit (Adrian et al., 2009; Woolway et al., 2020). It is crucial to understand that while SEB influences LIP and LSWT, SEB is also mediated by LIP and LSWT. LIP influences SEB by altering surface albedo and insulation properties, in turn, modifying energy fluxes. For instance, FU produces higher albedo and insulates the water body from the atmosphere, consequently reducing radiative fluxes (reducing absorption of shortwave radiation and release of longwave radiation) (Leppäranta, 2015; Leppäranta et al., 2019; Li et al., 2022). Additionally, a warmer LSWT causes a delay in freeze-up by necessitating a larger energy deficit to reach the freezing point (Woolway et al., 2020). To illustrate the interconnected relationship among SEB, LIP and LSWT, the following sub-sections describe how LSWT and LIP interact with each SEB energy flux (radiative, turbulent, conductive) as well as advective fluxes.

2.2.1.1 Turbulent fluxes

Turbulent fluxes are composed of sensible and latent heat fluxes. Sensible heat refers to the heat exchange at the lake-atmosphere interface due to thermal conduction, while latent heat is the energy absorbed and released during phase changes (Schmid & Read, 2022). The transfer of these fluxes is driven by air temperature, humidity and wind speed (Leppäranta, 2015; Woolway et al., 2020). The relationship between turbulent fluxes and lake state (open water versus ice-covered) is interrelated, thus, it poses an influence on each other (Brown, 2012; Leppäranta, 2015; Notaro et al., 2013). To capture the interrelated relationship, this section describes the turbulent fluxes during open water and ice-covered season separately, but first, it highlights the relationship between air temperature and lake ice, as it is a dominant control of ice phenology and turbulent fluxes.

Air temperature plays a dominant role in controlling LIP and turbulent fluxes, making it a crucial component in lake ice dynamics (M. A. Palecki & Barry, 1986; Stewart & Magnuson, 2009; Williams, 1965). Therefore, the timing of ice events strongly correlates with air temperatures one to two month(s) before the ice event, with regional variations. For instance, within northern regions, FU is typically associated with October to November climate, while BU is associated with April to May climate. Conversely, in southern regions, FU reflects January to February conditions while BU reflects February to March (Magnuson et al., 2000). Additionally, in the absence of other environmental changes, a 1°C increase in mean temperature shifts both BU and FU by approximately

4-6 days in mid-latitude Northern Hemisphere lakes (Duguay et al., 2006; Walsh et al., 1998). Moreover, the temperature difference between air temperature and the lake influences turbulent fluxes, which, in turn, influences lake ice phenology. Overall, air temperature is widely recognized as the primary driver of LIP, since it governs the cooling of LSWT towards freezing (producing ice formation) and governs the warming that causes melt. Air temperature is especially important due to the additive effect it has on albedo, sensible heat flux, incoming longwave and the amount of absorbed longwave and shortwave radiation (Woolway et al., 2020).

2.2.1.1.1 Open-water season

During late autumn and early winter, before ice formation, the LSWT is typically warmer than the atmosphere (Leppäranta, 2015), which drives strong latent and sensible heat loss (Woolway et al., 2020). During this period, latent heat loss occurs through evaporation, which produces moisture transfer to overlying, dry air masses. This increases humidity and, in turn, can promote cloud formation. Additionally, under suitable conditions, it can lead to downward precipitation (as lake effect snowfall) (Notaro et al., 2013; Prowse et al., 2011). The duration and magnitude of evaporation vary proportionally with lake size: for example, in the Mackenzie River Basin near Yellowknife, small/shallow lakes (<1 km²; average depth < 5 m) sustain ~22 weeks of evaporation, medium lakes (1–100 km²; average depth 5-70+ meters) ~24 weeks, and large lakes (>100 km²) up to ~30 weeks. As a result, lake-rich landscapes can experience an extended evaporation period, approximately 2-3 months longer during fall and early winter (Rouse et al., 2005). Simultaneously, the temperature difference between the warmer LSWT and the cooler atmosphere drives sensible heat loss from the lake (Prowse et al., 2011; Rouse et al., 2005; Woolway et al., 2020). This heat exchange at the lake-atmosphere interface can be amplified by wind. Specifically, the wind exposes cooler air to the lake surface, further increasing the temperature difference between the lake and the atmosphere. The sensible heat loss cools the surroundings, contributing to the gradual decline of LSWT as the season advances (Rouse et al., 2003, 2005). Additionally, sensible heat loss can moderate evaporation since evaporation peaks when the lake-atmosphere temperature and vapour pressure differences are maximized (Changnon & Jones, 1972; Rouse et al., 2008). Wind-driven turbulent mixing can further delay freeze-up by bringing warmer deep water to the surface, renewing the temperature difference. Therefore, prolonging the open-water period allows for increased solar absorption and higher latent heat loss late into autumn (Li et al., 2022; Woolway et al., 2020).

2.2.1.1.2 Ice-covered season

During ice-covered season, the ice acts as an insulator, nearly halting evaporation, causing a decrease in latent heat loss and sensible heat loss (through the ice insulating heat within the lake), while conductive transfer continues (Brown, 2012) (see Section 2.1.4 for more details). Wind affects lake ice differently depending on the strength of the ice cover (Jeffries et al., 2013; Prowse et al., 2011; Williams, 1965). Thus, since the strength of the ice cover evolves as it matures, the wind's influence differs based on ice stage. The presence of wind during early or initial freeze-up can cause the thin ice layer to break, preventing a solid ice layer from forming (Jeffries et al., 2013). However, if the presence of wind occurs after the formation of a solid ice cover, the wind can produce a 'freezing factor', hence, cooling the ice and aiding ice growth (Adams, 1976).

2.2.1.2 Conductive fluxes

Conduction refers to the heat transfer through a medium such as water, snow and ice (Sledd et al., 2024). Conductive heat transfer is defined by the medium's thermal conductivity, as higher thermal conductivity means the medium transfers heat more quickly. The thermal conductivity is relatively low (0.6 Wm^{-1} K^{-1}), and paired with water's high heat capacity, it allows for heat to be absorbed but slowly released (Ménard et al., 2002). Ice, on the other hand, also has a higher thermal conductivity (2.24 Wm^{-1} K^{-1}) but varies based on thickness, as thin ice allows heat to escape much more easily than thick ice. This ice growth occurs more rapidly compared to thick ice (Jeffries and Morris, 2006; Sturm et al., 1997; Leppäranta, 2015). Since snow has a low thermal conductivity (0.08-0.54 Wm^{-1} K^{-1}) compared to ice, it slows the downward transfer of heat, in turn, slowing ice growth (Adams & Roulet, 1980; Prowse et al., 2011; Sturm et al., 1997). The insulating effect of snow reduces the formation of congelation ice (also known as black ice) but can promote the formation of snow ice (Adams & Roulet, 1980; Bengtsson, 1986; Prowse et al., 2011). Although snow ice formation can increase the total ice thickness, its lower density compared to congelation ice causes a reduction in overall lake ice strength (Adams, 1976; Brown & Duguay, 2010; Kirillin et al., 2012) (further expanded in Section 2.3).

2.2.1.3 Radiative fluxes

Radiative fluxes encompass shortwave (solar) and longwave (thermal) radiation at the lake-atmosphere interface (Liston & Hall, 1995; Woolway et al., 2020). While both forms of radiation contribute to melting, shortwave radiation is the dominant source of melt, notably during the day.

During cloudy and nighttime conditions, longwave radiation and turbulent fluxes contribute more to melt than shortwave radiation (Kirillin et al., 2012; Leppäranta, 2015; Moukomla, 1999). However, the net longwave radiation depends on temperature differences at the lake-atmosphere interface, which can be affected by cloud cover (Moukomla, 1999; Woolway et al., 2020). While the amount of solar radiation absorbed can also be influenced by cloud cover, however, albedo is a larger influencing factor (Leppäranta, 2015). Thus, the following paragraphs expand on these influencing factors (albedo and cloud cover) and how they alter the amount of radiation absorbed.

Albedo governs the absorption and reflectance of shortwave radiation (Betts, 2001; Bounoua et al., 2002; Zheng et al., 2020). Albedo varies between mediums, where higher albedo represents higher shortwave radiation reflectance and lower absorption, therefore reducing surface warming (Bengtsson, 1986; Kirillin et al., 2012; Woolway et al., 2020). Snow has one of the highest albedos (~0.9), while ice has a moderate albedo (~0.5), and water has a low albedo (~0.1) (Leppäranta, 2015). Therefore, due to ice's albedo and the low solar radiation level during winter, the absorption of shortwave radiation is low; in other words, ice is self-protecting (Leppäranta, 2015). Additionally, during the ice-covered period, the presence of snow modulates radiative exchange through its high albedo, which causes it to reflect shortwave radiation, and through its low thermal conductivity, it traps longwave radiation (Sturm et al., 1997) (see Section 2.1.1.3 for more details regarding thermal conductivity). Snow's albedo also plays a key role during the melt period. As albedo lowers, there is an increase in albedo variability, producing a positive feedback that promotes the melt of the ice cover (typically during spring) and causes the melting to be patchy (Kirillin et al., 2012; Kirillin & Leppäranta, 2022).

Cloud cover has a dual effect, as its impact varies depending on which radiative flux is dominant (X. Wang & Key, 2005). During the day, when shortwave radiation is dominant, clouds attenuate shortwave radiation, thus producing a cooling effect (O'Reilly et al., 2015; X. Wang & Key, 2005). When longwave radiation is dominant, typically at night, the presence of clouds can trap longwave radiation, promoting a warming effect and ice melting. Alternatively, the absence of clouds during this time would increase outgoing longwave radiation, producing a cooling effect in turn, promoting ice growth (Curry et al., 1993; O'Reilly et al., 2015).

2.2.1.4 Advection

Advection is the transport of heat through the flow of liquid or air, and it plays a role in modulating lake temperatures (Marcé et al., 2024). Although advection plays a key role in lake thermal dynamics, it is often excluded from the SEB since it represents horizontal heat transport rather than vertical heat transport (Bonan, 1995; Liston & Hall, 1995). Within the lake, advection introduces liquid (via streams, snowmelt, rivers, and inflows) at ambient temperatures, which either prolongs or delays ice cover, depending on the ambient temperature (Ramón et al., 2021; Williams, 1965). A warm inflow can increase the lake temperature, thereby buffering radiative and turbulent cooling, which can delay ice formation or accelerate ice melting (Brown & Duguay, 2010; Williams, 1965, 1968). Conversely, cold meltwaters can enhance cooling and thereby accelerate ice formation or prolong ice cover (Ramón et al., 2021).

2.2.2 Freeze-up

Freeze-up is strongly controlled by lake properties and air temperature, leading to the following variables to be the most influential predictors of average FU date: lake morphology, latitude and elevation (Brown & Duguay, 2010; Efremova & Pal'shin, 2011; Kirillin et al., 2012). This paragraph expands on lake morphology, while the following covers latitude and elevation. Lake morphology is a key determinant of ice cover as it influences wind fetch, water circulation, water temperature and heat storage (Jeffries & Morris, 2007). The most important morphological characteristic is lake depth because it determines heat storage (Korhonen, 2006). Since water has a high heat capacity and deeper lakes tend to have larger water volume, this allows more heat to be retained, demonstrating greater heat storage capacity (Jeffries & Morris, 2007; Kheyrollah Pour, 2011; Woolway et al., 2020). Consequently, large heat storage causes a delay in the cooling and warming of the lake body. Thus, while air temperature produces heat gain and loss by the lake surface, FU is controlled by the combined effect of air temperature and depth. In general, for every meter of depth, there is an additional day in delay in water temperature response to air temperature (Haapala & Lepparanta, 1997; Kirillin et al., 2012; Leppäranta, 2009, 2015; Simojoki, 1940). Thus, ice formation is strongly controlled by the combined effect of air temperature and lake depth.

Ultimately, lake depth and air temperature play important roles in FU, but latitude and elevation above sea level also influence FU (Efremova & Pal'shin, 2011; Kirillin et al., 2012). The relationship between freeze-up timing and both latitude and elevation above sea level is relatively

simple. Firstly, latitude alters both freeze-up and break-up because it controls the amount of solar radiation reaching the surface, thus altering surface heating (Brown, 2012). In particular, solar radiation is most intense at the equator and progressively decreases towards the poles, reaching its lowest levels during periods of 24-hour darkness in the winter, known as polar night (Connan-McGinty et al., 2022; Matthias et al., 2016; Peixoto & Oort, 1993). Secondly, elevation above sea level alters ice seasons, with lakes at higher elevation experiencing longer ice seasons (Brown, 2012; Livingstone, 2000).

2.2.2.1 Process of Freeze-up

During the summer months when lakes are ice-free, there is an increase in turbulent fluxes and heat storage (Rouse et al., 2000, 2005). The dominant control of ice formation is air temperature; however, lake depth is also a key control on ice formation, as explained in the previous section (Bilello et al., 1980; Kirillin et al., 2012; M. A. Palecki & Barry, 1986; Stewart & Magnuson, 2009; Williams, 1968). Before ice formation, the lake surface is typically warmer than the atmosphere, causing intensive radiative and turbulent heat losses from the water surface (Kirillin et al., 2012; Leppäranta, 2015). The turbulent heat loss causes the lake surface to cool until it reaches the temperature of max density, which is approximately 3.98°C for freshwater but varies with pressure (0.02°C increase/bar) and salinity (0.22°C increase/ppt) (Kirillin et al., 2012). Once the surface water reaches 3.98°C, that surface water sinks, producing a downward buoyancy flux at the surface which drives vertical mixing via convection (Kirillin et al., 2012; Kirillin & Leppäranta, 2022). Eventually, the convection removes heat from the deeper water layers of the water column until the entire water column reaches a temperature of 3.98°C. Further cooling at the lake surface forms an inverse thermocline, in which water temperature increases with depth. So, lighter, cooler water remains at the surface stably stratified, while denser, warmer water remains at the lake bottom (Kirillin & Leppäranta, 2022). Consequently, preventing heat from deeper waters from rising to the surface, causing accelerated surface cooling, causing the surface to quickly reach freezing point (sometimes processes occur rapidly within hours); finally, forming lake ice (Haapala & Lepparanta, 1997; Kirillin & Leppäranta, 2022).

2.2.3 Ice growth

During ice formation, different ice types and stratigraphy occur due to climate conditions (Leppäranta, 2015). While lake ice types can be categorized in different ways, this section focuses on

three ice types, which are delineated based on formation conditions with consideration of different crystal structure and impurities: primary ice, secondary ice and snow ice (Kirillin et al., 2012; Michel & Ramseier, 1971). To briefly define each ice type, primary ice is the first stage of ice formation, providing a surface for secondary and snow ice to form. Secondary ice grows beneath the primary ice, whereas snow ice grows above the primary ice (Jeffries et al., 2013; Kirillin et al., 2012). With these broad definitions, the following sections expand on the formation conditions of each ice type.

The formation of primary ice may begin with frazil ice, a type of ice composed of fine crystals (~1 mm in diameter). Frazil ice forms in supercooled water, typically in the presence of surface waves that create turbulence, allowing supercooling to occur (Kirillin & Leppäranta, 2022). Frazil crystals form and move freely on the lake surface, which can be disturbed by wind/snow. But once their buoyancy overcomes the turbulence, frazil will consolidate into a thin ice sheet (Kirillin et al., 2012). However, this thin ice layer can be broken apart into ice crystals with the presence of wind or waves (Jeffries et al., 2013).

While secondary ice is significant to the structure and overall thickness of lake ice, this section first expands on secondary ice, but mainly focuses on snow ice, as it is more complex. Below the primary ice layer, secondary ice forms and grows downward, using the lake water as fuel; typically, it forms as clear congelation ice (also known as black ice), composed of large crystals (Jeffries et al., 2013; Kirillin et al., 2012; Michel & Ramseier, 1971). On the other hand, above the primary ice layer, snow ice forms, usually as snow ice formed from slush (a mix of snow and water). Snow ice typically forms either due to liquid precipitation, melted snow or flooding (Kirillin et al., 2012; Michel & Ramseier, 1971; Palosuo, 1965). Formation of snow ice via flooding can occur when the weight of overlying snow pushes the ice below the water surface, water then mixes with the snow forming slush which eventually freezes (Kirillin et al., 2012; Palosuo, 1965). Moving on, snow ice can form from snow melt, which typically occurs due to milder temperatures, such as spring temperatures, producing melt and refreeze between the day and night cycle. Snow melt causes water to percolate from overlying snow, forming slush and eventually freezing to form snow ice (Ashton, 1986; Bengtsson, 1986; Brown, 2012; Howell et al., 2009). Once snow ice forms, it grows downward from the topmost part of the slush. The freezing of slush can cause trapped slush pockets in the ice sheet for several weeks (Kirillin et al., 2012; Kirillin & Leppäranta, 2022).

Due to each ice layer forming under different conditions and inputs, the properties of each ice layer differ (Jeffries et al., 2013; Kirillin & Leppäranta, 2022). Notably, congelation and snow ice differ in density, spatial distribution, albedo and surface temperature (Bengtsson, 1986; Colbeck, 1987; Gray & Male, 1981; Heron & Woo, 1994). Firstly, the difference in density between congelation and snow ice is caused by the presence of air bubbles. Snow ice contains more air bubbles due to slush freezing, which traps air bubbles, whereas congelation ice has fewer and smaller air bubbles, typically originating from the water column or bottom sediments (Kirillin et al., 2012; Palosuo, 1965). At freezing point (0°C), the density of pure ice is ~917 kg m³, congelation ice is ~910 kg m³, while snow ice is ~850-900 kg m³ (Palosuo, 1965). Secondly, the spatial distribution differs due to formation conditions and influences from meteorological conditions. For instance, congelation ice typically forms more within the lake centre, while snow ice tends to form near shorelines due to wind causing snow drift (Bengtsson, 1986). Lastly, there are albedo and surface temperature differences between snow ice and congelation ice, such that congelation ice with minimal impurities and meltwater has a higher albedo and lower surface temperature compared to snow ice (Cheng et al., 2014; Colbeck, 1987; Gray & Male, 1981; Heron & Woo, 1994). The differences between these ice types affect the rate of melt and growth as described in Sections 2.2.1.2 and 2.2.1.3 due to their differences in properties, most notably albedo, density, and surface temperature.

2.2.4 Break-up

The process and timing of BU is controlled primarily by atmospheric heat gain, notably via solar radiation and air temperature (Jeffries & Morris, 2007; Kirillin et al., 2012; Woolway et al., 2020). However, other controls include snow and ice conditions, ice thickness, wind and heat inputs via inflow (Prowse et al., 2011; Williams, 1965). Starting with snow and ice conditions, snow and ice act as a diffusive filter for solar radiation, causing a reduction in solar radiation reaching the underlying water surface (Kirillin & Leppäranta, 2022; Mullen & Warren, 1988). Thus, the presence of snow causes a delay in initial BU due to snow's high albedo, causing high reflectance of solar radiation (Hicks et al., 2008; Kirillin & Leppäranta, 2022; Prowse et al., 2011). Once snow melt occurs, typically in the spring, due to increasing air temperature and solar radiation, ice begins to melt. Additionally, ice thickness determines the amount of heat required to completely melt the ice (Kirillin et al., 2012). Thus, BU is governed by air temperature and solar radiation, which notably alter radiative fluxes (Woolway et al., 2020). The close coupling between BU and air temperature has been documented in several studies. For example, Jeffries and Morris (2007) found that the timing of

BU is strongly determined by spring air temperature, specifically for April air temperatures for Alaskan ponds. They reported that a 1°C change in air temperature causes BU timing to change by 1.86 days. As the ice sheet melts, wind can accelerate the complete disappearance of ice. This occurs when the ice sheet is relatively thin, allowing the mechanical force of the wind to break the ice sheet apart (Brown, 2012; Williams, 1965). Thus, the ice sheet is no longer reducing solar radiation absorption by the water surface, causing increased heat input, accelerating melt (Kirillin & Leppäranta, 2022; Lindenschmidt et al., 2018). Overall, the timing and process of BU is primarily governed by air temperature and solar radiation, but other key influences include snow and ice conditions, ice thickness, wind and heat inputs via inflow. With this background on the key influences, the following section expands on the process of BU.

2.2.4.1 Process of break-up

Break-up begins once the heat balance of the ice turns positive, typically during springtime due to an increase in incoming solar radiation and ablation of highly reflective snow during clear skies conditions (Kirillin and Leppäranta, 2022). Consequently, producing a shift in the heat balance preceding ice melt due to heat fluxes at several interfaces: air-ice interface, ice-water interface and internal absorption of solar radiation within the ice (Kirillin and Leppäranta, 2022; Leppäranta, 2015; Woolway et al., 2020). The heat fluxes at the air-ice interface and internally within the ice occur simultaneously, as incoming solar radiation at the air-ice interface is then absorbed by the ice, causing a significant reduction in the ice's mechanical strength and increasing the porosity of ice (Hicks et al., 2008; Prowse et al., 2011). Subsequently, the heat-induced change in the ice's internal crystal structure weakens the ice, causing it to be easily broken by radiative and mechanical processes (Ashton, 1986). For instance, the ice sheet is unable to support its weight once ice porosity reaches 0.3-0.4, causing the ice sheet to break apart (Kirillin and Leppäranta, 2022). At the ice-water interface, the water beneath the ice is fixed at 0°C (melting point of ice), producing a heat flux from the water to the bottom of the ice. However, the heat flux is low due to weak turbulence due by the presence of ice. But once solar radiation penetrates the ice sheet, the underlying water will absorb heat. Consequently, this warming increases turbulence and convective mixing, which increases the heat flux from the water, accelerating melt (Kirillin and Leppäranta, 2022; Leppäranta, 2015; Kirillin et al., 2012).

2.2.5 Summary

To summarize, lake ice phenology refers to the timing and stages of lake ice, including formation (known as FU) and melt (known as BU). These processes are primarily governed by the surface energy balance (SEB), which is moderated by lake properties, hydrological influences, and meteorological variables. While air temperature is widely recognized as the dominant factor controlling lake ice phenology, other influencing variables include cloud cover, lake depth, snow, and wind.

Freeze-up timing is strongly dependent on the combined effects of lake depth and air temperature. In particular, lake depth determines the rate of cooling and air temperature produces heat loss from the water body to begin ice formation. Ice growth is influenced by wind, snow cover, cloud cover, and hydrological input (via inflow). Conversely, the dominant control of break-up is atmospheric heat gain (notably via solar radiation and air temperature), but other variables play key roles in BU timing, such as snow and ice conditions, ice thickness, wind and heat input via inflow.

Overall, this section has outlined the interactions between energy fluxes, meteorological conditions and lake ice processes. With this background, the following section describes the significance of lake incorporation within weather-climate models. It first reviews the general improvements that the parameterization of lakes has made to models, then introduces the central product of this study, ERA5-Land, and then finally summarizes previous assessments of its lake ice component.

2.3 Lake and lake ice inclusion in weather-climate modelling

As previously established (Section 2.2), lakes and lake ice play a crucial role in moderating the weather/climate, as they significantly influence the atmospheric boundary layer by altering surface fluxes of heat, moisture, and momentum (Mironov, 2008). Therefore, to produce comprehensive and precise weather or climate simulations, incorporating lakes within climate models is crucial. Accordingly, it has been found that including lakes tends to bring the model closer to observations within mesoscale modelling (Bates et al., 1993; Bonan, 1995; Hostetler et al., 1993). The improved accuracy of atmosphere models arises from capturing the following lake effects: lake thermal effect, thermal dampening and altering energy fluxes.

- Lake thermal inertia: Because of the high heat capacity of water, a lake requires a lot of energy to experience a temperature change; thus, it is resistant to temperature changes. This high thermal inertia consequently produces the lake thermal effect and the thermal dampening effect, as described below (Bates et al., 1993; Martynov et al., 2012; Notaro et al., 2013; Scott & Huff, 1996).
    - Lake thermal effect: The delayed response to temperature causes the lake temperature to be resistant to temperature change, most notably during seasonal shifts (Balsamo et al., 2012).
    - Lake dampening effect: Reduction in the magnitude of temperature fluctuations (diurnal and annual) (Bates et al., 1993; Notaro et al., 2013; Scott & Huff, 1996; Woolway et al., 2020).
- Altering energy fluxes: Lakes influence latent and sensible heat flux; the exact influence varies seasonally, and is related to thermal inertia (Notaro et al., 2013; Prowse et al., 2011; Woolway et al., 2020).

The inclusion of lakes produces realistic delays in seasonal shifts, demonstrating the lake thermal effect, which, in combination with the lake's dampening effect, causes cooler near-surface air temperature in the spring/summer and warmer in the autumn/winter (Balsamo et al., 2012). In fact, simulations that include lakes have been found to reduce forecast errors (notably during summer and spring), which can be attributed to the dampening and thermal effects (Balsamo et al., 2012; Bonan, 1995; Martynov et al., 2012). Additionally, lakes alter energy fluxes, notably turbulent fluxes, specifically producing an increase in latent heat flux and a decrease in sensible heat flux during the open water season (notably during summer and spring) (Notaro et al., 2013; Prowse et al., 2011). During this period, large or deep lakes cool more slowly than the surrounding land due to the lake's thermal inertia; therefore, the LSWT is warmer than the adjacent air, consequently driving sensible heat loss from the lake, in turn, cooling the surroundings (Lofgren, 1997; Lofgren & Zhu, 2000; Nagarajan et al., 2004). Simultaneously, lakes act as a moisture source, thus causing an increase in evaporation during the open water season, in turn, increasing turbulent heat flux (Notaro et al., 2013; Prowse et al., 2011; Rouse et al., 2005; Woolway et al., 2020). These changes in energy fluxes have been replicated within lake-incorporated models (Bonan, 1995; Martynov et al., 2012). Overall, the effect of lake inclusion has been quantified in which lakes have been shown to cause the air

temperature to cool by ~2-3°C, along with an increase in latent heat by 10-45 W m^{-2} and a decrease in sensible heat flux by 5-30 W m^{-2} in the month of July (Bonan, 1995).

2.3.1 European Centre for Medium-Range Weather Forecasts Fifth generation of European ReAnalysis

The European Centre for Medium-Range Weather Forecasts (ECMWF) Fifth generation of European ReAnalysis (ERA5-Land) is a reanalysis product that provides model-derived land variables describing the terrestrial water and Earth cycle at an hourly timescale. This product is a successor to ERA5 and thus shares most of its parameters with it. However, ERA5-Land has an improved spatial resolution of 9 km, interpolated from ERA5's 31 km resolution using a triangular-cubic-octahedral operational grid. The variable estimates of ERA5-Land are driven by ERA5 downscale meteorological forcing, achieved through numerical integration of the Cy45rl model cycle of ECMWF HTESSEL (Hydrology-Tiled ECMWF Scheme for Surface Exchanges over Land) surface model. Within the HTESSEL model, the lake scheme was introduced with the implementation of a lake tile (representing inland water bodies) based on the Freshwater Lake model (FLake), further described in the next section (lake parameterization) (European Centre for Medium-Range Weather Forecasts, 2018; Muñoz-Sabater et al., 2021).

Within the Cy45rl cycle of HTESSEL, lakes have been recently incorporated to account for how lake characteristics (e.g., state of the water surface) produce changes in thermal inertia, specific albedo, and roughness characteristics, consequently influencing the climate. To account for lakes, lake thermodynamics is incorporated within the surface parameterization through the implementation of a lake tile based on FLake. FLake is a 1D freshwater model that follows the concept of self-similarity for lake temperature profiles and a thermocline (further expanded in the lake parameterization section) (Mironov et al., 2010, 2012). FLake describes a lake's state with seven prognostic variables: mixed layer temperature, mixed layer depth, lake bottom temperature, mean water column temperature, shape factor (with respect to the temperature profile of the thermocline), lake ice surface temperature and lake ice thickness (Mironov et al., 2010, 2012; Muñoz-Sabater et al., 2021). To produce these prognostic variables, the following input variables are required: lake location/fractional cover, lake depth and initial lake conditions (Muñoz-Sabater et al., 2021).

2.3.1.1 Lake parameterization

The lake parameterization is provided by the FLake, a bulk-type numerical scheme that represents the lake's vertical profile with consideration of lake ice melt and formation (ECMWF, 2018; Mironov et al., 2010) (Figure 1). FLake was implemented into the HTESSEL surface scheme with ad-hoc simplification to remove components of FLake that were already present in HTESSEL. So, the following components were excluded: turbulent flux calculations, surface heat flux of moisture, heat and momentum, lake sediment parameterization (due to lack of global data), water balance (not accounted for), and consideration of snow cover over lake ice. Additionally, depth and surface area were treated as constant. (ECMWF, 2018). To understand the lake parameterization, the following sections expand on FLake and key equations used to represent the state of a lake.

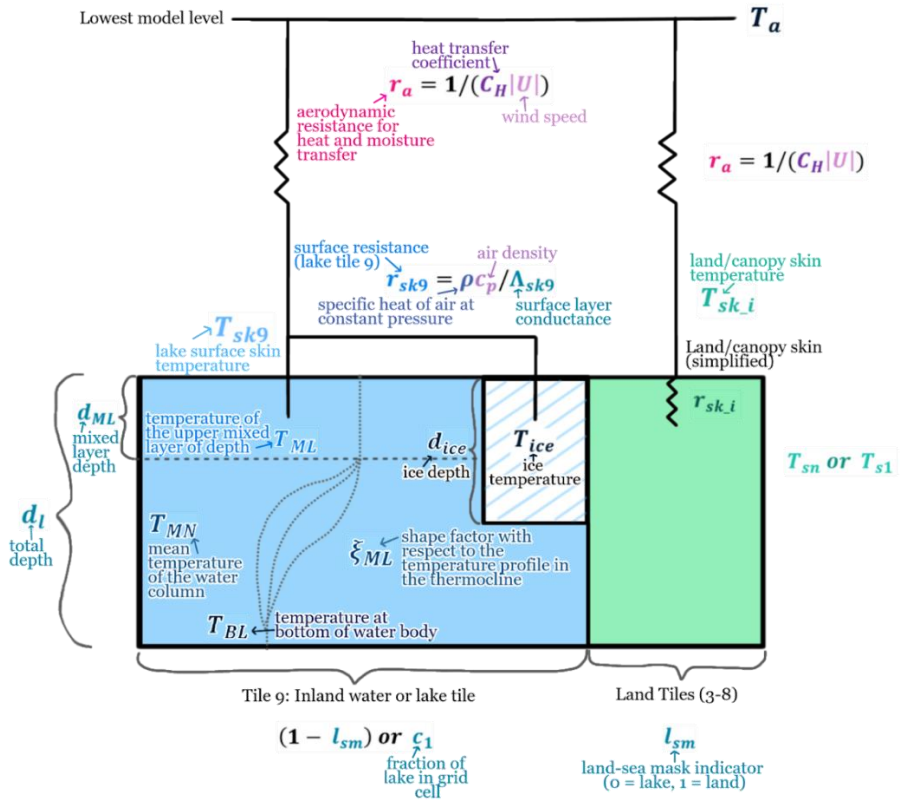


Figure 1: HTESSEL lake schematic (adapted from ECMWF, 2018)

FLake follows the concept of self-similarity, as such, the temperature-depth curve of the lake profile follows a predictable shape. Specifically, self-similarity depicts the mixed layer to be a

uniform temperature due to wind and thermal mixing (influenced by solar radiation) (Mironov et al. 2010, 2012). Then, past the mixed layer depth, the temperature follows a gradual curve (Figure 2) (Betts et al., 2020). The steepness of the temperature-depth curve is dependent on thermal stratification and mixing processes (Mironov et al. 2012).

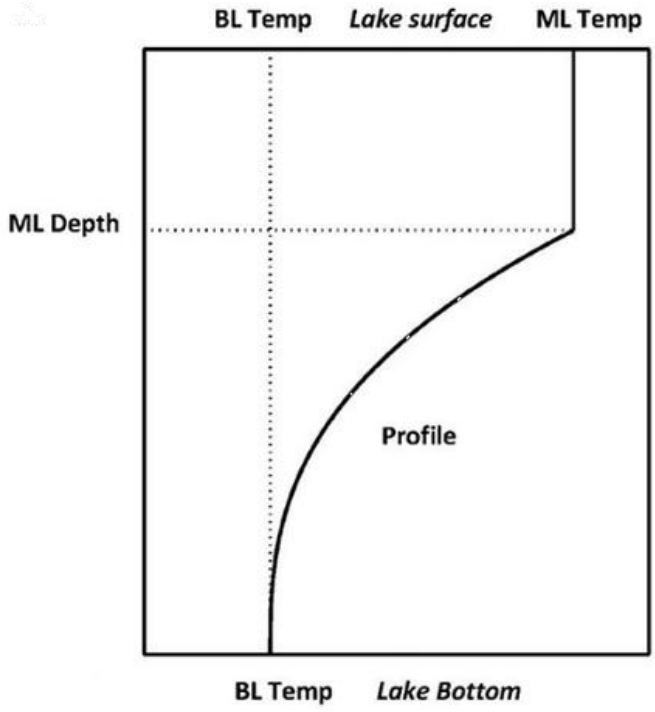


Figure 2: Diagram of self-similarity (Betts et al., 2020)

Thus, to parameterize self-similarity, FLake represents the lake profile as a 2-layer parametric equation (Equation 1) which considers, heat fluxes (e.g. albedo, solar radiation flux, heat flux from water to ice), wind-induced mixing, and lake thermal stratification (done so within the variables of the equation, most notably seen in Equation 3) (Mironov et al. 2012; ECMWF, 2018).

$$T_l(z) = \begin{cases} T_{ML} & if\ 0 < z \leq d_{ML} \\ T_{ML} - (T_{ML} - T_{BL}) \cdot \Phi_{T_l}(\zeta) & if\ d_{ML} < z \leq d_l \end{cases}$$

Equation 1: Two-layer parameterization of evolving lake temperature profile (ECMWF, 2018)

Where:

- $T_l(z)$ = temperature at depth function (z)
- T_{ML} = temperature of the upper mixed layer of depth (d_{ML})
- T_{BL} = temperature at the bottom of the water body ($z = d_l$)
- Φ_{T_l} = dimensionless function of dimensionless depth = $[z/d_{ML}(t)\ /\ d_l/d_{ML}(t)]$ satisfies boundary conditions
- d_l = lake depth
- z = function of depth
- d_{ML} = upper mixed layer of depth
- ζ = dimensionless depth

For Equation 1 to represent self-similarity, it relies on the dimensionless depth variable, T, to represent the relative depth within the lake profile. So, when $\zeta = 0$, it represents the depth within the mixed layer. So, at this point, within the mixed layer, Φ (0) equals 0, causing the temperature to be equal to the mixed layer temperature. Conversely, $\zeta=1$ represents the lake bottom, so at this depth the equation ensures that the temperature is equal to the lake bottom temperature. Thus, the top half of the equation ensures that the temperature within the mixed layer is constant. While the bottom half of the equation represents the thermocline, the temperature depth curve follows self-similarity, ensuring a smooth temperature transition as depth increases to avoid unrealistic temperature jumps (ECMWF, 2018)

2.3.1.2 Lake ice parameterization

The lake ice parameterization primarily determines ice formation based on surface temperature. Once the surface temperature surpasses the freezing point (273.15 K), and the atmospheric heat flux indicates heat loss, ice formation starts (Mironov et al. 2010, 2012). The rate of ice growth is influenced by the heat flux from the water to the ice (ECMWF, 2018; Mironov et al., 2012). Thus, this section will expand on two major parameterizations: firstly, the lake ice profile, as this provides the lake ice surface temperature, and secondly, the lake ice thickness parameterization.

The ice temperature profile is parameterized similarly to the lake temperature profile, following the concept of self-similarity (Equation 2).

$$T_{ice} = T_f - \left(T_f - T_{sk,i}\right)\phi_{ice}(\zeta_i)\ if\ -d_{ice} < z\ \leq 0$$

Equation 2: Lake ice temperature profile parameterization (ECMWF, 2018)

Where:

- T_f = freshwater freezing point (273.15 K)
- $T_{sk,i}$ = temperature at the upper ice surface
- ϕ_{ice} = $\left[T_f - T_{ice}(z,t)\right]/\left[T_f - T_{sk,i}\right]$, dimensionless universal function of dimensionless depth
- ζ_i = $z/d_{ice}(t)$, dimensionless depth that satisfies the boundary conditions
- d_{ice} = lake ice depth
- z = vertical coordinate (positive downward)

Unlike the depth representation in the lake profile parameterization (Equation 1), depth is inverse in Equation 2. So, when z = 0, this represents the ice-water interface, while $z = -d_{ice}$ represents the ice surface. Despite depth being inversed, it still follows similar logic to Equation 1; so, when ζ_i = 0, at the ice surface, the equation will provide the temperature as the ice surface temperature $T_{sk,i}$. Whereas ζ_i= 1, represents the ice bottom, causing the temperature output to be equal to the freezing point, T_f. In other words, at the bottom of the ice, the temperature output would be the temperature of the water surface beneath the ice (ECMWF, 2018).

To compute ice thickness, both ice growth and melting from below the ice surface is considered as demonstrated in Equation 3.

$$L_f \frac{d(p_{ice} d_{ice})}{dt} = G_w + \kappa_{ice} \frac{T_f - T_{ice}}{d_{ice}} \phi'_{ice}(0)$$

Equation 3: Parameterization of lake ice thickness (ECMWF, 2018)

Where:

- L_f = latent heat of fusion ($3.3\ 10^5\ J\ kg^{-1}$)
- p_{ice} = ice mean property for density ($9.1\ 10^2\ kg\ m^{-3}$)
- d_{ice} = lake ice depth
- $\frac{d}{dt}$ = time derivative
- G_w = heat flux in the near-surface water layer just beneath the ice
- κ_{ice} = thermal conductivity of ice ($2.29\ J\ m^{-1}\ s^{-1}\ K^{-1}$)
- T_f = freshwater freezing point (273.15 K)
- T_{ice} = ice temperature (Equation 2)
- $\phi'_{ice}(0)$ = dimensionless temperature gradient at the top of the ice; = $d\phi_{ice}/d\zeta_i$ at ζ_i=0

In Equation 3, the right side of the equation determines how much energy is entering and leaving the ice bottom. Therefore, if the right side equals a negative value, then ice ablation occurs, which can be due to negative G_w. Whereas if the right side of the equation is positive, then ice growth occurs. On the other hand, the left side of the equation determines the energy required to melt or form ice, accounting for the energy required for phase change between water and ice. If the left side of the equation is negative, then melt occurs, whereas if it is positive, then ice growth occurs (ECMWF, 2018).

2.3.2 Previous Assessments of FLake

The integration of FLake within land surface schemes has demonstrated the ability to account for lake processes such as lake ice and lake heat storage. In turn, it improves the representation of lake-atmosphere interactions, leading to improved predictions of LSWT and near-surface air temperature (Balsamo, 2013; Balsamo et al., 2012). These improvements are due to FLake producing a realistic seasonal delay in temperature (lake thermal effect), representing the realistic behaviour of high latitude lakes: storing heat in the summer, producing a cooling effect, whereas in the autumn, lakes release heat, producing a warming effect (Balsamo, 2013; Balsamo et al., 2012). As a result, FLake produces a significant reduction in forecast errors in the spring/summer, notably in regard to near-surface temperature (Balsamo, 2013). On the other hand, FLake reduces winter overestimation of lake (and ice) surface temperature as it allows the LSWT to adequately respond to atmospheric forcing (Mironov et al., 2010, 2012). Thus, in response to surface cooling, ice formation occurs, consequently, reducing LSWT (Mironov et al., 2010). Without the inclusion of FLake (or similar models), atmospheric model can produce unrealistic heat transfer at the lake-atmosphere interface, which can then inaccurately or falsely produce cold air outbreaks and cyclones over lakes (Mironov et al., 2012).

While FLake does produce improvements as described above, it still has its limitations. Firstly, FLake simplifies deep lakes, as it was originally intended for medium-depth lakes (Munoz-Sabater et al., 2021), by neglecting the abyssal/hypolimnion layer and, instead, using an artificial bottom about 40-60 m deep. Although the artificial bottom produces satisfactory results (since the abyssal layer rarely changes temperature), it is unable to represent partial ice coverage (Mironov et al., 2010; Martynov et al., 2012). Secondly, FLake neglects snow cover on top of lake ice despite the availability of snowfall rates through COSMO (Mironov et al., 2010). Instead, snow cover is implicitly accounted for by decreasing the surface albedo (typically between 0.2 and 0.3). However, this neglects the thermal insulation effect of snow (Dutra et al., 2009; Martynov et al., 2012), as well as simplifies how the change in snow's composition and cover (water content, density and patchiness of snow cover) alters albedo and in turn, alters the amount of absorbed radiation (Jakkila et al., 2009; Kirillin et al., 2012; Kirillin & Leppäranta, 2022; Leppäranta, 2015; Leppäranta et al., 2019).

Despite several studies assessing FLake as a standalone model, there is no comprehensive evaluation of FLake's performance within ERA5-Land, particularly regarding the accuracy of lake ice fraction and lake ice temperature. Lake ice fraction and temperature are of significant interest as they

influence other climatic variables within the model, notably evaporation and the availability of moisture for precipitation and cloud cover (Brown, 2012; Brown & Duguay, 2010; Kirillin & Leppäranta, 2022; Leppäranta et al., 2019). This thesis directly addresses the limited assessment through a spatial and temporally extensive evaluation of lake ice fraction and temperature through comparison with satellite-derived products.

Chapter 3
Methodology

3.1 Study areas

The study areas of this project are seven lakes across Canada: Great Bear Lake (GBL), Great Slave Lake (GSL), Lake Athabasca, Lake Winnipeg, Lake Superior, Lake Huron and Lake Erie. The lakes were selected as they all form annual seasonal ice cover. Additionally, they provide a latitudinal gradient, allowing for the assessment of different ice regimes (Figure 3, Table 2). The following section provides a description of the specific characteristics of each lake, such as lake morphology, ice regime and climate.

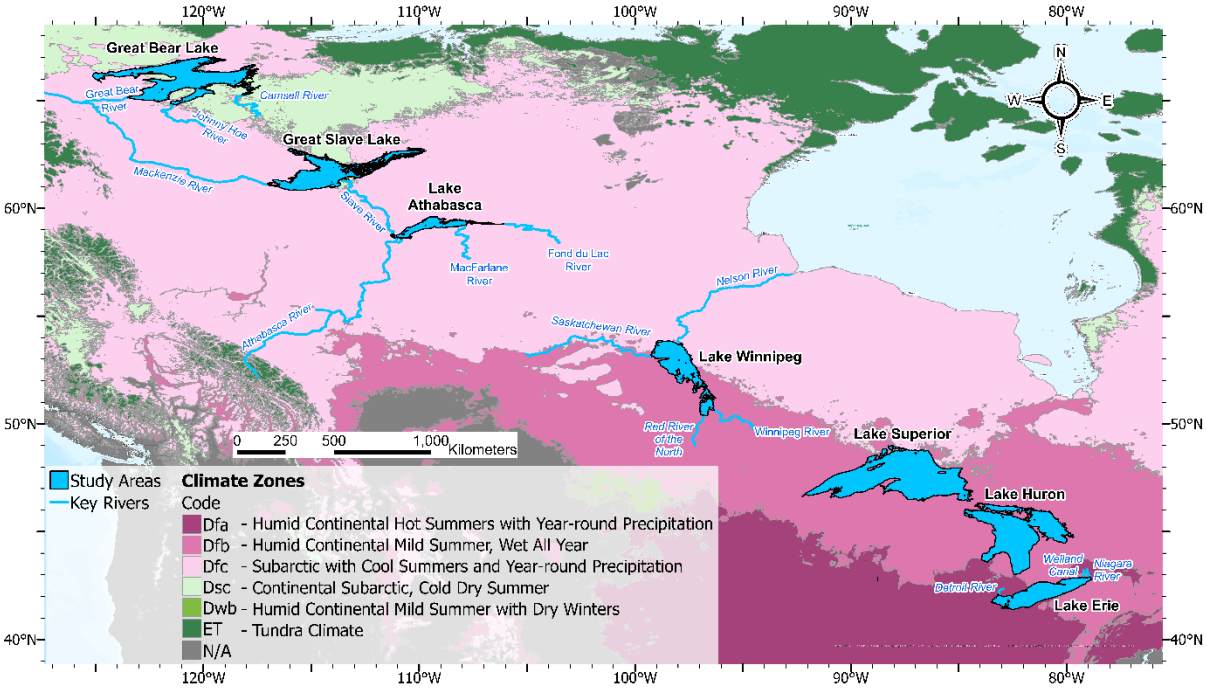


Figure 3: Climate zone map of study sites and key rivers (Data source: CEC, 2020)

Table 1: Climate zones (Adapted from Beck et al., 2018; CEC, 2020)

<table>
<tr><th>Climate Zone</th><th>Full Name</th><th>Climate Type</th><th>Precipitation Pattern</th><th>Temperature Subtype (3rd)</th></tr>
<tr><td>Dfa</td><td>Humid Continental Hot Summers with Year-round Precipitation</td><td rowspan="4">D: Cold
Criteria: Not (B); warmest month >10°C; coldest month ≥0°C</td><td rowspan="3">f: No dry season
Criteria:
Not (Ds - Dry Summer) or (Dw - Dry Winter)</td><td>a: Hot summer
Criteria: Warmest month≥22°C</td></tr>
<tr><td>Dfb</td><td>Humid Continental Mild Summer, Wet All Year</td><td>b: Warm summer
Criteria: ≥4 months>10°C</td></tr>
<tr><td>Dfc</td><td>Subarctic with Cool Summers and Year-round Precipitation</td><td rowspan="2">c: Cold summer
Criteria: Not (a), (b), or (d)</td></tr>
<tr><td>Dsc</td><td>Continental Subarctic - Cold Dry Summer</td><td>s: Dry summer
Criteria:
Summer driest month < 40mm and <⅓ winter wettest month</td></tr>
</table>

Table 2: Characteristics of study sites (Geological Survey of Canada, 1967; International Lake Environment Committee Foundation, n.d.; Lakepedia, n.d.; Peel et al., 2007; Statistics Canada, Environment, Energy and Transportation Statistics Division, 2009)

Drainage Basin	Lake Name	Latitude	Longitude	Elevation (m.a.s.l)	Catchment Area (km²)	Avg. Depth (m)	Frozen Period	Climate Zone
Mackenzie River Basin	**Great Bear Lake**	65.834	-120.752	186	114717	72	Nov-Jul	Dsc
	Great Slave Lake	61.500	-114.001	156	971000	73	Nov-Jun	Dfc/Dsc
	Lake Athabasca	59.367	-108.001	213	270000	26	Oct-Jun	Dsc
Lower Saskatchewan-Nelson	**Lake Winnipeg**	52.132	-97.261	217	953250	12	Nov-Mar	Dfb
Laurentian Great Lakes Basin	**Lake Erie**	42.327	-81.177	174	78769	18	80 days	Dfb/Dfa
	Lake Huron	44.944	-82.223	176	128464	53	80 days	Dfb
	Lake Superior	46.074	-81.332	183	124838	148	Nov-Apr	Dfb

3.1.1 Great Bear Lake

GBL is located in the northern area of Northwest Territories (NWT) and is among the largest and deepest lakes in Canada. Specifically, it is the eighth largest freshwater lake worldwide and the third largest in Canada, with an approximate surface area of 31,300 km² (Howell et al., 2009; Rafferty, 2023). GBL experiences a subarctic climate where winter is the dominant season. It is located between two subarctic climate zones, Dfc and Dsc (Figure 3). Dfc is characterized by year-round precipitation with cool summers, and Dsc, which is known for cold, dry summers (Beck et al., 2018; CEC, 2021; Peel et al., 2007). Thus, the summer months are relatively cool with higher rainfall and less total precipitation (snowfall plus rainfall) compared to winter due to the high amount of winter snowfall (Beck et al., 2018; Environment Climate Change Canada, 2023) as revealed by the climate normal of two nearby stations (Table 3). GBL is a cold monomictic lake, meaning the water temperature does not surpass 4°C; it experiences summer circulation with the water temperature at or below 4°C and reaches complete vertical mixing once every 3 years (Hutchinson & Löffler, 1956; Wetzel, 2001). The ice cover season occurs between late November to July but varies annually; in some years ice starts to form as early as September (Evans, 2000; Howell et al., 2009). On average, freeze-up starts on year date (YD) 321 (November), melt onset occurs on YD 139 (May), and complete melt occurs on YD 191 (July) (Howell et al., 2009).

Table 3: Climate normal (1991-2020) for Great Bear Lake (ECCC, 2023)

Note: blue represents the lowest value and red represents the highest value per climate normal element

Station	Location	Climate Normal Element	Jan	Feb	Mar	Apr	May	Jun	Jul	Aug	Sep	Oct	Nov	Dec	Year	Code*
Deline	65° 12' 31.090" N, 123° 26' 00.070" W	Daily Average Temperature (°C)	-24.7	-22.8	-18.7	-7.8	3.2	10.7	13.4	11.3	5.5	-3.4	-15.6	-22.3	-5.9	C
		StdDev Mean Monthly Temperature (°C)	3	2.9	3.6	2.6	2.3	1.2	1.3	1.7	1.8	2.1	2.7	3.7	5	C
		Daily Maximum Temperature (°C)	-20.6	-17.9	-12.8	-2	8.4	17	19.6	16.8	10.2	-0.3	-11.5	-18.2	-0.9	A
		Daily Minimum Temperature (°C)	-28.8	-27.6	-24.5	-13.8	-2.1	4.4	7.3	6	1	-6.5	-19.6	-26.3	-10.9	C
		Rainfall (mm)	0	0	0	0.2	12.7	23.5	39.9		38.5		0.3	0		
		Snowfall (cm)	13.4	16.2	15.1	12.1	3	0.3	0	0	2.1		34.5	17.6		
		Precipitation (mm)	11.8	11.7	9.5	11	14.7	23.7	40.2	42.9	38.6	31.7	21.6	11.9	269.2	D
Norman Wells	65° 17' 15.090" N, 126° 45' 12.084" W	Daily Average Temperature (°C)	-25.4	-22.8	-18.2	-5.3	6.9	15	16.8	13.7	6.5	-3.9	-17.4	-23.6	-4.8	A
		StdDev Mean Monthly Temperature (°C)	3.4	3.1	4	3	2.1	1.2	1.5	1.8	2.2	2.3	3	3.9	1	A
		Daily Maximum Temperature (°C)	-21.4	-18	-12	0.9	13	21	22.6	19.1	11.3	-0.5	-13.6	-19.6	0.2	A
		Daily Minimum Temperature (°C)	-29.4	-27.5	-24.3	-11.5	0.8	8.8	10.9	8.2	1.5	-7.2	-21.2	-27.5	-9.9	A
		Rainfall (mm)	0.2	0	0.4	1.3	11.6	35.7	46.4	49.1	23.9	3.3	0.1	0	171.9	C
		Snowfall (cm)	22.7	21.7	15.8	14.2	7.5	0.4	0	0.1	6.4	24.8	27.5	24.8	165.8	C
		Precipitation (mm)	18	17.2	11.3	11.1	20.5	35.8	49	52.5	33.9	23.5	27.2	21.6	321.6	C

**Code legend: A = WMO "3 and 5 rule" (i.e. no more than 3 consecutive and no more than 5 total missing for either temperature or precipitation); B = At least 25 years; C = At least 20 years; D = At least 15 years; + = First or oldest date of occurrence of the extreme value*

3.1.2 Great Slave Lake

GSL is located within southern NWT; it is the tenth largest freshwater lake worldwide and the fourth largest in Canada with an area of ~27,000km² and a maximum depth of 614 m (Gibson et al., 2006; Rafferty, 2023; Tang et al., 2023). The climate of GSL is similar to GBL, as it is also between the Dsc and Dfc climate zones, but more so within the Dfc zone, thus, it experiences higher amounts of precipitation (Beck et al., 2018; Environment Climate Change Canada, 2023). Also, compared to GBL, GSL experiences milder winters, which can be attributed to its lower latitude (Table 4). GSL can be divided into two sections: the main lake catchment and the eastern arm. The eastern arm is deeper in comparison to the main catchment with an average depth of 249 m and maximum depth of 614 m, whereas the main catchment has an average depth of 41 m and maximum depth of 163 m (Howell et al., 2009; Ménard et al., 2002). GSL is a dimictic lake, mixing twice a year during spring and fall and is stratified during summer and winter (Hoffman, 1987; Wetzel, 2001). The spatial pattern of ice phenology is as follows: the central basin is first to experience melt due to discharge from the Slave River into the lake, while the east arm is first to experience freezing, followed by the north and west arms. Typically, ice formation begins in November, on average on YD 330 (Howell et al., 2009). Ice coverage typically lasts from late November to early June, with annual variability (Ziyad et al., 2020). Melt typically begins in May, around YD 123, on average, and fully melts by YD 164, around June (Howell et al., 2009).

Table 4: Climate normal (1991-2020) for Great Slave Lake (ECCC, 2023)

Note: blue represents the lowest value and red represents the highest value per climate normal element

Station	Location	Climate Normal Element	Jan	Feb	Mar	Apr	May	Jun	Jul	Aug	Sep	Oct	Nov	Dec	Year	Code*
Hay River	65° 12' 31.090" N, 123° 26' 00.070" W	Daily Average Temperature (°C)	-21.4	-19.1	-13.7	-3.1	5.9	12.9	16.6	14.9	9.2	0.8	-10.7	-18.4	-2.2	A
		StdDev Mean Monthly Temperature (°C)	3.4	3.5	3.9	2.9	2.2	1.4	1.4	1.3	2.1	1.9	3	4.1	1.1	A
		Daily Maximum Temperature (°C)	-16.9	-13.7	-7.7	2.4	11.4	18.4	21.7	19.9	13.8	4.3	-7	-14.2	2.7	A
		Daily Minimum Temperature (°C)	-25.8	-24.3	-19.6	-8.6	0.3	7.4	11.5	9.8	4.5	-2.7	-14.4	-22.6	-7	A
		Rainfall (mm)	0.3	0.2	0.3	3.9	16.2	25.1	43.8	60.2	42.9	15.9	0.8	0.3	209.9	C
		Snowfall (cm)	22.2	16.6	16.8	8.9	4.3	0	0	0	1.1	19.1	34.4	22.1	145.5	C
		Precipitation (mm)	16.6	13.9	15.3	11.1	20.8	25.4	41.9	59.7	42.3	33	24	16.4	320.3	A
Yellowknife	65° 17' 15.090" N, 126° 45' 12.084" W	Daily Average Temperature (°C)	-25.5	-22.7	-16.6	-5.5	5.3	13.8	17.1	14.5	7.6	-1	-12.6	-21.8	-4	B
		StdDev Mean Monthly Temperature (°C)	3.1	3.8	3.8	2.9	2.7	1.2	1.4	1.3	2.1	2.2	2.8	4.6	2.4	B
		Daily Maximum Temperature (°C)	-21.6	-18	-10.6	0.3	10.4	18.6	21.5	18.4	10.9	1.5	-9	-18	0.4	B
		Daily Minimum Temperature (°C)	-29.4	-27.4	-22.5	-11.3	0.1	9	12.6	10.5	4.2	-3.6	-16.2	-25.6	-8.3	B
		Rainfall (mm)	0	0	0.2	2.9	12.2	28	40.4	44	39.9	12	0.5	0	180.2	C
		Snowfall (cm)	21.7	16.1	19.2	9.9	4.5	0	0	0	3	20.1	36.9	23.7	155	C
		Precipitation (mm)	15	11	14.1	11.6	16.3	28.9	40.4	44	43	28.8	25.8	15.1	293.9	C

**Code legend: A = WMO "3 and 5 rule" (i.e. no more than 3 consecutive and no more than 5 total missing for either temperature or precipitation); B = At least 25 years; C = At least 20 years; D = At least 15 years; + = First or oldest date of occurrence of the extreme value*

3.1.3 Lake Athabasca

Lake Athabasca is located at the border of Alberta and Saskatchewan. It is the eighth largest lake in Canada with a surface area of ~7,528 km² and average depth of 26 m (Bennett et al., 1973; International Lake Environment Committee, n.d.; Rafferty, 2023). The eastern side of the lake is significantly deeper than the western where the maximum depth is 124 m and 16 m, respectively (Leconte et al., 2001, 2008; Mitchell & Prepas, 1990). Similarly to GSL, Lake Athabasca is within the Dfc region, therefore experiences year-round precipitation, and due to its lower latitude, it experiences warmer temperatures than GSL (Beck et al., 2018; Environment Climate Change Canada, 2023) (Table 5). This lake is a dimictic lake, meaning it is stratified in summer, inversely stratified in the winter, and mixing occurs twice a year (Leconte et al., 2008; Wetzel, 2001). The ice season typically occurs from mid-November to late May (Brown, 2017).

Table 5: Climate normal for Lake Athabasca (ECCC, 2023)

Note: blue represents the lowest value and red represents the highest value per climate normal element

Station	Location	Climate Normal Element**	Jan	Feb	Mar	Apr	May	Jun	Jul	Aug	Sep	Oct	Nov	Dec	Year	Code*
Fort Chipewyan A*	58° 46' 00.000" N, 111° 07' 00.000" W	Daily Average Temperature (°C)	-21	-18.4	-11.7	-0.9	7.9	14.5	17.2	15.2	9	1	-10	-17.9	-1.3	A
		StdDev Mean Monthly Temperature (°C)	3.8	4.1	4.1	2.9	2.2	1.2	1.3	1.5	2.1	2.1	3.4	4.3	1.1	A
		Daily Maximum Temperature (°C)	-15.8	-12.3	-4.8	5.4	14.5	21	23.4	21.3	14.6	5.2	-5.7	-13.1	4.5	A
		Daily Minimum Temperature (°C)	-26.2	-24.5	-18.5	-7.3	1.2	8.1	10.9	9.1	3.4	-3.2	-14.2	-22.8	-7	A
		Rainfall (mm)	0.3	0.1	0.2	6.2	24.5	44.4	67.4	50.2	43.2	13.3	0.4	0.2	250.4	C
		Snowfall (cm)	14.8	14.4	15.7	9.8	2.7	0	0	0	0.7	15.5	24.7	18.5	116.9	C
		Precipitation (mm)	14.9	14.1	15.8	16	27.2	44.4	67.4	50.2	44	28.8	24.5	18.4	365.7	C

**Code legend: A = WMO "3 and 5 rule" (i.e. no more than 3 consecutive and no more than 5 total missing for either temperature or precipitation); B = At least 25 years; C = At least 20 years; D = At least 15 years; + = First or oldest date of occurrence of the extreme value*

*** The temperature climate normal is from 1991-2020, while the precipitation climate normals are 1981-2010 due to missing data for 1991-2020*

3.1.4 Lake Winnipeg

Lake Winnipeg is located in Manitoba. It is the 12th largest lake globally and the sixth largest in Canada with a surface area of ~24,514 km² (Cicek et al., 2006; Rafferty, 2023; Zhao et al., 2012). Lake Winnipeg is within the Dfb climate zone, characterized by a humid continental climate with mild summers and is wet year-round (Beck et al, 2018; ECCC, 2023). Thus, in comparison to Lake Athabasca, Lake Winnipeg experiences higher precipitation and slightly milder temperatures (Table 6). The lake is separated into two basins by a 2.5 km wide channel known as the Narrows (Zhao et al., 2012); the two basins are referred to as the north and south basins. The north basin is both larger and deeper, spanning ~100 km wide and with an average depth of 12 m, whereas the south basin is ~40 km wide with an average depth of 9 m. The shallow depth and wind-induced turbidity cause mixing to occur at irregular intervals, preventing stratification; thus, Lake Winnipeg is classified as polymictic (Dallosch, 2024; Environment Climate Change Canada, 2024; Zhao et al., 2012). The ice cover period is from mid-November to the end of May (Tang et al., 2023; Ziyad et al., 2020). However, the south basin experiences break-up two weeks earlier than the north basin due to its shallower depth (Dallosch, 2024; ECCC, 2024).

Table 6: Climate normal (1991-2020) for Lake Winnipeg (ECCC, 2023)

Note: blue represents the lowest value and red represents the highest value per climate normal element

Station	Location	Climate Normal Element	Jan	Feb	Mar	Apr	May	Jun	Jul	Aug	Sep	Oct	Nov	Dec	Year	Code*
Norway House	53° 57' 30.000" N, 97° 50' 39.000" W	Daily Average Temperature (°C)	-20.5	-18	-10.3	-0.3	7.9	14.5	17.9	16.6	10.5	2.4	-8.3	-16.9	-0.4	A
		StdDev Mean Monthly Temperature (°C)	3.9	4	3.4	3.1	1.7	1.6	1.4	1.4	1.7	2.1	3.3	4.4	1.9	A
		Daily Maximum Temperature (°C)	-15.5	-11.8	-3.6	6.1	14	20.5	23.5	22	15.6	6.3	-4.3	-12.2	5.1	A
		Daily Minimum Temperature (°C)	-25.5	-24.1	-17	-6.6	1.8	8.5	12.3	11.1	5.3	-1.5	-12.3	-21.6	-5.8	A
		Rainfall (mm)	0.4	0.6	4	9	39.8	75.1	82.9	66.6	60.5	26	2.2	0.4	367.5	D
		Snowfall (cm)	27.2	27	26.2	16	6.2	0	0	0	0.7	22	32.1	35	192.5	D
		Precipitation (mm)	18.3	16.6	23	21	46.5	74.5	79.3	65.9	58.9	42.3	25.7	22.5	494.6	D
Gimli	50° 38' 00.000" N, 97° 03' 00.000" W	Daily Average Temperature (°C)	-17.5	-14.8	-6.8	2.7	10	16.6	19.2	18.1	13	5	-4.5	-13.3	2.3	A
		StdDev Mean Monthly Temperature (°C)	3.3	4.1	3.7	2.8	1.9	1.3	1.1	1.4	1.5	2.1	3.6	4.2	3.2	A
		Daily Maximum Temperature (°C)	-12.2	-9.1	-1.2	8.7	16.4	22.4	25.3	24.4	18.9	9.7	-0.3	-8.6	7.9	A
		Daily Minimum Temperature (°C)	-22.7	-20.5	-12.4	-3.2	3.7	10.8	13.1	11.8	7.1	0.3	-8.7	-17.9	-3.2	A
		Rainfall (mm)	0	1.5	4.9		67.7	89.8	74.7	66.8	62.9					
		Snowfall (cm)	22.8	12.3	19.2	10.1	3.3	0	0	0	0					
		Precipitation (mm)	19.1	12.4	22.7	28.1	60.8	86.7	76.7	69.8	55.2	43.7	23.4	18.2	516.6	C

**Code legend: A = WMO "3 and 5 rule" (i.e. no more than 3 consecutive and no more than 5 total missing for either temperature or precipitation); B = At least 25 years; C = At least 20 years; D = At least 15 years; + = First or oldest date of occurrence of the extreme value*

*** The temperature climate normal is from 1991-2020, while the precipitation climate normals are 1981-2010 due to missing data for 1991-2020*

3.1.5 Lake Superior

Lake Superior is located between Canada and the U.S.A., specifically the province of Ontario and the states of Michigan, Wisconsin and Minnesota. It is the largest lake within Canada and the second largest worldwide with a surface area of ~82,000 km² (Assel, 1983; Notaro et al., 2023; Rafferty, 2023). Lake Superior has a volume of ~12,230 km³, a mean depth of 149 m and a maximum depth of 405 m, located in the southern basin (Assel, 1983; Environmental Protection Agency, 2025). Similar to Lake Winnipeg, Lake Superior falls within the Dfb climate zone (ECCC, 2023; Beck et al, 2018); however, Lake Superior experiences warmer temperatures and higher precipitation amounts compared to Lake Winnipeg (Table 7). A key feature of Lake Superior is the Keweenaw Peninsula, located in Michigan. The Peninsula is a subsurface ridge (~150-180 m deep) that extends from the south shore of Lake Superior, dividing the lake into eastern and western basins. The eastern basin is characterized by north-south valleys and ridges, while the bathymetry of the western basin is smoother (Assel, 1983). Lake Superior is a dimictic lake, meaning it is stratified and inversely stratified in the summer and winter, respectively, and mixes twice a year (Leconte et al., 2008; Wetzel, 2001). The ice phenology of Lake Superior is typically as follows: ice formation occurs around early/mid-December, reaching maximum ice coverage around mid-March, then melt onset occurs around shortly after (mid-March/late March) and finally, ice offs (i.e. water clear of ice) occurs around mid-May (North American Ice Service, n.d.).

Table 7: Climate normal (1991-2020) for Lake Superior (ECCC, 2023; Palecki et al., 2021)

Note: blue represents the lowest value and red represents the highest value per climate normal element

Station	Location	Climate Normal Element	Jan	Feb	Mar	Apr	May	Jun	Jul	Aug	Sep	Oct	Nov	Dec	Year	Code*
Wawa	47° 58' 01.000" N, 84° 47' 11.000" W	Daily Average Temperature (°C)	-21.4	-19.1	-13.7	-3.1	5.9	12.9	16.6	14.9	9.2	0.8	-10.7	-18.4	-2.2	A
		StdDev Mean Monthly Temperature (°C)	3.4	3.5	3.9	2.9	2.2	1.4	1.4	1.3	2.1	1.9	3	4.1	1.1	A
		Daily Maximum Temperature (°C)	-16.9	-13.7	-7.7	2.4	11.4	18.4	21.7	19.9	13.8	4.3	-7	-14.2	2.7	A
		Daily Minimum Temperature (°C)	-25.8	-24.3	-19.6	-8.6	0.3	7.4	11.5	9.8	4.5	-2.7	-14.4	-22.6	-7	A
		Rainfall (mm)	0.3	0.2	0.3	3.9	16.2	25.1	43.8	60.2	42.9	15.9	0.8	0.3	209.9	C
		Snowfall (cm)	22.2	16.6	16.8	8.9	4.3	0	0	0	1.1	19.1	34.4	22.1	145.5	C
		Precipitation (mm)	16.6	13.9	15.3	11.1	20.8	25.4	41.9	59.7	42.3	33	24	16.4	320.3	A
Duluth	46° 50' 13" N, 092° 11' 00" W	Average Temperature (°C)	-11.6	-9.2	-2.8	4.2	11.1	16.2	19.4	18.6	14.0	6.7	-1.2	-8.3	4.8	
		Maximum Temperature (°C)	-16.4	-14.4	-7.9	-1.2	5.0	10.1	13.4	12.9	8.5	2.0	-5.3	-12.4	10.0	
		Minimum Temperature (°C)	-22.7	-20.5	-12.4	-3.2	3.7	10.8	13.1	11.8	7.1	0.3	-8.7	-17.9	-0.5	
		Precipitation (mm)	24.1	25.7	37.1	64.3	85.6	111.5	99.6	94.7	88.4	73.9	49.8	37.3	792.0	
		Snowfall (cm)	42.7	38.4	32.5	23.1	2.0	0.0	0.0	0.0	0.3	6.9	35.8	47.5	229.1	

**Code legend: A = WMO "3 and 5 rule" (i.e. no more than 3 consecutive and no more than 5 total missing for either temperature or precipitation); B = At least 25 years; C = At least 20 years; D = At least 15 years; + = First or oldest date of occurrence of the extreme value*

3.1.6 Lake Huron

Lake Huron lies within both Canada (Ontario) and the United States (Michigan). Lake Huron, in terms of volume, is the third largest of the Laurentian Great Lakes with a volume of 3,537 km^3. Regarding surface area, it covers ~59,600 km^2, making it the second largest lake of Canada and the fourth largest in the world (Lewis et al., 2008; Rafferty, 2023). Lake Huron has an average depth of 59 m and a maximum depth of 229 m (Assel, 1983; Lewis et al., 2008). It falls within the Dfb climate zone (Beck et al, 2018), therefore, experiences higher precipitation and warmer temperatures compared to Lake Superior (ECCC, 2023) (Table 8). The lake can be divided into three basins: east, central and south. Starting with the eastern basin is the area from the North Channel to Georgian Bay. This basin is the shallowest of the lake, with waters less than 100 m deep, and the shore depth is typically 50 m (Assel, 1983; Lewis et al., 2008). Moving onto the central basin, it is characterized by a complex bathymetry and corresponds to the deepest part of the lake, with depths ranging from 100-229 m. Lastly, the southern basin includes Saginaw and Thunder Bay of Michigan. This basin is characterized by smoother bathymetry, with medium depths of 100 m in the lake center and 50 m near the shore (Assel, 1983; Lewis et al., 2008). Lake Huron is a dimictic lake, which means that mixing occurs during fall and spring, while summer and winter experience stratification. The ice phenology of Lake Huron is as follows: ice formation occurs in mid to late December (North American Ice Service, n.d.), starting along the shorelines (Assel, 1983). The peak of ice coverage occurs around mid-February, then break-up starts around early to mid-March, with significant melt beginning in the center of the lake. Following the initial break-up, complete ice melt occurs around late May, where some ice may remain in sheltered areas such as Bays and the southern shore (North American Ice Service, n.d.).

Table 8: Climate normal (1991-2020) for Lake Huron (ECCC, 2023; Palecki et al., 2021)

Note: blue represents the lowest value and red represents the highest value per climate normal element

Station	Location	Climate Normal Element	Jan	Feb	Mar	Apr	May	Jun	Jul	Aug	Sep	Oct	Nov	Dec	Year	Code*
Sarnia	42° 59' 32.058" N, 82° 18' 17.088" W	Daily Average Temperature (°C)	-4.6	-4	0.6	6.7	13.1	18.6	21.3	20.4	16.7	10.7	4.2	-1.2	8.5	A
		StdDev Mean Monthly Temperature (°C)	2.8	2.9	2.5	1.5	1.8	1.2	1.5	1.3	1.4	1.4	2	2.5	1.4	A
		Daily Maximum Temperature (°C)	-0.9	0	5	11.9	18.7	24	26.5	25.5	22.2	15.4	8	2.1	13.2	A
		Daily Minimum Temperature (°C)	-8.2	-7.9	-3.7	1.5	7.4	13	16	15.3	11.3	6	0.4	-4.4	3.9	A
		Rainfall (mm)	29	26.8	34.1	70.6	88.1	89.5	85.5	63.5	93.3	77.6	68.2	39	765.2	D
		Snowfall (cm)	34.2	20.2	22	3.5	0	0	0	0	0	0.5	7	25	112.4	D
		Precipitation (mm)	56.5	47.7	56.9	79.3	85.2	92.5	80.4	70.9	84.1	78.4	79.5	60	871.3	D
Alpena WWTP	45° 03' 38" N, 83° 25' 41" W	Average Temperature (°C)	-6.6	-6.3	-1.8	4.6	11.1	16.9	20.2	19.6	15.4	8.7	2.4	-2.8	6.8	
		Maximum Temperature (°C)	-2.7	-1.9	2.7	9.1	16.0	21.7	25.1	24.6	20.5	13.3	6.1	0.4	0.0	
		Minimum Temperature (°C)	-10.3	-10.7	-6.2	0.1	6.2	12.1	15.2	14.5	10.4	4.2	-1.2	-6.2	15.2	
		Precipitation (mm)	55.6	43.2	46.0	79.0	80.5	69.1	83.6	87.6	74.7	82.3	57.7	52.1	1325.9	
		Snowfall (cm)	39.6	36.6	15.7	8.9	0.0	0.0	0.0	0.0	0.0	0.3	7.6	42.2	91.9	

**Code legend: A = WMO "3 and 5 rule" (i.e. no more than 3 consecutive and no more than 5 total missing for either temperature or precipitation); B = At least 25 years; C = At least 20 years; D = At least 15 years; + = First or oldest date of occurrence of the extreme value*

3.1.7 Lake Erie

Lake Erie lies within Canada and the U.S.A., specifically Ontario, New York, Pennsylvania, Michigan and Ohio. Lake Erie is the smallest of the Laurentian Great Lakes in terms of volume (~483 km^3) and depth (average depth ~19m) (Assel, 1983). In terms of surface area, it is the fifth-largest lake in Canada and the 11^{th} largest in the world, with a surface area of 25,667 km^2 (Rafferty, 2023). Lake Erie is located between two climate zones, Dfb and Dfa (Figure 3). Dfb was described earlier while Dfa is characterized by hot summers and is wet all year, thus, it experiences high precipitation and warmer temperatures compared to Lake Huron (ECCC, 2023; Beck et al, 2018) (Table 9). The lake can be divided into three basins: western, central and eastern basins. The western basin spans from the western shore of Lake Erie to Point Pelee; this basin is the shallowest of the basins, with depths of 18 m or less. From Point Pelee to Long Point lies the central basin, which features moderate depths ranging from 10 m to 24 m. The deepest section of Lake Erie is located in the eastern basin, spanning from Long Point to the eastern shore with depths ranging from 36-55 m, and the deepest part is 64 m, located between Erie, Pennsylvania and Dunkirk, New York (EPA, 2020; Assel, 1983). Lake Erie is a dimictic lake, the same as Lake Huron, Lake Superior, Lake Athabasca, and GSL. Due to Lake Erie's shallow depth, it often experiences high ice cover, typically exceeding 90%, but with frequent melt and refreeze events (Assel, 1983; Fujisaki et al., 2012). The ice regime is typically characterized by ice formation beginning late December to early January and reaching maximum coverage around mid-February. Melt occurs shortly after around mid-February, with the disappearance of ice around mid-May (North American Ice Service, n.d.).

Table 9: Climate normal (1991-2020) for Lake Erie (ECCC, 2023)

Note: blue represents the lowest value and red represents the highest value per climate normal element

Station	Location	Climate Normal Element	Jan	Feb	Mar	Apr	May	Jun	Jul	Aug	Sep	Oct	Nov	Dec	Year	Code*
Windsor	58° 46' 00.000" N, 111° 07' 00.000" W	Daily Average Temperature (°C)	-3.6	-2.6	2.4	8.8	15.3	20.8	23.2	22.1	18.1	11.6	5.2	-0.4	10.1	B
		StdDev Mean Monthly Temperature (°C)	2.8	2.8	2.5	1.6	1.9	1.2	1.5	1.3	1.4	1.3	2.1	2.4	1.1	B
		Daily Maximum Temperature (°C)	0	1.3	6.8	14	20.7	26	28.3	27	23.1	16.1	8.9	2.7	14.6	A
		Daily Minimum Temperature (°C)	-7.1	-6.4	-2.1	3.5	9.8	15.5	18	17.1	13	6.9	1.4	-3.5	5.5	B
		Rainfall (mm)	39.1	34.3	50.9	86.5	97.7	83.7	99.3	75.7	88	72.2	70.6	47.2	845.2	C
		Snowfall (cm)	43.4	33.2	22.5	5.6	0	0	0	0	0	0.2	5	29.9	139.8	C
		Precipitation (mm)	70.8	60	71	92.2	97.3	82.9	99.3	75.7	88.3	73.9	73.2	69.2	953.8	C

**Code legend: A = WMO "3 and 5 rule" (i.e. no more than 3 consecutive and no more than 5 total missing for either temperature or precipitation); B = At least 25 years; C = At least 20 years; D = At least 15 years; + = First or oldest date of occurrence of the extreme value)*

3.2 Satellite-Derived Products: General Description

The following section describes the satellite products utilized to assess the ERA5-Land lake ice variables of interest (lake ice timing, fraction and surface temperature). Four satellite products are used: the Interactive Multisensor Snow and Ice Mapping System (IMS) Daily Northern Hemisphere Snow and Ice Analysis, the Canadian Ice Service (CIS) Weekly Lake Ice Product, the National Oceanic and Atmospheric Administration (NOAA) Lake Ice Product and the NASA MODIS Land Surface Temperature and Emissivity (MOD11C1) products.

3.2.1 Interactive Multisensor Snow and Ice Mapping System Daily Northern Hemisphere Snow and Ice Analysis at 1 km, 4 km, and 24 km Resolutions, Version 1

The U.S. National Ice Center (USNIC) Interactive Multisensor Snow and Ice Mapping System (IMS) provides daily surface type maps of the Northern Hemisphere at various spatial resolutions. The surface type maps are produced using an operational software for snow and ice coverage monitoring known as IMS. The IMS software uses various data sources as input, such as in-situ and satellite imagery data (Table 10). The data inputs are preprocessed in the IMS GUI to reformat and reproject the data to match IMS projections and format (the spatial resolution and north stereographic projection). The reformatted data are then visually assessed by Office of Satellite Products and Operations analysts to determine and label the surface types within the image. Finally, the output is produced as daily surface type maps of the Northern Hemisphere and the variables within the output are as seen in Table 11 (U.S. National Ice Center, 2008).

Table 10: Data sources of IMS (UNIC, 2008)

Sensor or Source	Platform or Organization	Data Version*
Arctic Cap Nowcast/Forecast System (ACNFS) sea ice area fraction and sea ice thickness	U.S. National Ice Center (USNIC)	1.3
Advanced Microwave Scanning Radiometer – Earth Observing System (AMSR-2)	Global Change Observation Mission for Water (GCOM-W)	1.3
Advanced Microwave Sounding Unit (AMSU)	National Oceanic and Atmospheric Administration (NOAA) Polar Operational Environmental Satellites (POES) (15 - 18), Aqua, European Organisation for the Exploitation of Meteorological Satellites (EUMETSAT) MetOp-A	1.1, 1.2, 1.3
Advanced Scatterometer (ASCAT)	European Organisation for the Exploitation of Meteorological Satellites (EUMETSAT) MetOp-A	1.2, 1.3
ATMS (MIRS based)	Suomi National Polar-orbiting Partnership (S-NPP)	1.3
Automated snow detection layers	National Environmental Satellite, Data, and Information Service (NESDIS) and National Centers for Environmental Prediction (NCEP)	1.1, 1.2, 1.3
Advanced Very High Resolution Radiometer (AVHRR)	NOAA POES Satellites (14 - 19), European Organisation for the Exploitation of Meteorological Satellites (EUMETSAT) MetOp-A	1.1, 1.2, 1.3
Canadian snow analysis	Environment Canada	1.3
Global Forecast System (GFS) daily snow depth	National Centers for Environmental Prediction (NCEP)	1.3
Geostationary Meteorological Satellite (GMS) Imager	Japan Meteorological Agency (JMA) Geostationary Meteorological Satellite - 5 (GMS-5) (Himawari 5)	1.1, 1.2
Geostationary Operational Environmental Satellite (GOES) Imager	National Oceanic and Atmospheric Administration (NOAA) Global Operational Environmental Satellites (GOES) (9, 10, 11, 13)	1.1, 1.2, 1.3
Hourly surface weather reports	Aviation Routine Weather Report (METAR)	1.3
Moderate Resolution Imaging Spectroradiometer (MODIS)	Aqua and Terra	1.2, 1.3
Multi-function Transport Satellite-1R (MTSAT-1R) Imager	JMA MTSAT-1R (Himawari 6)	1.2
Multi-function Transport Satellite-2 (MTSAT-2) Imager	JMA MTSAT-2 (Himawari 7)	1.3
Meteosat Visible Infra-Red Imager (MVIRI)	Meteosat First Generation (MFG)	1.1, 1.2
Radar	Various radar published from Europe, Japan, China, South Korea, Canada, or U.S.	1.3

Synthetic Aperture Radar (SAR)	Radarsat-2	1.3
Synthetic Aperture Radar (SAR) (C-band)	Sentinel-1A	1.3
Spinning Enhanced Visible and Infrared Imager (SEVIRI)	MSG	1.3
Snow Data Assimilation System (SNODAS)	NOHRSC	1.1, 1.2, 1.3
Special Sensor Microwave Imager (SSM/I)	DMSP Satellites	1.1, 1.2, 1.3
Special Sensor Microwave Imager/Sounder (SSMIS)	DMSP Satellites	1.2, 1.3
U.S. Air Force Snow and Ice Analysis Product	USAF	1.1, 1.2, 1.3
Various weather reports, ice charts, and snow depth reports	In situ data from U.S. and other foreign countries	1.3
Visible Infrared Imaging Radiometer (VIIRS) (visible channels 1,2,3, IR channel 15, day/night bands)	S-NPP Satellites	1.3
Visible Infrared Imaging Radiometer (VIIRS) Binary Snow Cover EDR	NASA Goddard	1.3
Visible Infrared Imaging Radiometer (VIIRS) Sea Ice Characterization EDR	NASA Goddard	1.3
Weekly sea ice analysis and ice edge	USNIC	1.1, 1.2, 1.3
*** may not apply exclusively to the specified version(s)**		

Table 11: Variables of IMS surface type maps (UNIC, 2008)

Variable	Description
IMS_Surface_Values	The surface types in the IMS product. There are open water, land, sea/lake ice, and snow cover with the following values: 0: Outside Coverage Area, 1: Open Water, 2: Land Without Snow, 3: Sea Ice or Lake Ice, 4: Snow Covered Land
projection	Projection description for the data
time	Time stamp for the data in seconds since 1970-01-01T00:00:00Z. This is the 00Z reference time. Note that products are nowcasted (WMO, 2017) to be valid specifically at the time given here.
x	X coordinate of grid cell. Values, in m, are the centers of the grid cells
y	Y coordinate of grid cell. Values, in m, are the centers of the grid cells

3.2.2 Canadian Ice Service Lake Ice Product

The Canadian Ice Service (CIS) lake ice product provides weekly lake-wide ice fraction for approximately 140 lakes within Northern U.S.A and Canada. The lake ice fraction estimates are obtained from visual interpretation of imagery from optical and SAR imagery. Consequently, due to the nature of data processing (visual interpretation), once per week, the occurrence date of lake ice varies ±7 days (Howell et al., 2009). This lake ice fraction product covers 3 of the project's studied lakes: Great Bear Lake (GBL), Great Slave Lake (GSL), Lake Athabasca and Lake Winnipeg.

3.2.3 National Oceanic and Atmospheric Administration Lake Ice Product

The National Oceanic and Atmospheric Administration (NOAA) Coast Watch Program provides daily lake ice fraction of the Laurentian Great Lakes through combining the ice charts of the CIS and U.S. National Ice Center (USNIC). The ice charts are produced through analysis of satellite imagery (SAR, visible and optical) and meteorological data (Yang et al. 2020). The output represents the ice coverage at 1800 UTC (Simard et al., 2005). The NOAA Laurentian Great Lakes Environment Research Laboratory (GLERL) reprocesses the ice charts of CIS and USNIC to provide lake ice data as daily average lake ice fraction, annual maximum ice cover and gridded shape files of ice cover concentration (GLERL, 2023).

3.2.4 MODIS Land Surface Temperature and Emissivity

The Terra Moderate Resolution Spectroradiometer (MODIS) Land Surface and Emissivity product (MOD11C1) provides daily daytime and nighttime land surface temperature (LST) and emissivity values (~2 values per day) at a 0.05° resolution (~5 km) (see Table 12 for data variables). The surface emissivity and LST values are derived from reprojecting and averaging the MOD11B1 product after filtering cloud-contaminated pixels (as the presence of clouds interferes with LST and emissivity readings) (Institute for Computational Earth System Sciences, n.d.). Cloud filtering is done through a double-screen scheme; this scheme is based on the LST values of the day/night algorithm (5 km) and the generalized-split window (1 km). Details on the differences between the day/night algorithm and the generalized-split window can be found in Table 13 (Wan et al. 2002).

Table 12: Variables of interest within MOD11C1. (Institute for Computational Earth System Sciences, n.d.).

SDS Name	Description	Units	Data Type	Fill Value	Valid Range	Scale Factor	Offset
LST_Day_CMG	Day Land Surface Temperature	Kelvin	16-bit unsigned integer	0	7500 to 65535	0.02	N/A
QC_Day	Daytime LST Quality Indicators	Bit Field	8-bit unsigned integer	N/A	0 to 255	N/A	N/A
Day_view_time	Local time of day observation	Hours	8-bit unsigned integer	255	0 to 120	0.2	N/A
Day_view_angl	View zenith angle of day observation	Degree	8-bit unsigned integer	255	0 to 130	N/A	-65
LST_Night_CMG	Night Land Surface Temperature	Kelvin	16-bit unsigned integer	0	7500 to 65535	0.02	N/A
QC_Night	Nighttime LST Quality indicators	Bit Field	8-bit unsigned integer	N/A	0 to 255	N/A	N/A
Night_view_time	Local time of night observation	Hours	8-bit unsigned integer	255	0 to 120	0.2	N/A
Night_view_angl	View zenith angle of night observation	Degree	8-bit unsigned integer	255	0 to 130	N/A	-65

Table 13: MOD11C1 algorithms (information from Wan et al. 2002)

Day/Night Algorithm	Generalized Split Window
• LST retrieval specifically for day and night conditions • Uses TIR data, algorithm then uses different approaches/equations for day and night conditions (considering difference in solar radiation) • Explicitly accounts differences in atmospheric conditions between day and night and uses different empirical coefficients to do so • Dual retrieval	• LST retrieval through differences in TIR radiance between two adjacent bands (MODIS band 31 and 32) • Doesn't explicitly consider day and night differences but rather is optimized for specific conditions (ex. surface types) • Uses split window technique to account for atmospheric effects (uses one equation) • Uses empirical coefficients for atmospheric conditions to account for aerosols and atmospheric gases • Single retrieval approach

3.3 Datasets: Variables of Interest and Preprocessing Procedure

3.3.1 ERA5-Land

ERA5-Land is a reanalysis product developed by the ECMWF which describes the global terrestrial water and energy cycle hourly at a spatial resolution of 9 km. ERA5-Land provides a total of 50 variables, but the variables of interest are the lake variables (Table 14). Out of the seven lake variables available, two were selected for their evaluation: lake ice depth (referred to as lake ice thickness) and lake ice surface temperature (LIST). These variables were selected as based on two reasons. Firstly, are the only lake ice variables available and secondly, they were selected based on the availability of satellite-derived data. Moreover, LIST was selected because it is a crucial variable in determining lake ice formation in ERA5-Land. Also, evaluating biases/errors for this variable can provide insight into errors with lake ice thickness (Kheyrollah Pour et al., 2017). Lake ice thickness was used to derive lake ice fraction and timing, as these variables are not directly provided in ERA5-Land. The threshold values selected to determine whether a grid cell was ice-covered or open-water; these threshold values were 10 mm, 20 mm, and 50 mm. These values were selected based on the preliminary results for 1 mm, 5 mm, and 10 mm. The 10 mm yielded the best (closest to 0) mean bias error (MBE) when compared to CIS weekly ice fraction data, prompting the replacement of the 1 mm and 5 mm thresholds with higher values (20 mm and 50 mm). In terms of selecting a thickness threshold for satellite-derived ice detection, Balsamo et al. (2011) recommended a threshold of 20 cm for comparison with FLake output. However, the thresholds selected in this study are lower to capture the full projected ice season, allowing for a more comprehensive assessment of ice growth and melt, as this affects lake ice timing. It is important to note that several satellites used for the generation of the selected ice fraction/timing datasets (CIS, NOAA and IMS) demonstrate the ability to detect ice of a few mm thick, such as AVHRR, VIIRS, GOES, and SARs, further justifying the lower threshold values (Key et al., 2020; Dorofy, 2017; Weber et al., 2016; Murfitt et al., 2018).

Table 14: Lake variables provided in ERA5-Land with the selected variables highlighted in blue (Muñoz et al., 2019)

Variable	Unit	Short description
Lake bottom temperature	K	Water temperature at the bottom of lakes, reservoirs, rivers, and coastal waters. A lake model was added to the Integrated Forecasting System in May 2015 to simulate water temperature and ice cover for major inland water bodies. The model assumes constant depth and surface area.
Lake ice depth	m	Ice thickness on water bodies (inland water bodies like lakes, reservoirs, and rivers, and coastal waters) is represented in the ECMWF Integrated Forecasting System. The system models the formation and melting of a single ice layer on these water bodies. This parameter provides the thickness of the ice layer.
Lake ice temperature	K	Surface temperature of ice on inland water bodies (lakes, reservoirs, rivers) and coastal waters. The ECMWF Integrated Forecasting System models the formation and melting of a single ice layer on lakes, and this variable represents the temperature of the uppermost surface of that ice layer.
Lake mix-layer depth	m	represents the thickness of the uppermost layer of a well-mixed inland water body or coastal waters, where the temperature is almost constant with depth. The ECMWF Integrated Forecasting System divides inland water bodies into two layers: the mixed layer and the thermocline. The thermocline is located below the mixed layer and extends to the bottom of the lake or water body. Mixing in the mixed layer can occur due to differences in water density or wind action on the surface.
Lake mix-layer temperature	K	temperature of the uppermost well-mixed layer of inland water bodies (lakes, reservoirs, rivers) or coastal waters. The ECMWF Integrated Forecasting System represents these water bodies with two layers: the mixed layer above and the thermocline below. The thermocline's upper boundary is located at the bottom of the mixed layer, and the lower boundary is at the lake bottom. Mixing within the mixed layer can occur due to differences in water density or the action of wind on the lake surface.
Lake shape factor	N/A	describes the temperature gradient in the thermocline layer of inland water bodies (lakes, reservoirs, and rivers) and coastal waters. It is used to calculate the temperature at the bottom of the lake and other related parameters. In the ECMWF Integrated Forecasting System, the inland and coastal water bodies are represented with two layers in the vertical, the mixed layer above and the thermocline below, where the temperature changes with depth.
Lake total layer temperature	K	Mean temperature of the entire water column in inland water bodies (lakes, reservoirs, and rivers) and coastal waters. The ECMWF Integrated Forecasting System represents inland water bodies with two vertical layers: the mixed layer above and the thermocline below. The parameter is the mean temperature of the two layers.

Data from the ERA5-Land lake variables of interest were retrieved through an API request to the Climate Data Store, providing yearly NetCDF files per lake and for the years of interest (2004-2023). To improve processing efficiency, the data from NetCDF were extracted into CSV format using Python. The CSV output retained spatial and temporal information; the fields of the CSV files are latitude, longitude, date, time and the selected variables (lake ice thickness or surface

temperature). Since the API request defines an area of interest with a rectangular bounding box, the output CSVs include land pixels surrounding the lake. To eliminate the land pixels, spatial filtering was applied using a lake mask from HydroLAKES (Messager et al., 2016), producing new CSV files limiting the data to only the lake area. To allow for direct comparison with satellite observations, the hourly ERA5-Land data were averaged to daily values.

To characterize surface type for ERA5-Land, lake ice thickness was converted into the IMS surface values (Table 11) by applying three thresholds: 10 mm, 20 mm and 50 mm. This means that if the lake ice thickness is equal to or greater than the threshold, it is classified as lake ice (value 3), and cells with ice thickness less than the threshold are classified as open water (value 1). These surface values were also used to define lake ice fraction, where for each date and each of the three ice thickness thresholds, the count of cells classified as lake ice was divided by the total number of lake cells to provide lake ice fraction.

3.3.2 IMS Daily Ice Cover

IMS provides daily surface-type maps for the Northern Hemisphere at various spatial resolutions: 1 km, 4 km and 24 km. The 4 km product was selected as it is the grid spacing closest to ERA5-Land's 9 km product. The surface type classifications are described in Table 11, specifically focusing on surface values 1 (representing open water) and 3 (representing lake ice), which are of interest.

The data were downloaded through the file transfer protocol via Python. The data are formatted as daily GeoTIFFs, which were converted to CSV format for faster processing. The CSVs were spatially filtered to the lake area using HydroLAKES lake masks and further filtered to remove cells classified as land (cells with surface type values 2 and 4 as described in Table 11). There are several missing dates in the IMS dataset (the full list is included in Table A.1). Most notably, there is no data between January 1 and February 25, 2004.

3.3.3 CIS Weekly Ice Cover

CIS provides weekly lake-wide ice fraction values, which are obtained through visual interpretation of satellite imagery (e.g. AVHRR, MODIS, VIIRS, and RADARSAT/Sentinel-1). Ice fraction values are expressed in tenths, with 0 corresponding to no ice (open water) and 10 to full ice cover. This dataset provides ice cover fractions for ~140 of the largest lakes across Canada and

northern U.S. states, excluding the Laurentian Great Lakes which are monitored independently for the production of daily ice charts (see 3.2.4). Therefore, only four of the seven lakes of this study are included in the weekly CIS product: GBL, GSL, Lake Athabasca, and Lake Winnipeg. The larger lakes are divided into two sections, which are divided as follows: GSL is divided into northwest and southeast, GBL and Lake Winnipeg are both divided into north and south.

For the lake ice fraction of the lakes divided into two sections (GBL, GSL, and Lake Winnipeg), the average of the two sections was computed to represent the lake-wide ice fraction. The lake ice fractions were converted to percentages to match the NOAA dataset. Minor data filtering was performed, with only four dates removed due to concerns regarding consistency or quality. Consistency concerns refer to dates (2006-10-05 and 2007-12-15) that contained a duplicate value between the weekly values; these were removed due to redundancy and inconsistency. Quality concerns refer to dates (2006-06-14 and 2012-11-07) removed due to suspiciously sudden and large peaks in lake ice fraction, followed by rapid melt (refer to Table A.2).

3.3.4 NOAA Daily Ice Charts

The NOAA GLERL provides reprocessed ice charts of CIS and USNIC, offering lake ice data in the form of daily average lake ice fraction, annual maximum ice cover, and gridded shape files of ice cover concentration (per cell) (GLERL, 2023). Only the daily average lake ice fraction is used, as it is most compatible for ERA5-Land comparison, since the gridded data provides the ice cover concentration (lake ice fraction per cell), which cannot be obtained through ERA5-Land, as ERA5-Land only provides ice thickness per cell.

The raw data of NOAA is in CSV format, in which the headings are the years, and each row is a different date. The raw data was first filtered to the years of interest, following this, the CSV data were reformatted to separate the raw CSV with all the years to separate CSVs for each year, allowing for empty values for each year to be easily removed and for easier merging with ERA5-Land CSVs.

3.3.5 MOD11C1

MOD11C1 uses thermal infrared bands to generate a LST and emissivity product, derived from reprojecting and averaging the MOD11B1 product. Providing approximately two observations daily: nighttime and daytime observation on a 5 km grid. Only LST values were used as emissivity is not of concern for this project. To address the limited assessments of winter lake surface temperatures

of ERA5-Land, our assessment focuses on the ice-on period (the period between FUE and BUS, determined based on the dates derived from CIS/NOAA and ERA5-Land)

The data were obtained through the Level-1 and Atmosphere Archive and Distribution System Distributed Active Archive Center (LAADS DAAC), providing the data in GeoTIFF format, in which each variable (Table 12) has a separate GeoTIFF per date. Data from the GeoTIFFs were extracted into CSV format to improve processing time and to allow for easier merging (merging dates into CSVs to produce yearly CSVs and merging with ERA5-Land CSVs). Data within the CSVs were then converted from unsigned integers to floating point values through Python using the fill values, scale factors and offset as described in Table 12. The CSVs were then filtered to the lake area by applying the lake masks, and then the quality assurance flags were used to exclude LST values that were obscured by clouds. Furthermore, pixels with an average LST error of ≥ 3 K were removed (Table 15) and missing dates pre-filtering can be found in Table A.3.

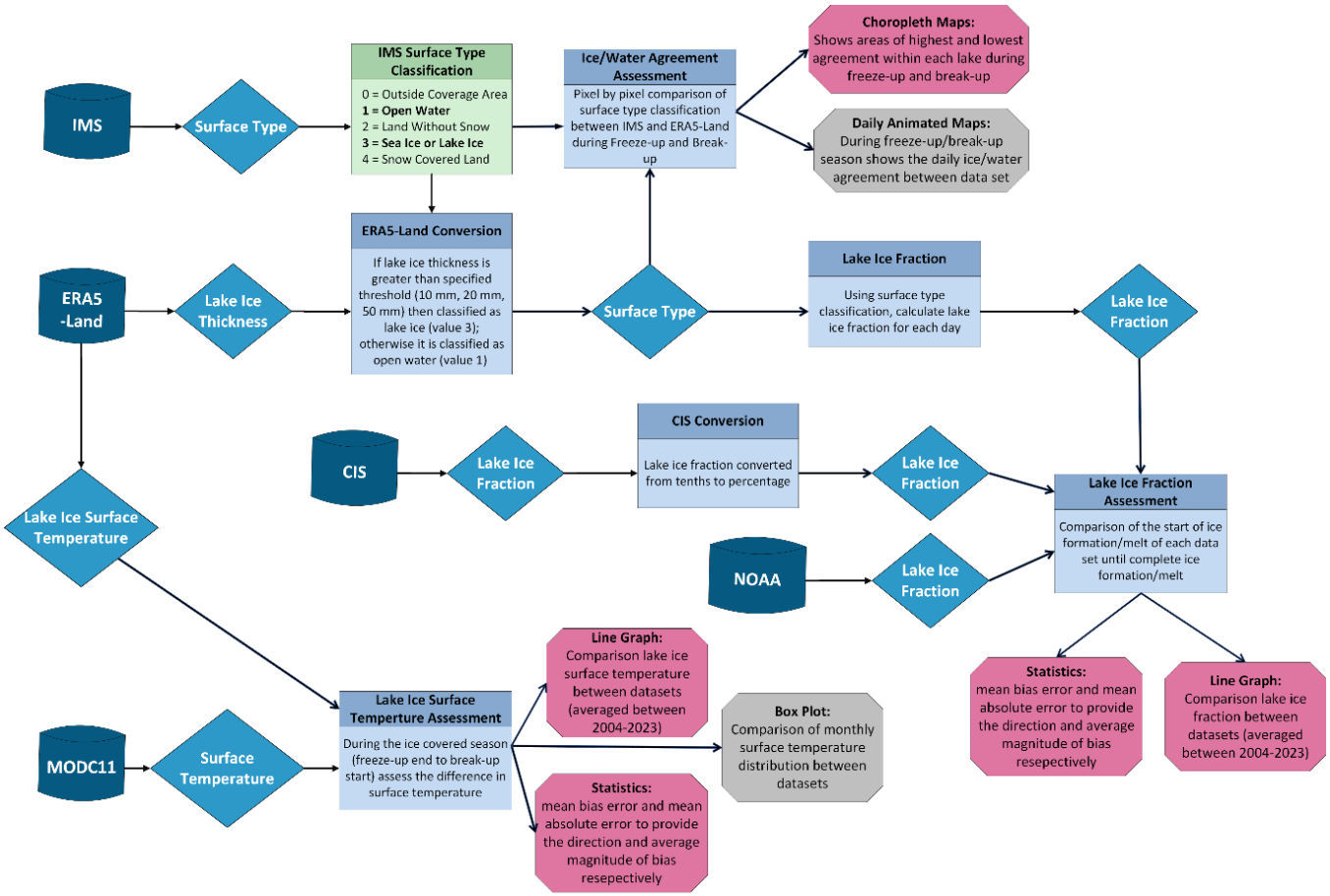
Table 15: MOD11C1 quality assurance (Institute for Computational Earth System Sciences, n.d.).

Note: cells in blue represent the QA that were considered in filtering, strikethrough text represents the QA codes that were filtered out

Bits	Long Name	Key
1 and 0	Mandatory QA flags	00=LST produced good quality not necessary to examine more detailed QA 01=LST produced other quality recommend examination of more detailed QA ~~10=LST not produced due to cloud effects~~ ~~11=LST not produced primarily due to reasons other than cloud~~
3 and 2	Data quality flag	00=good data quality 01=other data quality pixel ~~10=LST affected by nearby clouds and/or sub-grid clouds and/or ocean~~ ~~11=LST screened off~~
5 and 4	Emis Error flag	00=average emissivity error <= 0.01// 01=average emissivity error <= 0.02// 10=average emissivity error <= 0.04// 11=average emissivity error > 0.04
7 and 6	LST Error flag	00=average LST error <= 1K 01=average LST error <= 2K ~~10=average LST error <= 3K~~ ~~11=average LST error > 3K~~

3.4 Assessments

The goal of this thesis is to assess ERA5-Land's proficiency at estimating lake ice related variables, with a focus on lake ice timing, fraction and surface temperature. Thus, this section describes how this goal is accomplished through comparative assessment with satellite products (IMS, NOAA, CIS and MOD11C1) (as shown in Figure 4). Specifically, assessing lake ice timing and fraction through a surface type assessment (ice and open water) between ERA5-Land and IMS, as well as through a lake ice fraction assessment between ERA5-Land and CIS/NOAA. Also, assessing LIST by comparing ERA5-Land values to MOD11C1. To describe the process and results of each assessment, this section will proceed as follows: Section 3.4.1 describes the lake ice fraction and timing assessment, which is broken down into two subsections: lake ice fraction assessment (Section 3.4.1.1) and ice and water agreement assessment (Section 3.4.1.2). Then, Section 3.4.2 describes the LIST assessment.



Note: dark blue cylinders = datasets, blue diamonds = variables, blue and green boxes = process description, pink boxes = results within thesis body and grey boxes = supplementary results

Figure 4: Overall flowchart of the methodology

3.4.1 Lake Ice Fraction and Timing

3.4.1.1 Lake Ice Fraction Assessment (NOAA/CIS and ERA5-Land)

To evaluate ERA5-Land's proficiency at estimating lake ice, timing, and fraction, these have been assessed as they vary with different ice regimes. Such as some lakes form full ice coverage while some form partial ice coverage, and the timing of ice will differ due to differences in the environment. Thus, the difference in fraction, timing and rate of ice growth and melt between ERA5-Land and either NOAA or CIS was evaluated (as these datasets cover different study areas as described in Sections 3.3.4 and 3.3.3, respectively). This evaluation was visualized through line graphs to capture the change in ice fraction over time between ERA5-Land and CIS or NOAA.

To account for the differences between break-up (BU) and freeze-up (FU), these seasons are graphed separately. As their processes, specifically their timing and influencing factors, differ as described in Sections 2.2.4 and 2.2.2 respectively. Thus, this separation assesses how well ERA5-Land captures the difference in processes and controls. The seasonal line graphs also demonstrate how each ERA5-Land thickness threshold performs relative to CIS/NOAA. The consideration of multiple thresholds provides a comprehensive evaluation of the rate of growth/decay and compensates for the different nature of the datasets, as CIS/NOAA are derived from visual assessment of satellite imagery, while ERA5-Land is computationally derived.

The ice seasons (BU and FU) follow slightly different definitions between CIS and NOAA, as they cover different lakes, thus covering different ice regimes. As such, CIS covers GBL, GSL, Lake Winnipeg and Lake Athabasca, which all experience 100% ice fraction annually; in turn, the definitions for FU and BU are relatively simple. BU is defined as starting from consistent decrease in ice from 100% fraction (BUS) and when 0% fraction is reached (BUE). On the other hand, FU is defined similarly, starting from the date of consistent increase in ice fraction from 0% (FUS) and ends the date when 100% ice coverage is reached (FUE). A buffer of three weeks before the start date and three weeks after the end date is used to fully capture ice growth and melt of ERA5-Land.

NOAA covers the Laurentian Great Lakes (Lake Superior, Lake Huron and Lake Erie), which experience varying amounts of partial ice coverage. Therefore, BU and FU are defined around the maximum ice fraction rather than 100% fraction. So, BU is defined as starting the date of decrease from maximum ice fraction (BUS) and ends when 0% fraction is reached (BUE). While FU is defined the date when ice growth occurs from 0% fraction (FUS) and ends the date maximum ice fraction occurs (FUE). A buffer of three days before the start date and three days after the end date was

applied to fully capture the ice season. But there are some exceptions to NOAA's ice season definitions, as there are instances where NOAA does not record multiple or any dates of 0% ice fraction prior to ice growth. Also, since ERA5-Land's ice season sometimes occurs earlier or later than NOAA, then more than 3 days may be used if available. The dates selected to defined FU and BU from the CIS and NOAA definitions can be found in Appendix B.

To quantify bias and errors in lake ice timing and fraction, several measures were utilized. Firstly, the degree of overestimation/underestimation is calculated using the mean bias error (MBE). Secondly, the mean absolute error (MAE) is calculated to provide the average magnitude of error. So, for each season, MBE and MAE is calculated where ERA5-Land is treated as the "predicted" fraction and CIS or NOAA as the "reference" fraction (Equation 4 and Equation 5). Thirdly, to evaluate errors in timing, the difference between ERA5-Land start and end of BU and FU will be compared to CIS/NOAA. This will be done through evaluating the full range of the difference between the dates and the average difference between dates.

Equation 4: Mean Bias Error

$$MBE = \frac{1}{n}\sum_{i=1}^{n}(P_i - O_i)$$

n = number of observations

P_i = predicted value

O_i = observed value

Equation 5: Mean absolute error

$$MAE = \frac{1}{n}\sum_{i=1}^{n}|P_i - O_i|$$

n = number of observations

P_i = predicted value

O_i = observed value

3.4.1.2 Ice and Water Agreement Assessment (ERA5-Land and IMS)

To assess ERA5-Land's ability to capture the spatial patterns of ice formation and melt, IMS is used to identify highest and lowest regions of ice and water agreement. Similar to the ice fraction assessment, this surface type assessment evaluates lake ice fraction and timing, but unlike the fraction assessment, it allows pixel-by-pixel assessment rather than being limited to lake-wide evaluation.

Modifications and filtering were required to ensure datasets are comparable spatially and contextually. The modification made was to derive ice/water surface types from ERA5-Land's lake ice thickness to conform to the IMS surface scheme (shown in Table 11 and further described in Section 3.3.1). Following the derivation of ice/water surface types from ERA5-Land, the datasets were merged while accounting for differences in spatial resolution. For this merge, cells of the same date between datasets are grouped together, then points between the datasets are paired together based on proximity; if the closest cell between them is greater than 4 km (spatial resolution of IMS), then those points are excluded. The paired points (ERA5-Land and IMS points) of the merged data typically had a distance difference of 2 km or less. Once ERA5-Land and IMS data have been merged and filtered, to pinpoint how the datasets disagree, a nominal variable was created called "comparison code" (Table 16).

The results of the ice and water agreement assessment are visualized through two different maps: choropleth and animated maps. The choropleth map shows broad regional patterns of agreement and disagreement over the 20-year period, expressed as percentages. The regions are user-defined by first dividing along the shoreline using a 9 km buffer (the resolution of ERA5-Land), then divide the center of the lake based on bathymetry data, if available. The daily animated map provides pixel-specific timing differences per year, allowing for yearly variation to be captured (animated

maps can be found here). Overall, both maps provide insight into ERA5-Land's ability to accurately capture spatial patterns of ice formation and melt which encapsulates both lake ice timing and fraction.

Table 16: Agreement of IMS and ERA5-Land via Comparison Codes

Note: Comparison codes 0 and 3 flags surface type agreement, whereas codes 1 and 2 identifies whether ERA5-Land predicted ice formation or melting too early or too late, relative to IMS surface values and ice season (BU or FU).

IMS Surface Value	ERA5-Land Surface Value	Comparison Code	Explanation
3	3	0	Ice agreement
3	1	1	During FU = ERA5-Land produce early melt; During BU = ERA5-Land produce delay ice
1	3	2	During FU = ERA5-Land produce early ice; During BU = ERA5-Land produce early melt
1	1	3	Water agreement

3.4.2 Lake ice surface temperature assessment

Lake ice formation within ERA5-Land is primarily based on surface temperature (as detailed in Section 2.3.1); therefore, this assessment of lake ice surface temperature (LIST) is conducted to potentially explain the observed biases and errors in the lake ice fraction and timing assessments. Thus, the biases observed in LIST are treated as a potential influence of biases previously observed. Due to ERA5-Land's assumption of freezing point temperature (273.15K) even when ice is not present LIST comparison is limited to the ice-covered period (FUE to BUS) to filter out ERA5-Land's assumption.

To perform the LIST assessment, ERA5-Land and MOD11C1 observations were merged to match each ERA5-Land pixel to the MOD11C1 pixel based on closest distance and with consideration of date and time as well. The spatial merge only paired points together within 5 km (the spatial resolution of MOD11C1) of each other. Simultaneously, the temporal merge would round the observation time of MOD11C1 to the nearest hour, to then merge that observation with the ERA5-

Land observation of that hour. Using the merged data, the filtered and merged data were then computed using Python to produce the line graphs and compute the statistics as described below.

The results of the LIST assessment are presented as daily line graphs within the body of the thesis, and boxplots are provided as supplemental figures within Appendix C. The daily line graphs used the lake-wide average temperature (averaged over 2004-2023) and graphed it over the same freeze-up period as used in the lake ice fraction assessment (refer to Appendix B). Whereas the boxplots found in Appendix C provide more precise information, which captures the yearly distributions, variation and biases. Additionally, within both graphs, biases will be quantified through MBE (Equation 4) and MAE (Equation 5), specifically treated ERA5-Land as the "predicted" value and MOD11C1 as the "observed" value. The combination of these statistics provides a comprehensive picture of the accuracy of ERA5-Land's predicted LIST, as MBE describes the direction of the average bias (overestimation or underestimation) while MAE describes the magnitude of the average bias.

Chapter 4
Results and Discussion

4.1 Introduction

ERA5-Land is a widely used reanalysis product; however, comprehensive evaluations of its lake ice parameters remain scarce. Such assessments are crucial as lake ice strongly influences the local energy balance and, in turn, influences the regional climate and weather. Since ERA5-Land parameterizes these interactions, quantifying biases in lake ice estimates helps reveal broader model biases in energy fluxes, temperature, and albedo.

To address the scarcity of evaluations of ERA5-Land's lake ice parameters, this study quantifies bias in three lake ice variables: fraction, timing, and surface temperature. These variables were selected based on the availability of satellite-derived datasets for validation and their critical role in moderating climate and weather (see Section 2.2). To produce a spatial and temporally extensive assessment, the lake ice biases were examined across seven Canadian lakes from 2004 to 2023. The selection of these lakes provides a latitudinal gradient that allows evaluation of ERA5-Land's ability to accurately represent various lake ice regimes and climatic conditions.

To quantify biases in ERA5-Land lake ice parameters, three assessments are conducted corresponding to each of the selected variables: fraction, timing, and temperature. Each variable is defined as follows. Firstly, lake ice fraction is the total area of the lake that is ice-covered, represented by a percentage. Secondly, lake ice timing refers to the date of the start and end of ice formation and melt; also referred to as freeze-up (FU) and break-up (BU), respectively. Lastly, lake ice temperature is the surface temperature of the ice represented in Kelvin.

To quantify bias in the three selected lake ice variables, four satellite-derived products were used to evaluate ERA5-Land estimates (Table 17). Each product was used for one of the three assessments: fraction, timing and surface temperature, except for CIS and NOAA, which were used for both fraction and timing assessments. It is important to note that while CIS and NOAA are used for the same assessments, they have different characteristics. The most notable difference is that CIS covers the northern lakes (GBL, GSL, Athabasca, Winnipeg) while NOAA covers the Laurentian Great Lakes (Superior, Huron, Erie). Overall, these satellite products and variable definitions provide the foundation for evaluating the performance of ERA5-Land.

Table 17: Characteristics of selected satellite products and their associated assessment

Satellite product	ERA5-Land Assessment(s)	Lakes covered	Temporal resolution	Purpose / Notes
CIS (Canadian Ice Service)	Fraction, Timing	GBL, GSL, Athabasca, Winnipeg	Approximately weekly	Observed data for northern lakes
NOAA (National Oceanic and Atmospheric Administration)	Fraction, Timing	Superior, Huron, Erie	Daily	Higher temporal resolution than CIS; data is a combination of CIS and UNIC data
IMS (Interactive Multisensor Snow and Ice Mapping System)	Timing	All lakes	Daily	Validates CIS/NOAA; enables spatial bias assessment.
MOD11C1 (MODIS Land Surface Temperature)	Temperature	All lakes (ice period only, FUE to BUS)	Twice daily (daytime and nighttime observations)	Evaluates ERA5-Land ice temperature; identifies potential sources of bias.

The results are organized into three sections: *Freeze-up Differences*, *Break-up Differences*, and *Lake Ice Temperature Differences.* This structure is designed to build on the observed biases, enabling each section to conclude with a targeted discussion identifying potential explanations for biases. Both *Freeze-up Differences* and *Break-up Differences* follow the same order of analyses: First, evaluating lake ice fraction differences, then assessing differences in lake ice timing, and finally examining spatial patterns of agreement and disagreement. The progression of the *Freeze-up Differences* and *Break-up Differences* sections builds from general patterns to detailed spatial insights. The final section, *Lake Ice Temperature Differences*, serves to provide potential explanations for the biases observed in previous analyses (lake ice fraction and timing).

4.2 Freeze-up Differences

Freeze-up refers to the formation of lake ice, which is dominantly controlled by air temperature, lake morphology, latitude and elevation (expanded on in Section 2.2.2). Within this study, FU is defined as the period between the first appearance of ice (FUS) and the formation of the maximum ice cover (FUE) (for specific definitions see Section 3.4.1).

4.2.1 Lake Ice Fraction

Across all lakes, ERA5-Land consistently overestimates lake ice fraction for each threshold (Figure 5), as indicated by the positive MBE (Table 18). However, the magnitude of overestimation

in ERA5-Land varies across lakes, notably exhibiting greater overestimation among the Laurentian Great Lakes compared to the northern lakes. Specifically, Lake Superior and Lake Huron depict the highest overestimation (50 mm MAE = 47% and 24% respectively). For these lakes, ERA5-Land substantially overestimates the peak ice fraction, showing near-complete ice cover, whereas NOAA observations indicate only a moderate ice fraction (Figure 5). Lake Superior exhibits the largest difference in peak ice fraction and, correspondingly, the highest overestimation. Conversely, Lake Erie shows the lowest overestimation out of the Laurentian Great Lakes (50 mm MAE = 13%).

The trend of overestimation is also evident in the northern lakes, although the average magnitude is lower than that observed in the Laurentian Great Lakes. Across all lakes, Lake Winnipeg shows the lowest overestimation (50 mm MAE = 7%). While Lake Superior exhibits the greatest overall overestimation, within the northern lakes, Lake Athabasca shows the highest overestimation (50 mm MAE = 13%). Overall, ERA5-Land consistently overestimates lake ice fraction, with the Laurentian Great Lakes showing higher biases than the northern lakes.

However, lake ice timing also contributes to this overestimation, as discussed in the next section. Since the 50 mm threshold performed best across all lakes, it was applied in the subsequent analyses (timing and spatial agreement).

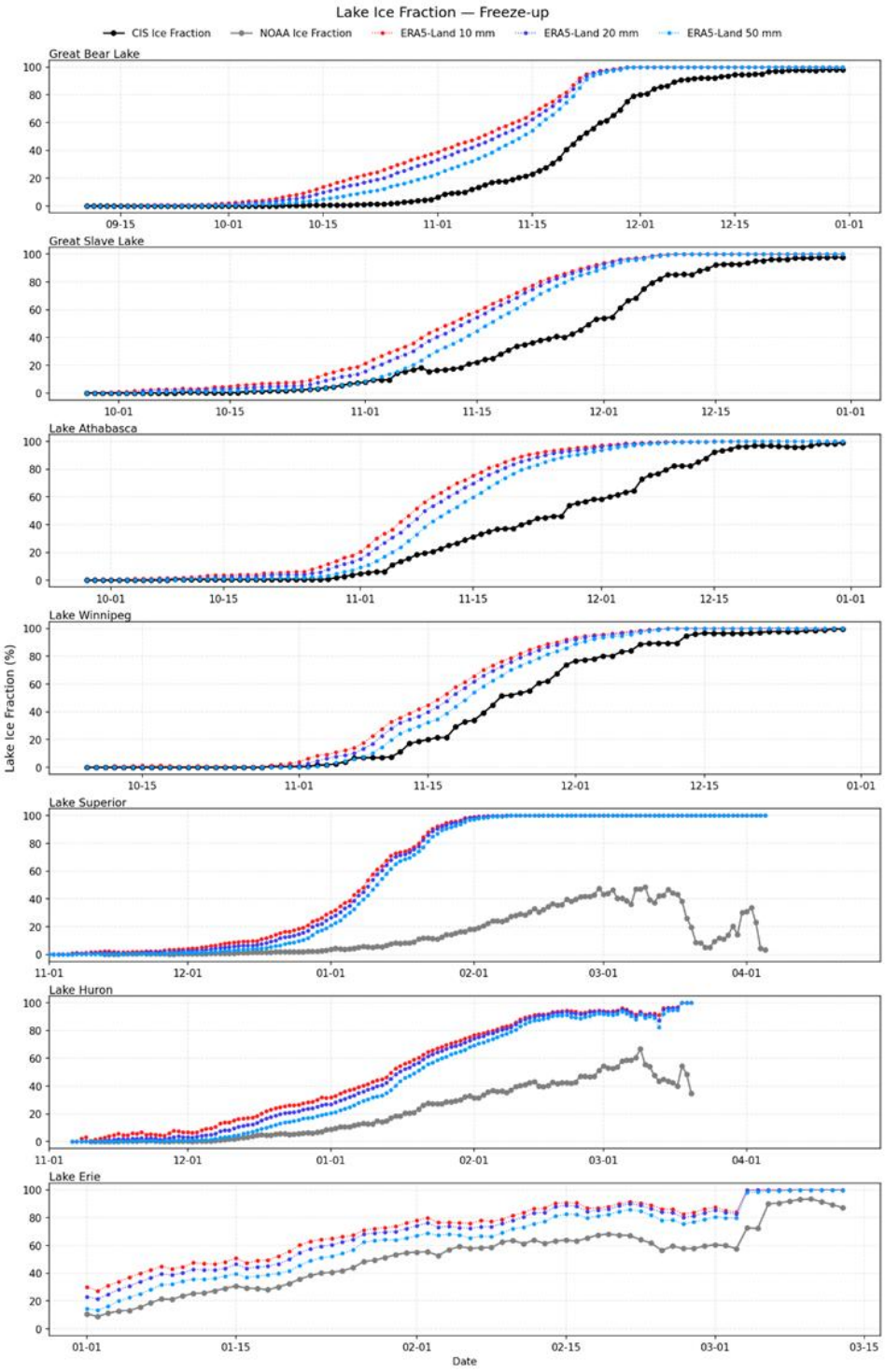


Figure 5: Average (2004-2023) ice fraction (%) for all lakes of this study during freeze-up

Table 18: Direction and magnitude of bias in lake ice fraction (%) during freeze-up per lake

Note: Values blue–red scale (red = highest value, blue = lowest value; intensity reflects magnitude)

Lake	10 mm MBE	10 mm MAE	20 mm MBE	20 mm MAE	50 mm MBE	50 mm MAE
Great Bear Lake	14	14	12	12	10	10
Great Slave Lake	15	15	14	14	10	11
Lake Athabasca	18	18	16	16	13	13
Lake Winnipeg	10	11	9	9	6	7
Lake Superior	52	52	50	50	47	47
Lake Huron	32	32	28	29	24	24
Lake Erie	23	23	18	19	11	13

4.2.2 Lake Ice Timing

Differences in FUS and FUE across both CIS/NOAA and IMS comparisons demonstrate a consistent pattern, where ERA5-Land estimates early FUS and FUE dates than those observed (Table 19). While both FUS and FUE exhibit similar patterns, there are notable outliers and differences to note.

Agreement for FUS is relatively high, with satellite-derived products differing by an average of 4 days. Both FUS comparisons also indicate GBL has the largest difference, followed by Athabasca and Winnipeg/GSL. However, outliers exist; NOAA observations of Lake Huron and Lake Erie show slightly later timing in ERA5-Land, while IMS comparison typically observes ERA5-Land earlier timing.

Unlike FUS, FUE differences only show moderate agreement, with ERA5-Land and satellite observations on average differing by 13 days. However, both satellite-derived datasets indicate that Lake Superior has the earliest FUE. Overall, both comparisons show that ERA5-Land typically

produces early FUS and FUE, with GBL showing the most significant difference in FUS, and Lake Superior depicts the greatest difference in FUE.

Table 19: Difference in freeze-up dates of ERA5-Land to satellite-derived products

Note: Lakes highlighted pink uses CIS data while lakes highlighted blue uses NOAA data

	ERA5-Land (50 mm) timing – dataset timing			
Lake	**CIS/NOAA FUS Difference***	**IMS FUS Difference**	**CIS/NOAA FUE Difference***	**IMS FUE Difference**
Great Bear Lake	-22	-22	-27	-7
Great Slave Lake	-6	-10	-24	-3
Lake Athabasca	-12	-12	-15	-1
Lake Winnipeg	-6	-8	-20	-6
Lake Superior	-9	-11	-32	-27
Lake Huron	1	-9	-17	-8
Lake Erie	2	-4	-4	5

Areas of the Lakes with Highest and Lowest Agreement

All lakes, except Huron and Superior, reveal that the lowest agreement typically occurs along the shores, notably the northern and eastern shores, which correspond to areas that experience FU first. In contrast, areas of highest agreement tend to occur within the lake center, which corresponds to areas that experience FU last (Figure 6 and Figure 7). Conversely, Superior and Huron show the opposite pattern, with the highest agreement along their shores. Meanwhile, the areas of lowest agreement are within the lake center, specifically the northern area where lake ice rarely reaches (Figure 8).

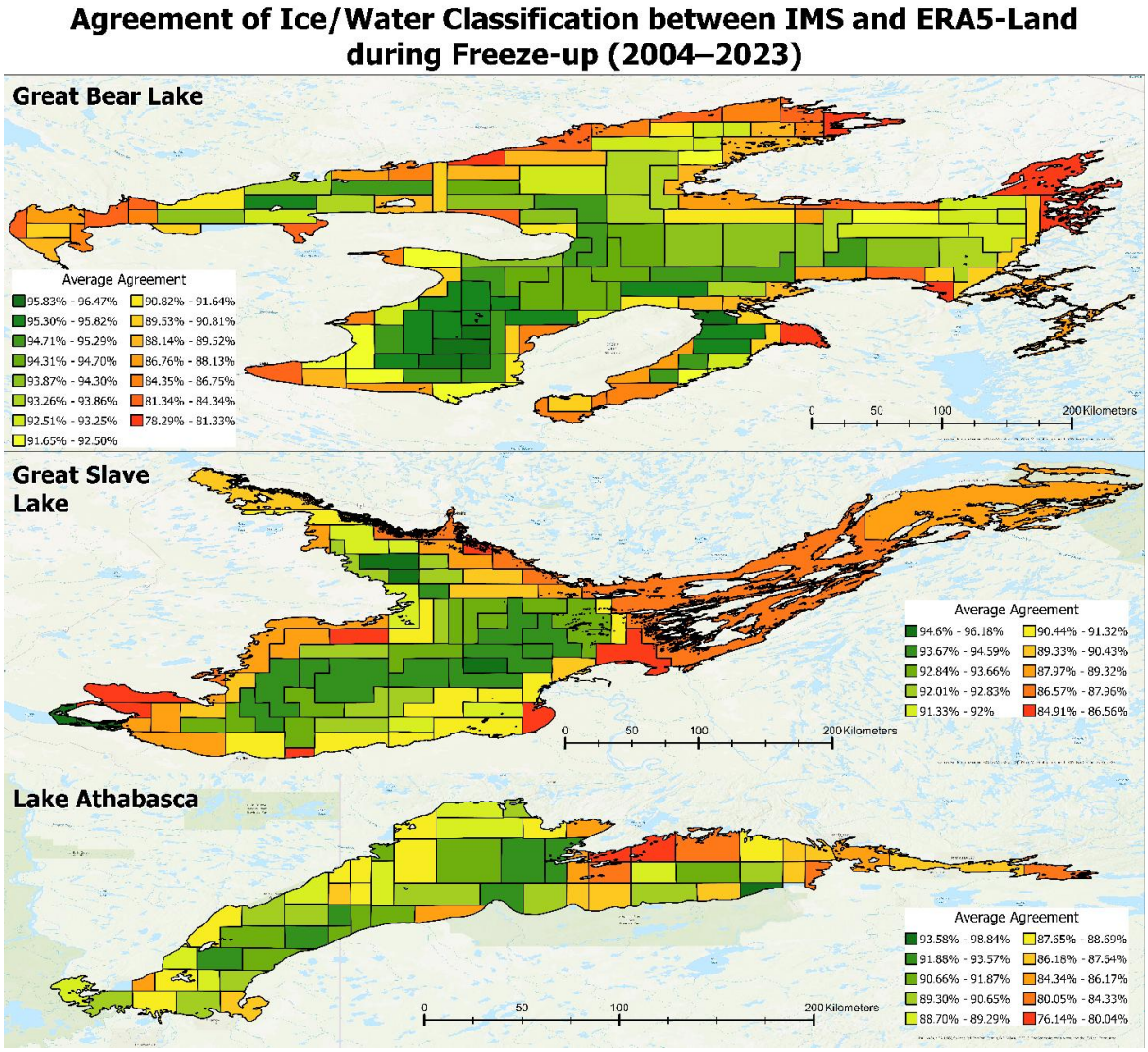


Figure 6: Average (2004-2023) ice to water transition agreement (%) during freeze-up between ERA5-Land and IMS for Great Bear Lake, Great Slave Lake and Lake Athabasca

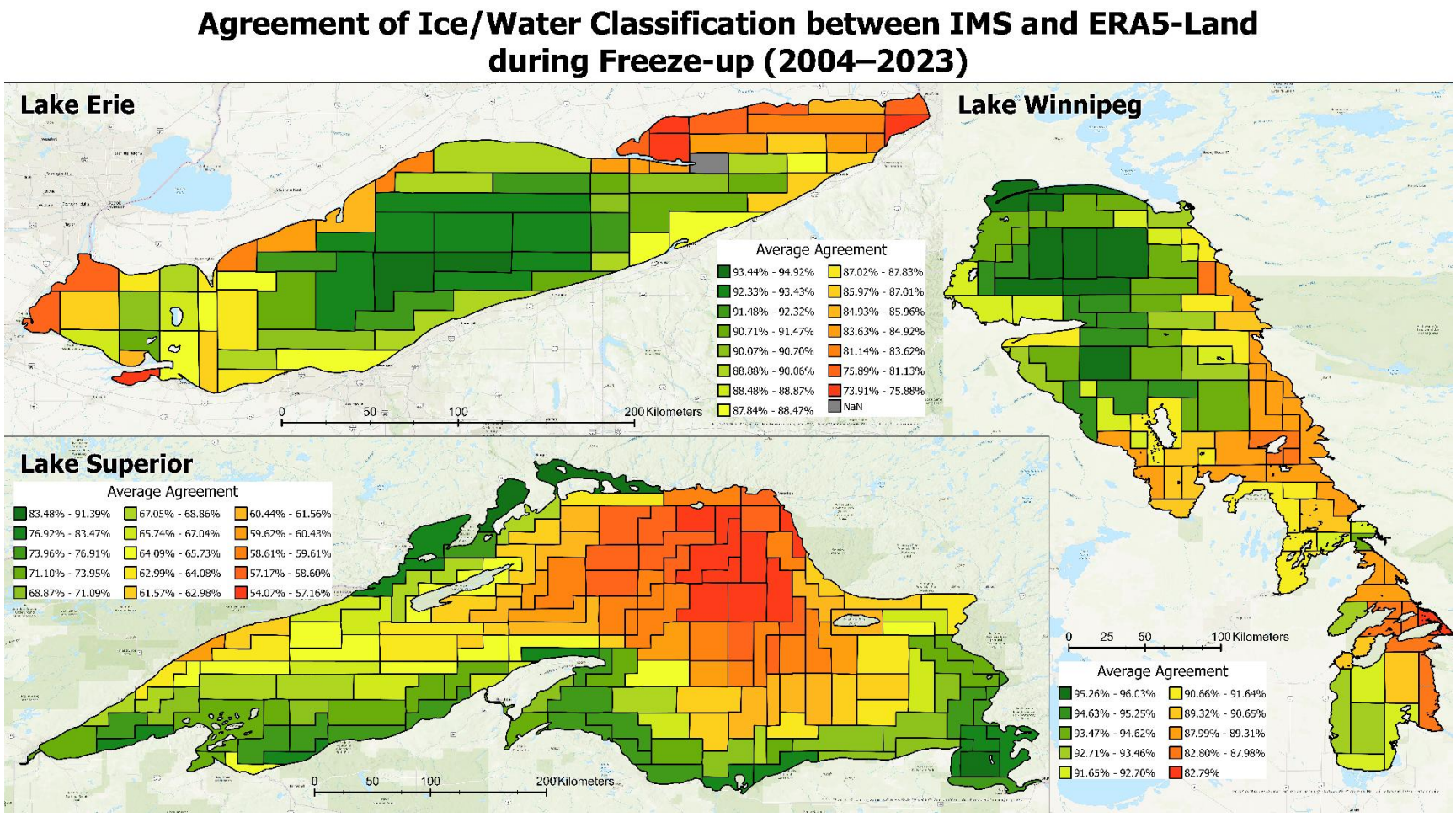


Figure 7: Average (2004-2023) ice to water transition agreement (%) during freeze-up between ERA5-Land and IMS for Lake Erie, Lake Superior and Lake Winnipeg

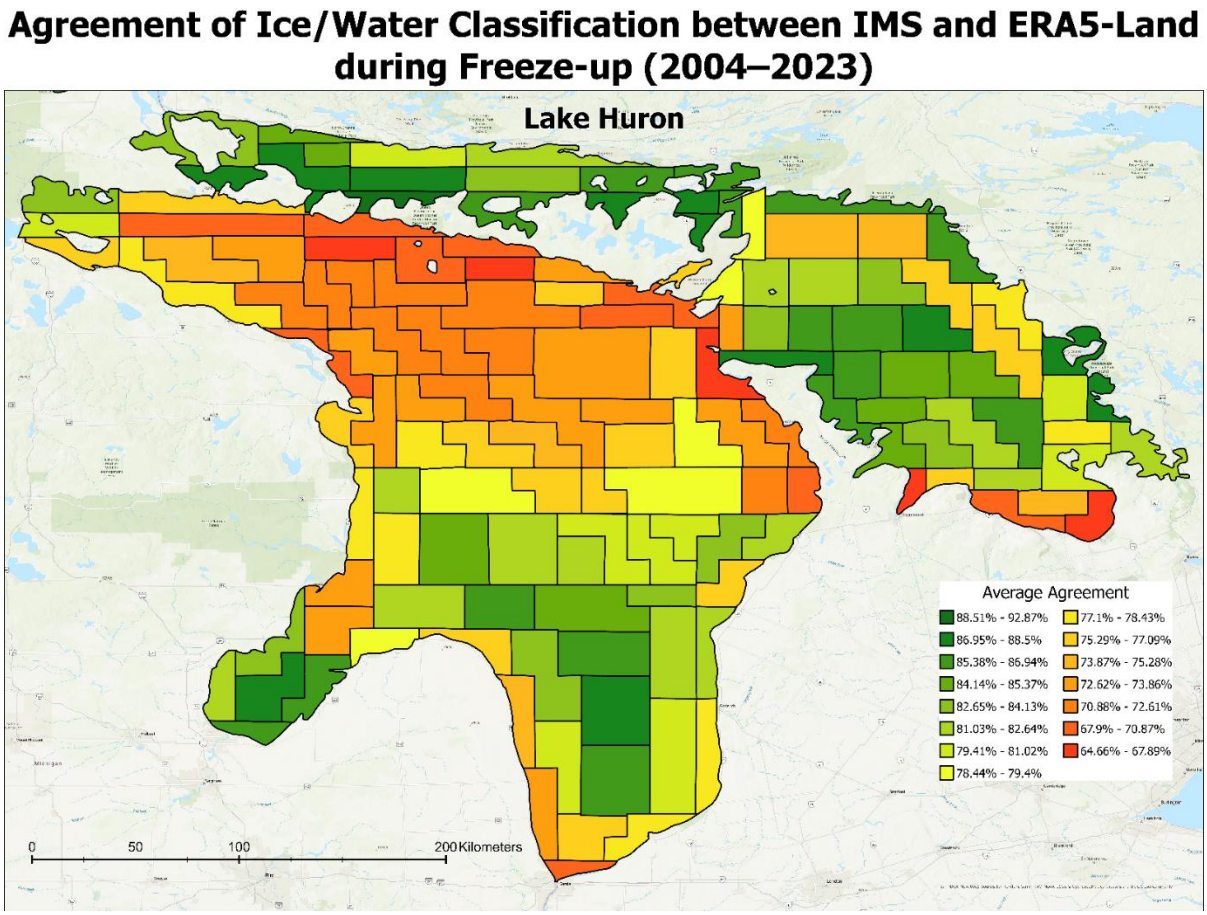


Figure 8: Average (2004-2023) ice to water transition agreement (%) during freeze-up between ERA5-Land and IMS for Lake Huron

4.2.3 Discussion

4.2.3.1 Lake Ice Fraction

ERA5-Land consistently overestimates lake ice fraction during FU, with the Laurentian Great Lakes showing larger bias compared to the northern lakes. The higher bias found in deep lakes corresponds to ERA5-Land's unrealistically rapid ice formation and high ice cover. The lower bias in ERA5-Land for shallow lakes corresponds to these lakes typically experiencing faster ice formation and full ice coverage. These results suggest that depth significantly affects the overestimation bias in ERA5-Land ice cover.

The most notable contributor to the larger overestimation of ice fraction in the Laurentian Great Lakes is due to FLake's ability in its simulation of ice cover on large, deep lakes at mid latitudes. Indeed, this is attributed to FLake's use of a false bottom (~40-60 m depth), causing FLake to typically simulate full or near full ice coverage (Martynov et al., 2012; Mironov et al., 2010) (see Section 2.3.2 for more details). Thus, lakes that experience partial ice coverage, notably Lake Superior and Lake Huron, produce a larger overestimation bias in ERA5-Land. Conversely, shallow lakes such as Lake Erie and Lake Winnipeg reveal lower overestimation, which aligns with FLake's optimal configuration for medium depth lakes (<50 m depth).

Although lake depth is a significant contributor to the overestimation of lake ice cover in ERA5-Land, latitude also influences this overestimation, which is notably observed in the northern lakes due to their varying latitudes, unlike the Laurentian Great Lakes, which lie at similar latitudes. Within the northern lakes, as latitude decreases there is an increase in ERA5-Land's overestimation of lake ice fraction, except for Lake Winnipeg, which is located at the lowest latitude and displays the lowest overestimation. GBL is the highest latitude lake and exhibits the lowest bias despite its considerable depth, likely due to the higher latitude producing consistently colder temperatures to facilitate faster full ice coverage, counteracting FLake's depth related bias. Whereas GSL is only slightly deeper but at a lower latitude than GBL, it produces a higher bias than GBL, which continues to follow a pattern of bias increasing with a decrease in latitude until Lake Athabasca with the highest overestimation and third lowest latitude.

4.2.3.2 Lake Ice Timing

ERA5-Land estimates earlier FUS and FUE timing across all lakes; in other words, it produces an early bias. However, before interpreting the potential causes of the earlier FU timing, it is important to note a notable discrepancy: lower agreement in FUE differences between the two comparisons (IMS vs CIS/NOAA) than in FUS differences. The lower agreement in FUE is a known weakness of IMS, as previous research found that IMS FUE dates had only a moderate correlation (R=0.41) with ground-based observations (Du et al., 2017). Noting this FUE timing error enables the discussion to focus solely on CIS/NOAA for FUE timing differences and to avoid incorrectly attributing this bias to ERA5-Land. Therefore, while both satellite-derived datasets are used to assess FUS differences, only the CIS/NOAA product is used for FUE, as their dates are more accurate.

Similarly, lake ice fraction, lake depth, and latitude influence the timing of FUS. However, the combined influence of latitude and depth complicates the trend in early bias. This confounding influence is best observed in the northern lakes, which vary more in latitude than the Laurentian Great Lakes. Overall, ERA5-Land shows a larger early timing bias in the northern lakes than in the Laurentian Great Lakes. The larger differences in FUS among the northern lakes may be partly attributed to the sparsity of weather stations (used in reanalysis production) in northern Canada, whereas southern Canada has much higher station density (Milewska & Hogg, 2001). However, while the low density of weather stations at higher latitudes likely amplifies these biases in FU, lake depth also contributes. For example, Lake Athabasca, which is located at a lower latitude and shallower than GSL, unexpectedly exhibits earlier timing than GSL. The earlier timing in Lake Athabasca is most likely attributed to its shallower depth, while latitude has a lesser influence. Lake Winnipeg is the shallowest and lowest latitude northern lakes, and its FUS timing shows the closest agreement with CIS observations. Lake Winnipeg's shallow depth is within the optimized configuration for FLake, contributing to more accurate FUS timing.

The dominant influence of the early FUS timing within the Laurentian Great Lakes is lake depth, as unlike the northern lakes, these lakes lie at similar latitudes. For example, Lake Superior is the deepest and displays the largest early bias, while Lake Erie is the shallowest and shows the smallest bias. This variation in bias supports the argument that the larger early bias in FUS for the deeper lakes can be attributed to FLake's known limitation for simulations above ca. 50 m. There is one exception to this pattern, which is seen in NOAA's estimates of Lake Huron. Specifically, NOAA depicts slightly later timing, but IMS follows the described trend with earlier timing. However, this

outlier in the NOAA comparison is likely due to ice thickness threshold sensitivity, as when using the smaller thresholds for ERA5-Land the FUS difference follows the trend of earlier timing with greater depth.

The consistent early onset of FUS in ERA5-Land is the primary contributor to the early timing of FUE, as an early start to freeze-up naturally leads to an earlier end. However, ERA5-Land's omission of snow cover on top of lake ice may also contribute to its earlier timing for FUE, since snow slows ice growth (and therefore ice thickness in ERA5-Land) due to the difference in thermal conductivity (See Section 2.2.2.1 for more details). Therefore, including snow cover over lake ice could delay ERA5-Land's FUE estimates and potentially reduce the early bias, but this cannot be concluded conclusively as snow cover on lake ice is not considered in FLake/ERA5-Land.

4.2.3.2.1 Spatial Assessment of Highest and Lowest Agreement

The spatial assessment evaluates the agreement of timing of water and ice transitions between IMS and ERA5-Land; thus, this agreement integrates ice date timing and fraction agreement. For all lakes except Lake Superior and Huron, the lowest agreement occurs along the lake shores, notably the northern and eastern shores, while the highest agreement occurs within the center of the lake. Conversely, within Superior and Huron, the lowest agreement occurs in the northern center, and the highest agreement occurs along the shores, notably within bay areas. This pattern of agreement within Superior and Huron can be primarily attributed to ERA5-Land's large overestimation of lake ice fraction and the location of consistent lake ice, as ERA5-Land consistently produces full or near full ice fraction for these lakes. However, observations indicate that lake ice rarely occurs in the northern center, resulting in low agreement there, while the areas of highest agreement, the shores and bays, are areas that consistently experience lake ice.

For the other lakes, the pattern of lowest agreement along the shores and highest agreement in the center is largely due to differences in FU timing. As previously mentioned, ERA5-Land consistently produces earlier FU. Since the shores experience FU first, this would cause larger differences in FU timing and, consequently, lower agreement. Whereas, since the center of the lakes is last to freeze, the difference in FU timing would be shorter in comparison, hence the larger agreement in this area of the lakes.

4.3 Break-up Differences

4.3.1 Lake Ice Fraction

Across all lakes except for GBL, ERA5-Land overestimates lake ice fraction as indicated by the positive MBE (Figure 9, Table 20). GBL is the one exception, showing an underestimation as indicated by the negative MBE across all thresholds (10 mm = -10% ; 20 mm = -11%; 50 mm = -12%). The overestimation of lake ice fraction is greater in the Laurentian Great Lakes than in the northern lakes (Table 20). The overestimation for the Laurentian Great Lakes can be attributed to ERA5-Land producing full or near-full ice cover, whereas observations showed low to moderate ice fractions for Lake Superior and Huron (Figure 9). Lake Superior shows the greatest overestimation across all lakes (50 mm MAE = 62%), followed by Lake Huron (50 mm MAE = 42%), while Lake Erie reveals the lowest overestimation among the Laurentian Great Lakes, but the overestimation is still greater than observed in most of the northern lakes (50 mm MAE = 12%).

The northern lakes also depict this trend in overestimation, with GBL as the only exception (Figure 9, Table 20). This exception in GBL appears to be due to a more accelerated melt rate than that observed in the other northern lakes (Figure 9). Along with the accelerated melt, which contributes to underestimation, GBL shows the largest bias among the northern lakes (50 mm MAE = 15%). Conversely, while the other northern lakes showed overestimation, GSL exhibited the lowest bias across all lakes (50 mm MAE = 7%).

Overall, ERA5-Land consistently overestimates lake ice fraction, with GBL as the one exception. Among the trend of overestimation, the Laurentian Great Lakes depict larger overestimation compared to the northern lakes, with Lake Superior depicting the largest overestimation, while GSL depicts the lowest overestimation.

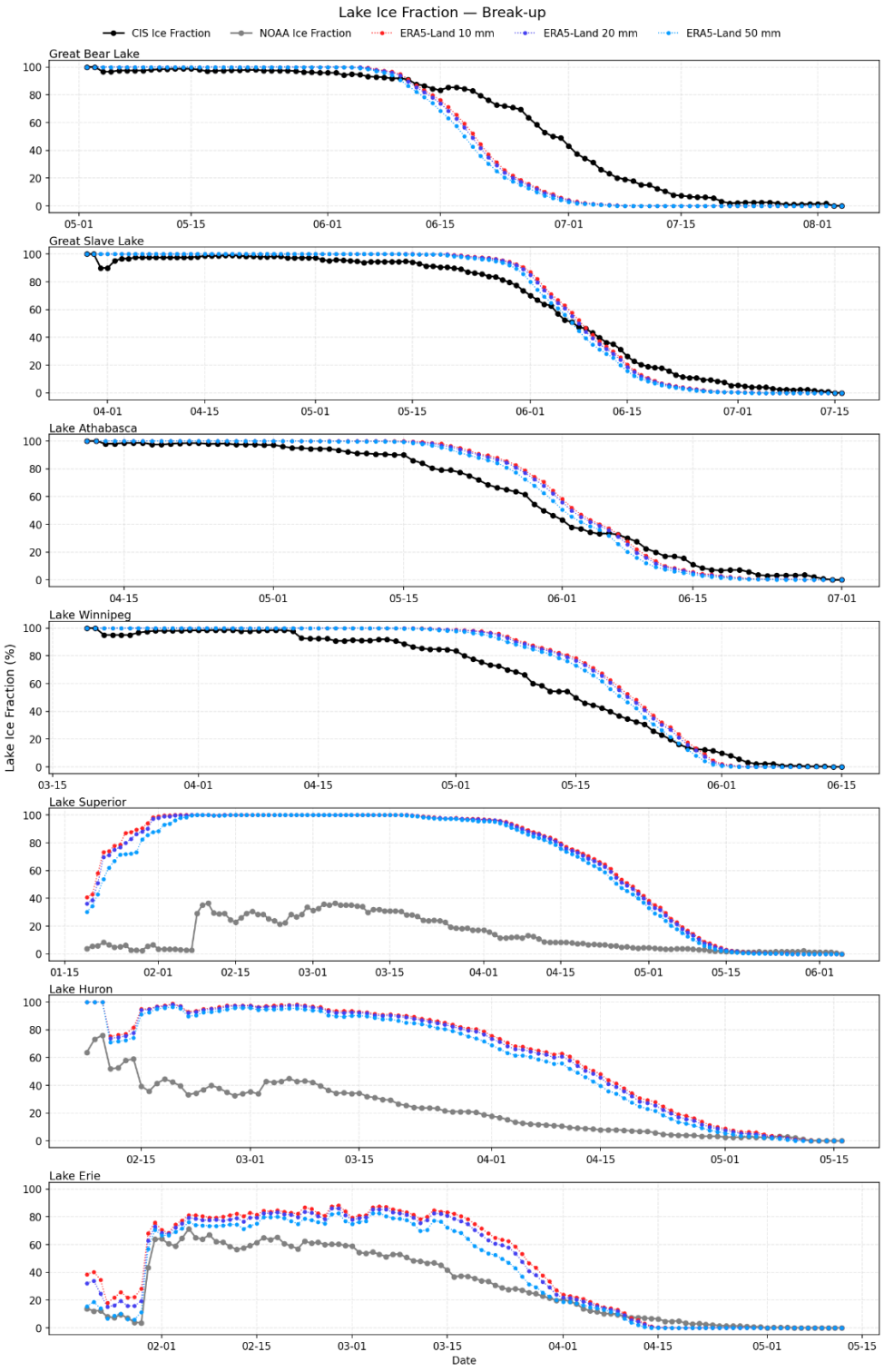


Figure 9: Average (2004-2023) ice fraction (%) for all lakes of this study during break-up

Table 20: Direction and magnitude of bias in lake ice fraction (%) during break-up per lake

Note: Values blue–red scale (red = highest value, blue = lowest value; intensity reflects magnitude)

Lake	10 mm MBE	10 mm MAE	20 mm MBE	20 mm MAE	50 mm MBE	50 mm MAE
Great Bear Lake	-10	13	-11	14	-12	15
Great Slave Lake	2	7	1	7	0	7
Lake Athabasca	4	8	4	8	3	8
Lake Winnipeg	9	11	8	11	7	10
Lake Superior	65	65	64	64	62	62
Lake Huron	46	46	45	45	41	42
Lake Erie	22	23	18	18	11	12

4.3.2 Lake Ice Timing

Across all lakes, ERA5-Land consistently provides delayed BUS and early BUE relative to satellite-derived observations, with few exceptions (Table 21). The few exceptions to this pattern are Lake Superior and Huron, which show late BUE (Superior = NOAA: 6 days and IMS: 9 days; Huron = NOAA and IMS: 0 days). Another exception is within Athabasca, where IMS found BUE timing to be marginally early (5 days) while CIS observed late BUE timing (1 day).

The Laurentian Great Lakes show the most significant delay in BUS and the closest timing in BUE compared to the northern lakes in both comparisons. The larger delay in BUS can be attributed to the overestimation of lake ice fraction within these lakes. Specifically, Lake Superior shows the largest delay in BUS across all lakes (NOAA: 44 days; IMS: 46 days). For BUE, across all lakes, Huron shows the closest timing (NOAA and IMS: 0 days), and Superior shows the greatest delay (NOAA: 6 days; IMS: 9 days). Lastly, Lake Erie depicts the closest BUS timing (NOAA: 15 days; IMS: 5 days) and BUE timing (NOAA: -13 days; IMS: -9 days) among the Laurentian Great Lakes.

The northern lakes depict the shortest delay in BUS and earlier timing in BUE compared to the Laurentian Great Lakes. In particular, Athabasca shows the closest BUS timing across all the

lakes (CIS: 7 days; IMS: 5 days), while GSL shows the most significant delay in BUS timing (CIS: 5 days; IMS: 1 day) among the northern lakes. For BUE, GBL depicts the earliest timing across all lakes (CIS: -17 days; IMS: -14 days).

Generally, ERA5-Land estimates later BUS and earlier BUE, with the Laurentian Great Lakes typically depicting larger timing differences than the northern lakes.

Table 21: Difference in break-up dates of ERA5-Land to satellite-derived products

Note: Lakes highlighted pink uses CIS data while lakes highlighted blue uses NOAA data

	ERA5-Land (50 mm) timing – dataset timing			
Lake	**CIS/NOAA BUS Difference**	**IMS BUS Difference**	**CIS/NOAA BUE Difference**	**IMS BUE Difference**
Great Bear Lake	5	1	-17	-14
Great Slave Lake	13	7	-14	-9
Lake Athabasca	7	4	-5	1
Lake Winnipeg	9	5	-7	-3
Lake Superior	44	46	6	9
Lake Huron	25	25	0	0
Lake Erie	15	5	-13	-9

4.3.2.1 Areas of the Lakes with Highest and Lowest Agreement

Overall, the spatial agreement patterns do not show a single pattern applicable across all lakes (Figure 11-Figure 13). Instead, the spatial agreement mainly aligns in areas where ERA5-Land's estimated BUS and BUE timing is closest to observation. Because agreement is influenced by both BUS and BUE, the combined effects make it more difficult to delineate potential reasons for the spatial pattern. However, there appears to be a latitudinal pattern across all lakes, most notably among the northern lakes (Figure 10).

Within the northern lakes, high-latitude lakes (e.g., GBL and GSL) show peak agreement in areas that experience BU early in the season, whereas as latitude decreases (e.g., Athabasca and Winnipeg), the peak agreement occurs in areas that experience BU later (Figure 10). This pattern of peak agreement corresponds to the timing of closest agreement in lake ice extent (Figure 9). However, the exact cause for this pattern is challenging to delineate because several variables

influence BU (e.g., air temperature, ice thickness, albedo), and the accuracy and biases of these variables were not assessed within the study. Additionally, because agreement is determined by both BUS and BUE timing, these combined influences complicate the interpretation of potential reasons.

The Laurentian Great Lakes appear to follow a latitudinal pattern; however, overestimation of lake ice extent is a significant contributor to the areas of lowest agreement. The lowest agreement occurs in the north-central regions, where lake ice rarely forms. But ERA5-Land consistently produces full or near full ice coverage for these lakes, and this contributes to the low agreement within these regions. Conversely, the highest agreement occurs within the areas that experience BU later in the season, which can be attributed to ERA5-Land's estimated BUE matching closer to observation. However, the closer BUE timing does not accurately reflect the melt process. While agreement is high within these areas, it does not occur for the right reasons. FLake in ERA5-Land grows ice too thick due to the lack of consideration of snow on ice, and melts the ice faster for the same reason, although some accommodation is made through the surface albedo parameterization to slow the melt process that would otherwise be faster without the presence of snow (i.e. only clear ice).

Lake Erie does not follow the latitudinal pattern; instead, there are several peaks in agreement over a broader period, suggesting that multiple controls influence its spatial pattern. Because Lake Erie typically exhibits high ice fraction (~70%), the full ice assumption of ERA5-Land's leads to comparatively lower bias for Lake Erie compared to Lake Huron and Superior. Therefore, ERA5-Land's inability to produce partial ice coverage does contribute to the biases in Lake Erie, but to a lower magnitude to Huron and Superior. Also, while lake morphology is not a significant contributor to the BU process, it does influence lake ice thickness and extent, as more ice produces a longer BU period. Therefore, the rapid melt produced by ERA5-Land is closely aligned with what occurs in shallow lakes. It should then be expected that Lake Winnipeg would have a lower lake ice extent bias, but this is not the case, which once again indicates collinearity among other controls of BU, such as albedo, air temperature, and lake ice thickness.

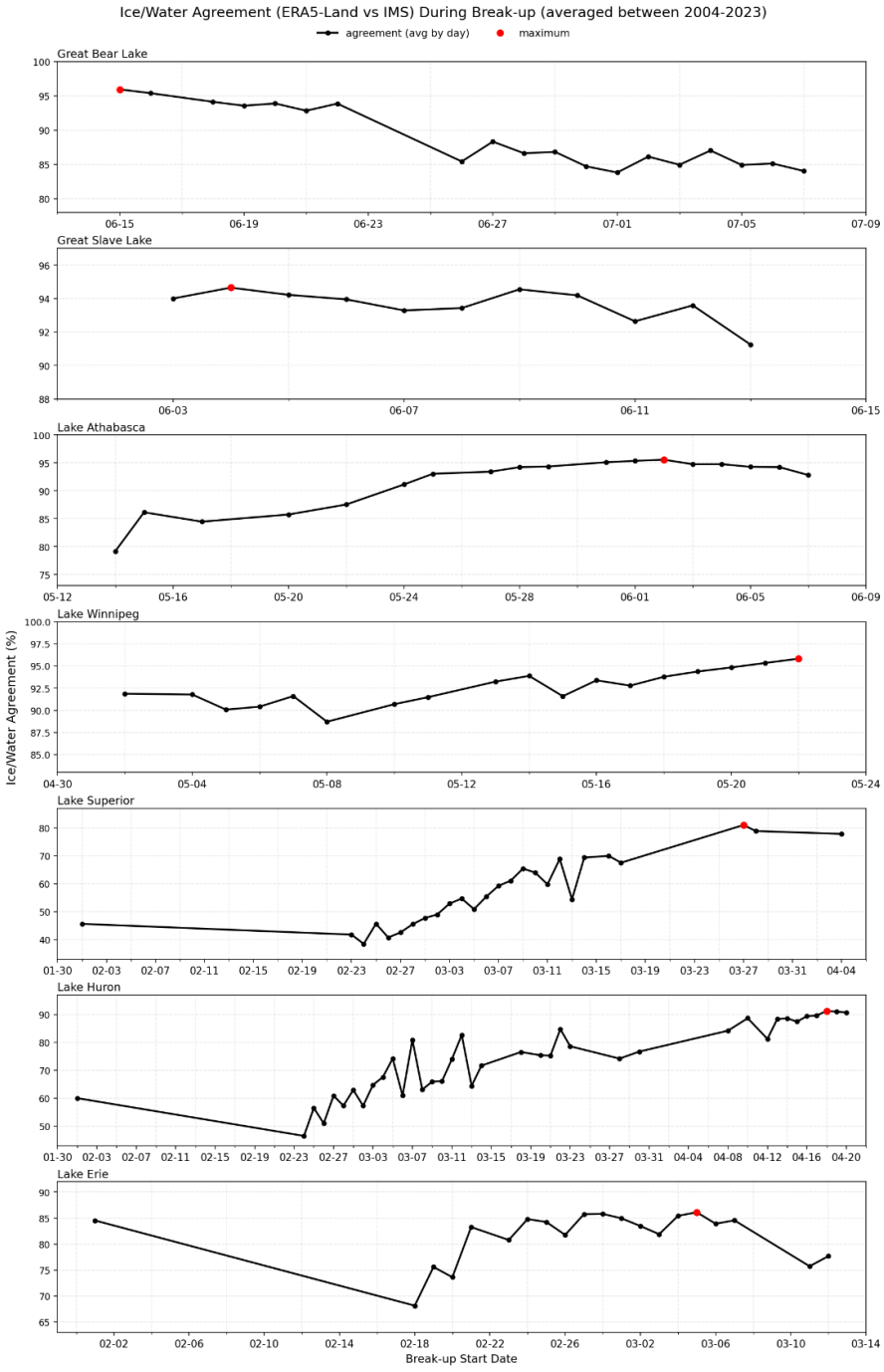


Figure 10: Ice–water agreement (%) between ERA5-Land and IMS during break-up (2004–2023)

Note: computed using only pixels with IMS break-up starting on each plotted date.

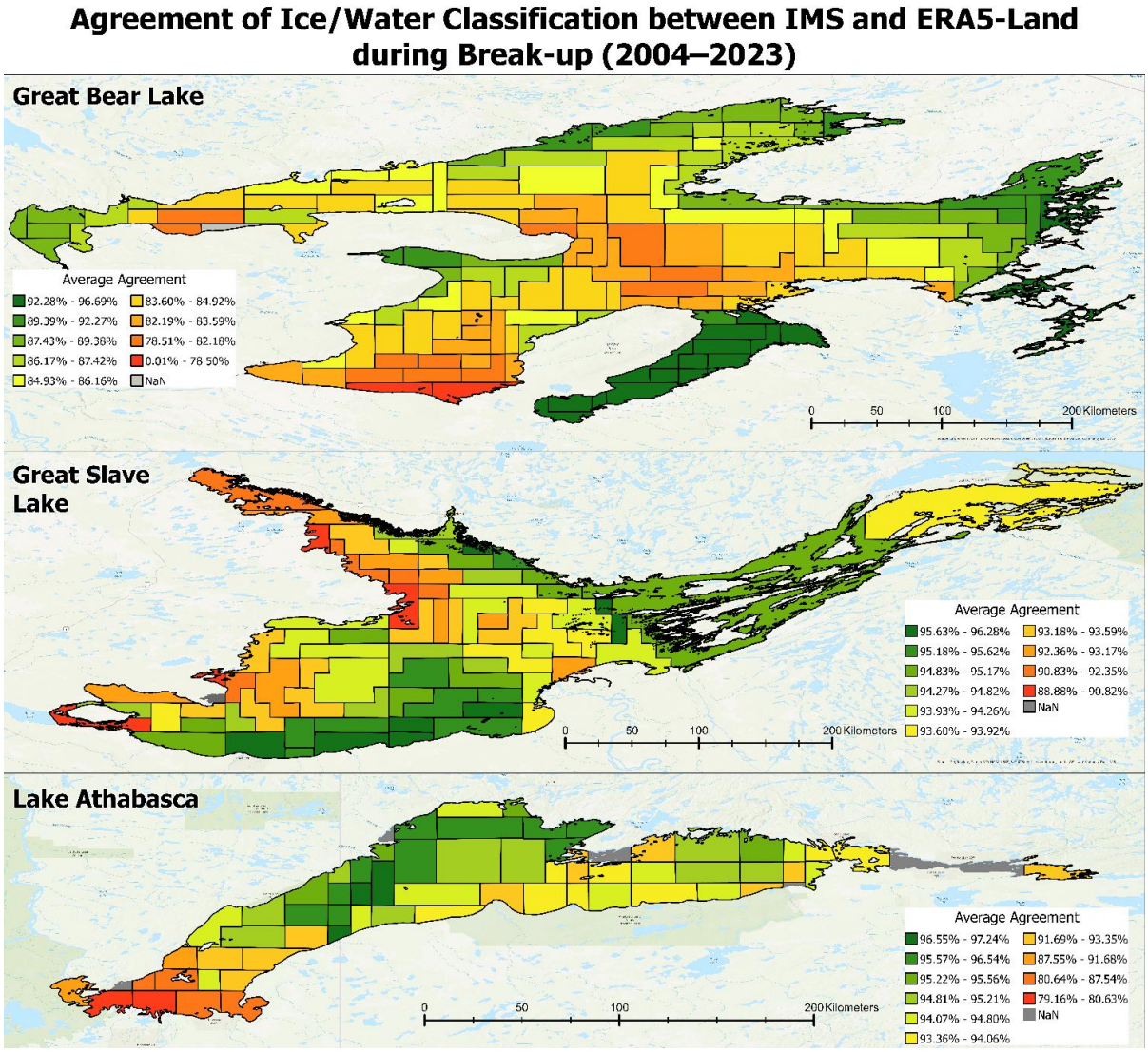


Figure 11: Average (2004-2023) ice to water transition agreement (%) during break-up between ERA5-Land and IMS for Great Bear Lake, Great Slave Lake and Lake Athabasca

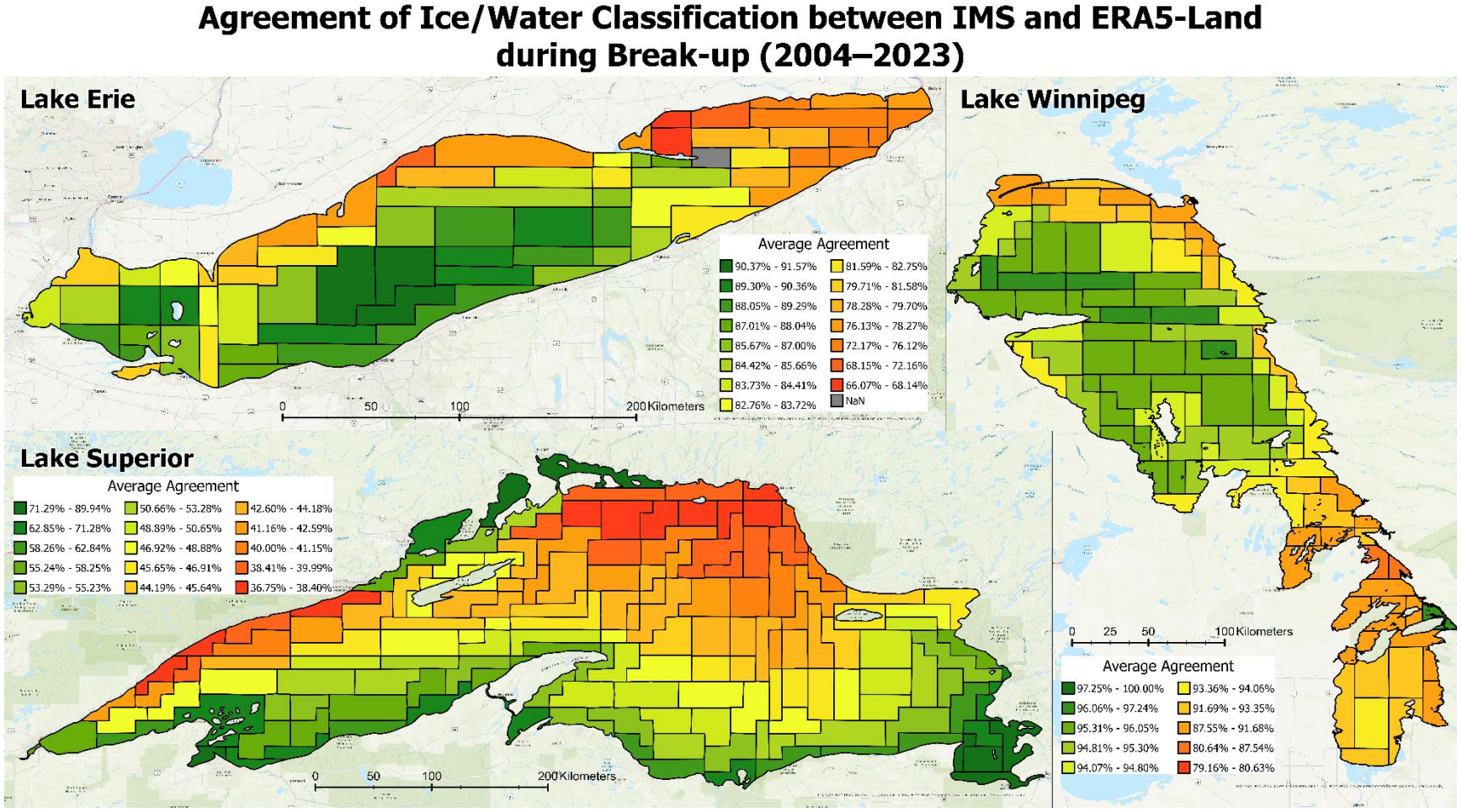


Figure 12: Average (2004-2023) ice to water transition agreement (%) during break-up between ERA5-Land and IMS for Lake Erie, Lake Superior and Lake Winnipeg

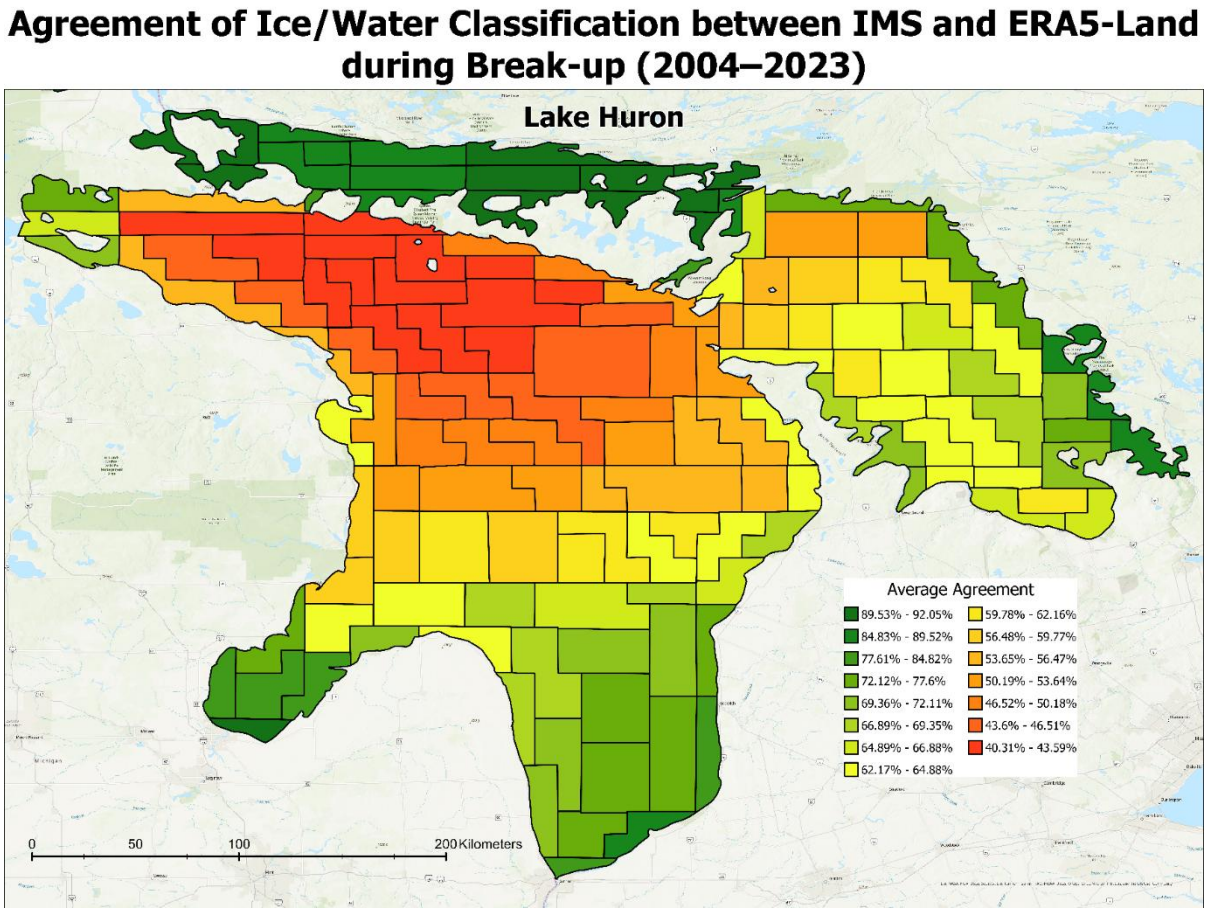


Figure 13: Average (2004-2023) ice to water transition agreement (%) during break-up between ERA5-Land and IMS for Lake Huron

4.3.3 Discussion

4.3.3.1 Summary of findings

Generally, ERA5-Land overestimates lake ice fraction during break- up across all lakes. This overestimation can be attributed to the consistently delayed timing of BUS in ERA5-Land's estimates relative to satellite-derived observations. The delay timing of BUS causes ERA5-Land to estimate a higher ice fraction during the early break-up season, while the consistently early BUE timing would offset that overestimation. However, there is one exception to the overestimation trend: GBL. While GBL follows the pattern of late BUS and early BUE, the exception of underestimation stems from GBL having the closest BUS timing to the observation. Therefore, the cause of overestimation (the delayed timing of BUS) is minimized in GBL, and ERA5-Land's accelerated melt causes it to have the earliest BUE, producing underestimation in lake ice fraction.

The spatial agreement of ice and water does not demonstrate a consistent pattern across all lakes, unlike during freeze-up. To clarify, the areas of highest agreement were not confined to specific areas within the lakes (e.g., shores/bays); instead, the areas of highest agreement correspond to locations where the average difference between ERA5-Land and IMS for BUS and BUE is lowest. Consequently, the congruent influences of BUS and BUE complicate spatial patterns within the lake. While there are no apparent spatial patterns across the lakes, a latitudinal pattern emerges, with peak agreement timing, notably among the northern lakes.

Within the northern lakes, the latitudinal pattern of peak agreement shows that high-latitude lakes (e.g., GBL and GSL) exhibit peak agreement in areas that experience melt first or earlier during the BU period. Whereas, as latitude decreases (e.g., Athabasca and Winnipeg), the peak agreement occurs within areas that experience BU later. While the Laurentian Great Lakes appear to follow this pattern, it is not fully applicable due to the ERA5-Land's large overestimation of lake ice fraction within these lakes. The areas of lower agreement are mainly attributed to regions where lake ice rarely forms (north central regions), rather than to higher average differences in BUS and BUE timing. Thus, ERA5-Land consistently produces full or near full ice coverage for these lakes, complicating the trend of lower BUS and BUE differences to produce higher agreement.

An interesting finding is that the timing of peak agreement in the spatial assessment using IMS corresponds to the timing of closest agreement in lake ice fraction seen using NOAA/CIS. This alignment in peak agreement reinforces the reliability of these datasets as validation data.

4.3.3.2 Examination of Potential Causes for Observed Biases

Break-up is influenced by multiple interconnected processes that influence heat absorption and melt (Brown & Duguay, 2010; Kirillin & Leppäranta, 2022; Woolway et al., 2020). Therefore, to identify potential influences on the biases of ERA5-Land during break-up, several controls of break-up are discussed: albedo, lake ice thickness, snow cover and air temperature. The potential biases of these controls and how they contributed to the biases observed (lake ice fraction overestimation, delayed BUS timing and early BUE timing) are provided below.

Albedo is recognized as influencing the timing and rate of break-up through its control of absorbed solar radiation. This influence of albedo is captured in ERA5-Land by parameterizing albedo as a function of the decay law for solar radiation flux, which is one of the parameters that influence the rate and timing of melt. Given albedo's recognized influence on break-up in the model and in reality, albedo was examined as a possible contributor to why GBL deviates from the overestimation pattern and instead produces an underestimation.

Examination of ERA5-Land's albedo was performed through comparison of GBL and GSL, as these lakes, or at similar latitudes, act as an appropriate reference point for understanding why GBL deviates from the pattern of lake ice fraction overestimation. For this examination, three years (2004, 2009 and 2015) were selected based on the highest underestimation of lake ice fraction within GBL. Overall, this examination found that GBL has a lower average albedo during pre-BUS (on average, lower by 0.007) and typically has a faster rate of decrease during the pre-BUS period (Figure 14). The one exception to the faster rate of decrease during pre-BUS is 2004, which instead shows a faster decrease during the BU period. This indicates that GBL absorbs more solar radiation, leading to earlier and faster melt and, in turn, an underestimation of the lake ice fraction.

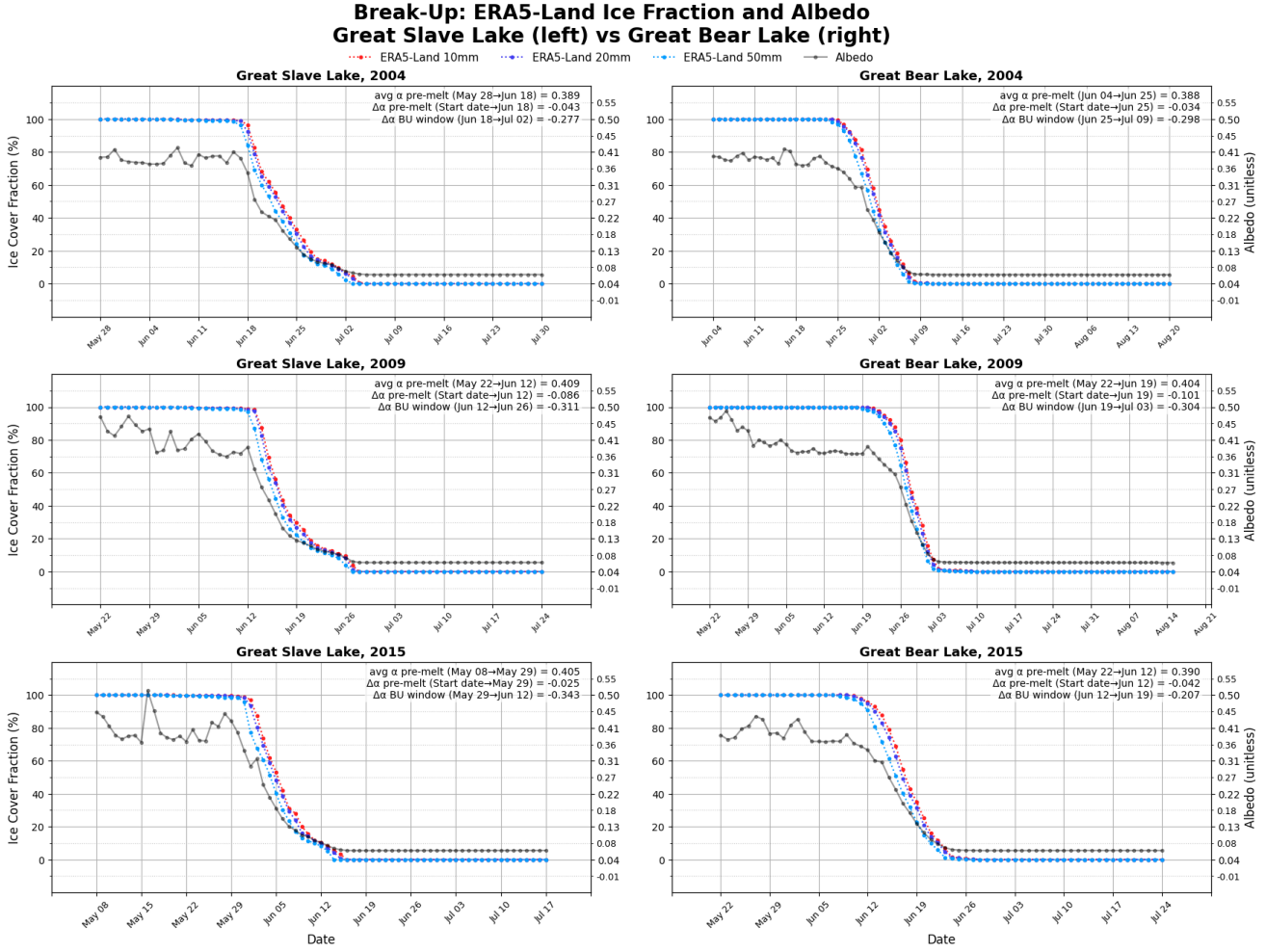


Figure 14: Break-up evolution of ERA5-Land ice fraction and albedo for Great Slave Lake (left) and Great Bear Lake (right) for the years 2004, 2009, and 2015

The influence of albedo extends beyond the GBL exception and contributes to the pattern of early BUE timing in ERA5-Land. In reality, snow cover would highly reflect incoming solar radiation due to its high albedo (~0.7-0.9), in turn insulating the underlying ice (Leppäranta, 2015). Thus, snow cover reduces heat penetration into the ice and reduces heat absorption, thereby delaying melting (Hicks et al., 2008; Kirillin & Leppäranta, 2022; Prowse et al., 2011). However, ERA5-Land omits snow cover on lake ice which neglects its reflective and insulating influence (European Centre for Medium-Range Weather Forecasts, 2018; Martynov et al., 2012; Mironov et al., 2010). Thus, the underestimation of GBL is likely due to the omission of snow cover as GBL is a cold monomictic lake which causes break-up to be largely driven by snow. Consequently, the omission of snow produces overestimation of solar radiation absorption, leading to accelerated melt and earlier BUE relative to satellite-derived observations.

The Laurentian Great Lakes exemplify the overestimation of lake ice thickness, as ERA5-Land produces full or near full ice coverage when partial ice coverage occurs, thereby prolonging break-up and delaying BUS. In reality, partial ice coverage would melt more quickly because it provides insulation and exposes more open water, increasing solar radiation absorption due to lower albedo (Arp et al., 2015; Garrett et al., 2010; Leppäranta, 2015; Williams, 1968). Consequently, the increased absorption of solar radiation enhances the heat flux beneath the ice and accelerates basal melting (Kirillin & Leppäranta, 2022). However, ERA5-Land's assumption of full or near full ice coverage fails to capture the partial insulation and increase in solar radiation that is occurring within the Laurentian Great Lakes because of their partial ice coverage. Therefore, the overestimation of lake ice coverage effectively produces thicker lake ice, which causes the Laurentian Great Lakes to experience the largest delay in BUS.

The final break-up control considered is air temperature, which governs the amount of atmospheric heat available to melt lake ice. However, there are limited air temperature evaluations of ERA5-Land's air temperature. But ERA5-Land derives air temperature from its predecessor, ERA5, so evaluations of ERA5's air temperature will serve as a proxy. These assessments may not directly reflect ERA5-Land, but there is a potential that ERA5 biases are carried over into ERA5-Land. Likely, these biases would exist within ERA5-Land at a lower magnitude due to adjustments made within the model (adjusted for altitude differences and use of a daily environmental lapse rate). ERA5 has been found to produce a warm bias of 0-8°C in the Arctic, which is reaffirmed by another study that found a warm bias across all months (Wang et al., 2019; Yu et al., 2021). The month of highest warm bias occurred in April (3.73 ± 2.84 °C), and lowest bias occurred between August to November

(less than 2 °C) (Yu et al., 2021). The warm bias of ERA5 could have carried over into ERA5-Land, which could have also contributed to the accelerated melt observed in this study.

4.4 Lake Ice Temperature Differences during Ice-covered Period

ERA5-Land generally exhibits a warm bias, with nighttime temperatures showing a larger warm bias than daytime temperatures (Figure 15 and Figure 16). Daytime values show a decreasing trend in MAE over the ice-covered period (FUE to BUS) (Table 22). To clarify, the average bias decreases as melt approaches. Specifically, MAE is highest during the month of FUE and lowest during the month of BUS across all lakes (Table 22). Although warm bias dominates the ice-covered period, occasional cold biases occur mainly in the Laurentian Great Lakes and less frequently in the northern lakes. Among the northern lakes, daytime cold bias typically occurred near BUS; specifically in May for both GSL and Athabasca, and in March for GBL. In the Laurentian Great Lakes, a daytime cold bias occurred during most months except BUS. In particular, cold bias occurred in all months in Lake Huron, from January to March in Lake Superior, and from November to December in Lake Erie (Table 22). Across all lakes, daytime temperatures reveal a consistent seasonal trend with MAE decreasing towards BUS (typically late spring), suggesting that ERA5-Land's temperature estimates become more accurate as ice reaches its maximum thickness before the beginning of melt.

Nighttime temperatures exhibit a stronger warm bias, and unlike daytime values there appears to be no clear trend across all lakes (Figure 16). However, some lake-specific patterns are observed; for instance, Lake Winnipeg and GSL show increasing MAE through the ice-covered period. Specifically, MAE increases through the period but sharply decreases near BUS (Table 23). Whereas Huron and Superior show the opposite trend: highest bias at FUE, decreasing steadily until BUS, which shows the lowest bias (Table 23). Despite the overall stronger warm bias at night, occasional cold biases still occur in the Laurentian Great Lakes. Specifically, cold bias occurred from February to March in Lake Superior and in November for Lake Erie (Table 23). Generally, while there appears to be no seasonal trend in bias across all lakes, nighttime values demonstrate a stronger warm bias compared to daytime values.

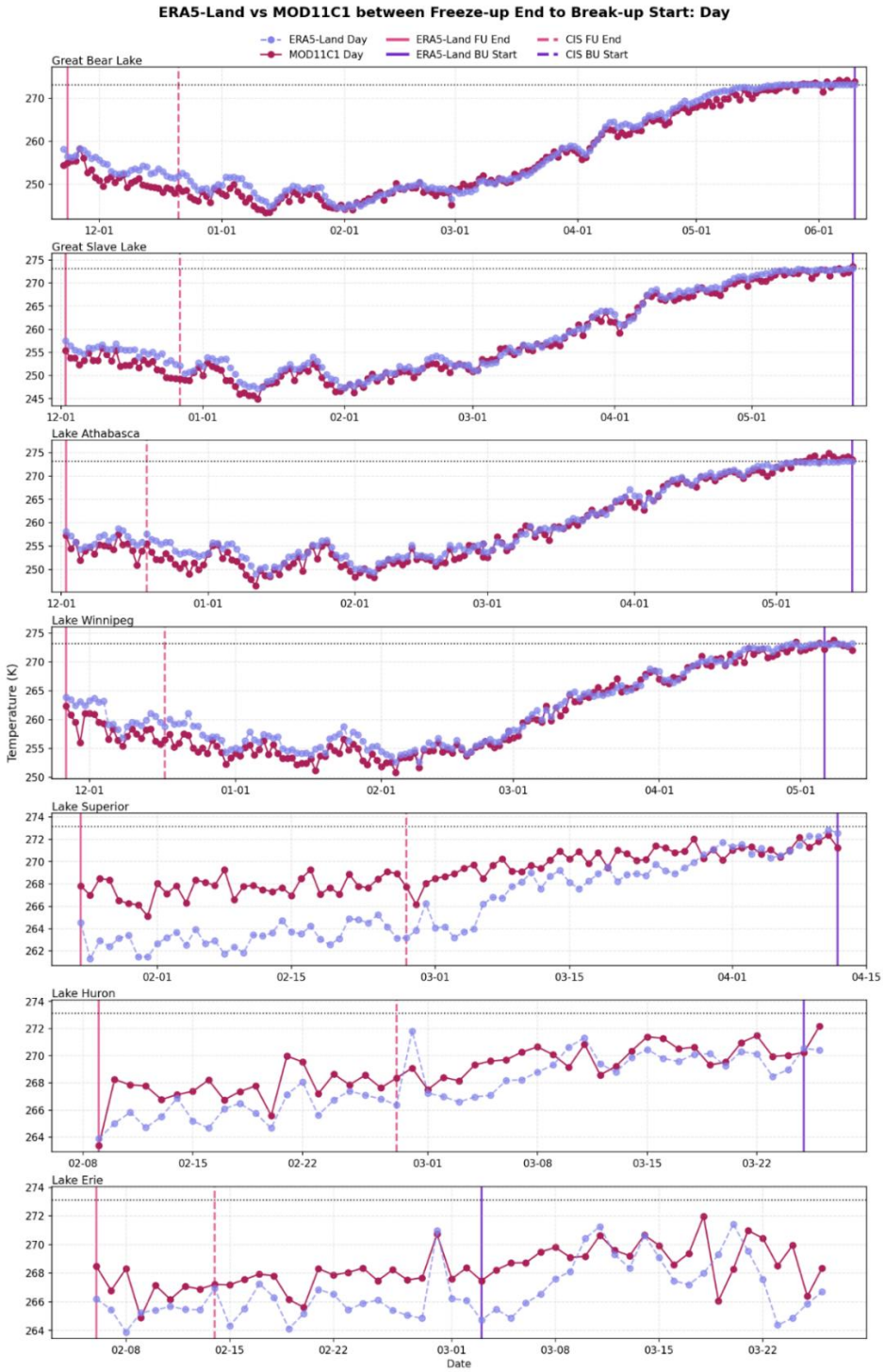


Figure 15: Average lake-wide surface temperature of MOD11C1 and ERA5-Land during daytime

Table 22: Daytime biases (MBE and MAE) during ERA5-Land's ice-covered period

Note: MBE uses a red–green scale (red = negative, green = positive; intensity reflects magnitude). MAE uses a white–red scale (white = lowest error, red = highest; intensity reflects magnitude).

	GBL		GSL		Athabasca		Winnipeg		Superior		Huron		Erie	
Month	MBE	MAE	MBE	MAE	MBE	MAE	MBE	MAE	MBE	MAE	MBE	MAE	MBE	MAE
Nov													-7.339	7.598
Dec	2.270	4.733	2.492	4.481	1.939	3.960	2.141	3.270					-1.259	3.454
Jan	1.481	3.962	1.577	3.550	1.565	3.593	1.815	3.363	-1.267	6.056			0.653	2.916
Feb	0.028	3.409	0.637	3.206	0.577	3.145	0.663	2.919	-4.835	6.639	-1.120	4.352	0.741	3.033
Mar	-0.436	3.024	0.144	3.029	0.096	2.976	0.055	3.022	-2.399	4.494	-0.798	3.456		
Apr	0.768	2.872	0.441	2.713	0.249	2.744	0.150	2.713	0.209	2.582	-0.467	2.718		
May	0.948	2.329	-0.023	2.265	-1.513	3.302								

Table 23: Nighttime biases (MBE and MAE) during ERA5-Land's ice-covered period

Note: MBE uses a red–green scale (red = negative, green = positive; intensity reflects magnitude). MAE uses a white–red scale (white = lowest error, red = highest; intensity reflects magnitude).

	GBL		GSL		Athabasca		Winnipeg		Superior		Huron		Erie	
Month	MBE	MAE	MBE	MAE	MBE	MAE	MBE	MAE	MBE	MAE	MBE	MAE	MBE	MAE
Nov													-5.549	7.807
Dec	2.483	5.025	3.949	5.715	3.872	5.585	4.913	5.483					2.141	5.543
Jan	2.590	4.390	3.604	5.021	4.251	5.395	5.281	5.847	2.524	8.445			4.409	6.097
Feb	2.572	4.647	4.169	5.431	3.913	6.153	5.866	6.320	-0.869	8.140	2.477	7.047	3.824	5.455
Mar	4.842	5.593	6.247	6.672	6.718	6.959	7.227	7.331	-0.387	5.719	0.761	4.987		
Apr	7.733	7.805	6.770	6.809	6.044	6.115	5.047	5.288	0.613	3.490	0.684	3.404		
May	5.535	5.636	2.803	3.250	1.480	3.325								

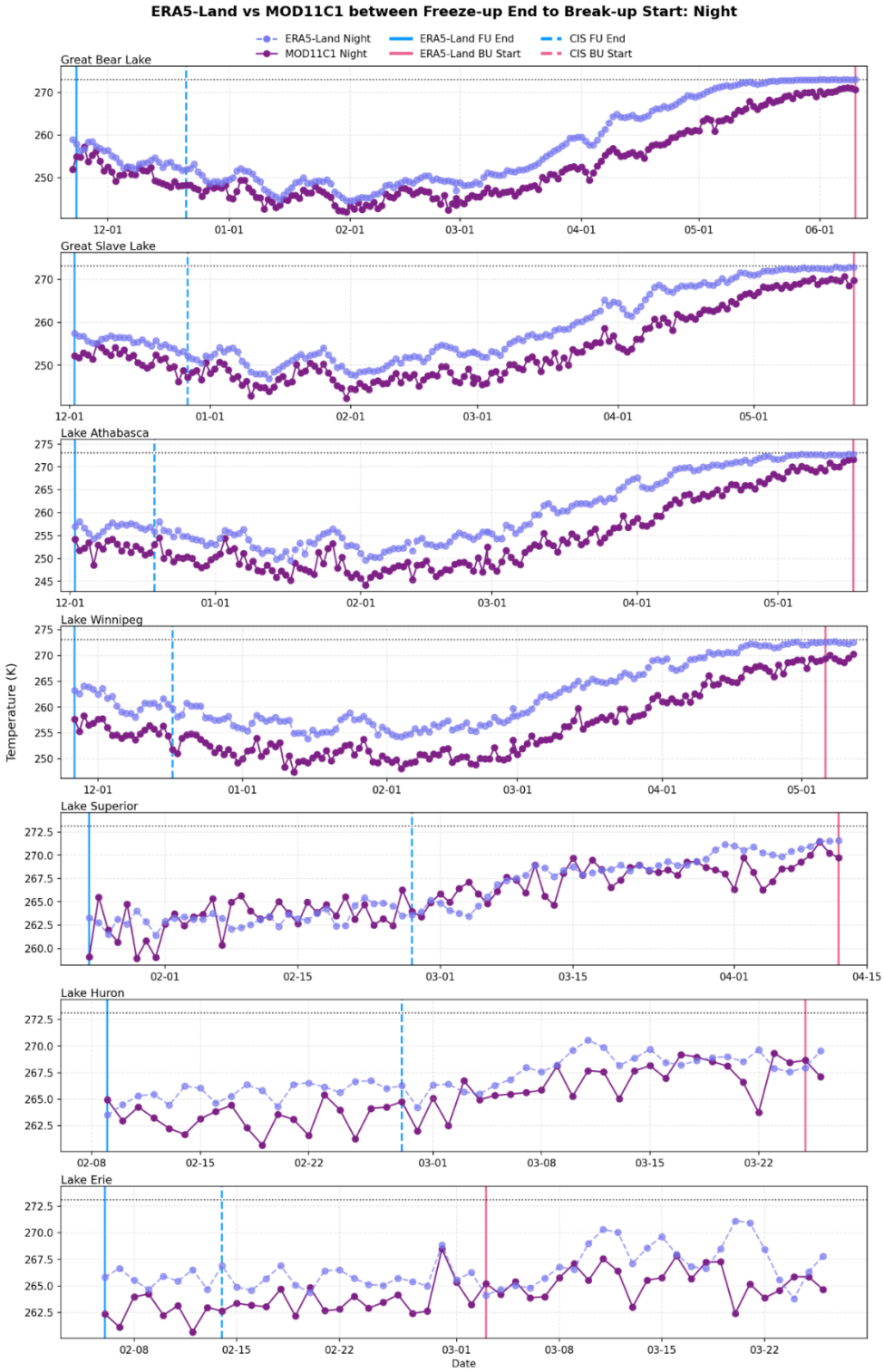


Figure 16: Average lake-wide surface temperature of MOD11C1 and ERA5-Land during nighttime

4.4.1 Discussion

In summary, ERA5-Land's daytime lake ice temperature shows a warm bias during the ice-covered period (FUE to BUS) for the northern lakes, while the Laurentian Great Lakes generally exhibit a cold bias. Across all lakes, daytime MAE decreases as season progresses, reaching its minimum near BUS and maximum near FUE. Unlike the daytime temperatures, nighttime biases do not follow a clear or consistent temporal pattern. But the stronger nighttime warm bias indicates ERA5-Land does not capture nighttime cooling effectively. Despite the stronger nighttime warm bias across all lakes, there are still instances of cold bias in the Laurentian Great Lakes.

The overall warm bias in the northern lakes is likely attributed to ERA5-Land's omission of snow cover. The surface temperature is controlled by the overlying air temperature and conductive heat flow through the ice/snow (Gould & Jeffries, 2005; National Snow and Ice Data Center, n.d.). The lack of snow on the ice surface leads to a higher conductive heat flow, which can help explain the warm bias. Also, the months with the highest snowfall correspond to months with the highest warm bias (Table 22, Table 24). Likewise, months of lower snowfall correspond with lower warm bias or cold bias. However, GBL is an exception, as March shows a cold bias despite typically experiencing high snowfall. This exception could be due to MOD11C1 potentially capturing snow melting and snow drift, leading to bare ice to be intermittently exposed, in turn, causing MOD11C1 to observe warmer surface temperature (Bengtsson, 1986; Bernhardt et al., 2012; Kirillin et al., 2012).

The overall cold bias in the Laurentian Great Lakes is likely due to both ERA5-Land's overestimation of lake ice fraction and does not explicitly account for precipitation influence on lake ice, though lake ice fraction appears to exert a stronger influence (European Centre for Medium-Range Weather Forecasts, 2018). The largest cold biases occur near FUE, consistent with the influence of lake ice fraction overestimation. This occurs because MOD11C1 includes the temperature of the open-water pixels, which lower the observed lake-wide temperature relative to ERA5-Land's full ice cover estimation. Thus, it would have been expected that Lake Erie, which shows the lowest lake ice overestimation, would exhibit the lowest cold bias but that is not observed. During January and February, Lake Erie shows the lowest overestimation in lake ice fraction (Figure 9), which corresponds to a cold bias, yet the MAE of Lake Erie is similar to Huron and Superior. The similar MAE suggests precipitation acts as a complicating factor, as Lake Erie experiences high snowfall and rainfall in January and February (Table 24 and Table 25). While snowfall can insulate the ice and reduce cold bias, freezing rain can have the opposite effect (Table 22). As freezing rain

events accompanied by rising air temperature can cause the ice to rapidly warm and sometimes drive it towards isothermal condition, even over brief periods (Gould et al., 2005). Because ERA5-Land does explicitly represent freezing rain effect on ice, its estimated surface temperature remains colder than observed in MOD11C1, contributing to the cold bias. Although ERA5-Land does parameterize frozen precipitation in HTESSEL, it does not appear to explicitly consider its effect on lake ice temperatures which could contribute to the cold bias of Erie and Huron (as they both experience high rainfall in freezing temperature; Table 25 and Table 26). Overall, the biases of these lakes suggest that the ice fraction errors are the biggest contributors to the daytime cold bias with snow cover and freezing rain also producing contributing effect on the cold bias.

Table 24: Snowfall climate normal for all lakes of this study during the ice-covered period (FUE-BUS) (Environment Climate Change Canada, 2023)

Note: Values red-blue scale (red = lowest value, blue = highest value; intensity reflects magnitude per lake). Bolded values represent the months specifically evaluated in surface temperature assessment for each lake.

SNOWFALL (cm)								
LAKE	Nov	Dec	Jan	Feb	Mar	Apr	May	Notes
Great Bear	*31.0*	**21.2**	**18.1**	**19.0**	**15.5**	**13.2**	**5.3**	Averaged climate normals of Norman Wells and Deline Stations (see Table 3 for details)
Great Slave	*35.7*	**22.9**	**22.0**	**16.4**	**18.0**	**9.4**	**4.4**	Averaged climate normals of Hay River and Yellowknife Stations (see Table 4 for details)
Athabasca	*24.7*	**18.5**	**14.8**	**14.4**	**15.7**	**9.8**	**2.7**	Climate normals of Fort Chipewyan A Station (see Table 5 for details)
Winnipeg	*32.1*	**35.0**	**25.0**	**19.7**	**22.7**	**13.1**	*4.8*	Averaged climate normals of Norway House and Gimli Stations (see Table 6 for details)
Superior	*35.1*	*34.8*	**32.5**	**27.5**	**24.7**	**16.0**	*3.2*	Averaged climate normals of Wawa and Duluth Stations (see Table 7 for details)
Huron	*7.3*	*33.6*	**36.9**	**28.4**	**18.9**	**6.2**	*0.0*	Averaged climate normals of Sarnia and Alpena WWTP Stations (see Table 8 for details)
Erie	**5.0**	**29.9**	**43.4**	**33.2**	*22.5*	*5.6*	*0.0*	Climate normals of Windsor Station (see Table 9 for details)

Table 25: Air temperature climate normal for all lakes of this study during the ice-covered period (FUE-BUS) (Environment Climate Change Canada, 2023)

Note: Values blue–red scale (red = highest value, blue = lowest value; intensity reflects magnitude per lake). Bolded values represent the months specifically evaluated in surface temperature assessment for each lake.

AIR TEMPERATURE (°C)								
LAKE	Nov	Dec	Jan	Feb	Mar	Apr	May	Notes
Great Bear	-16.5	**-23.0**	**-25.1**	**-22.8**	**-18.5**	**-6.6**	**5.1**	Averaged climate normals of Norman Wells and Deline Stations (see Table 3 for details)
Great Slave	-11.7	**-20.1**	**-23.5**	**-20.9**	**-15.2**	**-4.3**	**5.6**	Averaged climate normals of Hay River and Yellowknife Stations (see Table 4 for details)
Athabasca	-10.0	**-17.9**	**-21.0**	**-18.4**	**-11.7**	**-0.9**	**7.9**	Climate normals of Fort Chipewyan A Station (see Table 5 for details)
Winnipeg	-6.4	**-15.1**	**-19.0**	**-16.4**	**-8.6**	**1.2**	9.0	Averaged climate normals of Norway House and Gimli Stations (see Table 6 for details)
Superior	-6.0	-13.4	**-16.5**	**-14.2**	**-8.3**	**0.6**	8.5	Climate normals of Wawa Station (see Table 7 for details)
Huron	3.3	-2.0	**-5.6**	**-5.2**	**-0.6**	**5.7**	12.1	Climate normals of Sarnia Station (see Table 8 for details)
Erie	**5.2**	**-0.4**	**-3.6**	**-2.6**	2.4	8.8	15.3	Climate normals of Windsor Station (see Table 9 for details)

Table 26: Rainfall climate normal for all lakes of this study during the ice-covered period (FUE-BUS) (Environment Climate Change Canada, 2023)

Note: Values red-blue scale (red = lowest value, blue = highest value; intensity reflects magnitude per lake). Bolded values represent the months specifically evaluated in surface temperature assessment for each lake.

RAINFALL (mm)								
LAKE	Nov	Dec	Jan	Feb	Mar	Apr	May	Notes
Great Bear	*0.2*	**0.0**	**0.1**	**0.0**	**0.2**	**0.8**	**12.2**	Averaged climate normals of Norman Wells and Deline Stations (see Table 3 for details)
Great Slave	*0.7*	**0.2**	**0.2**	**0.1**	**0.3**	**3.4**	**14.2**	Averaged climate normals of Hay River and Yellowknife Stations (see Table 4 for details)
Athabasca	*0.4*	**0.2**	**0.3**	**0.1**	**0.2**	**6.2**	**24.5**	Climate normals of Fort Chipewyan A Station (see Table 5 for details)
Winnipeg	*2.2*	**0.4**	**0.2**	**1.1**	**4.5**	**9.0**	53.8	Averaged climate normals of Norway House and Gimli Stations (see Table 6 for details)
Superior	*0.8*	0.3	**0.3**	**0.2**	**0.3**	**3.9**	16.2	Climate normals of Wawa Station (see Table 7 for details)
Huron	*68.2*	39.0	**29.0**	**26.8**	**34.1**	**70.6**	88.1	Climate normals of Sarnia Station (see Table 8 for details)
Erie	**70.6**	**47.2**	**39.1**	**34.3**	50.9	86.5	97.7	Climate normals of Windsor Station (see Table 9 for details)

Chapter 5
Conclusion

5.1 Summary of Findings

Lakes and lake ice are essential components of the climatic system due to their interrelated relationship with the surface energy balance (SEB) as both influence and respond to changes in each other (Belward et al., 2016; Global Climate Observing System, 2022; Brown & Duguay, 2010; Brown, 2012; Leppäranta, 2015; Notaro et al., 2013). Lake ice formation and melt respond to changes in energy fluxes (notably radiative and turbulent), allowing lake ice processes to serve as integrated indicators of net heat gain and loss (Liston & Hall, 1995). Lakes and lake ice also modify surface fluxes of heat, moisture and momentum, strongly influencing the atmospheric boundary layer which is intrinsically connected to the SEB (Mironov, 2008).

The strong coupling between the SEB and lake ice underscores the importance of including lake ice in climate/weather models to produce accurate simulations. The inclusion of lakes in climate models has been shown to reduce forecast errors in all seasons, but particularly in spring/summer (Bates et al., 1993; Bonan, 1995; Hostetler et al., 1993). The accuracy of air temperature estimates across all seasons is improved by delaying seasonal shifts through representation of the lake thermal effect (Balsamo et al., 2012; Bonan, 1995; Martynov et al., 2012). Despite the known importance of lake ice inclusion, there are currently few evaluations of the lake component within ERA5-Land, a widely used reanalysis product.

This thesis, therefore, evaluates and quantifies ERA5-Land's proficiency in estimating lake ice conditions. Estimates of lake ice fraction, timing and surface temperature were compared to satellite-derived observations. Biases were quantified through MBE and MAE, providing the direction and average magnitude of bias, respectively. Additionally, to assess ERA5-Land's proficiency at capturing spatial patterns of lake ice fraction and timing, a spatial assessment was conducted and presented using choropleth maps to depict areas of highest and lowest agreement.

The findings show an overall overestimation of lake ice fraction during both freeze-up and break-up. During freeze-up, ERA5-Land initiates FUS and FUE earlier than satellite observations, while during break-up, ERA5-Land initiates BUS later and BUE earlier. During the ice-covered period (FUE to BUS), nighttime surface temperatures generally display a consistent warm bias

whereas daytime shows weaker warm bias for the northern lakes and cold bias for the Laurentian Great Lakes.

These findings confirm that the known limitations of FLake persist within ERA5-Land's implementation of the model, namely

- optimization for medium-depth lakes (Munoz-Sabater et al., 2021)
- inability to produce partial ice coverage (Martynov et al., 2012; Mironov et al., 2010)
- omission of snow cover on lake ice (Dutra et al., 2009; Martynov et al., 2012).

The influence of these limitations on each assessment (lake ice timing, fraction, and temperature) is provided below, followed by other considerations that may influence the biases.

The optimization for medium-depth lakes is most apparent during freeze-up as depth strongly controls the timing of freeze-up (Korhonen, 2006). This is reflected in the pattern of rapid lake ice fraction growth produced by ERA5-Land across all lakes which is an expected pattern for medium depth lakes. As a result, shallow lakes such as Lake Winnipeg and Lake Erie (shallowest out of the Laurentian Great Lakes) exhibit lower lake ice fraction bias during freeze-up.

The inability to represent partial ice coverage is due to the use of a false bottom (~40-60 m) (Martynov et al., 2012; Mironov et al., 2010), which results in persistent high overestimation of lake ice fraction for lakes that rarely produce full ice cover. This overestimation was observed for the Laurentian Great Lakes, with Lake Superior producing the highest overestimation because it typically experiences low to moderate ice cover. Additionally, the full ice cover assumption contributes to the daytime cold surface temperature biases in the Laurentian Great Lakes. Because MOD11C1 incorporates warmer open water pixels which elevates the observed lake-wide surface temperature, while ERA5-Land only captures lake ice temperature, which leads to a cold bias when compared to MOD11C1.

The last limitation of FLake is the omission of snow cover on top of lake ice, failing to consider the interaction between snow and lake ice, specifically the insulation effect of snow, which has a significant influence on ice thickness and break-up. During break-up, snow's high albedo reduces heat absorption at the ice surface by reflecting solar radiation (Leppäranta, 2015; Kirillin et al., 2012; Woolway et al., 2020). Because ERA5-Land does not account for this cooling effect, its surface temperatures remain warmer than observations, producing a warm surface temperature bias,

particularly in the northern lakes during months of heavy snowfall. Additionally, the snow cover omission fails to consider that presence of snow on ice slows ice growth due to its low thermal conductivity (Adams & Roulet, 1980; Prowse et al., 2011; Sturm et al., 1997). Thus, the omission of snow cover likely causes ice thickness to continuously increase and produce thicker lake ice. The increased thickness in lake ice contributes to the delay in BUS while the warm bias would contribute to the accelerated melt.

While biases observed within this thesis are linked to the known limitations of FLake, bias outside of the lake parameterization of ERA5-Land was also considered as lakes are also influenced by climatic variables, notably air temperature but also freezing rain. However, air temperature was not directly evaluated within this thesis and there are limited evaluations of ERA5-Land's air temperature. But, the predecessor, ERA5, which provides atmospheric forcing to ERA5-Land has been found to have a warm air temperature bias. While all seasons show a warm bias, the warm bias is highest in the cold season and lowest in the warm season (Betts et al., 2019; Wang et al., 2019; Yu et al., 2021). Potentially, this bias was carried over into ERA5-Land, likely at a lower magnitude which would contribute to ERA5-Land's accelerated melt. On the other hand, freezing rain is not a significant consideration as its influence is not prevalent in all lakes and there are more significant influences (air temperature, lake depth, albedo, snow, etc.). But freezing rain is a potential contributor to why Lake Erie demonstrates similar MAE to Superior and Huron, despite the main contributor of cold bias in these lakes being overestimation of lake ice fractions which is lowest for Lake Erie. Thus, Lake Erie should have lower cold bias but that is not what occurred, which suggests there is another contributor to the observed warmer temperatures such as freezing rain. As brief events of freezing rain and warming air temperatures have been observed to produce rapid warming of the lake ice surface (Gould et al., 2005). Overall, while the limitations of FLake appear to significantly contribute to the observed biases, air temperature bias is a consideration and to a lesser extent freezing rain.

5.2 Limitations

Since ERA5-Land does not directly provide lake ice fraction or timing, these variables were derived from lake ice thickness using 10, 20, and 50 mm thresholds, with increased focus on the 50 mm threshold. The use of these thresholds is reasonable because the sensors used in IMS, CIS and NOAA (AVHRR and SAR) can detect very thin ice (few millimeters thick). However, these satellite

products rely on visual interpretation, so it is unknown whether the thresholds correspond closely to the ice detection within the satellite-derived products.

The satellite-derived products used (IMS, CIS, NOAA and MOD11C1) contain several limitations which are subjectivity of visual interpretation, data availability constraints and spatial resolution errors. Human errors arise in IMS, CIS and NOAA because they all rely on visual interpretation of imagery, which introduces subjectivity and affects both reliability and accuracy (Helfrich et al., 2018; Howell et al., 2009; Yang et al., 2020). Data availability constraints affect every product, but additional constraints also apply. For IMS, availability is partially dependent on IRDL/ENVI licensing (Helfrich et al., 2018). For NOAA, inconsistent frequency of ice reports from CIS and UNSIC produce inconsistent data availability between 1973 and 2010 (Yang et al., 2020). For MOD11C1, data are restricted to clear-sky conditions (Wan, 1999).

All satellite-derived products are subject to spatial error, notably the mixed-pixel effect (and potentially unresolved cloud contamination in MOD11C1), but the severity varies with resolution. NOAA and CIS have finer resolution (AVHRR = 1.1/4 km and SAR = 8-100 meters), which makes it less affected by the mixed-pixel effect compared to IMS (4 km) and MOD11C1 (5 km). However, all products were compared to ERA5-Land's 9 km grid using nearest-pixel matching, which can introduce representativeness errors due to differences in pixel area and distance.

5.3 Future Work

To further assess ERA5-Land's lake ice parameterization, several additional evaluations could provide valuable insight into the sources of error, specifically, air temperature, albedo and lake ice thickness. Air temperature influences both break-up and freeze-up, particularly freeze-up, thus could help explain the cause of overestimation of lake ice fraction and early timing of ice formation. On the other hand, break-up is strongly influenced by snow cover with lake ice thickness contributing to a lesser extent. Currently, albedo within ERA5-Land does not consider snow, thus evaluating the magnitude of bias would clarify its significance and influence on lake ice fraction and break-up timing. While lake ice thickness bias determines the duration of melt, therefore it would provide insight into the timing biases observed during break-up.

Several potential improvements to ERA5-Land could aid in correcting or offsetting the biases observed. Notably the inclusion of snow cover and partial ice cover parameterization. Partial ice cover could be represented by using historical lake information of annual/seasonal peak ice fractions

and the corresponding air temperature to train the model for the lakes that typically experience partial ice cover. Alternatively, or in conjunction with the training data, the criteria of freeze-up could be adjusted based on lake depth. Because ERA5-Land already includes lake depth information, this variable could be used to allow ERA5-Land to represent partial ice coverage. For example, deep lake pixels could be assigned lower freezing thresholds, since these areas require much colder temperature to freeze. Snow cover parameterization could be added using the existing snowfall estimate of ERA5, modulated by surface temperature and wind speed. Although freezing rain has a weaker influence on lake ice (compared to snow cover, lake depth, ice fraction, etc.), it could be included in the lake parameterization by extending the existing frozen precipitation parameterization to capture its occasional influence on lake ice temperature. Together, these improvements would improve ERA5-Land's ability to simulate lake ice processes and reduce the key biases identified in this study.

References

ACIA. (2004). *Impacts of a warming Arctic: Arctic climate impact assessment*. Cambridge Univ. Press.

Adams, W. P. (1976). Diversity of lake cover and its implications. *Musk-Ox*, *18*, 86–98.

Adams, W. P., & Roulet, N. T. (1980). Illustration of the roles of snow in the evolution of the winter cover of a lake. *Arctic*, *33*, 100–116.

Adrian, R., O'Reilly, C. M., Zagarese, H., Baines, S. B., Hessen, D. O., Keller, W., Livingstone, D. M., Sommaruga, R., Straile, D., Van Donk, E., Weyhenmeyer, G. A., & Winder, M. (2009). Lakes as sentinels of climate change. *Limnology and Oceanography*, *54*(6part2), 2283–2297. https://doi.org/10.4319/lo.2009.54.6_part_2.2283

Arp, C. D., Jones, B. M., Liljedahl, A. K., Hinkel, K. M., & Welker, J. A. (2015). Depth, ice thickness, and ice-out timing cause divergent hydrologic responses among Arctic lakes. *Water Resources Research*, *51*(12), 9379–9401. https://doi.org/10.1002/2015WR017362

Ashton, G. D. (1986). *River and Lake Ice Engineering*. Water Resources Publications. https://books.google.ca/books?id=xglYVjAsnt8C

Assel, R. A. (1983). *Great Lakes Ice Atlas*. US Department of Commerce, National Oceanic and atmospheric Administration. https://books.google.ca/books?id=uRi4nQAACAAJ

Balsamo, G. (2013). *Interactive lakes in the Integrated Forecasting System*. https://doi.org/10.21957/RFFV1GIR

Balsamo, G., Salgado, R., Dutra, E., Boussetta, S., Stockdale, T., & Potes, M. (2012). On the contribution of lakes in predicting near-surface temperature in a global weather forecasting model. *Tellus A: Dynamic Meteorology and Oceanography*, *64*(1), 15829. https://doi.org/10.3402/tellusa.v64i0.15829

Bates, G. T., Giorgi, F., & Hostetler, S. W. (1993). Toward the Simulation of the Effects of the Great Lakes on Regional Climate. *Monthly Weather Review*, *121*(5), 1373–1387. https://doi.org/10.1175/1520-0493(1993)121%253C1373:TTSOTE%253E2.0.CO;2

Beck, H. E., Zimmermann, N. E., McVicar, T. R., Vergopolan, N., Berg, A., & Wood, E. F. (2018). Present and future Köppen-Geiger climate classification maps at 1-km resolution. *Scientific Data*, *5*(1), 180214. https://doi.org/10.1038/sdata.2018.214

Belward, A., Bourassa, M., Dowell, M., Briggs, S., Dolman, H., Holmlund, K., & Verstraete, M. (2016). The Global Observing System for Climate: Implementation Needs. *The Global Observing System for Climate*.

Bengtsson, L. (1986). *Spatial Variability of Lake Ice Covers*. *68*, 113–121. https://doi.org/10.1080/04353676.1986.11880164

Bennett, R. M., Card, J. R., & Hornby, D. M. (1973). HYDROLOGY OF LAKE ATHABASCA: PAST, PRESENT AND FUTURE. *Hydrological Sciences Bulletin*, *18*(3), 337–345. https://doi.org/10.1080/02626667309494045

Bernhardt, J., Engelhardt, C., Kirillin, G., & Matschullat, J. (2012). Lake ice phenology in Berlin-Brandenburg from 1947–2007: Observations and model hindcasts. *Climatic Change*, *112*(3–4), 791–817. https://doi.org/10.1007/s10584-011-0248-9

Betts, A. K., Reid, D., & Crossett, C. (2020). Evaluation of the FLake Model in ERA5 for Lake Champlain. *Frontiers in Environmental Science*, *8*, 609254. https://doi.org/10.3389/fenvs.2020.609254

Bilello, M. A., Research, C. R., & Laboratory (U.S.), E. (1980). *Maximum Thickness and Subsequent Decay of Lake, River, and Fast Sea Ice in Canada and Alaska*. U.S. Army, Corps of Engineers, Cold Regions Research and Engineering Laboratory. https://books.google.ca/books?id=dg00en300uIC

Bonan, G. B. (1995). Sensitivity of a GCM Simulation to Inclusion of Inland Water Surfaces. *Journal of Climate*, *8*(11), 2691–2704. https://doi.org/10.1175/1520-0442(1995)008%253C2691:SOAGST%253E2.0.CO;2

Brown, L. (2012). *Modelling lake ice cover under contemporary and future climate conditions*.

Brown, L. (2017, June). Lake ice monitoring. In *Canadian Cryospheric Information Network*. https://ccin.ca/ccw/lakeice/current/monitoring

Brown, L., & Duguay, C. (2010). The response and role of ice cover in lake-climate interactions. *Progress in Physical Geography: Earth and Environment*, *34*(5), 671–704. https://doi.org/10.1177/0309133310375653

Brown, L., & Duguay, C. (2012). Modelling Lake Ice Phenology with an Examination of Satellite-Detected Subgrid Cell Variability. *Advances in Meteorology*, *2012*, 1–19. https://doi.org/10.1155/2012/529064

CEC, C. for E. (2021). Climate zones of North America. In *Commission for Environmental Cooperation*. https://www.cec.org/north-american-environmental-atlas/climate-zones-of-north-america

Changnon Jr, S. A., & Jones, D. M. (1972). Review of the influences of the Great Lakes on weather. *Water Resources Research*, *8*(2), 360–371.

Changnon, S. A., & Jones, D. M. A. (1972). Review of the influences of the Great Lakes on weather. *Water Resources Research*, *8*(2), 360–371. https://doi.org/10.1029/WR008i002p00360

Cheng, B., Vihma, T., Rontu, L., Kontu, A., Pour, H. K., Duguay, C., & Pulliainen, J. (2014). Evolution of snow and ice temperature, thickness and energy balance in Lake Orajärvi, northern Finland. *Tellus A: Dynamic Meteorology and Oceanography*, *66*(1), 21564. https://doi.org/10.3402/tellusa.v66.21564

Cicek, N., Lambert, S., Venema, H. D., Snelgrove, K. R., Bibeau, E. L., & Grosshans, R. (2006). Nutrient removal and bio-energy production from Netley-Libau Marsh at Lake Winnipeg through annual biomass harvesting. *Biomass and Bioenergy*, *30*(6), 529–536. https://doi.org/10.1016/j.biombioe.2005.12.009

Colbeck, S. C. (1987). Snow Metamorphism and Classification. In H. G. Jones & W. J. Orville-Thomas (Eds.), *Seasonal Snowcovers: Physics, Chemistry, Hydrology* (pp. 1–35). Springer Netherlands. https://doi.org/10.1007/978-94-009-3947-9_1

Connan-McGinty, S., Banas, N. S., Berge, J., Cottier, F., Grant, S., Johnsen, G., Kopec, T. P., Porter, M., & McKee, D. (2022). Midnight Sun to Polar Night: A Model of Seasonal Light in the Barents Sea. *Journal of Advances in Modeling Earth Systems*, *14*(10), e2022MS003198. https://doi.org/10.1029/2022MS003198

Curry, J. A., Schramm, J. L., & Ebert, E. E. (1993). Impact of clouds on the surface radiation balance of the Arctic Ocean. *Meteorology and Atmospheric Physics*, *51*(3–4), 197–217. https://doi.org/10.1007/BF01030494

Dallosch, M. A. (2024). Assessment of Drivers of Algal Biomass in North American Great Lakes via Satellite Remote Sensing. *University of Waterloo*.

Duguay, C. R., Prowse, T. D., Bonsal, B. R., Brown, R. D., Lacroix, M. P., & Ménard, P. (2006). Recent trends in Canadian lake ice cover. *Hydrological Processes*, *20*(4), 781–801. https://doi.org/10.1002/hyp.6131

Dutra, E., Stepanenko, V. M., Balsamo, G., Viterbo, P., Miranda, P. M. A., Mironov, D., & Schär, C. (2009). *An offline study of the impact of lakes on the performance of the ECMWF surface scheme*. *15*.

Eerola, K., Rontu, L., Kourzeneva, E., & Shcherbak, E. (2009). *A study on effects of lake temperature and ice cover in*. *15*.

Efremova, T. V., & Pal'shin, N. I. (2011). Ice phenomena terms on the water bodies of Northwestern Russia. *Russian Meteorology and Hydrology*, *36*(8), 559–565. https://doi.org/10.3103/S1068373911080085

Environment Climate Change Canada. (2023). *Canadian Climate Normals*. Government of Canada. https://climate.weather.gc.ca/climate_normals/index_e.html

Environment Climate Change Canada. (2024). *Lake Winnipeg Water Quality—Ice Cores*. Government of Canada. https://data-donnees.az.ec.gc.ca/data/sites/areainterest/lake-winnipeg-basin-initiative/lake-winnipeg-water-quality-ice-cores?lang=en

Environmental Protection Agency. (2025). Lake Superior. In *EPA*. Environmental Protection Agency. https://www.epa.gov/greatlakes/lake-superior

European Centre for Medium-Range Weather Forecasts. (2018). *IFS DOCUMENTATION – Cy45r1 PART IV: PHYSICAL PROCESSES*. European Centre for Medium-Range Weather Forecasts. https://www.ecmwf.int/en/elibrary/80895-ifs-documentation-cy45r1-part-iv-physical-processeshttps://www.ecmwf.int/en/elibrary/80895-ifs-documentation-cy45r1-part-iv-physical-processes

Evans, M. S. (2000). The large lake ecosystems of northern Canada. *Aquatic Ecosystem Health & Management*, *3*(1), 65–79. https://doi.org/10.1080/14634980008656992

Fujisaki, A., Wang, J., Hu, H., Schwab, D. J., Hawley, N., & Rao, Y. R. (2012). A modeling study of ice–water processes for Lake Erie applying coupled ice-circulation models. *Journal of Great Lakes Research*, *38*(4), 585–599. https://doi.org/10.1016/j.jglr.2012.09.021

Garrett, A. J., Casterline, M., & Salvaggio, C. (2010). *Thermodynamics of partially frozen cooling lakes* (R. B. Dinwiddie & M. Safai, Eds.; p. 766105). https://doi.org/10.1117/12.849349

Gibson, J. J., Prowse, T. D., & Peters, D. L. (2006). Hydroclimatic controls on water balance and water level variability in Great Slave Lake. *Hydrological Processes*, *20*(19), 4155–4172. https://doi.org/10.1002/hyp.6424

Global Climate Observing System. (2022). *The 2022 GCOS Implementation Plan*.

Gould, M., & Jeffries, M. (2005). Temperature variations in lake ice in central Alaska, USA. *Annals of Glaciology*, *40*, 89–94. https://doi.org/10.3189/172756405781813825

Gray, D. M., & Male, D. H. (1981). *Handbook of Snow: Principles, Processes, Management & Use*. New York. https://books.google.ca/books?id=5OMsAQAAMAAJ

Haapala, J., & Lepparanta, M. (1997). The Baltic Sea ice season in changing climate. *Boreal Environment Research*, 93–108.

Helfrich, S., Li, M., Kongoli, C., Nagdimunov, L., & Rodriguez, E. (2018). *IMS ALGORITHM THEORETICAL BASIS DOCUMENT VERSION 2.4*.

Heron, R., & Woo, M.-K. (1994). Decay of a High Arctic lake-ice cover: Observations and modelling. *Journal of Glaciology*, *40*(135), 283–292. https://doi.org/10.3189/S0022143000007371

Hewitt, B., Lopez, L., Gaibisels, K., Murdoch, A., Higgins, S., Magnuson, J., Paterson, A., Rusak, J., Yao, H., & Sharma, S. (2018). Historical Trends, Drivers, and Future Projections of Ice Phenology in Small North Temperate Lakes in the Laurentian Great Lakes Region. *Water*, *10*(1), 70. https://doi.org/10.3390/w10010070

Hicks, F., Cui, W., & Ashton, G. D. (2008). Heat transfer and ice cover decay. *River Ice Breakup*, 67–123.

Hoffman, P. F. (1987). Continental transform tectonics: Great Slave Lake shear zone (ca. 1.9 Ga), northwest Canada. *Geology*, *15*(9), 785. https://doi.org/10.1130/0091-7613(1987)15%253C785:CTTGSL%253E2.0.CO;2

Hostetler, S. W., Bates, G. T., & Giorgi, F. (1993). Interactive coupling of a lake thermal model with a regional climate model. *Journal of Geophysical Research: Atmospheres*, *98*(D3), 5045–5057. https://doi.org/10.1029/92JD02843

Howell, S. E. L., Brown, L. C., Kang, K.-K., & Duguay, C. R. (2009). Variability in ice phenology on Great Bear Lake and Great Slave Lake, Northwest Territories, Canada, from SeaWinds/QuikSCAT: 2000–2006. *Remote Sensing of Environment*, *113*(4), 816–834. https://doi.org/10.1016/j.rse.2008.12.007

Hutchinson, G. E., & Löffler, H. (1956). THE THERMAL CLASSIFICATION OF LAKES. *Proceedings of the National Academy of Sciences*, *42*(2), 84–86. https://doi.org/10.1073/pnas.42.2.84

International Lake Environment Committee. (n.d.). List of lakes: World Lake Database—ILEC. In *World Lake Database: International Lake Environment Committee Foundation (ILEC)*. https://wldb.ilec.or.jp/Lake/NAM-270

Jakkila, J., Leppäranta, M., Kawamura, T., Shirasawa, K., & Salonen, K. (2009). Radiation transfer and heat budget during the ice season in Lake Pääjärvi, Finland. *Aquatic Ecology*, *43*(3), 681–692. https://doi.org/10.1007/s10452-009-9275-2

Jeffries, M. O., & Morris, K. (2007). Some aspects of ice phenology on ponds in central Alaska, USA. *Annals of Glaciology*, *46*, 397–403. https://doi.org/10.3189/172756407782871576

Jeffries, M. O., Morris, K., & Kozlenko, N. (2013). Ice Characteristics and Processes, and Remote Sensing of Frozen Rivers and Lakes. In C. R. Duguay & A. Pietroniro (Eds.), *Geophysical Monograph Series* (pp. 63–90). American Geophysical Union. https://doi.org/10.1029/163GM05

Kheyrollah Pour, H. (2011). *On the Use of MODIS for Lake and Land Surface Temperature Investigations in the Regions of Great Bear Lake and Great Slave Lake, N.W.T.* University of Waterloo.

Kheyrollah Pour, H., Duguay, C. R., Martynov, A., & Brown, L. C. (2012). Simulation of surface temperature and ice cover of large northern lakes with 1-D models: A comparison with MODIS satellite data and *in situ* measurements. *Tellus A: Dynamic Meteorology and Oceanography*, *64*(1), 17614. https://doi.org/10.3402/tellusa.v64i0.17614

Kirillin, G., & Leppäranta, M. (2022). Lake Ice Formation and Melt. Under-Ice Dynamics. In *Encyclopedia of Inland Waters* (pp. 534–545). Elsevier. https://doi.org/10.1016/B978-0-12-819166-8.00003-7

Kirillin, G., Leppäranta, M., Terzhevik, A., Granin, N., Bernhardt, J., Engelhardt, C., Efremova, T., Golosov, S., Palshin, N., Sherstyankin, P., Zdorovennova, G., & Zdorovennov, R. (2012). Physics of seasonally ice-covered lakes: A review. *Aquatic Sciences*, *74*(4), 659–682. https://doi.org/10.1007/s00027-012-0279-y

Korhonen, J. (2006). Long-term changes in lake ice cover in Finland*. *Hydrology Research*, *37*(4–5), 347–363. https://doi.org/10.2166/nh.2006.019

Leconte, R., Chaouch, N., Temimi, M., Brissette, F., & Toussaint, T. (2008). *Cold region atmospheric and hydrologic studies: The Mackenzie GEWEX experience*. Springer.

Leconte, R., Pietroniro, A., Peters, D. L., & Prowse, T. D. (2001). Effects of flow regulation on hydrologic patterns of a large, inland delta. *Regulated Rivers: Research & Management*, *17*(1), 51–65. https://doi.org/10.1002/1099-1646(200101/02)17:1%253C51::AID-RRR588%253E3.0.CO;2-V

Leppäranta, M. (2009). Modelling the Formation and Decay of Lake Ice. In G. George (Ed.), *The Impact of Climate Change on European Lakes* (pp. 63–83). Springer Netherlands. https://doi.org/10.1007/978-90-481-2945-4_5

Leppäranta, M. (2015). *Freezing of Lakes and the Evolution of their Ice Cover*. Springer Berlin Heidelberg. https://doi.org/10.1007/978-3-642-29081-7

Leppäranta, M., Lindgren, E., Wen, L., & Kirillin, G. (2019). Ice cover decay and heat balance in Lake Kilpisjärvi in Arctic tundra: Ice decay in Lake Kilpisjärvi. *Journal of Limnology*, *78*(2). https://doi.org/10.4081/jlimnol.2019.1879

Lewis, C. F. M., Paul F. Karrow, Stefan M. Blasco, Francine M. G. McCarthy, John W. King, Theodore C. Moore, & David K. Rea. (2008). Evolution of lakes in the Huron basin: Deglaciation to present. *Aquatic Ecosystem Health & Management*, *11*(2), 127–136. https://doi.org/10.1080/14634980802095263

Li, X., Peng, S., Xi, Y., Woolway, R. I., & Liu, G. (2022). Earlier ice loss accelerates lake warming in the Northern Hemisphere. *Nature Communications*, *13*(1), 5156. https://doi.org/10.1038/s41467-022-32830-y

Lindenschmidt, K.-E., Baulch, H., & Cavaliere, E. (2018). River and Lake Ice Processes—Impacts of Freshwater Ice on Aquatic Ecosystems in a Changing Globe. *Water*, *10*(11), 1586. https://doi.org/10.3390/w10111586

Liston, G. E., & Hall, D. K. (1995). An energy-balance model of lake-ice evolution. *Journal of Glaciology*, *41*(138), 373–382. https://doi.org/10.3189/S0022143000016245

Livingstone, D. M. (2000). Large-scale climatic forcing detected in historical observations of lake ice break-up. *SIL Proceedings, 1922-2010*, *27*(5), 2775–2783. https://doi.org/10.1080/03680770.1998.11898171

Lofgren, B. M. (1997). Simulated Effects of Idealized Laurentian Great Lakes onRegional and Large-Scale Climate*. *Journal of Climate*, *10*(11), 2847–2858. https://doi.org/10.1175/1520-0442(1997)010%253C2847:SEOILG%253E2.0.CO;2

Lofgren, B. M., & Zhu, Y. (2000). Surface Energy Fluxes on the Great Lakes Based on Satellite-Observed Surface Temperatures 1992 to 1995. *Journal of Great Lakes Research*, *26*(3), 305–314. https://doi.org/10.1016/S0380-1330(00)70694-0

Magnuson, J. J., Robertson, D. M., Benson, B. J., Wynne, R. H., Livingstone, D. M., Arai, T., Assel, R. A., Barry, R. G., Card, V., Kuusisto, E., Granin, N. G., Prowse, T. D., Stewart, K. M., & Vuglinski, V. S. (2000). Historical Trends in Lake and River Ice Cover in the Northern Hemisphere. *Science*, *289*(5485), 1743–1746. https://doi.org/10.1126/science.289.5485.1743

Marcé, R., Gómez-Gener, L., & Carey, C. C. (2024). Chapter 11—Oxygen. In I. D. Jones & J. P. Smol (Eds.), *Wetzel's Limnology (Fourth Edition)* (pp. 237–274). Academic Press. https://doi.org/10.1016/B978-0-12-822701-5.00011-2

Martynov, A., Sushama, L., Laprise, R., Winger, K., & Dugas, B. (2012). Interactive lakes in the Canadian Regional Climate Model, version 5: The role of lakes in the regional climate of North America. *Tellus A: Dynamic Meteorology and Oceanography*, *64*(1), 16226. https://doi.org/10.3402/tellusa.v64i0.16226

Matthias, V., Dörnbrack, A., & Stober, G. (2016). The extraordinarily strong and cold polar vortex in the early northern winter 2015/2016. *Geophysical Research Letters*, *43*(23). https://doi.org/10.1002/2016GL071676

Ménard, P., Duguay, C. R., Flato, G. M., & Rouse, W. R. (2002). Simulation of ice phenology on Great Slave Lake, Northwest Territories, Canada. *Hydrological Processes*, *16*(18), 3691–3706. https://doi.org/10.1002/hyp.1230

Michel, B., & Ramseier, R. O. (1971). Classification of river and lake ice. *Canadian Geotechnical Journal*, *8*(1), 36–45. https://doi.org/10.1139/t71-004

Milewska, E., & Hogg, W. D. (2001). Spatial representativeness of a long-term climate network in Canada. *Atmosphere-Ocean*, *39*(2), 145–161. https://doi.org/10.1080/07055900.2001.9649671

Mironov, D. (2005). *Parameterization of Lakes in Numerical Weather Prediction. Part 1: Description of a Lake Model*. http://www.cosmo-model.org/content/model/documentation/techReports/docs/techReport11.pdf

Mironov, D. (2008). *COSMO Technical Report No. 11: Parameterization of Lakes in Numerical Weather Prediction. Description of a Lake Model*. https://doi.org/10.5676/DWD_PUB/NWV/COSMO-TR_11

Mironov, D., Heise, E., Kourzeneva, E., Ritter, B., Schneider, N., & Terzhevik, A. (2010). *Implementation of the lake parameterisation scheme FLake into the numerical weather prediction model COSMO*. *15*.

Mironov, D., Ritter, B., Schulz, J.-P., Buchhold, M., Lange, M., & Machulskaya, E. (2012). Parameterisation of sea and lake ice in numerical weather prediction models of the German Weather Service. *Tellus A: Dynamic Meteorology and Oceanography*, *64*(1), 17330. https://doi.org/10.3402/tellusa.v64i0.17330

Mitchell, P., & Prepas, E. E. (1990). *Atlas of Alberta Lakes*. University of Alberta Press. https://books.google.ca/books?id=uPgDwqflBNsC

Moukomla, S. (1999). *THE ESTIMATION OF THE SURFACE ENERGY BALANCE OF THE NORTH AMERICAN LAURENTIAN GREAT LAKES USING SATELLITE REMOTE SENSING AND MERRA REANALYSIS*.

Mullen, P. C., & Warren, S. G. (1988). Theory of the optical properties of lake ice. *Journal of Geophysical Research: Atmospheres*, *93*(D7), 8403–8414. https://doi.org/10.1029/JD093iD07p08403

Muñoz Sabater, J. (2019). *ERA5-Land hourly data from 1950 to present* [Dataset]. Copernicus Climate Change Service (C3S) Climate Data Store (CDS). https://doi.org/10.24381/CDS.E2161BAC

Muñoz-Sabater, J., Dutra, E., Agustí-Panareda, A., Albergel, C., Arduini, G., Balsamo, G., Boussetta, S., Choulga, M., Harrigan, S., Hersbach, H., Martens, B., Miralles, D. G., Piles, M., Rodríguez-Fernández, N. J., Zsoter, E., Buontempo, C., & Thépaut, J.-N. (2021). ERA5-Land: A state-of-the-art global reanalysis dataset for land applications. *Earth System Science Data*, *13*(9), 4349–4383. https://doi.org/10.5194/essd-13-4349-2021

Nagarajan, B., Yau, M. K., & Schuepp, P. H. (2004). The effects of small water bodies on the atmospheric heat and water budgets over the MacKenzie River Basin. *Hydrological Processes*, *18*(5), 913–938. https://doi.org/10.1002/hyp.1338

National Snow and Ice Data Center. (n.d.). *Why it matters*. https://nsidc.org/learn/parts-cryosphere/snow/why-snow-matters

North American Ice Service. (n.d.). *Seasonal Summary Great Lakes Winter 2021-2022*. Government of Canada. https://publications.gc.ca/collections/collection_2022/eccc/En55-6-2022-eng.pdf

Notaro, M., Holman, K., Zarrin, A., Fluck, E., Vavrus, S., & Bennington, V. (2013). Influence of the Laurentian Great Lakes on Regional Climate*. *Journal of Climate*, *26*(3), 789–804. https://doi.org/10.1175/JCLI-D-12-00140.1

O'Reilly, C. M., Sharma, S., Gray, D. K., Hampton, S. E., Read, J. S., Rowley, R. J., Schneider, P., Lenters, J. D., McIntyre, P. B., Kraemer, B. M., Weyhenmeyer, G. A., Straile, D., Dong, B., Adrian, R., Allan, M. G., Anneville, O., Arvola, L., Austin, J., Bailey, J. L., … Zhang, G.

(2015). Rapid and highly variable warming of lake surface waters around the globe. *Geophysical Research Letters*, *42*(24). https://doi.org/10.1002/2015GL066235

Palecki, M. A., & Barry, R. G. (1986). Freeze-up and Break-up of Lakes as an Index of Temperature Changes during the Transition Seasons: A Case Study for Finland. *Journal of Climate and Applied Meteorology*, *25*(7), 893–902. https://doi.org/10.1175/1520-0450(1986)025%253C0893:FUABUO%253E2.0.CO;2

Palecki, M., Durre, I., Applequist, S., Arguez, A., & Lawrimore, J. (2021). *U.S. Climate Normals 2020: U.S. Hourly Climate Normals (1991–2020)*. NOAA National Centers for Environmental Information. https://doi.org/DOI

Palosuo, E. (1965). *Frozen slush on lake ice*. Geophysical Society of Finland.

Peel, M. C., Finlayson, B. L., & McMahon, T. A. (2007). Updated world map of the K¨oppen-Geiger climate classification. *Hydrol. Earth Syst. Sci.*

Peixoto, J. P., & Oort, A. H. (1993). *Physics of climate* (3. print). American Institute of Physics.

Prowse, T., Alfredsen, K., Beltaos, S., Bonsal, B., Duguay, C., Korhola, A., McNamara, J., Vincent, W. F., Vuglinsky, V., & Weyhenmeyer, G. A. (2011). Arctic Freshwater Ice and Its Climatic Role. *AMBIO*, *40*(S1), 46–52. https://doi.org/10.1007/s13280-011-0214-9

Rafferty, J. (2023, July 28). *World's largest lakes | Description, Area, & Facts | Britannica*. World's Largest Lakes. https://www.britannica.com/topic/worlds-largest-lakes-2228655

Ramón, C. L., Ulloa, H. N., Doda, T., Winters, K. B., & Bouffard, D. (2021). Bathymetry and latitude modify lake warming under ice. *Hydrology and Earth System Sciences*, *25*(4), 1813–1825. https://doi.org/10.5194/hess-25-1813-2021

Rosenzweig, C., Casassa, G., Karoly, D. J., Imeson, A., Rawlins, S., Root, T. L., Seguin, B., Tryjanowski, P., Abeku, T., Côté, I., Dyurgerov, M., Edwards, M., Ebi, K. L., Estrella, N., Forbes, D. L., Francou, B., Githeko, A., Gornitz, V., Haeberli, W., … Tryjanowski, P. (2007).

Assessment of observed changes and responses in natural and managed systems. *Climate Change 2007: Impacts, Adaptation and Vulnerability. Contribution of Working Group II to the Fourth Assessment Report of the Intergovernmental Panel on Climate Change*, 79–131.

Rouse, W. R., Blanken, P. D., Bussières, N., Walker, A. E., Oswald, C. J., Schertzer, W. M., & Spence, C. (2008). An Investigation of the Thermal and Energy Balance Regimes of Great Slave and Great Bear Lakes. *Journal of Hydrometeorology*, *9*(6), 1318–1333. https://doi.org/10.1175/2008JHM977.1

Rouse, W. R., Blanken, P. D., Eaton, A. K., Petrone, R. M., Schertzer, W. M., & Spence, C. (2000). Energy and water balance of high latitude surfaces. *MAGS: Final Reports and Proceedings, 6th Scientific Workshop for MAGS*, *1517*.

Rouse, W. R., Oswald, C. J., Binyamin, J., Spence, C., Schertzer, W. M., Blanken, P. D., Bussières, N., & Duguay, C. R. (2005). The Role of Northern Lakes in a Regional Energy Balance. *Journal of Hydrometeorology*, *6*(3), 291–305. https://doi.org/10.1175/JHM421.1

Rouse, W. R., Oswald, C. M., Binyamin, J., Blanken, P. D., Schertzer, W. M., & Spence, C. (2003). Interannual and Seasonal Variability of the Surface Energy Balance and Temperature of Central Great Slave Lake. *Journal of Hydrometeorology*, *4*(4), 720–730. https://doi.org/10.1175/1525-7541(2003)004%253C0720:iasvot%253E2.0.co;2

Schmid, M., & Read, J. (2022). Heat Budget of Lakes. In *Encyclopedia of Inland Waters* (pp. 467–473). Elsevier. https://doi.org/10.1016/B978-0-12-819166-8.00011-6

Scott, R. W., & Huff, F. A. (1996). Impacts of the Great Lakes on Regional Climate Conditions. *Journal of Great Lakes Research*, *22*(4), 845–863. https://doi.org/10.1016/S0380-1330(96)71006-7

Siles, G. L., & Leconte, R. (2023). Reservoir Ice Conditions from Multi-Sensor Remote Sensing and ERA5-Land: The Manicouagan Hydroelectric Reservoir Case Study. *Hydrology*, *10*(5), 108. https://doi.org/10.3390/hydrology10050108

Simojoki, H. (1940). *Über die Eisverhältnisse der binnenseen Finnlands....* https://books.google.ca/books?id=pHl2zwEACAAJ

Sledd, A., Shupe, M. D., Solomon, A., Cox, C. J., Perovich, D., & Lei, R. (2024). Snow thermal conductivity and conductive flux in the Central Arctic: Estimates from observations and implications for models. *Elem Sci Anth*, *12*(1), 00086. https://doi.org/10.1525/elementa.2023.00086

Stewart, K. M., & Magnuson, J. J. (2009). Ice. *Encyclopedia of Inland Waters*, *2*, 664–670. https://uwmadison.box.com/s/oauy4bw8qwbpnhxu6e5c3ahodl5dbrtu

Sturm, M., Holmgren, J., König, M., & Morris, K. (1997). The thermal conductivity of seasonal snow. *Journal of Glaciology*, *43*(143), 26–41. https://doi.org/10.3189/S0022143000002781

Tang, F., Chen, P., An, Z., Xiong, M., Chen, H., & Qiu, L. (2023). A Dual-Threshold Algorithm for Ice-Covered Lake Water Level Retrieval Using Sentinel-3 SAR Altimetry Waveforms. *Sensors*, *23*(24), 9724. https://doi.org/10.3390/s23249724

U.S. National Ice Center. (2008). *IMS Daily Northern Hemisphere Snow and Ice Analysis at 1 km, 4 km, and 24 km Resolutions, Version 1*. NSIDC. https://doi.org/10.7265/N52R3PMC

Walsh, S. E., Vavrus, S. J., Foley, J. A., Fisher, V. A., Wynne, R. H., & Lenters, J. D. (1998). Global patterns of lake ice phenology and climate: Model simulations and observations. *Journal of Geophysical Research: Atmospheres*, *103*(D22), 28825–28837. https://doi.org/10.1029/98JD02275

Wan, Z. (1999). *Contract Number: NAS5-31370*.

Wang, C., Graham, R. M., Wang, K., Gerland, S., & Granskog, M. A. (2019). Comparison of ERA5 and ERA-Interim near-surface air temperature, snowfall and precipitation over Arctic sea ice: Effects on sea ice thermodynamics and evolution. *The Cryosphere*, *13*(6), 1661–1679. https://doi.org/10.5194/tc-13-1661-2019

Wang, X., & Key, J. R. (2005). Arctic Surface, Cloud, and Radiation Properties Based on the AVHRR Polar Pathfinder Dataset. Part I: Spatial and Temporal Characteristics. *Journal of Climate*, *18*(14), 2558–2574. https://doi.org/10.1175/JCLI3438.1

Wetzel, R. G. (2001). *Limnology* (R. G. WETZEL, Ed.; Third Edition). Academic Press. https://doi.org/10.1016/C2009-0-02112-6

Williams, G. P. (1965). Correlating Freeze-Up and Break-Up with Weather Conditions. *Canadian Geotechnical Journal*, *2*(4), 313–326. https://doi.org/10.1139/t65-047

Williams, G. P. (1968). *Freeze-up and break-up of fresh water lakes*.

Woolway, R. I., Kraemer, B. M., Lenters, J. D., Merchant, C. J., O'Reilly, C. M., & Sharma, S. (2020). Global lake responses to climate change. *Nature Reviews Earth & Environment*, *1*(8), 388–403. https://doi.org/10.1038/s43017-020-0067-5

Yang, T.-Y., Kessler, J., Mason, L., Chu, P. Y., & Wang, J. (2020). A consistent Great Lakes ice cover digital data set for winters 1973–2019. *Scientific Data*, *7*(1), 259. https://doi.org/10.1038/s41597-020-00603-1

Yu, Y., Xiao, W., Zhang, Z., Cheng, X., Hui, F., & Zhao, J. (2021). Evaluation of 2-m Air Temperature and Surface Temperature from ERA5 and ERA-I Using Buoy Observations in the Arctic during 2010–2020. *Remote Sensing*, *13*(14), 2813. https://doi.org/10.3390/rs13142813

Zhao, J., Rao, Y. R., & Wassenaar, L. I. (2012). Numerical modeling of hydrodynamics and tracer dispersion during ice-free period in Lake Winnipeg. *Journal of Great Lakes Research*, *38*, 147–157. https://doi.org/10.1016/j.jglr.2011.02.005

Ziyad, J., Goïta, K., Magagi, R., Blarel, F., & Frappart, F. (2020). Improving the Estimation of Water Level over Freshwater Ice Cover using Altimetry Satellite Active and Passive Observations. *Remote Sensing*, *12*(6), 967. https://doi.org/10.3390/rs12060967

Appendix A - Missing and Filtered Data

Year	Total Missing Dates	Notes
2004	57	Missing dates: 01-01 to 02-25 and 11-13
2005	4	Missing dates: 02-11, 06-05, 07-05 and 10-12
2009	1	Missing Date: 03-27
2017	1	Missing Date: 11-04

Table A.1: Missing dates within IMS between 2004-2023

Date	Reason	Details
2006-06-14	Temporal redundancy; GBL: Quality	2006-06-14 was redundant of 2006-06-16 which fit the weekly interval better than filtered date GBL: Ice fraction abruptly dropped to 30%, inconsistent with surrounding values (the previous date was 90% and the following date was 70%)
2006-10-05	Temporal redundancy	2006-10-05 was redundant of 2006-10-06 which fit the weekly interval better than filtered date
2007-12-15	Temporal redundancy	2007-12-15 was redundant of 2007-12-14 which fit the weekly interval better than filtered date
2012-11-07	Quality	All lakes show abrupt jump in lake ice fraction, inconsistent with adjacent dates. Athabasca: increased to 70% despite the date prior was 10% and 20% the following date GBL: jumped to 100% despite 10% ice fraction prior and 20% the following date GSL: jumped to 95% despite 10% ice fraction prior and 25% the following date Winnipeg: jumped to 100% despite 0% ice fraction prior and after this date

Note: CIS represent Great Bear Lake (GBL), Great Slave Lake (GSL), Lake Athabasca and Lake Winnipeg

Table A.2: Filtered dates within CIS and explanation for filtering

Lake	Day Count	Night Count	Total Ice-Covered Days (2004-2023)
Great Bear Lake	353	165	4005
Great Slave Lake	168	159	3465
Lake Athabasca	224	193	3345
Lake Winnipeg	420	171	3245
Lake Huron	41	23	905
Lake Superior	46	31	1585
Lake Erie	82	40	525

Table A.3: Missing dates in MOD11C1 pre-filtering

Appendix B – Supplementary Lake Ice Fraction Figures and Tables

Year	*Break-up Start*	*Break-up End*	*Freeze-up Start*	*Freeze-up End*
2004	2004-06-04	2004-08-20	2004-09-17	2005-02-04
2005	2005-05-06	2005-08-05	2005-09-09	2006-01-27
2006	2006-04-28	2006-07-21	2006-09-22	2006-12-15
2007	2007-05-18	2007-08-03	2007-09-14	2007-12-21
2008	2008-05-16	2008-08-01	2008-09-26	2009-01-09
2009	2009-05-22	2009-08-15	2009-09-18	2010-01-15
2010	2010-04-16	2010-07-16	2010-09-24	2010-12-31
2011	2011-04-29	2011-07-29	2011-09-30	2012-01-06
2012	2012-05-11	2012-07-20	2012-09-21	2012-12-21
2013	2013-05-24	2013-07-26	2013-09-27	2014-01-24
2014	2014-05-16	2014-08-01	2014-09-12	2014-12-26
2015	2015-05-22	2015-07-24	2015-09-18	2016-01-01
2016	2016-05-13	2016-07-22	2016-09-16	2017-01-06
2017	2017-05-12	2017-07-21	2017-09-22	2017-12-22
2018	2018-05-25	2018-08-03	2018-08-31	2019-01-04
2019	2019-05-10	2019-08-02	2019-09-27	2019-12-20
2020				
2021	2021-05-28	2021-07-30	2021-09-24	2022-01-07
2022	2022-05-20	2022-07-29	2022-09-30	2023-01-06
2023	2023-05-19	2023-07-14		

Table B.1: Great Bear Lake freeze-up and break-up periods used in this study

Year	Break-up Start	Break-up End	Freeze-up Start	Freeze-up End
2004	2004-03-12	2004-07-30	2004-10-01	2005-01-28
2005	2005-04-15	2005-07-29	2005-10-07	2006-01-27
2006	2006-04-14	2006-06-30	2006-09-29	2007-01-05
2007	2007-04-20	2007-07-20	2007-10-12	2008-01-11
2008	2008-04-18	2008-08-01	2008-10-10	2009-01-02
2009	2009-04-17	2009-07-24	2009-09-25	2010-01-01
2010	2010-04-02	2010-07-09	2010-10-08	2010-12-31
2011	2011-04-29	2011-07-15	2011-10-14	2012-02-03
2012	2012-04-20	2012-06-29	2012-10-05	2013-01-11
2013	2013-04-05	2013-07-26	2013-10-11	2014-02-07
2014	2014-04-25	2014-07-11	2014-10-10	2015-01-16
2015	2015-04-03	2015-07-17	2015-10-09	2016-01-08
2016	2016-04-15	2016-07-01	2016-09-30	2017-01-27
2017	2017-05-05	2017-07-07	2017-10-13	2018-01-05
2018	2018-05-04	2018-07-13	2018-09-14	2018-12-28
2019	2019-04-19	2019-07-05	2019-10-11	2019-12-20
2020	2020-04-24	2020-07-17		
2021	2021-05-07	2021-07-16	2021-10-15	2022-01-07
2022	2022-05-13	2022-07-15	2022-10-07	2022-12-30
2023				

Table B.2: Great Slave Lake freeze-up and break-up periods used in this study

Year	Break-up Start	Break-up End	Freeze-up Start	Freeze-up End
2004	2004-03-26	2004-07-16	2004-10-01	2004-12-24
2005	2005-04-15	2005-07-01	2005-10-14	2006-01-27
2006	2006-03-31	2006-06-16	2006-09-22	2006-12-15
2007	2007-04-20	2007-06-29	2007-09-28	2007-12-14
2008	2008-04-25	2008-07-04	2008-10-10	2009-01-02
2009	2009-04-24	2009-07-17	2009-09-25	2010-01-01
2010	2010-04-09	2010-06-18	2010-10-08	2011-01-14
2011	2011-04-22	2011-07-01	2011-10-14	2012-01-20
2012	2012-04-06	2012-06-29	2012-10-12	2013-01-04
2013	2013-04-12	2013-07-05	2013-10-04	2014-01-17
2014	2014-05-09	2014-07-04	2014-10-10	2015-01-02
2015	2015-04-17	2015-06-26	2015-10-09	2016-01-01
2016	2016-04-15	2016-06-24	2016-09-30	2017-01-13
2017	2017-04-21	2017-06-23	2017-10-13	2017-12-22
2018	2018-04-20	2018-06-29	2018-09-14	2018-12-21
2019	2019-04-26	2019-07-05	2019-10-11	2020-01-03
2020	2020-05-01	2020-07-10		
2021	2021-04-30	2021-07-16	2021-10-08	2021-12-31
2022	2022-05-13	2022-07-15	2022-10-14	2022-12-23
2023	2023-04-21	2023-06-16		

Table B.3: Lake Athabasca freeze-up and break-up periods used in this study

Year	Break-up Start	Break-up End	Freeze-up Start	Freeze-up End
2004	2004-03-26	2004-06-25	2004-10-22	2004-12-31
2005	2005-03-25	2005-06-17	2005-10-28	2006-01-27
2006	2006-03-03	2006-06-02	2006-10-13	2007-01-12
2007	2007-04-13	2007-06-08	2007-10-19	2007-12-21
2008	2008-04-18	2008-06-20	2008-10-24	2008-12-26
2009	2009-03-27	2009-06-19	2009-10-16	2010-01-22
2010	2010-03-19	2010-06-11	2010-10-29	2010-12-31
2011	2011-04-22	2011-06-17	2011-10-21	2012-01-20
2012	2012-04-13	2012-06-01	2012-10-19	2012-12-21
2013	2013-04-12	2013-06-21	2013-10-25	2013-12-27
2014	2014-04-25	2014-06-27	2014-10-24	2014-12-12
2015	2015-04-03	2015-06-19	2015-10-30	2016-01-15
2016	2016-04-08	2016-06-10	2016-11-04	2017-01-06
2017	2017-03-31	2017-06-16	2017-10-13	2017-12-08
2018	2018-04-20	2018-06-22	2018-10-19	2018-12-14
2019	2019-04-19	2019-06-28	2019-10-11	2019-12-20
2020	2020-04-10	2020-06-19		
2021	2021-04-09	2021-06-18	2021-10-22	2022-01-07
2022	2022-04-22	2022-07-01	2022-10-21	2022-12-23
2023	2023-04-21	2023-06-16		

Table B.4: Lake Winnipeg freeze-up and break-up periods used in this study

Year	Break-up Start	Break-up End	Freeze-up Start	Freeze-up End
2004	2004-02-16	2004-05-21	2004-11-23	2005-03-20
2005	2005-03-14	2005-05-16	2005-11-16	2006-03-05
2006	2006-02-27	2006-05-08	2006-11-16	2007-03-11
2007	2007-03-05	2007-05-13	2007-11-20	2008-03-13
2008	2008-03-07	2008-05-23	2008-11-15	2009-03-05
2009	2009-02-27	2009-05-24	2009-11-28	2010-02-25
2010	2010-02-19	2010-05-02	2010-11-18	2011-04-05
2011	2011-03-30	2011-05-19	2011-11-16	2012-02-05
2012	2012-01-19	2012-05-05	2012-11-12	2013-02-20
2013	2013-02-14	2013-05-28	2013-11-10	2014-02-28
2014	2014-02-28	2014-06-05	2014-11-08	2015-03-03
2015	2015-02-25	2015-05-26	2015-11-20	2016-02-17
2016	2016-02-11	2016-05-11	2016-11-19	2017-03-07
2017	2017-03-01	2017-05-11	2017-11-05	2018-02-14
2018	2018-02-08	2018-05-23	2018-11-08	2019-03-11
2019	2019-03-05	2019-05-21	2019-10-30	2020-02-20
2020	2020-02-14	2020-05-20	2020-11-13	2021-02-22
2021	2021-02-16	2021-05-07	2021-11-17	2022-03-18
2022	2022-03-12	2022-05-19	2022-11-11	2023-02-27
2023	2023-02-21	2023-05-20		

Table B.5: Lake Superior freeze-up and break-up periods used in this study

Year	Break-up Start	Break-up End	Freeze-up Start	Freeze-up End
2004	2004-02-17	2004-05-01	2004-11-29	2005-03-12
2005	2005-03-06	2005-05-03	2005-11-22	2006-03-05
2006	2006-02-27	2006-04-26	2006-11-29	2007-03-11
2007	2007-03-05	2007-05-03	2007-11-22	2008-03-20
2008	2008-03-14	2008-05-04	2008-11-17	2009-03-05
2009	2009-02-27	2009-05-10	2009-12-04	2010-02-21
2010	2010-02-15	2010-04-21	2010-12-02	2011-02-27
2011	2011-02-21	2011-05-11	2011-12-02	2012-03-08
2012	2012-03-02	2012-04-09	2012-12-05	2013-02-21
2013	2013-02-15	2013-05-07	2013-11-22	2014-03-09
2014	2014-03-03	2014-05-16	2014-11-12	2015-03-09
2015	2015-03-03	2015-05-16	2015-11-13	2016-02-17
2016	2016-02-11	2016-04-30	2016-12-07	2017-03-17
2017	2017-03-11	2017-04-20	2017-12-06	2018-02-14
2018	2018-02-08	2018-05-16	2018-11-10	2019-03-12
2019	2019-03-06	2019-05-07	2019-11-06	2020-03-04
2020	2020-02-27	2020-04-25	2020-11-10	2021-02-23
2021	2021-02-17	2021-04-16	2021-11-25	2022-03-01
2022	2022-02-23	2022-05-04	2022-11-30	2023-02-27
2023	2023-02-21	2023-04-29		

Table B.6: Lake Huron freeze-up and break-up periods used in this study

Year	*Break-up Start*	*Break-up End*	*Freeze-up Start*	*Freeze-up End*
2004	2004-01-31	2004-05-02	2004-01-02	2004-02-05
2005	2005-02-05	2005-04-16	2004-12-09	2005-02-10
2006	2006-03-02	2006-03-31	2006-02-03	2006-03-05
2007	2007-02-16	2007-05-02	2007-01-16	2007-02-22
2008	2008-03-08	2008-04-26	2007-12-29	2008-03-13
2009	2009-02-03	2009-04-17	2008-11-18	2009-02-08
2010	2010-02-06	2010-04-01	2009-12-05	2010-02-11
2011	2011-01-30	2011-04-22	2010-12-01	2011-02-04
2012	2012-01-21	2012-03-03	2012-01-02	2012-01-26
2013	2013-02-21	2013-04-11	2012-12-29	2013-02-25
2014	2014-03-07	2014-05-12	2013-12-06	2014-03-09
2015	2015-02-16	2015-04-24	2014-12-06	2015-02-21
2016	2016-02-13	2016-03-11	2016-01-01	2016-02-18
2017	2017-02-06	2017-02-25	2016-12-08	2017-02-11
2018	2018-02-08	2018-04-20	2017-12-07	2018-02-12
2019	2019-02-28	2019-05-07	2019-01-09	2019-03-05
2020	2020-02-28	2020-03-12	2020-01-16	2020-03-03
2021	2021-02-18	2021-03-27	2020-12-24	2021-02-23
2022	2022-02-03	2022-04-10	2022-01-02	2022-02-03
2023	2023-02-03	2023-02-21	2022-12-13	2023-02-08

Table B.7: Lake Erie freeze-up and break-up periods used in this study

Appendix C – MOD11C1 Monthly boxplots

C.1 Great Bear Lake

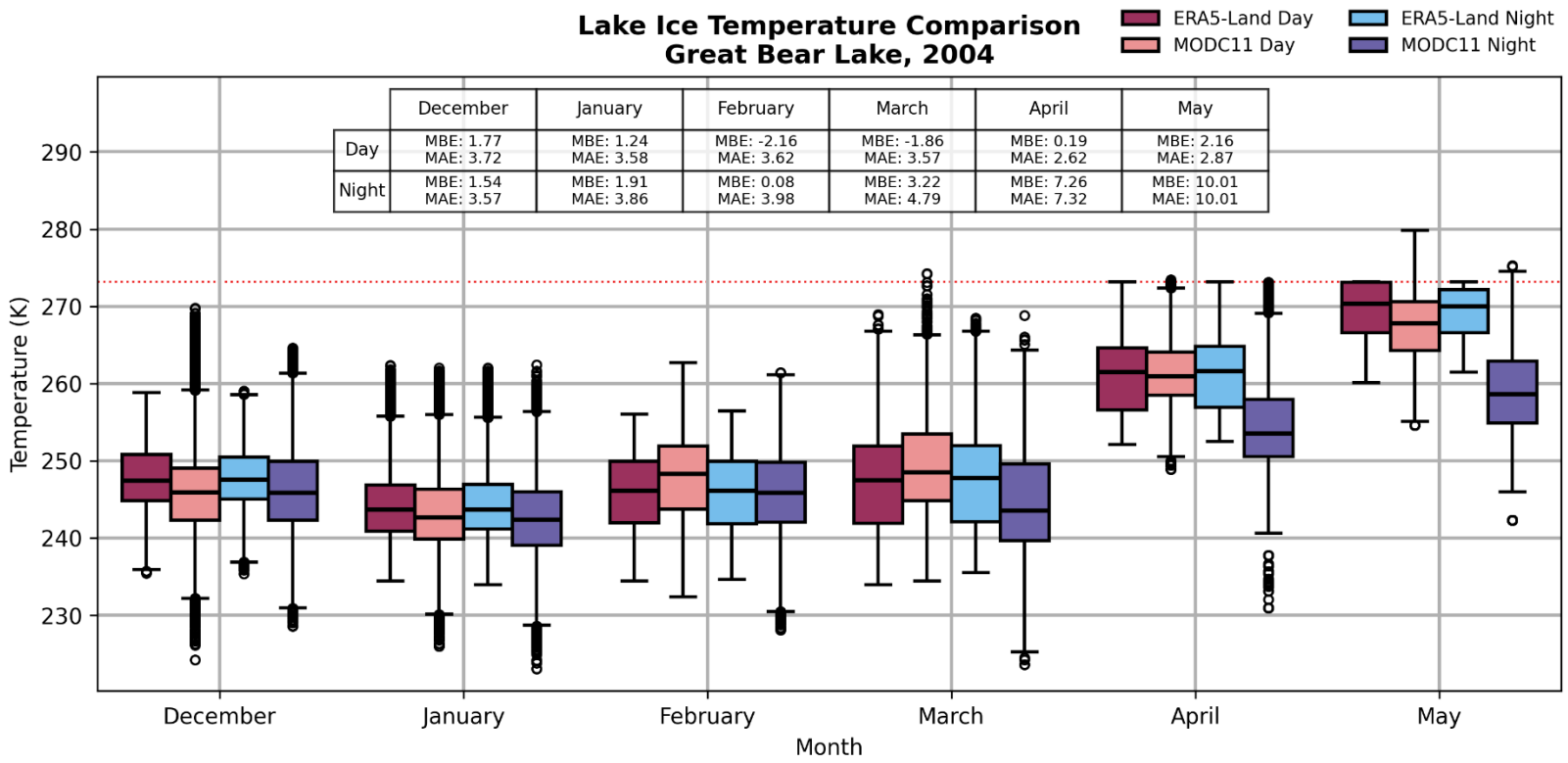


Figure C.1.1: Boxplot of monthly lake ice surface temperatures during ice-on period of ERA5-Land and MODIS for Great Bear Lake, 2004

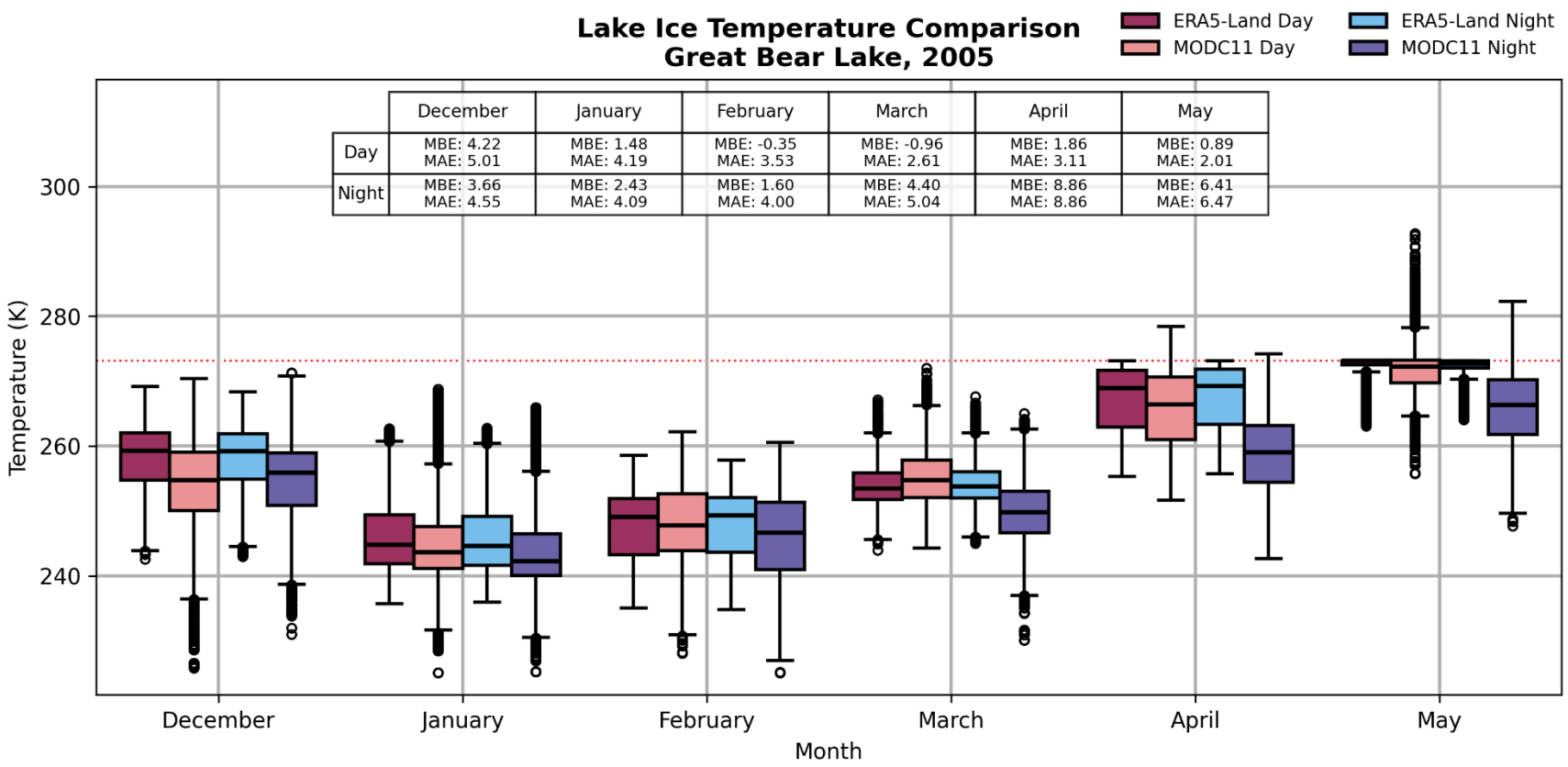


Figure C.1.2: Boxplot of monthly lake ice surface temperatures during ice-on period of ERA5-Land and MODIS for Great Bear Lake, 2005

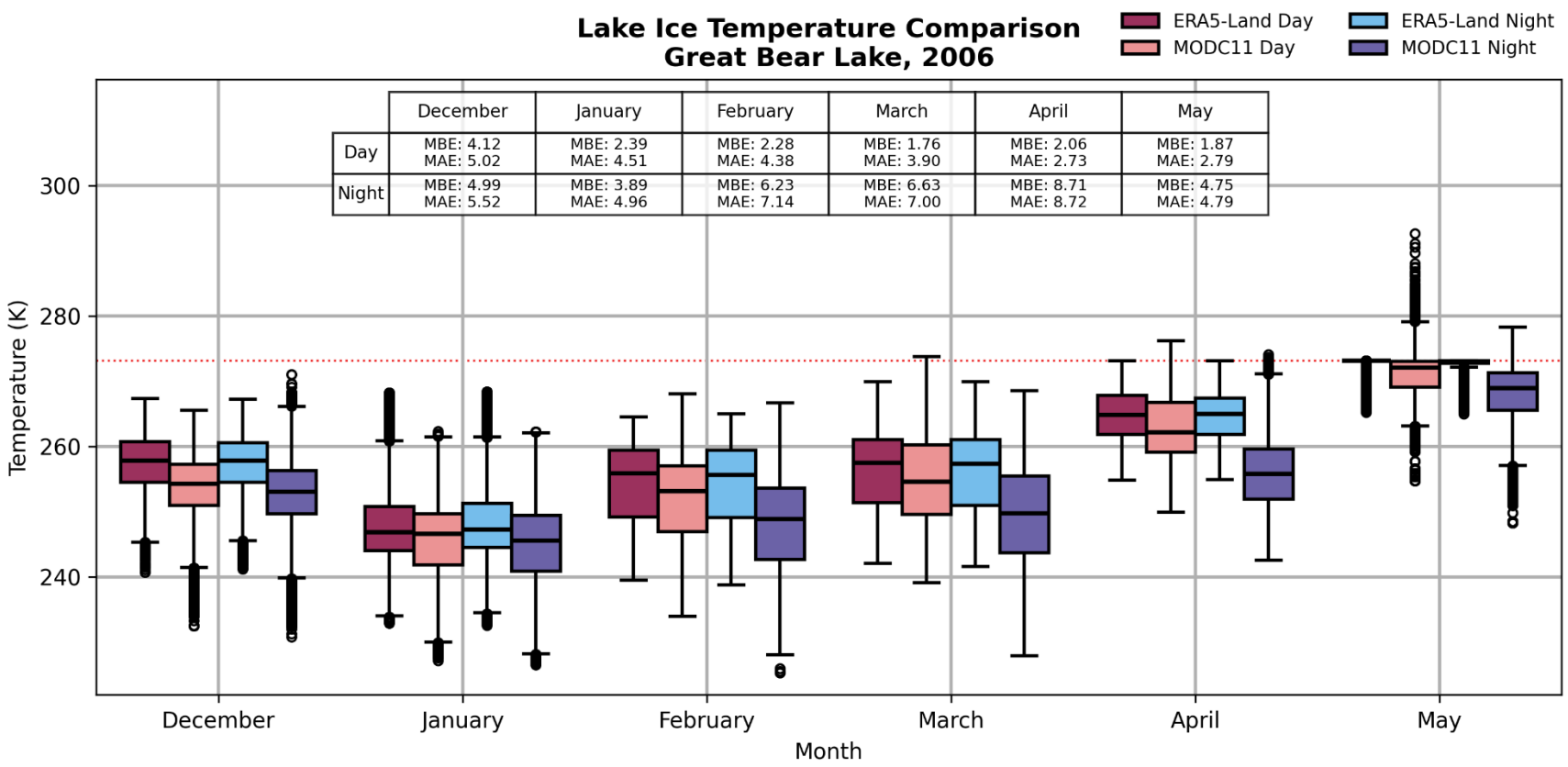


Figure C.1.3: Boxplot of monthly lake ice surface temperatures during ice-on period of ERA5-Land and MODIS for Great Bear Lake, 2006

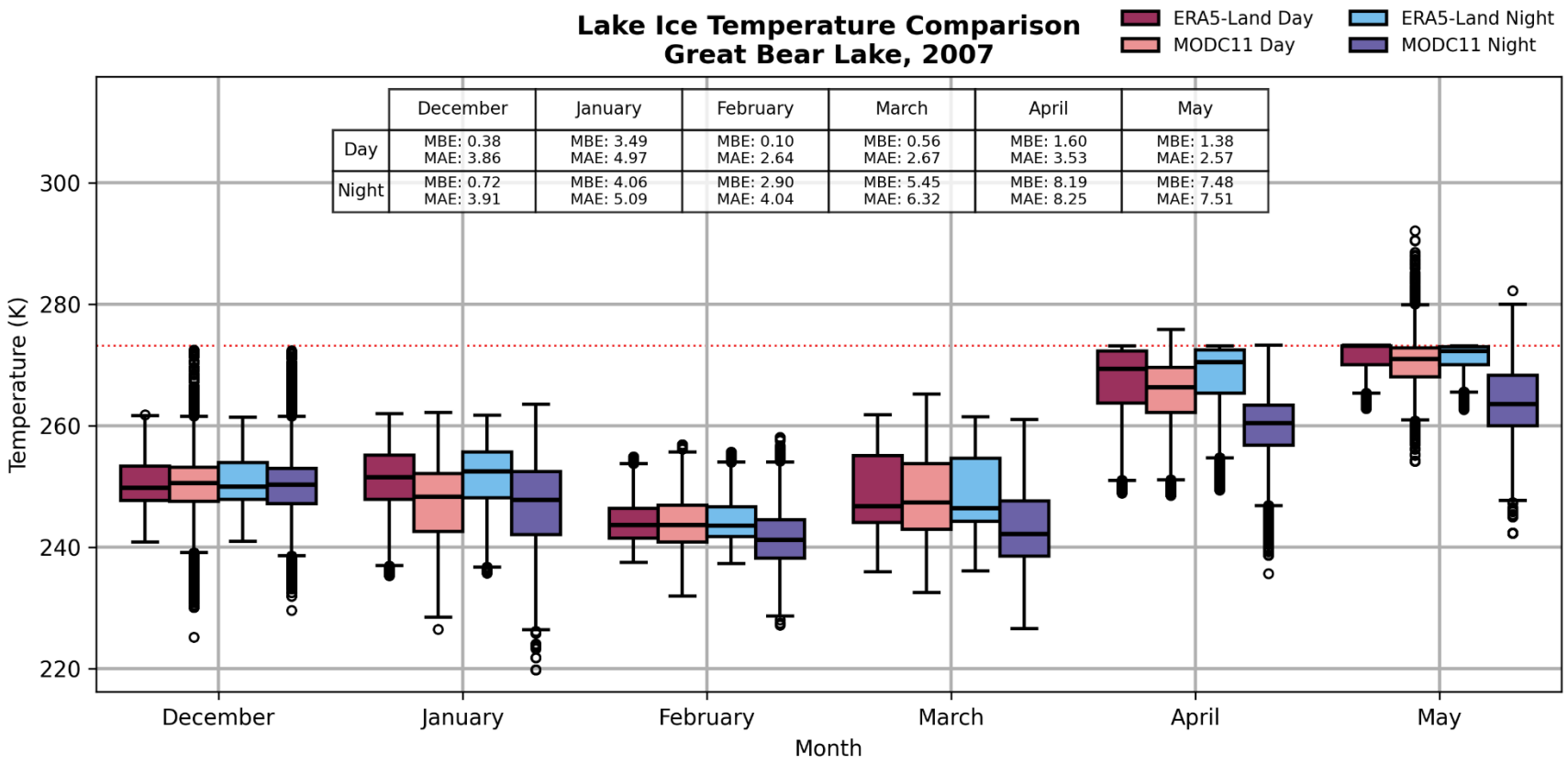


Figure C.1.4: Boxplot of monthly lake ice surface temperatures during ice-on period of ERA5-Land and MODIS for Great Bear Lake, 2007

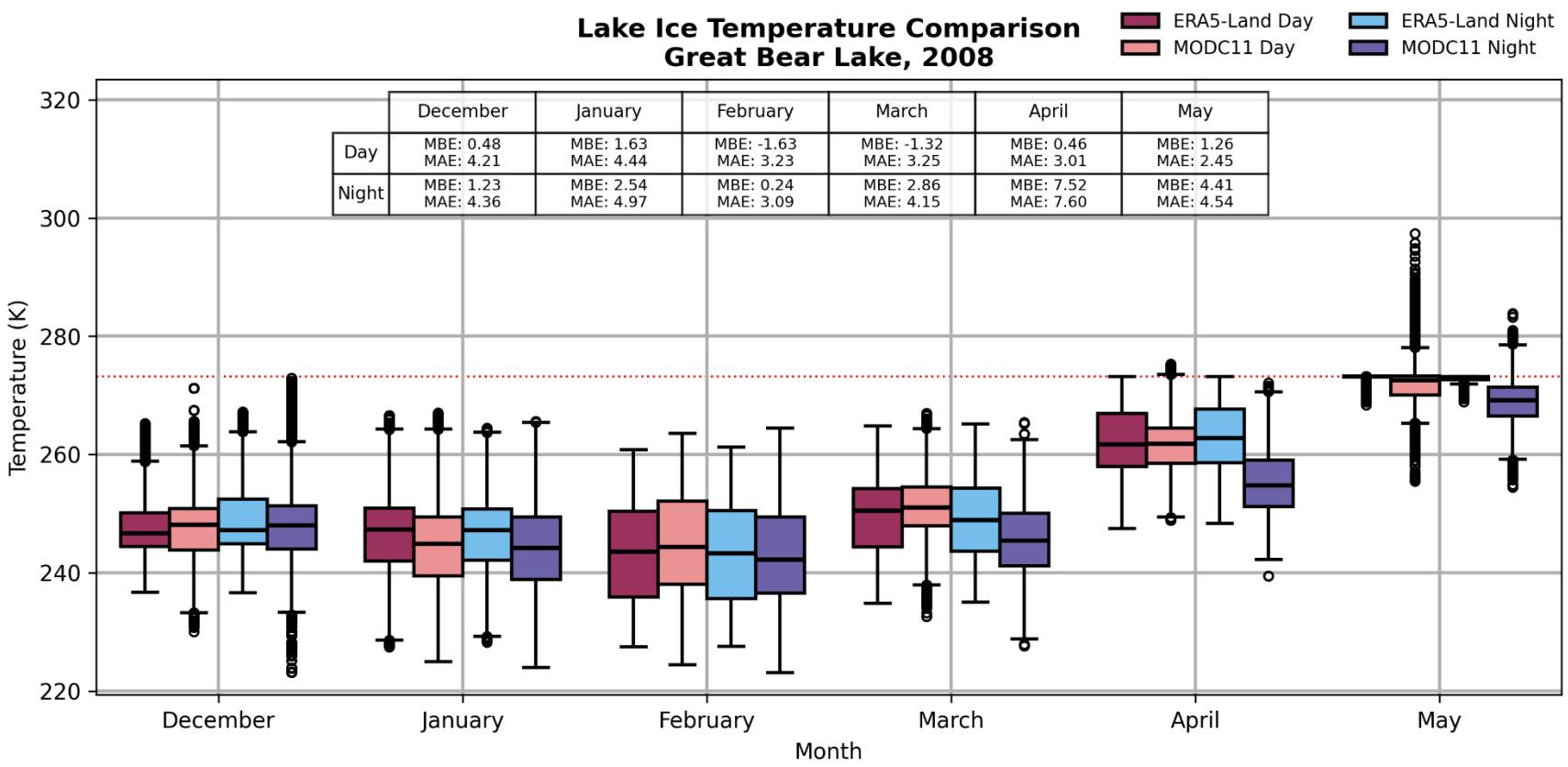


Figure C.1.5: Boxplot of monthly lake ice surface temperatures during ice-on period of ERA5-Land and MODIS for Great Bear Lake, 2008

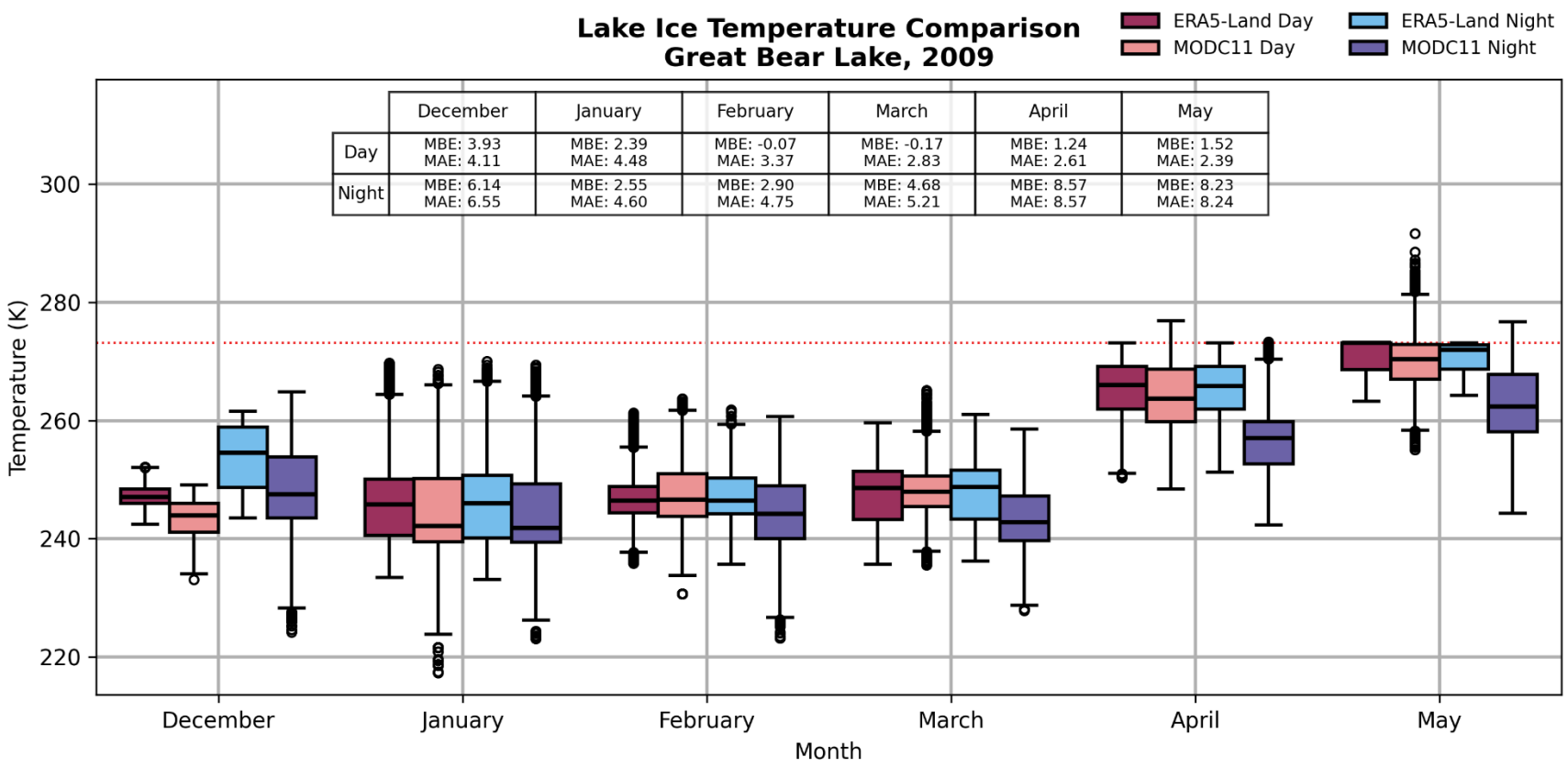


Figure C.1.6: Boxplot of monthly lake ice surface temperatures during ice-on period of ERA5-Land and MODIS for Great Bear Lake, 2009

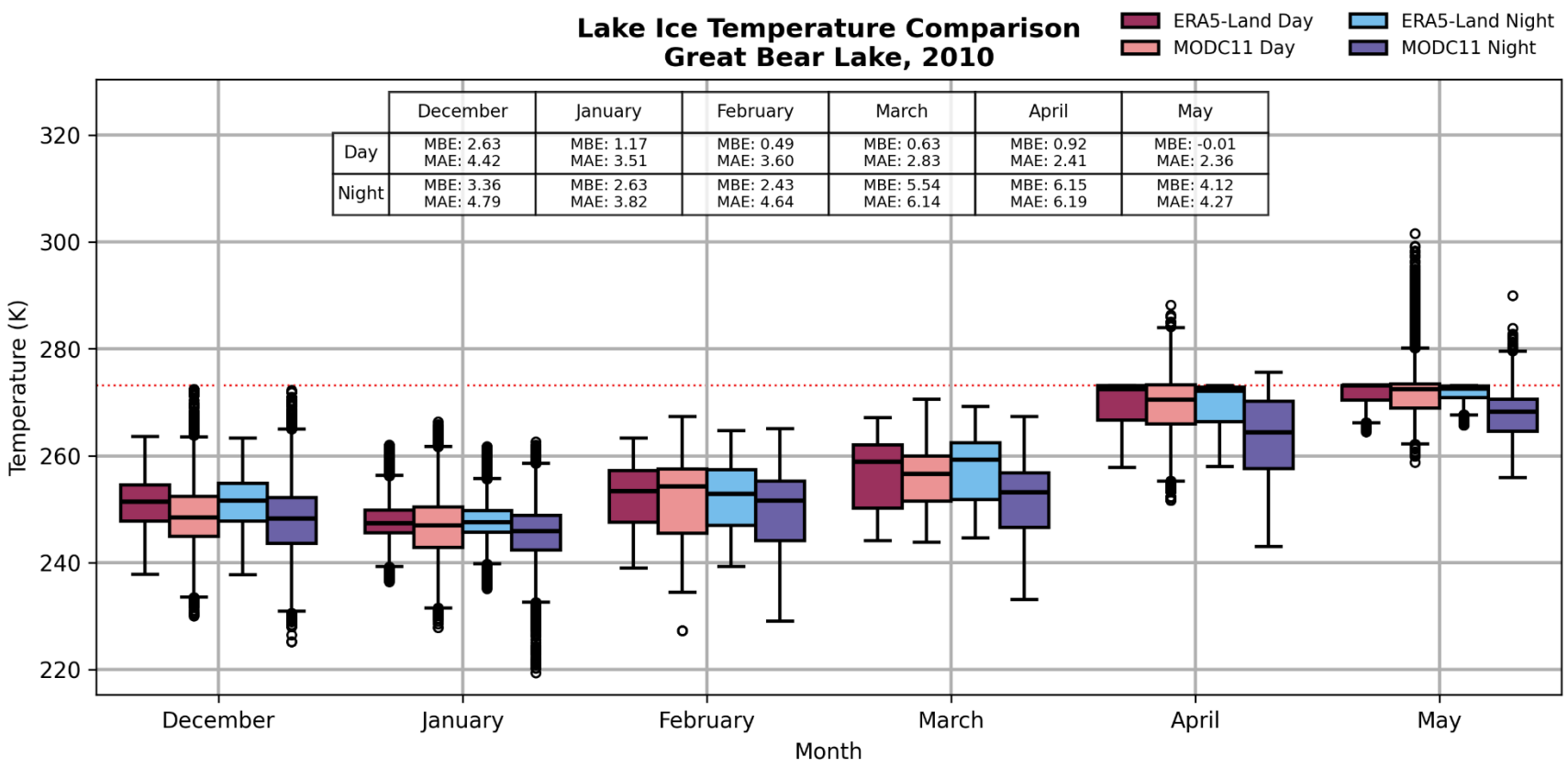


Figure C.1.7: Boxplot of monthly lake ice surface temperatures of ERA5-Land and MODIS for Great Bear Lake, 2010

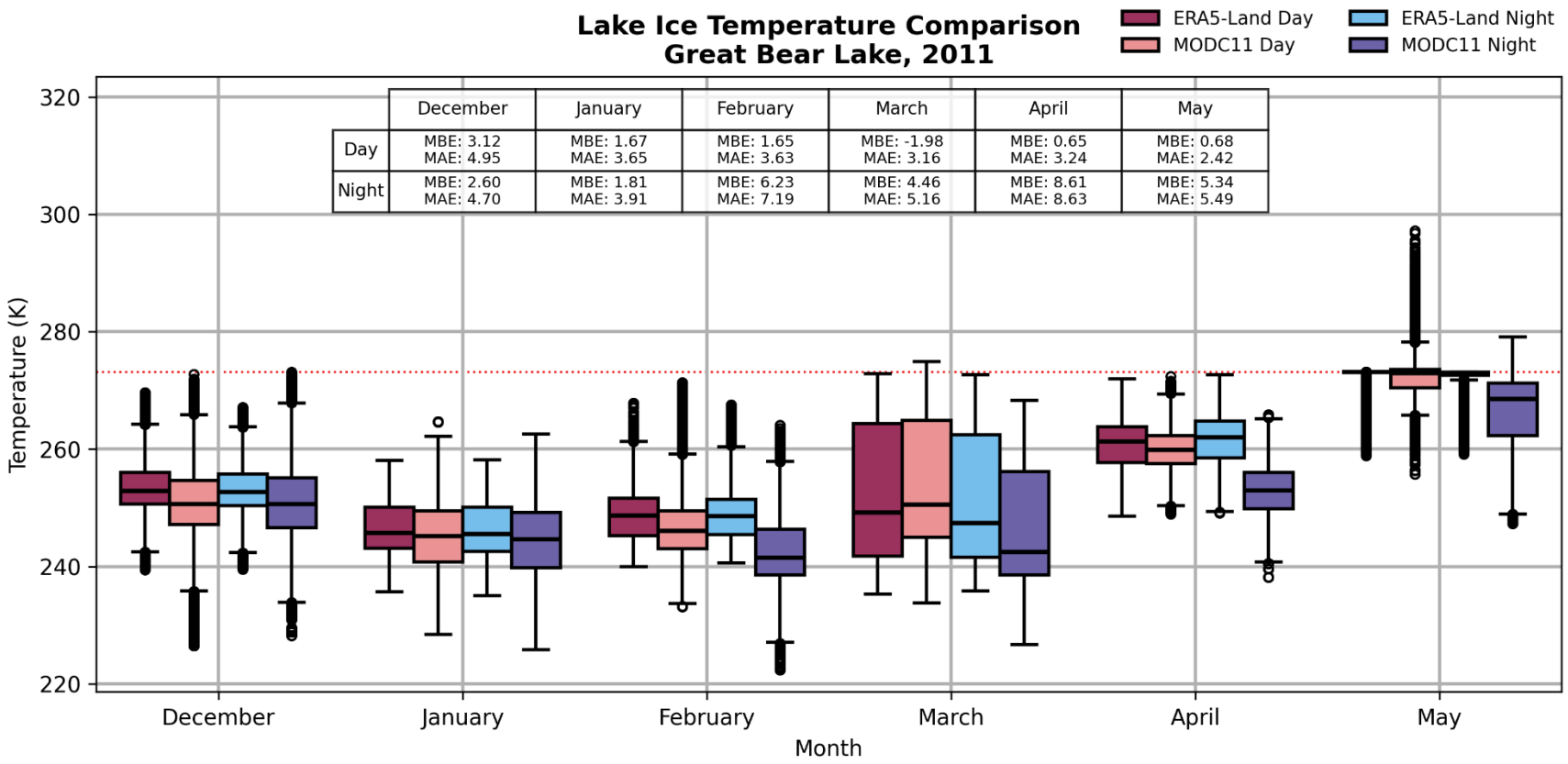


Figure C.1.8: Boxplot of monthly lake ice surface temperatures during ice-on period of ERA5-Land and MODIS for Great Bear Lake, 2011

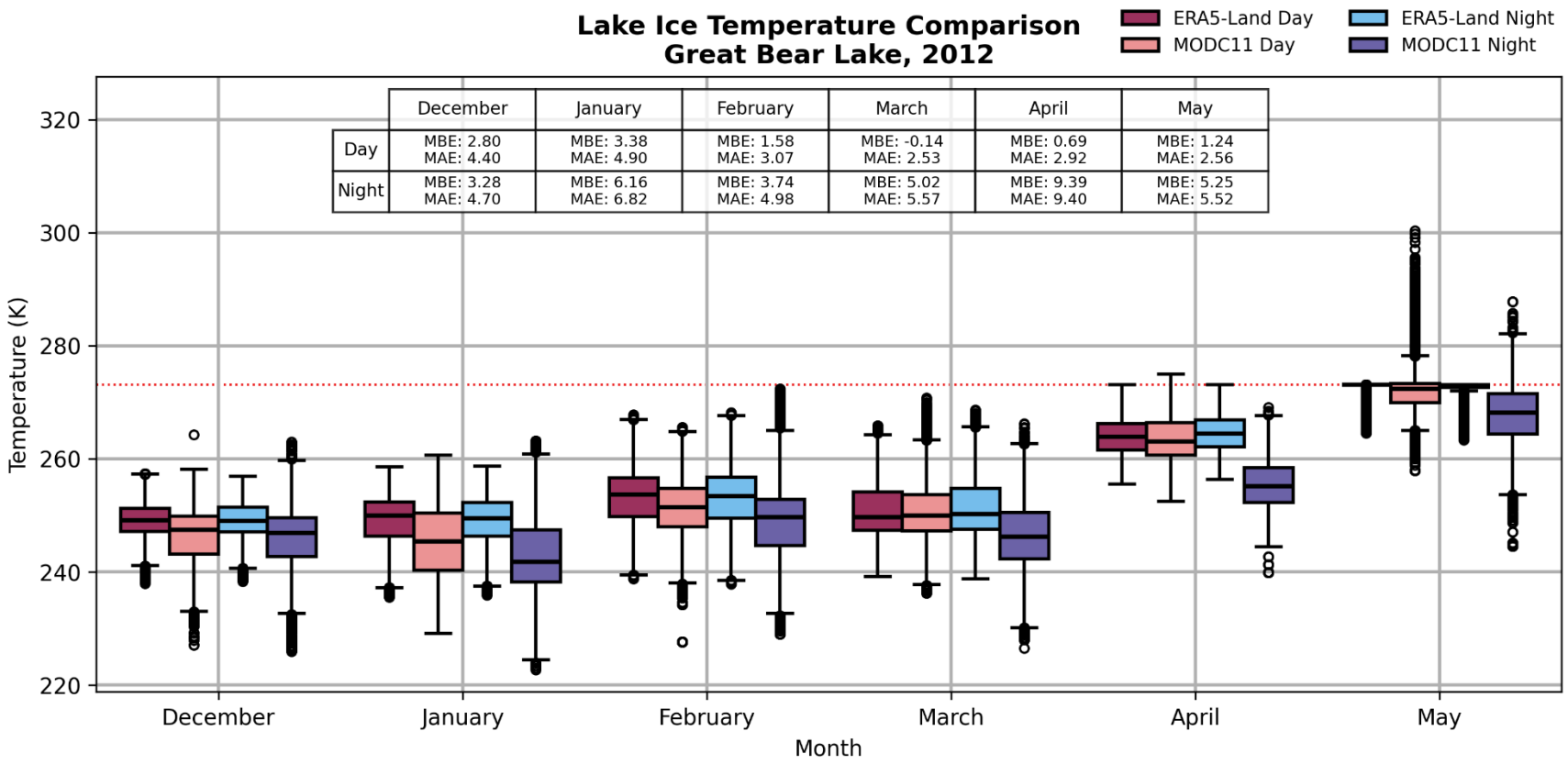


Figure C.1.9: Boxplot of monthly lake ice surface temperatures during ice-on period of ERA5-Land and MODIS for Great Bear Lake, 2012

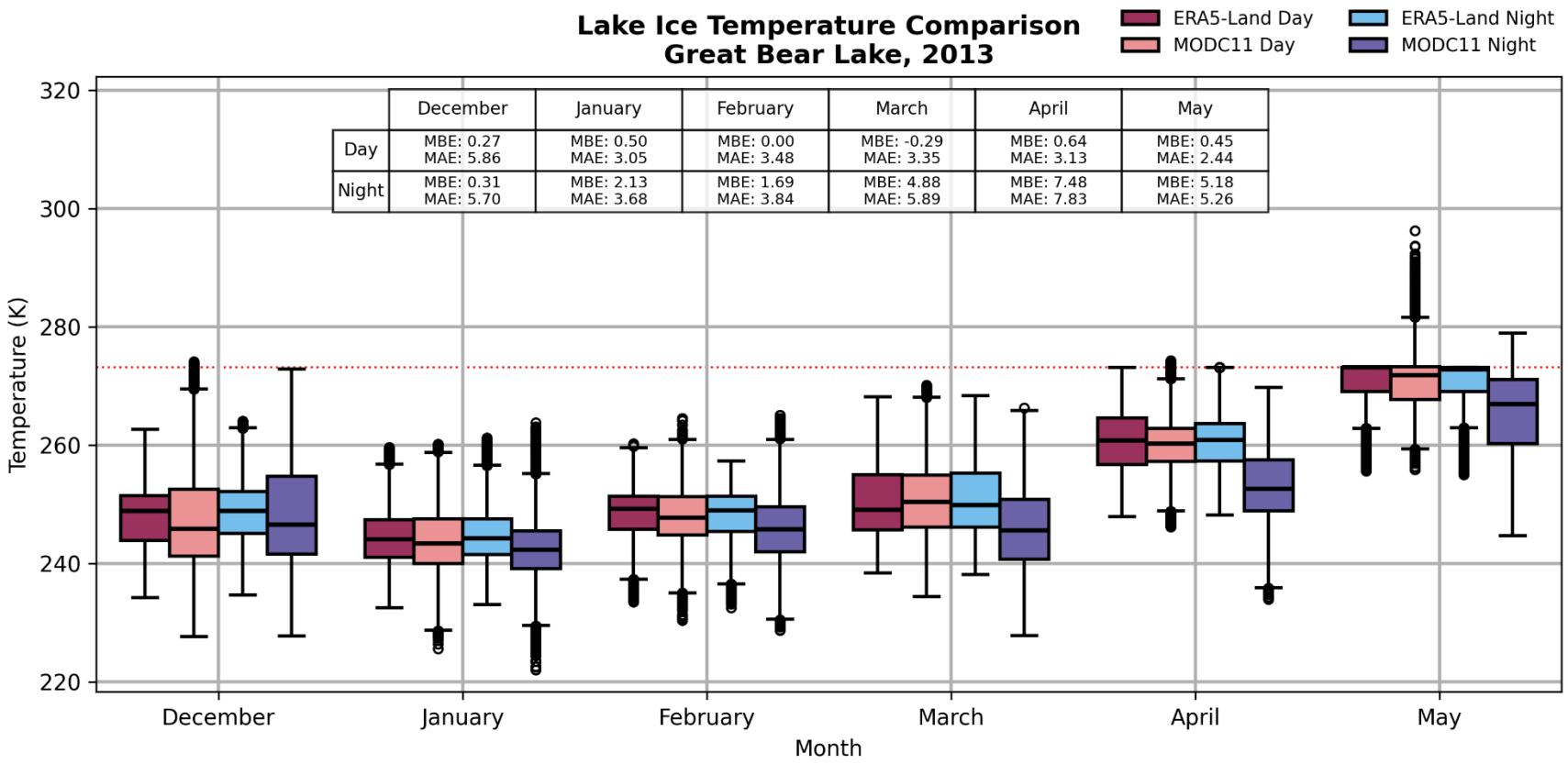


Figure C.1.10: Boxplot of monthly lake ice surface temperatures during ice-on period of ERA5-Land and MODIS for Great Bear Lake, 2013

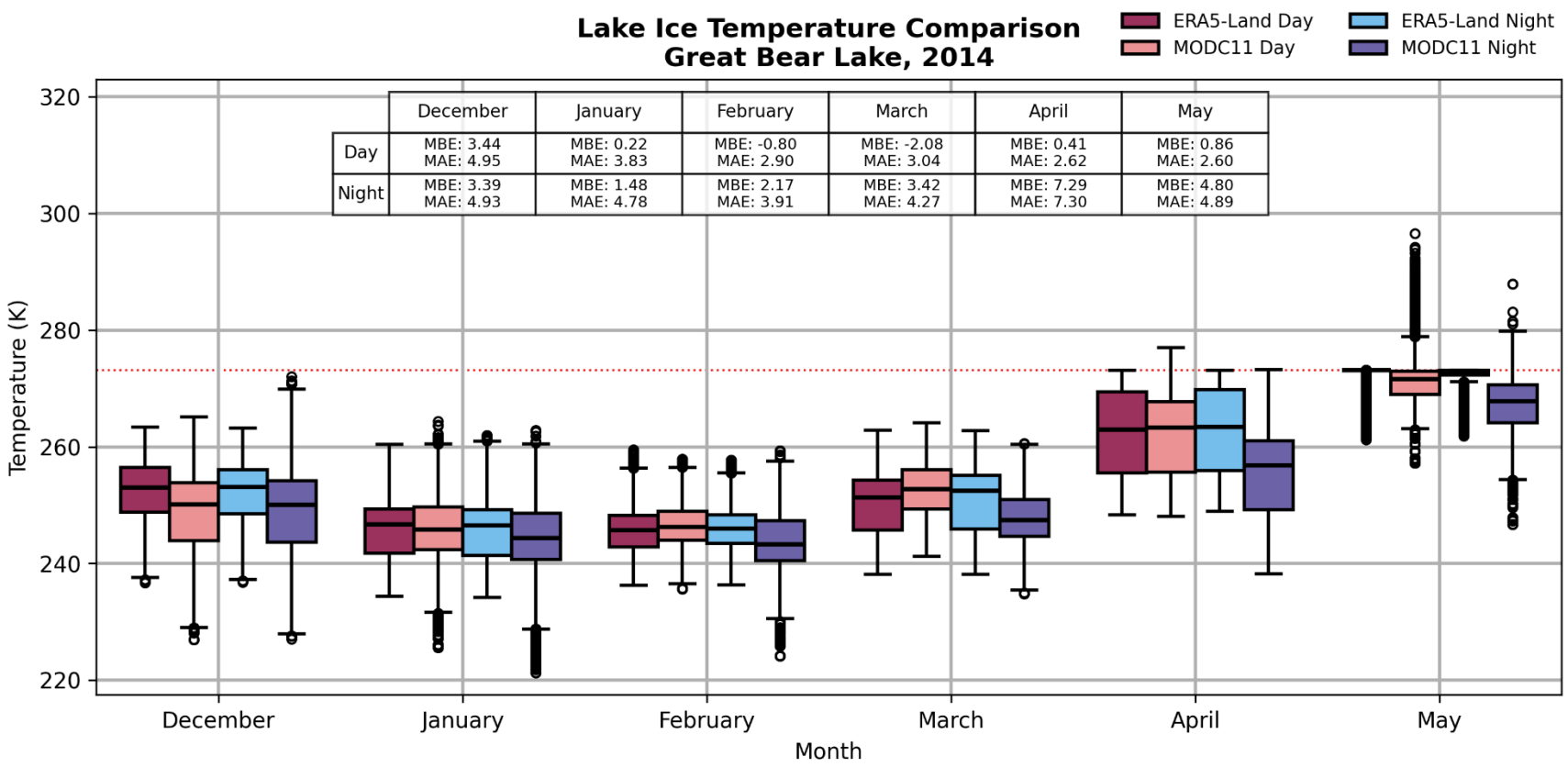


Figure C.1.11: Boxplot of monthly lake ice surface temperatures during ice-on period of ERA5-Land and MODIS for Great Bear Lake, 2014

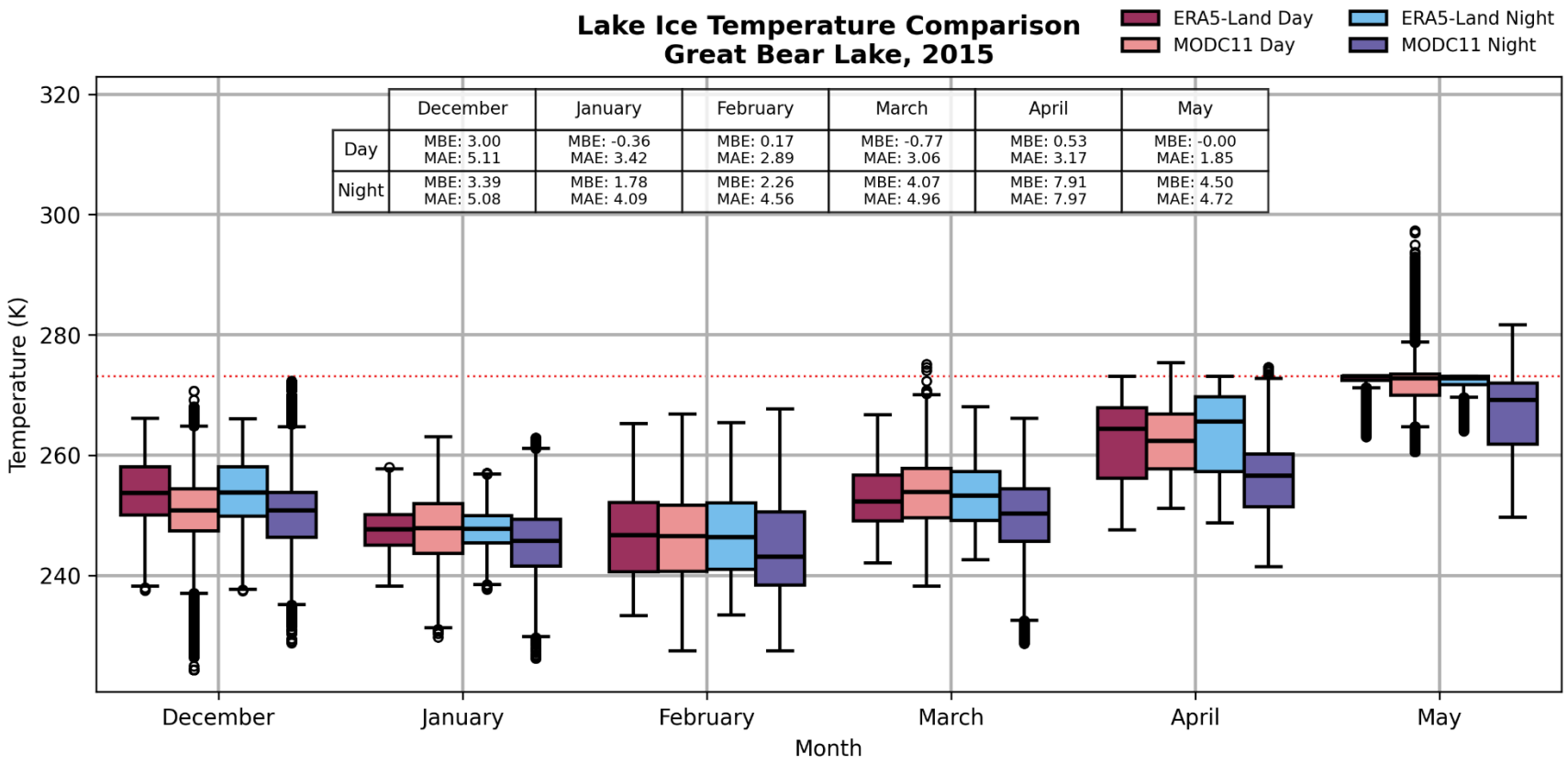


Figure C.1.12: Boxplot of monthly lake ice surface temperatures during ice-on period of ERA5-Land and MODIS for Great Bear Lake, 2015

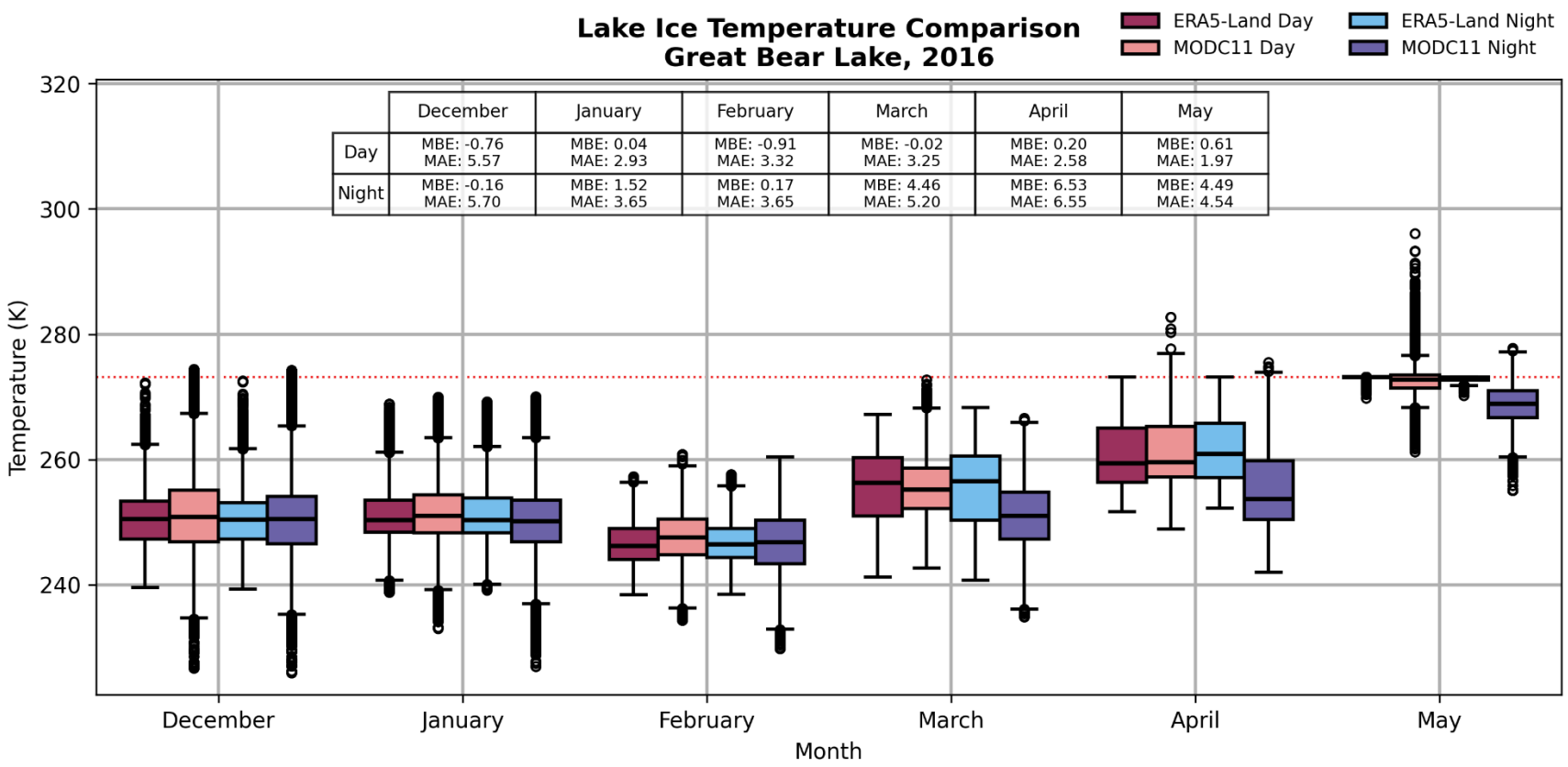


Figure C.1.13: Boxplot of monthly lake ice surface temperatures during ice-on period of ERA5-Land and MODIS for Great Bear Lake, 2016

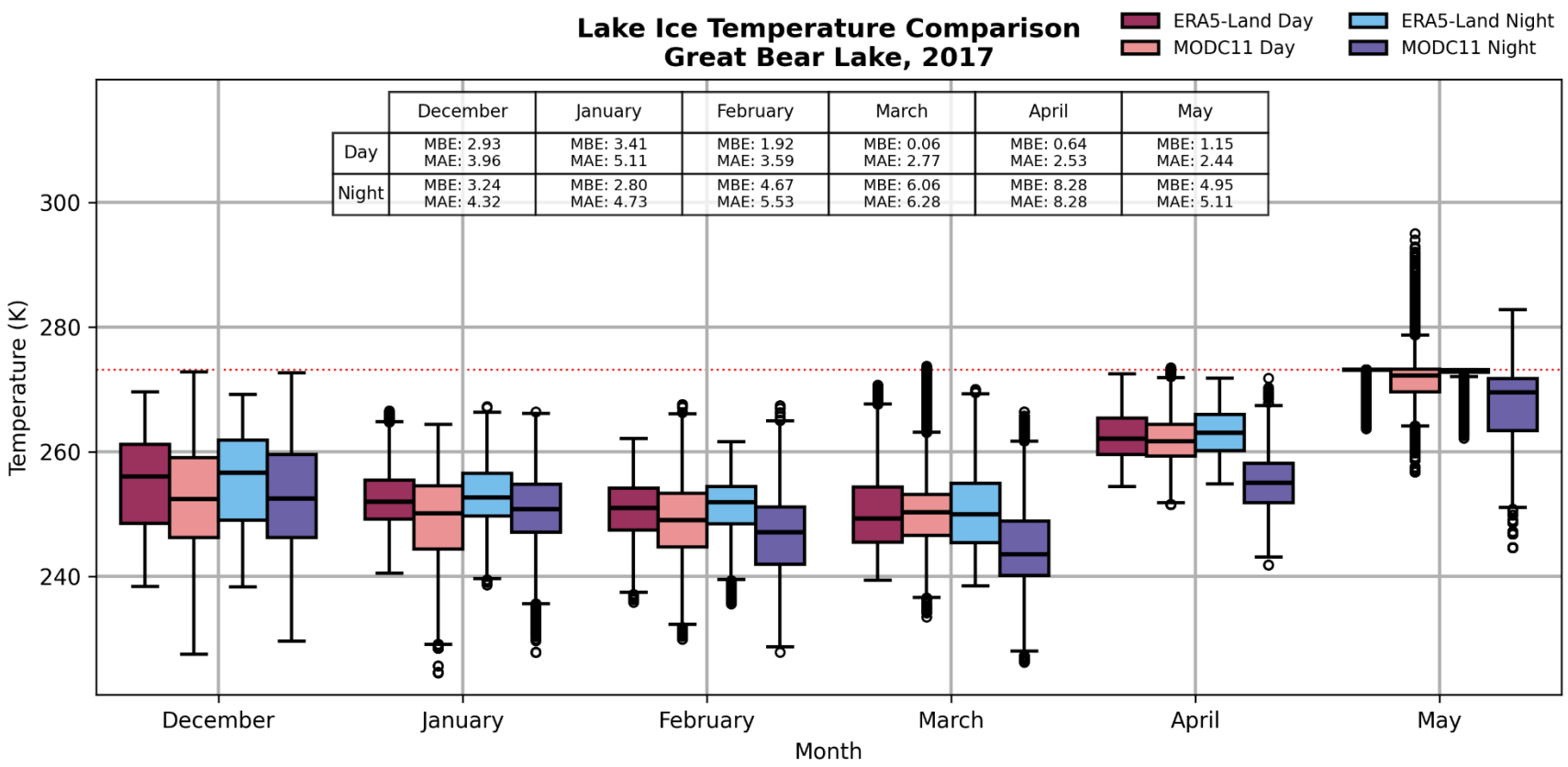


Figure C.1.14: Boxplot of monthly lake ice surface temperatures during ice-on period of ERA5-Land and MODIS for Great Bear Lake, 2017

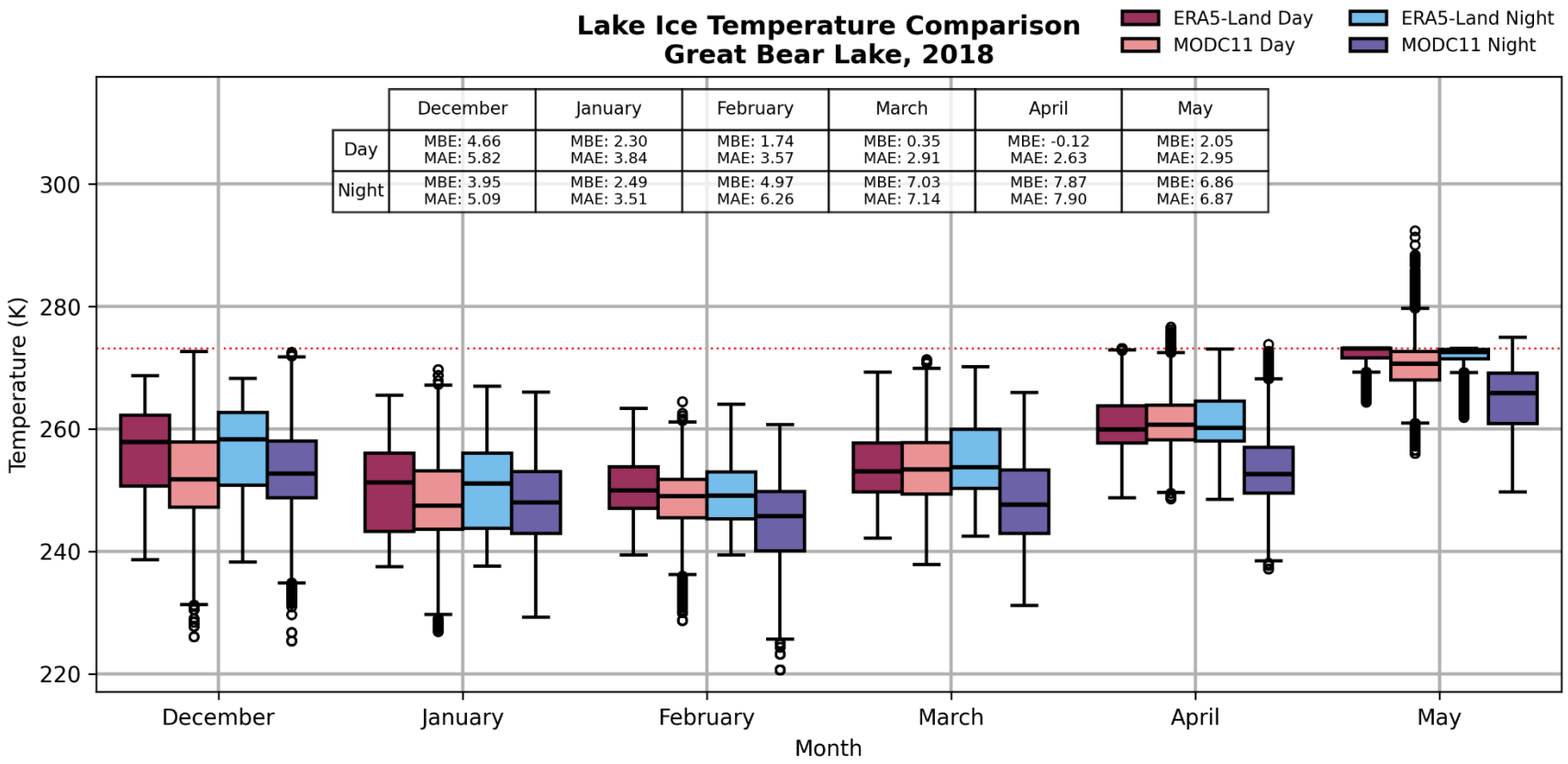


Figure C.1.15: Boxplot of monthly lake ice surface temperatures during ice-on period of ERA5-Land and MODIS for Great Bear Lake, 2018

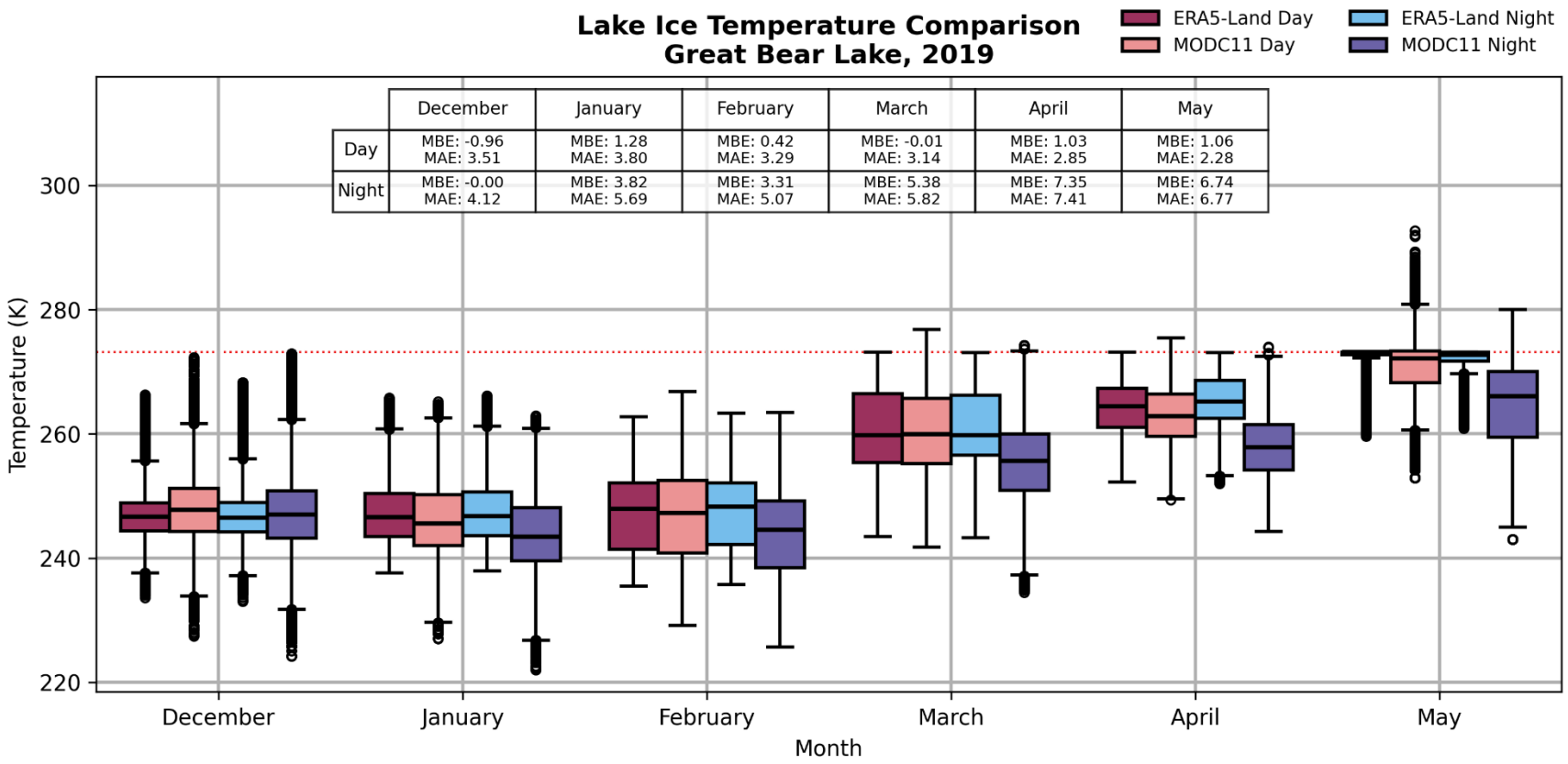


Figure C.1.16: Boxplot of monthly lake ice surface temperatures during ice-on period of ERA5-Land and MODIS for Great Bear Lake, 2019

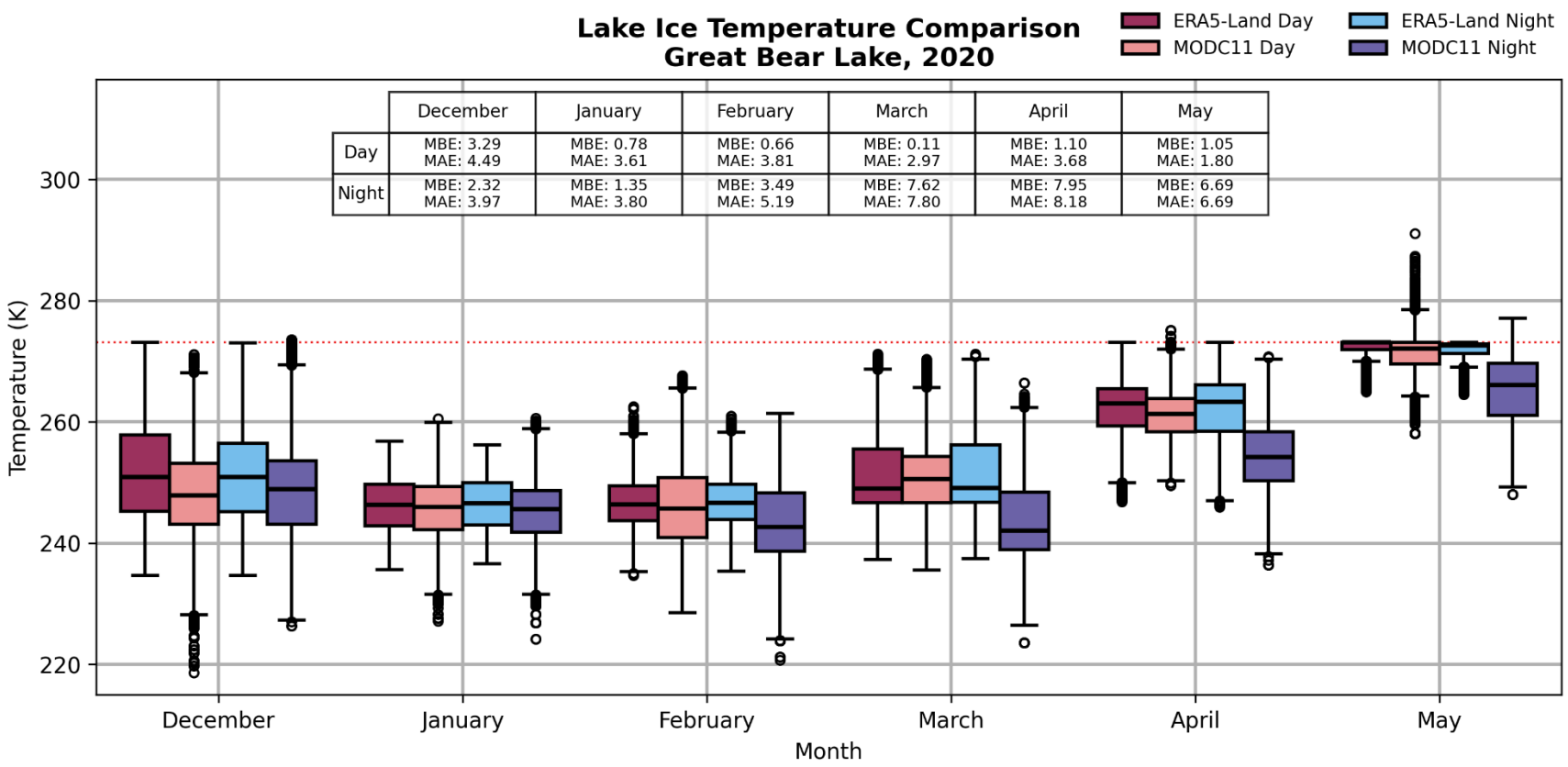


Figure C.1.17: Boxplot of monthly lake ice surface temperatures during ice-on period of ERA5-Land and MODIS for Great Bear Lake, 2020

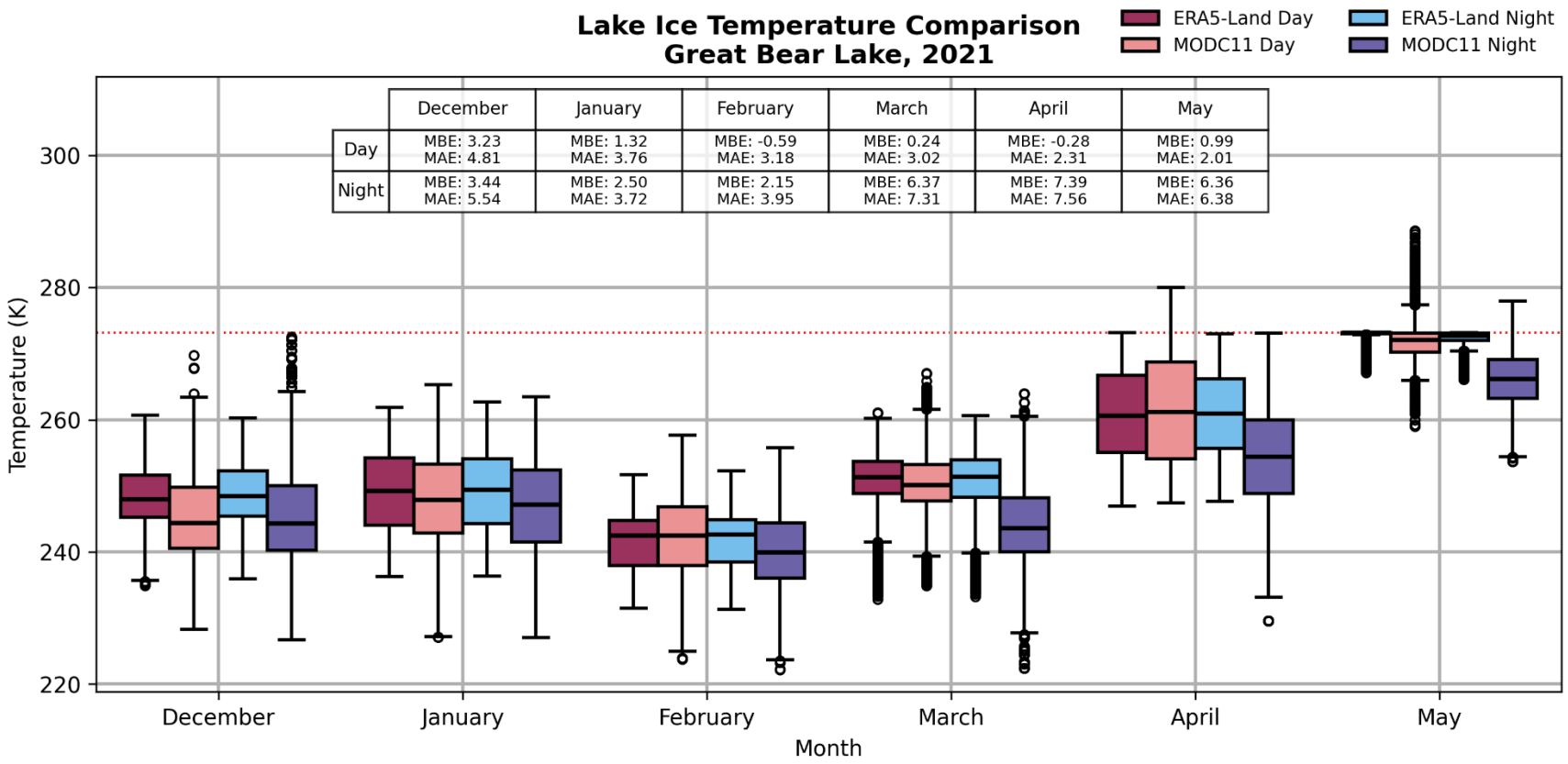


Figure C.1.18: Boxplot of monthly lake ice surface temperatures during ice-on period of ERA5-Land and MODIS for Great Bear Lake, 2021

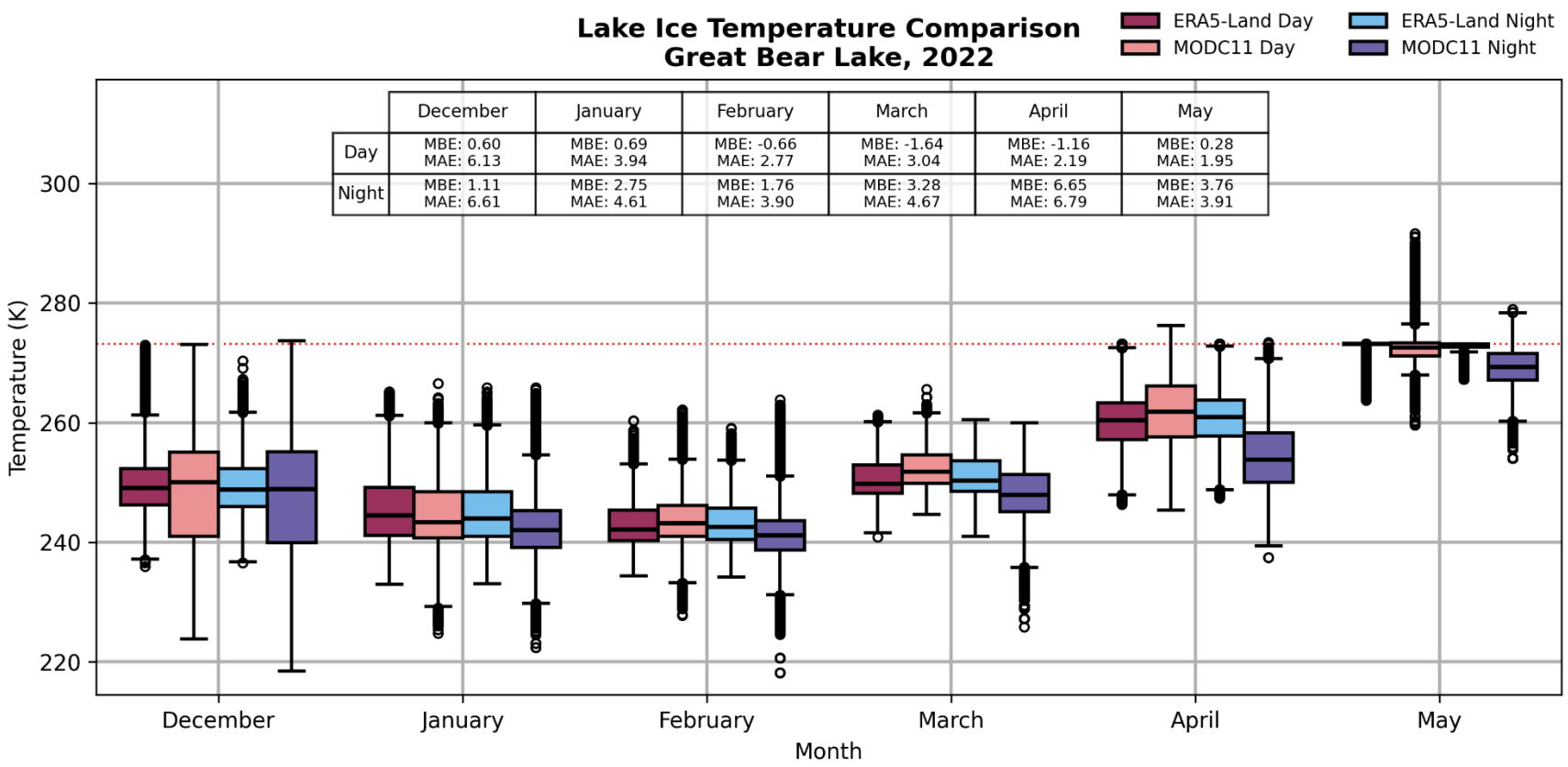


Figure C.1.19: Boxplot of monthly lake ice surface temperatures during ice-on period of ERA5-Land and MODIS for Great Bear Lake, 2022

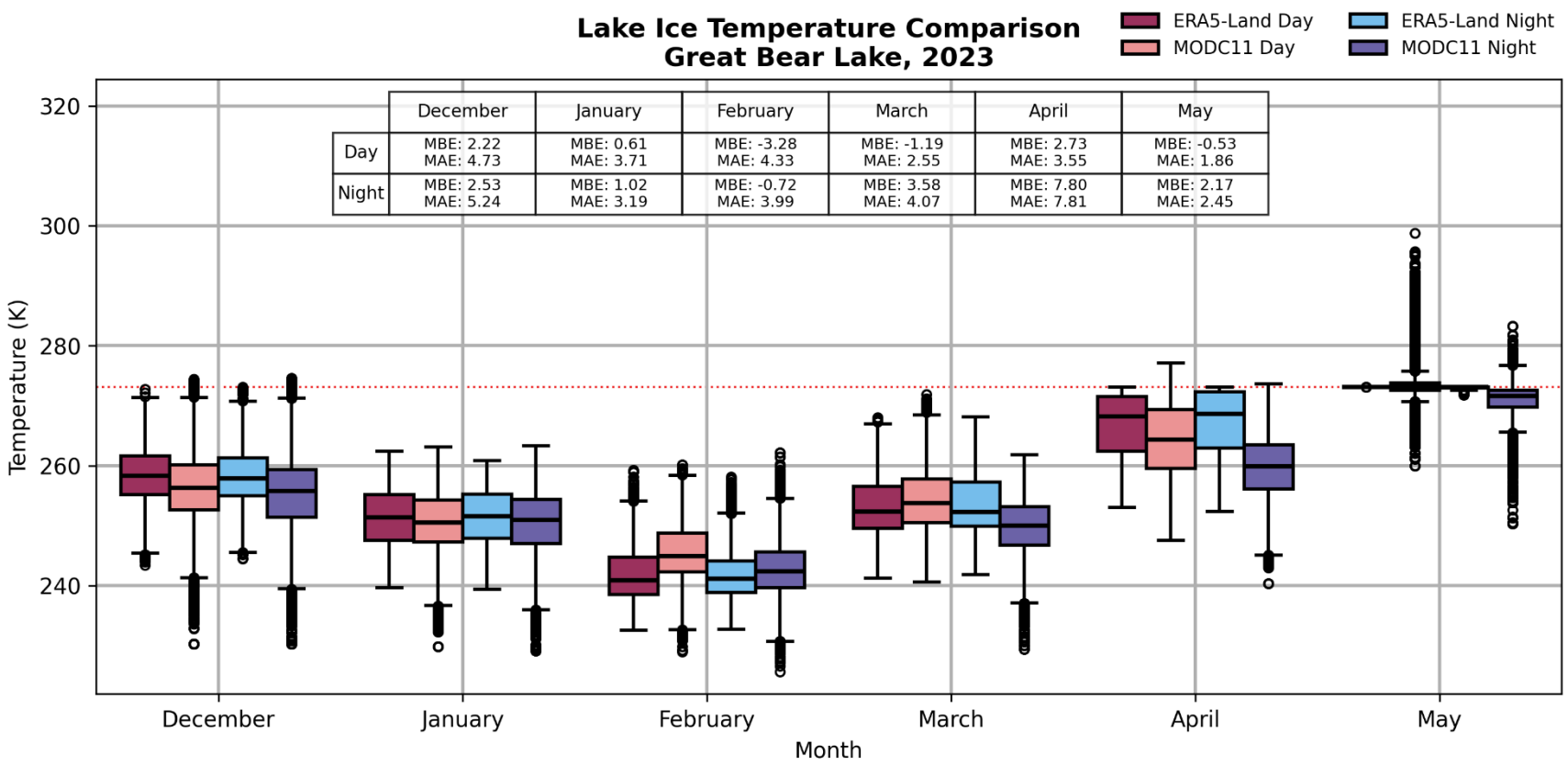


Figure C.1.20: Boxplot of monthly lake ice surface temperatures during ice-on period of ERA5-Land and MODIS for Great Bear Lake, 2023

C.2 Great Slave Lake

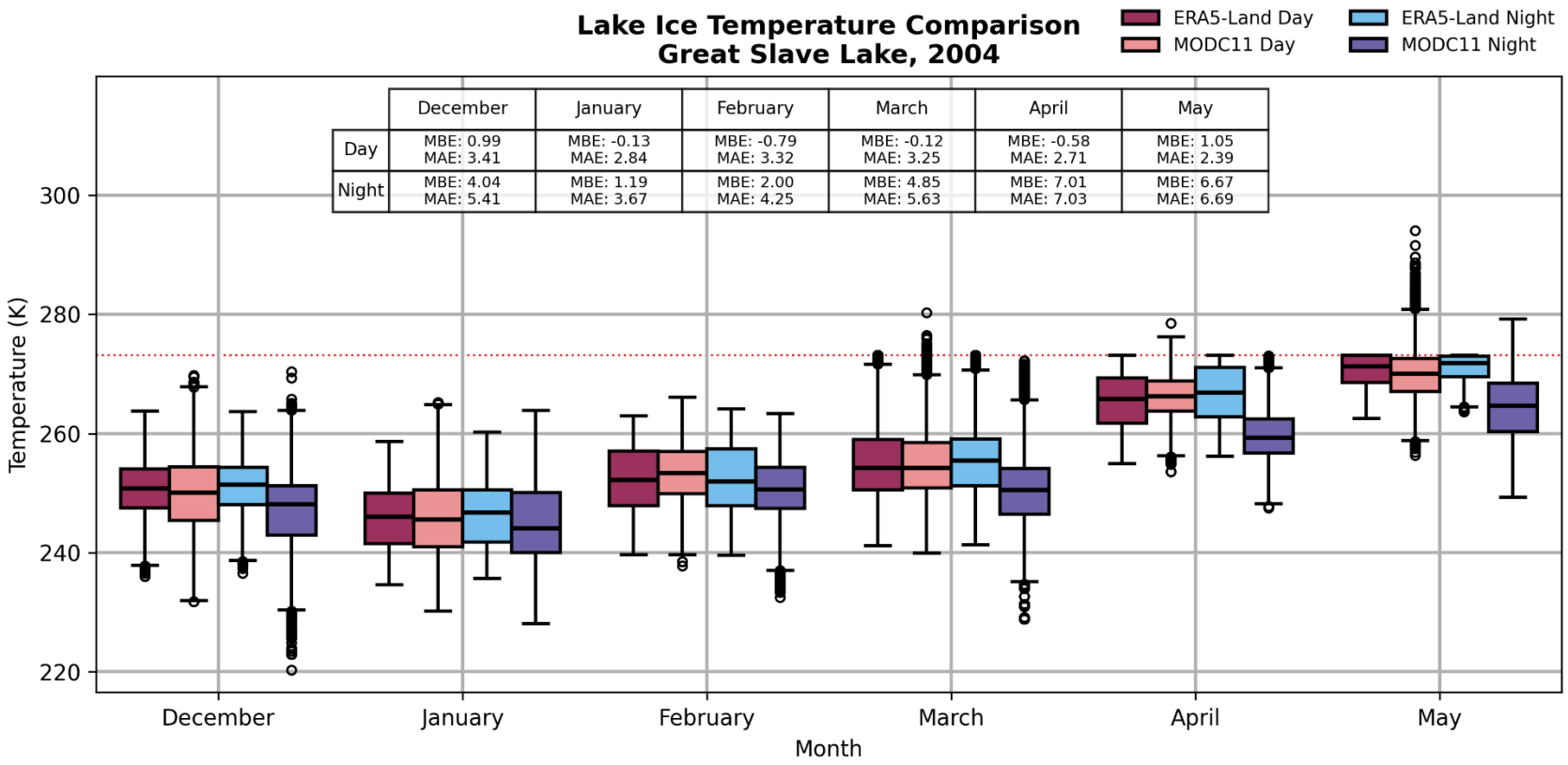


Figure C.2.1: Boxplot of monthly lake ice surface temperatures during ice-on period of ERA5-Land and MODIS for Great Slave Lake, 2004

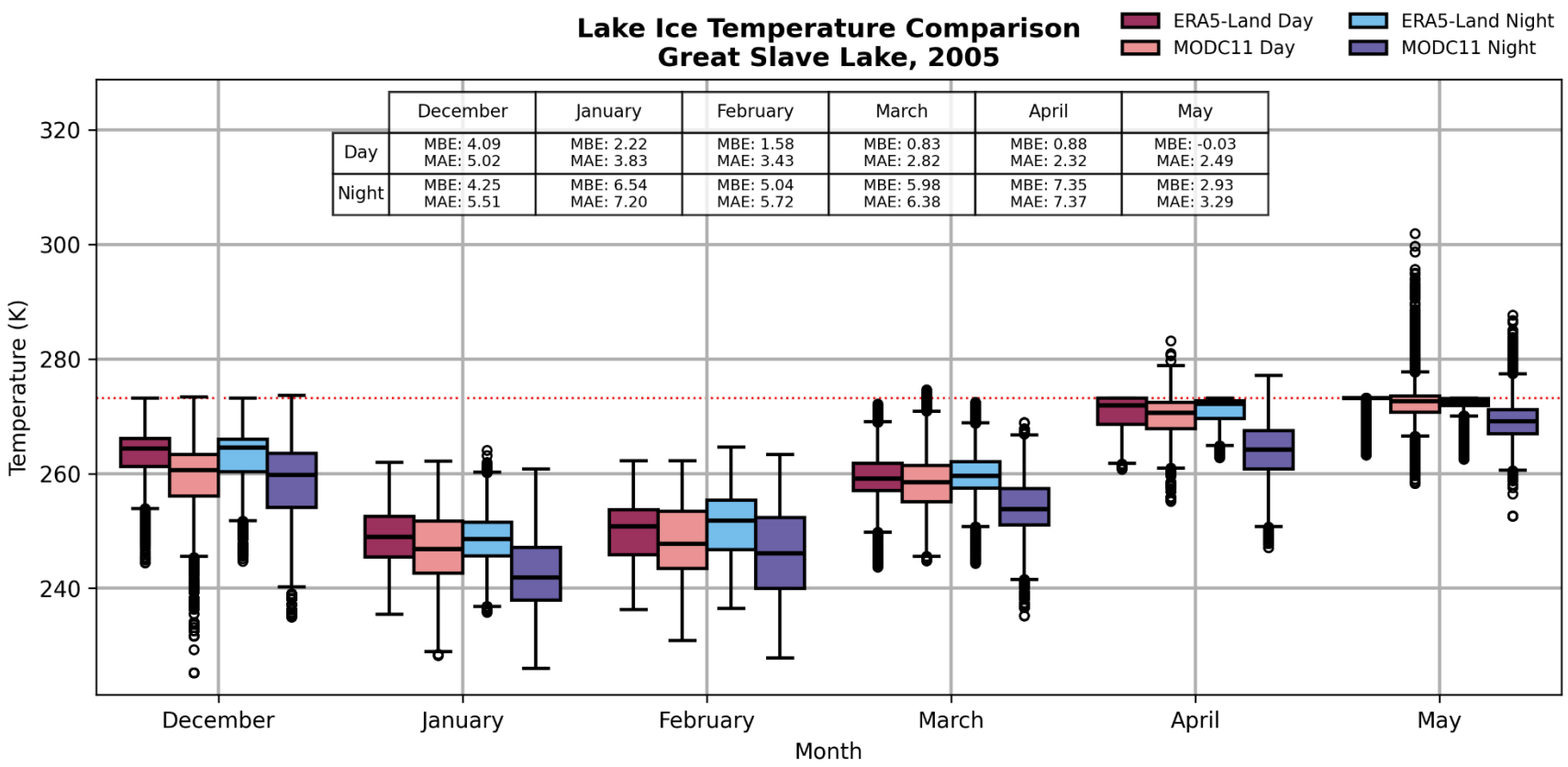


Figure C.2.2: Boxplot of monthly lake ice surface temperatures during ice-on period of ERA5-Land and MODIS for Great Slave Lake, 2005

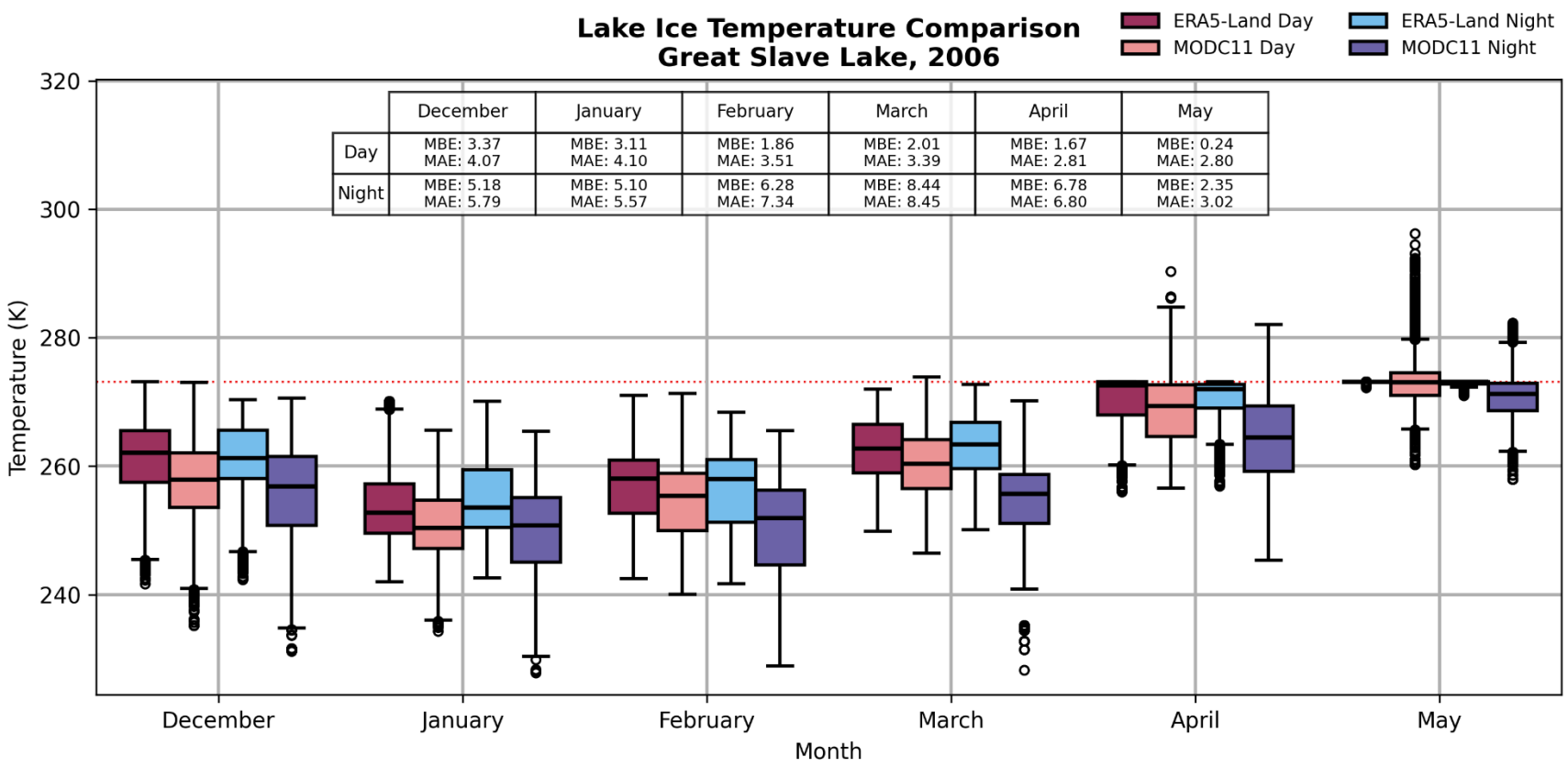


Figure C.2.3: Boxplot of monthly lake ice surface temperatures during ice-on period of ERA5-Land and MODIS for Great Slave Lake, 2006

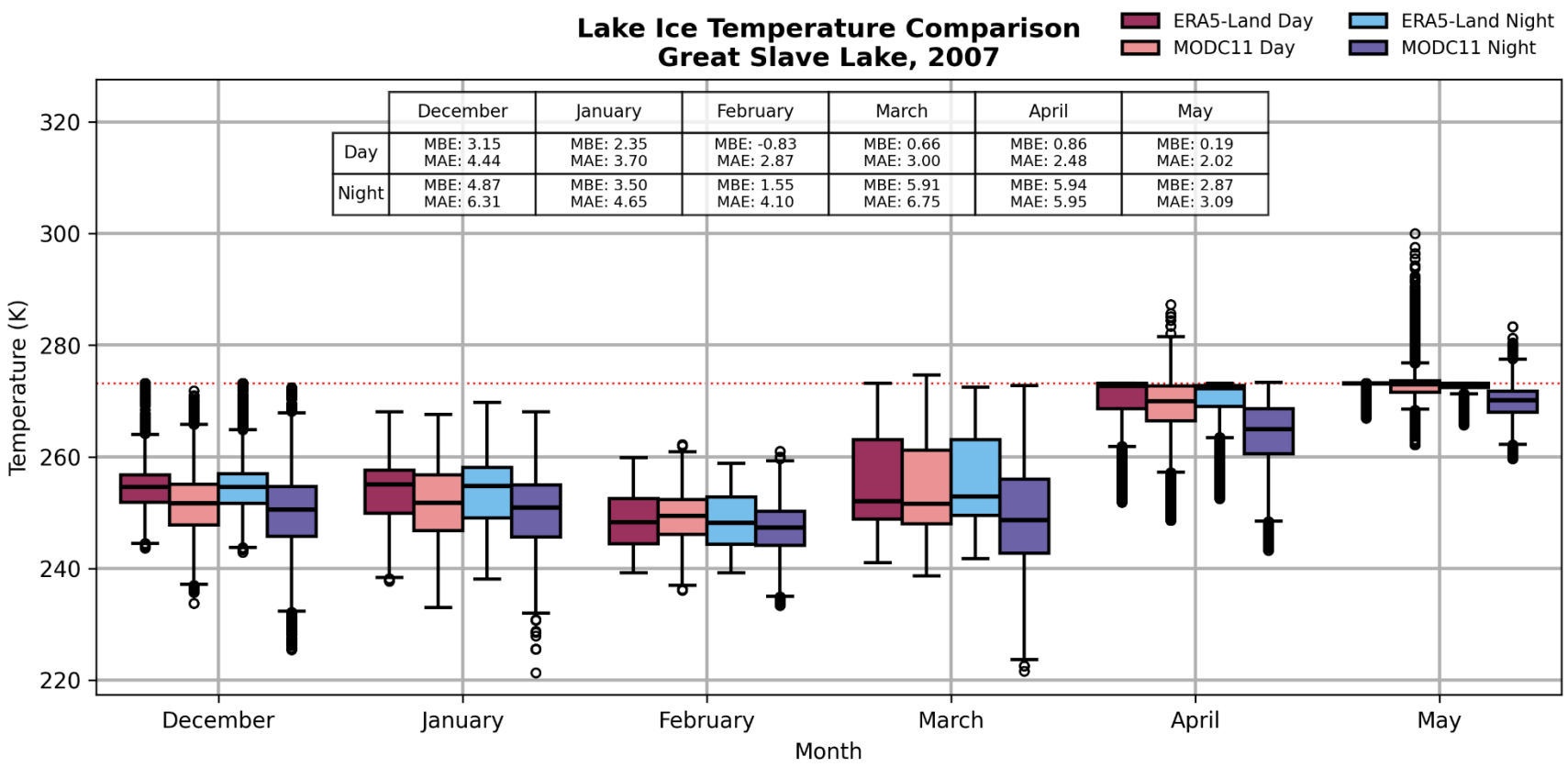


Figure C.2.4: Boxplot of monthly lake ice surface temperatures during ice-on period of ERA5-Land and MODIS for Great Slave Lake, 2007

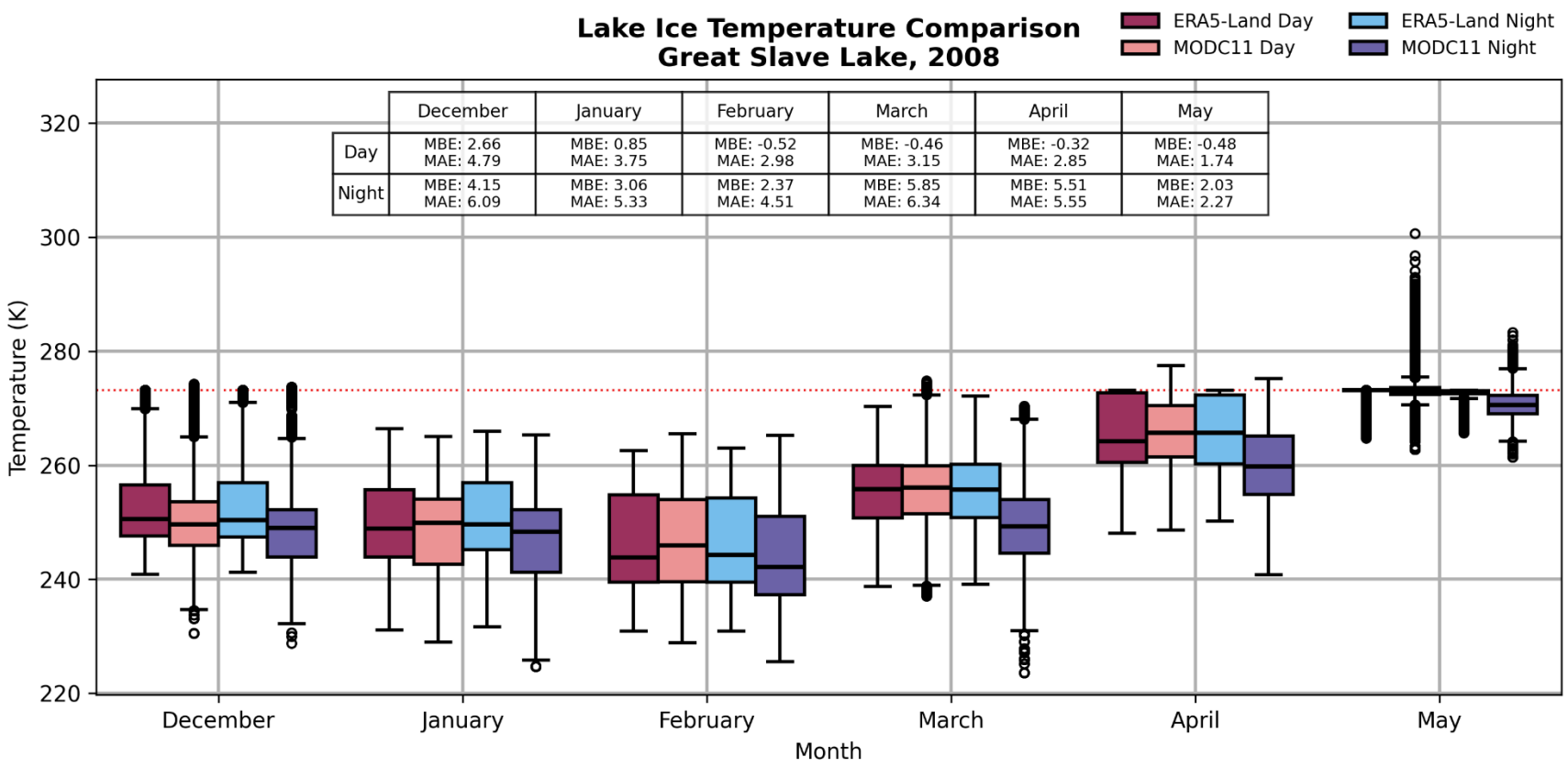


Figure C.2.5: Boxplot of monthly lake ice surface temperatures during ice-on period of ERA5-Land and MODIS for Great Slave Lake, 2008

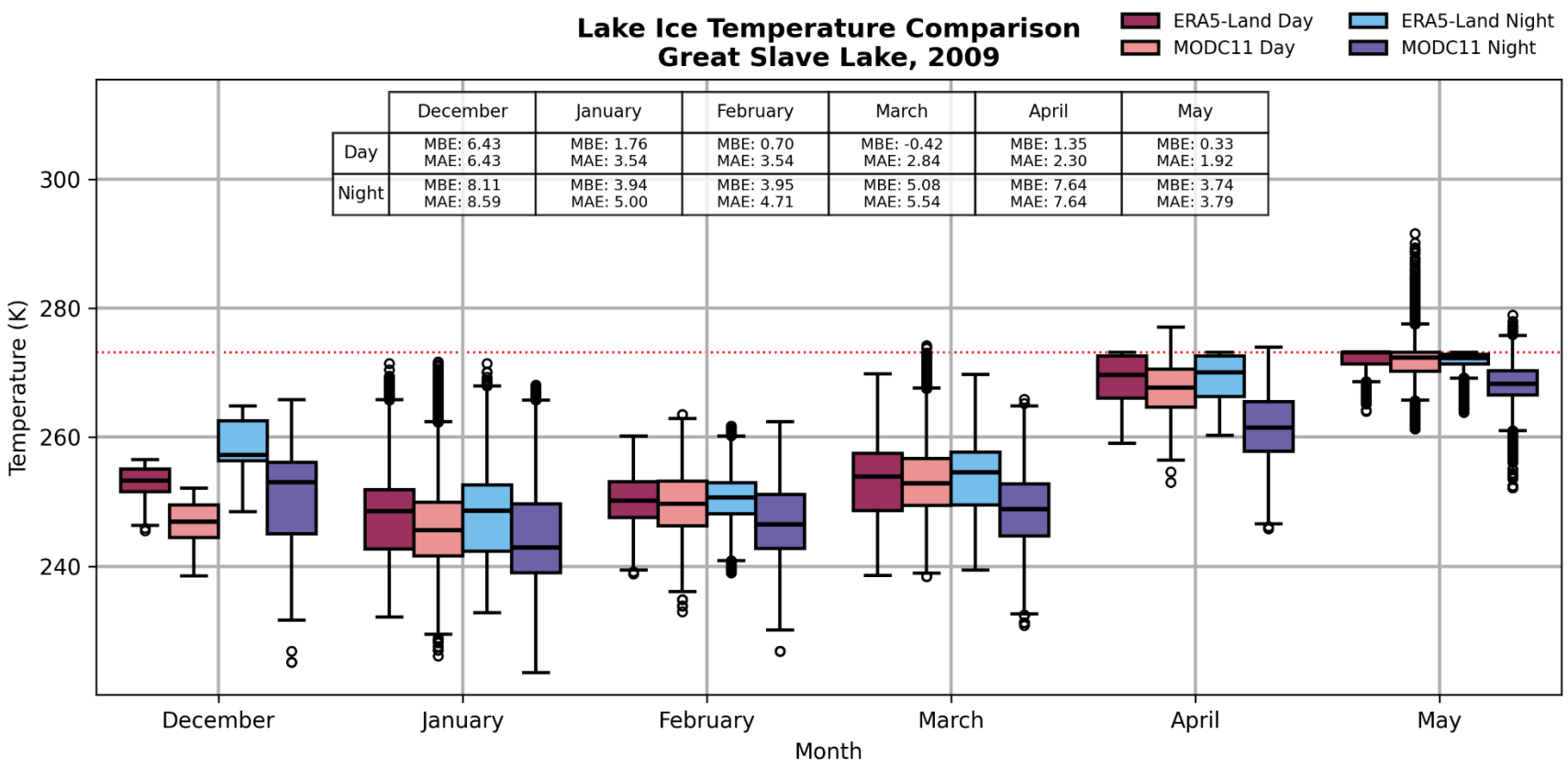


Figure C.2.6: Boxplot of monthly lake ice surface temperatures during ice-on period of ERA5-Land and MODIS for Great Slave Lake, 2009

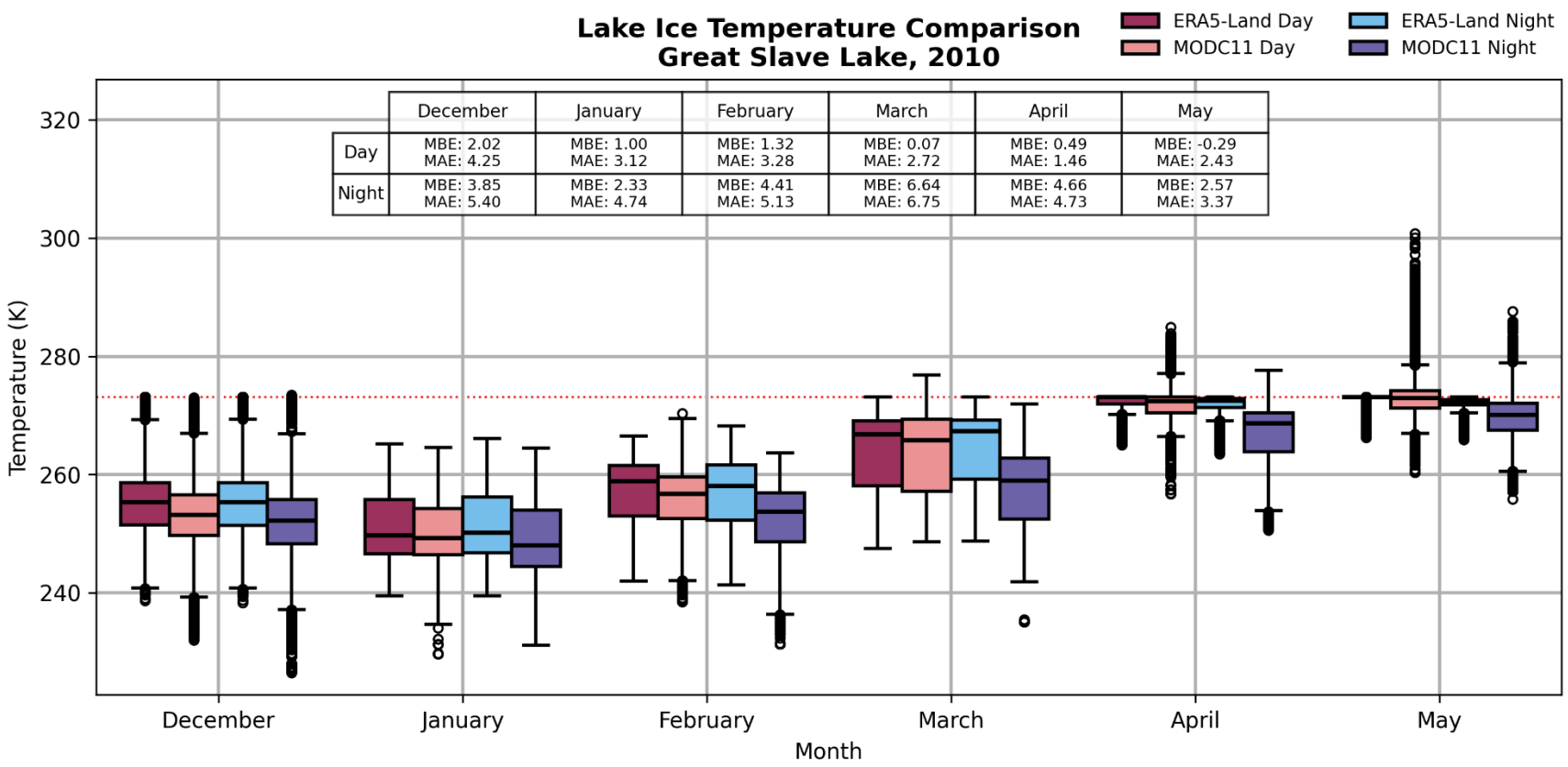


Figure C.2. 7: Boxplot of monthly lake ice surface temperatures during ice-on period of ERA5-Land and MODIS for Great Slave Lake, 2010

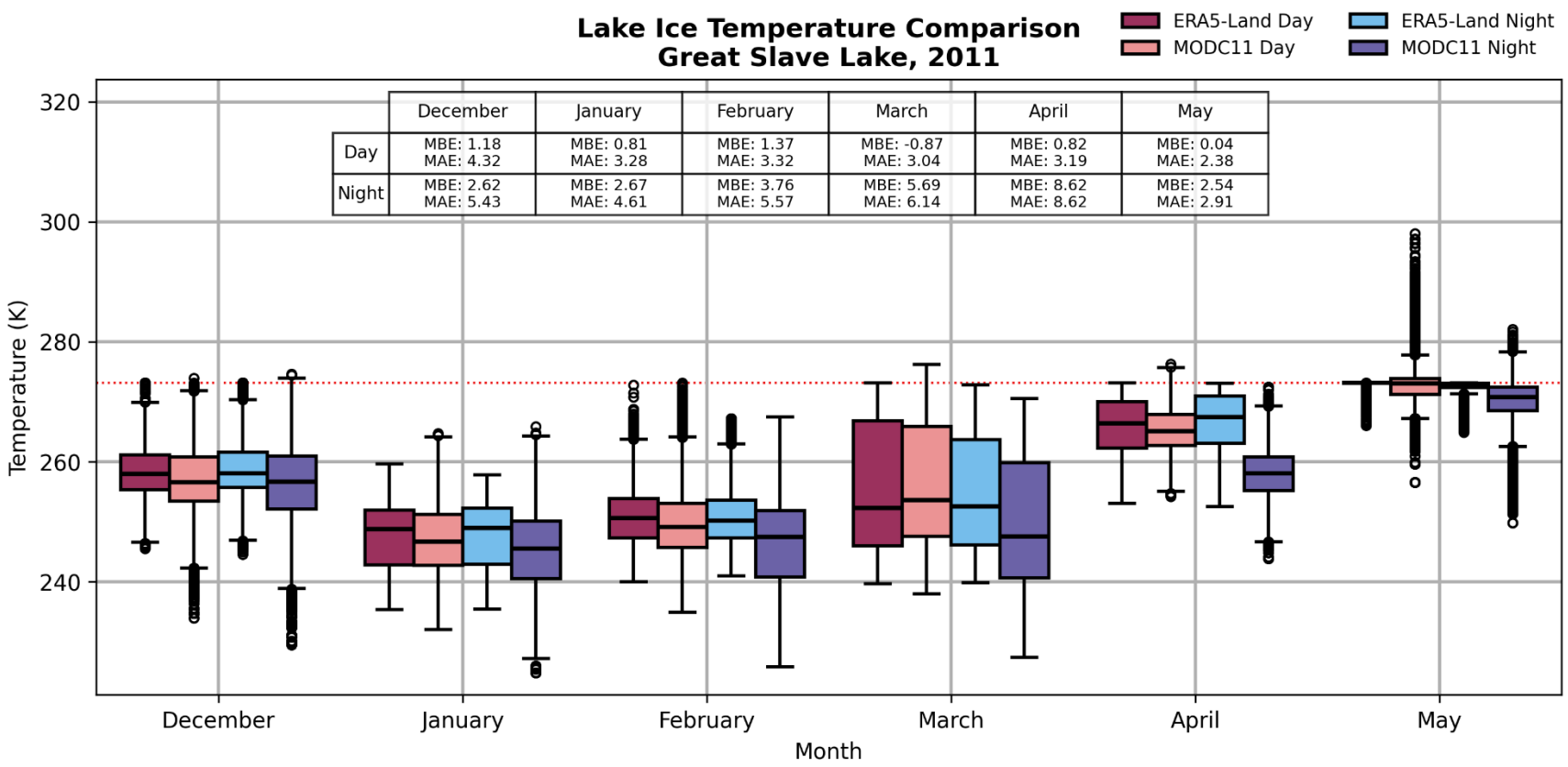


Figure C.2. 8: Boxplot of monthly lake ice surface temperatures during ice-on period of ERA5-Land and MODIS for Great Slave Lake, 2011

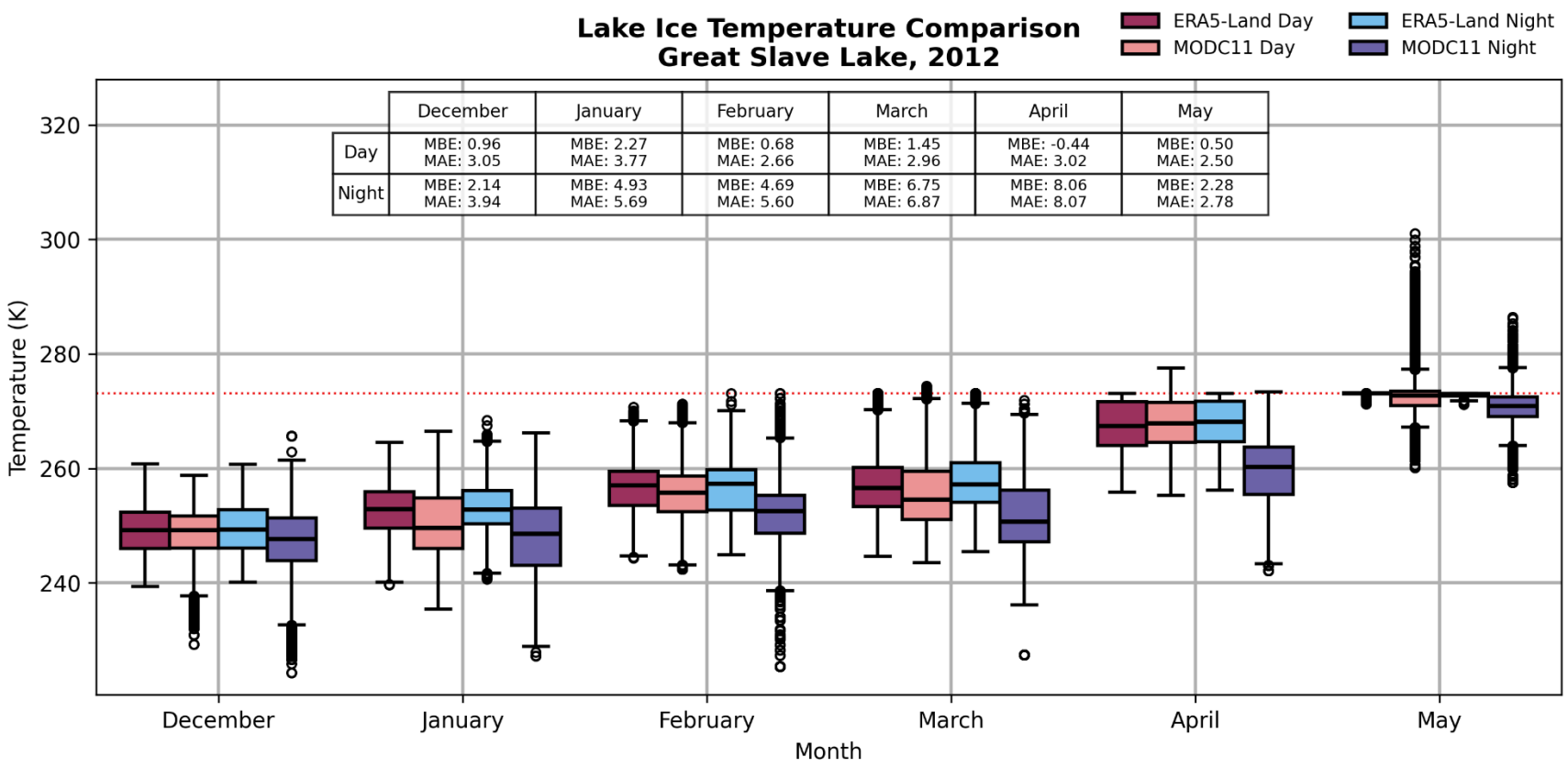


Figure C.2. 9: Boxplot of monthly lake ice surface temperatures during ice-on period of ERA5-Land and MODIS for Great Slave Lake, 2012

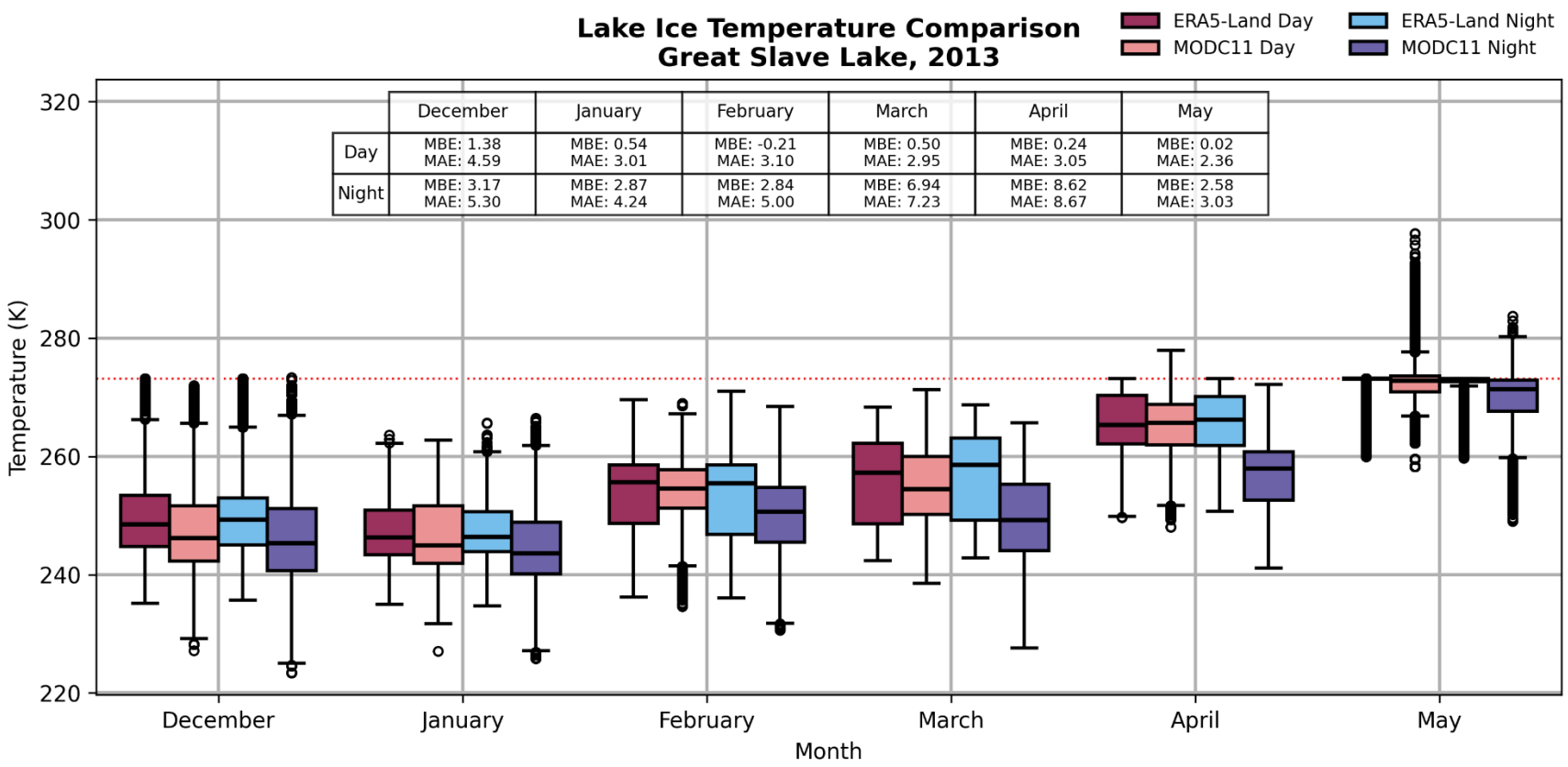


Figure C.2. 10:Boxplot of monthly lake ice surface temperatures during ice-on period of ERA5-Land and MODIS for Great Slave Lake, 2013

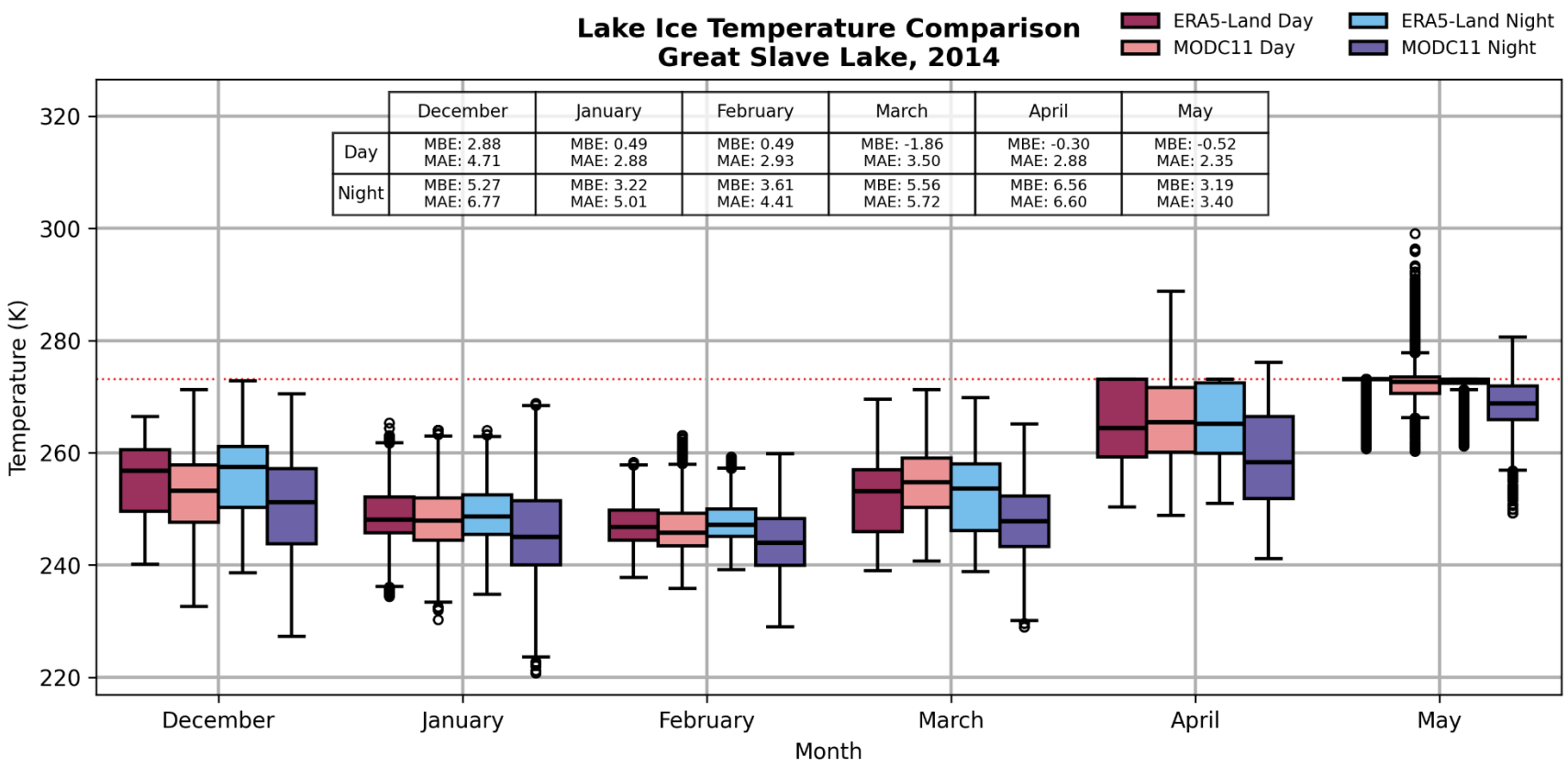


Figure C.2.11: Boxplot of monthly lake ice surface temperatures during ice-on period of ERA5-Land and MODIS for Great Slave Lake, 2014

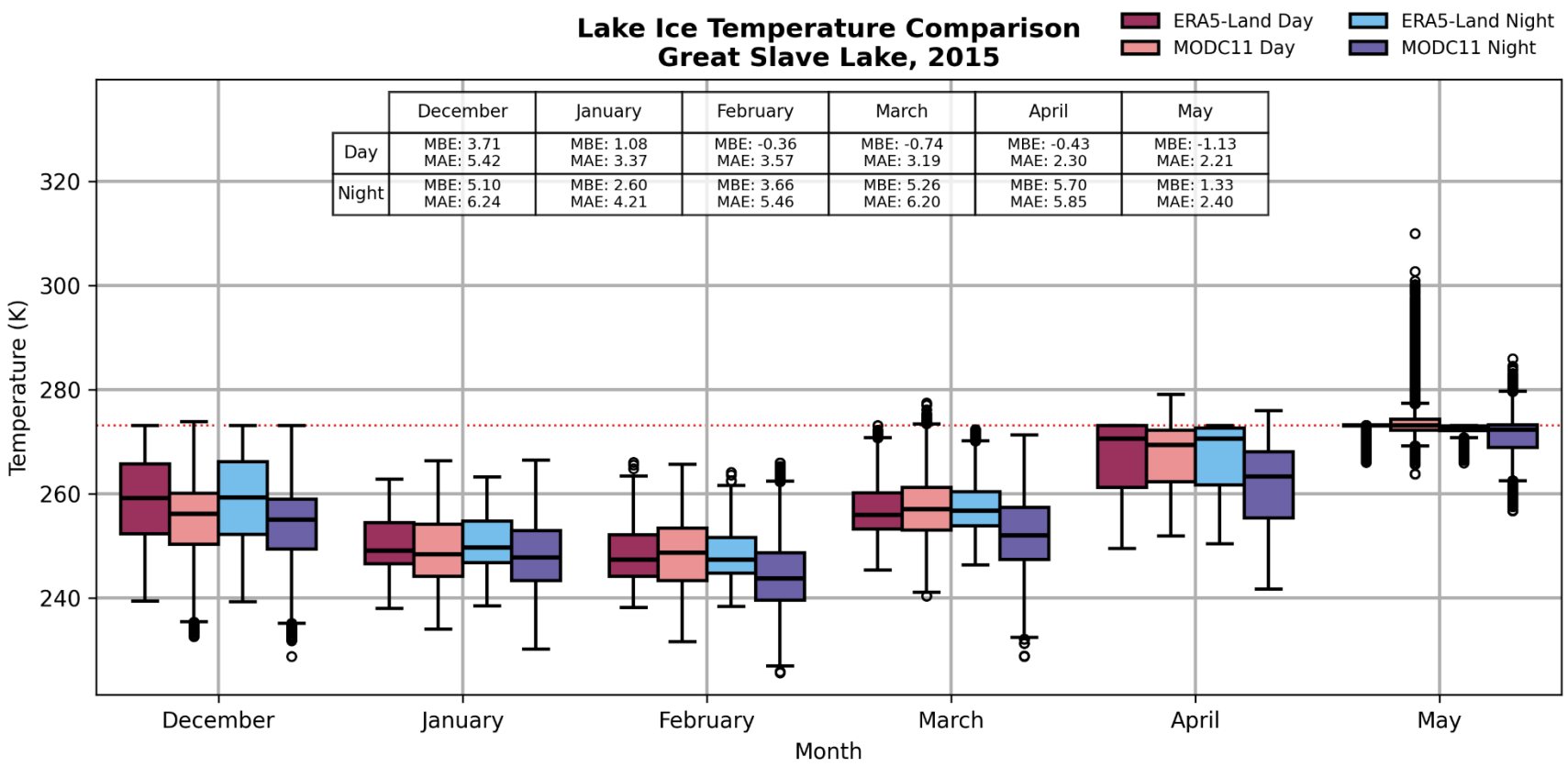


Figure C.2. 12: Boxplot of monthly lake ice surface temperatures during ice-on period of ERA5-Land and MODIS for Great Slave Lake, 2015

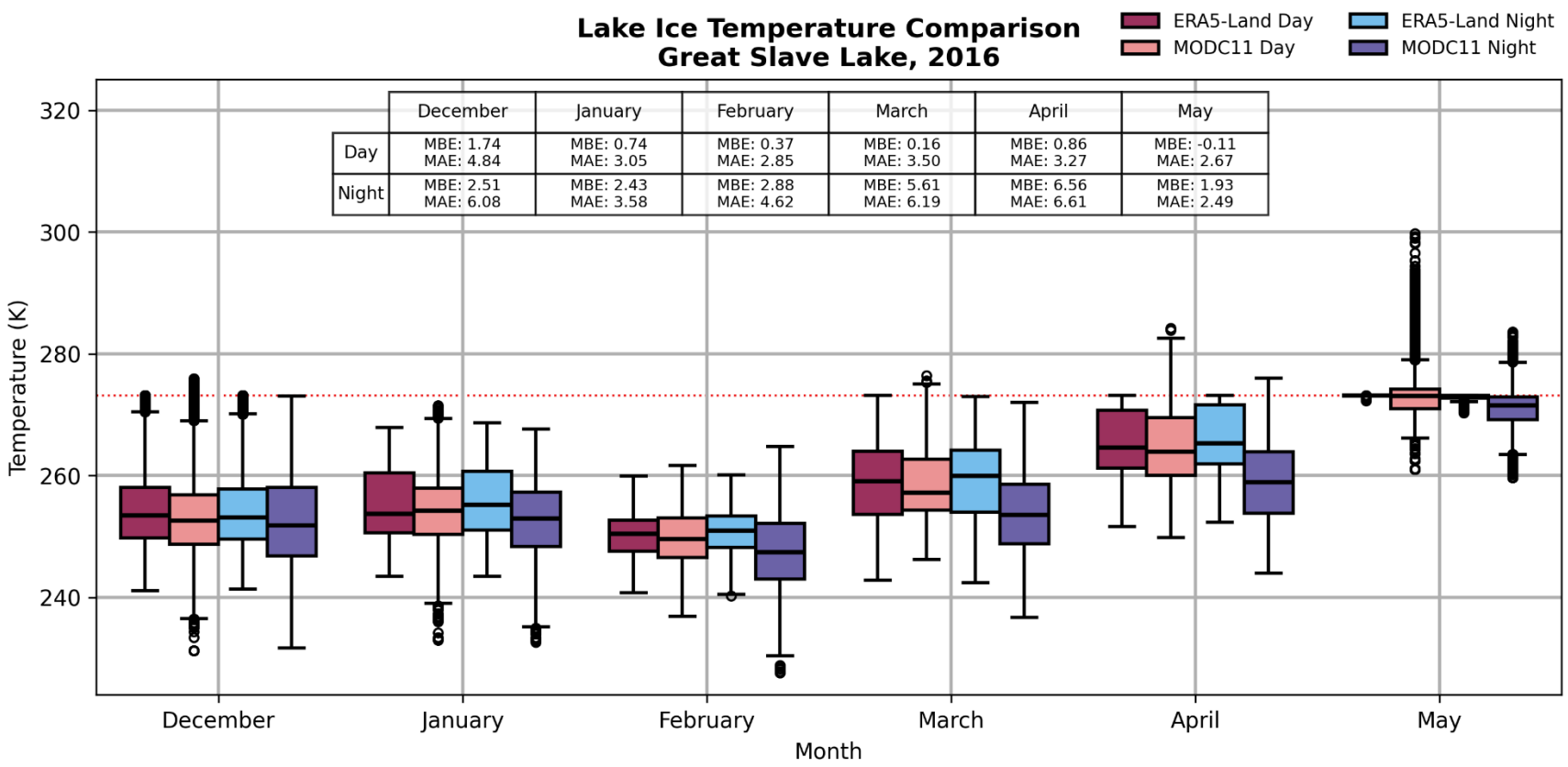


Figure C.2. 13: Boxplot of monthly lake ice surface temperatures during ice-on period of ERA5-Land and MODIS for Great Slave Lake, 2016

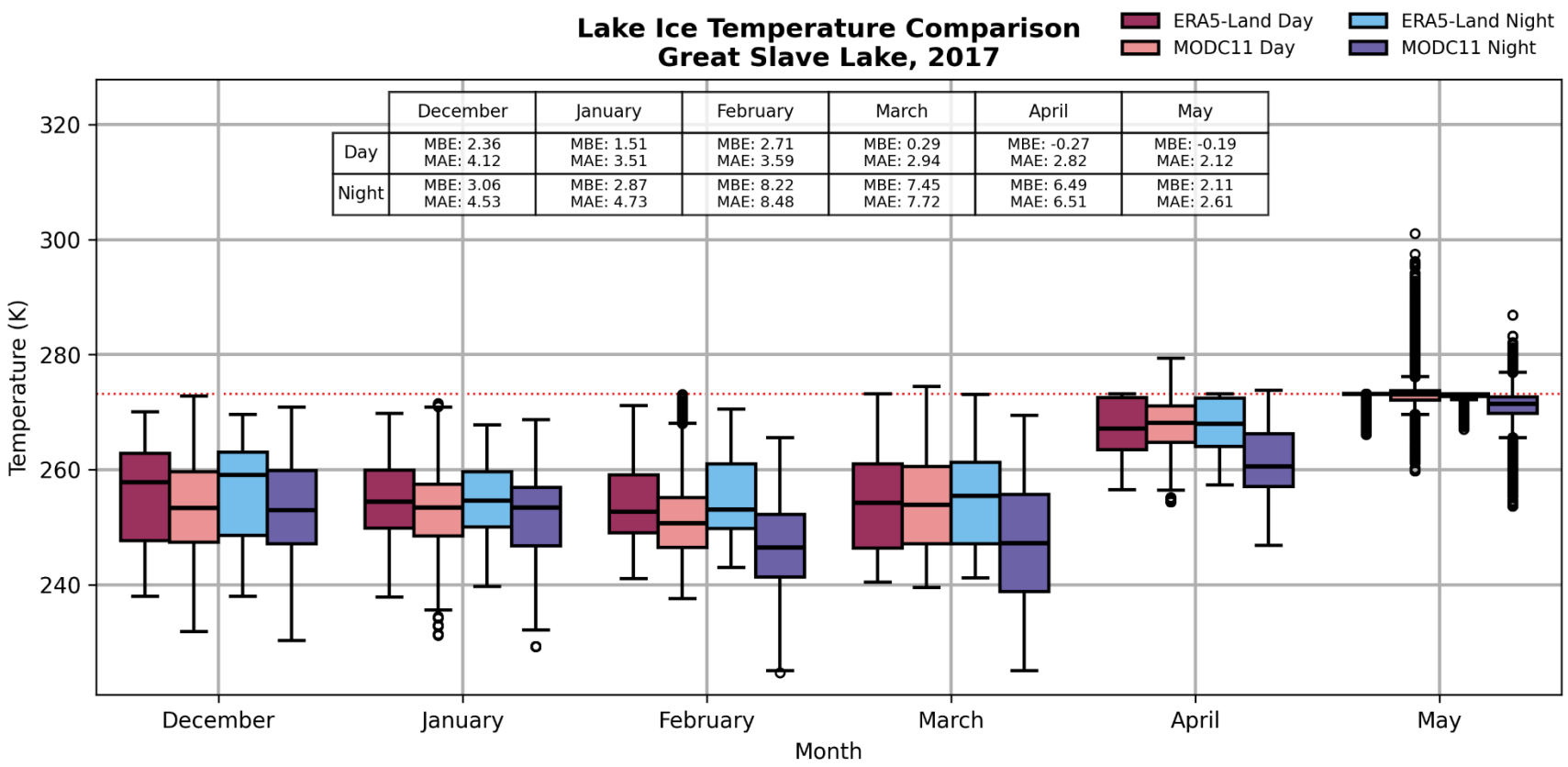


Figure C.2. 14: Boxplot of monthly lake ice surface temperatures during ice-on period of ERA5-Land and MODIS for Great Slave Lake, 2017

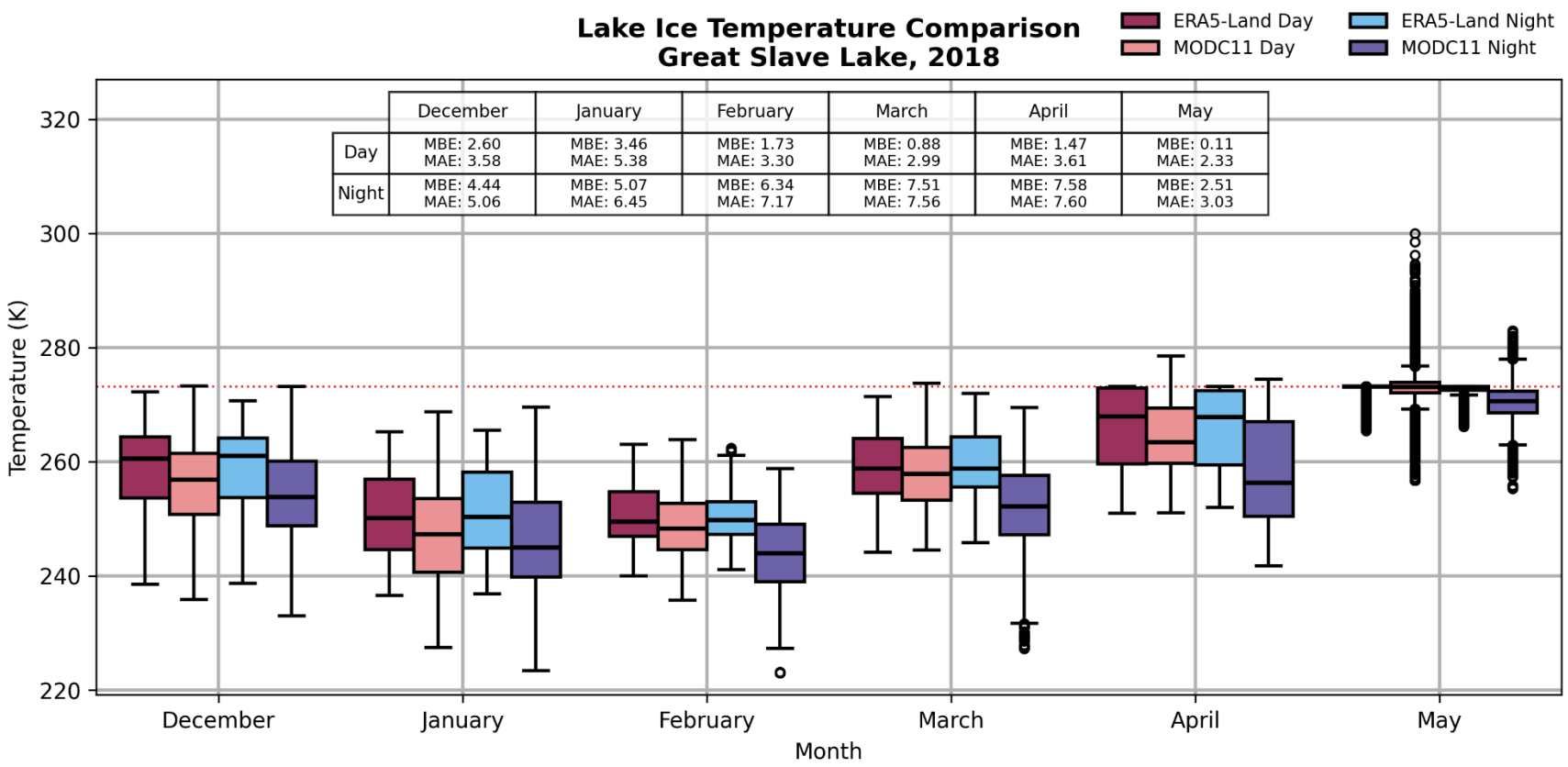


Figure C.2. 15: Boxplot of monthly lake ice surface temperatures during ice-on period of ERA5-Land and MODIS for Great Slave Lake, 2018

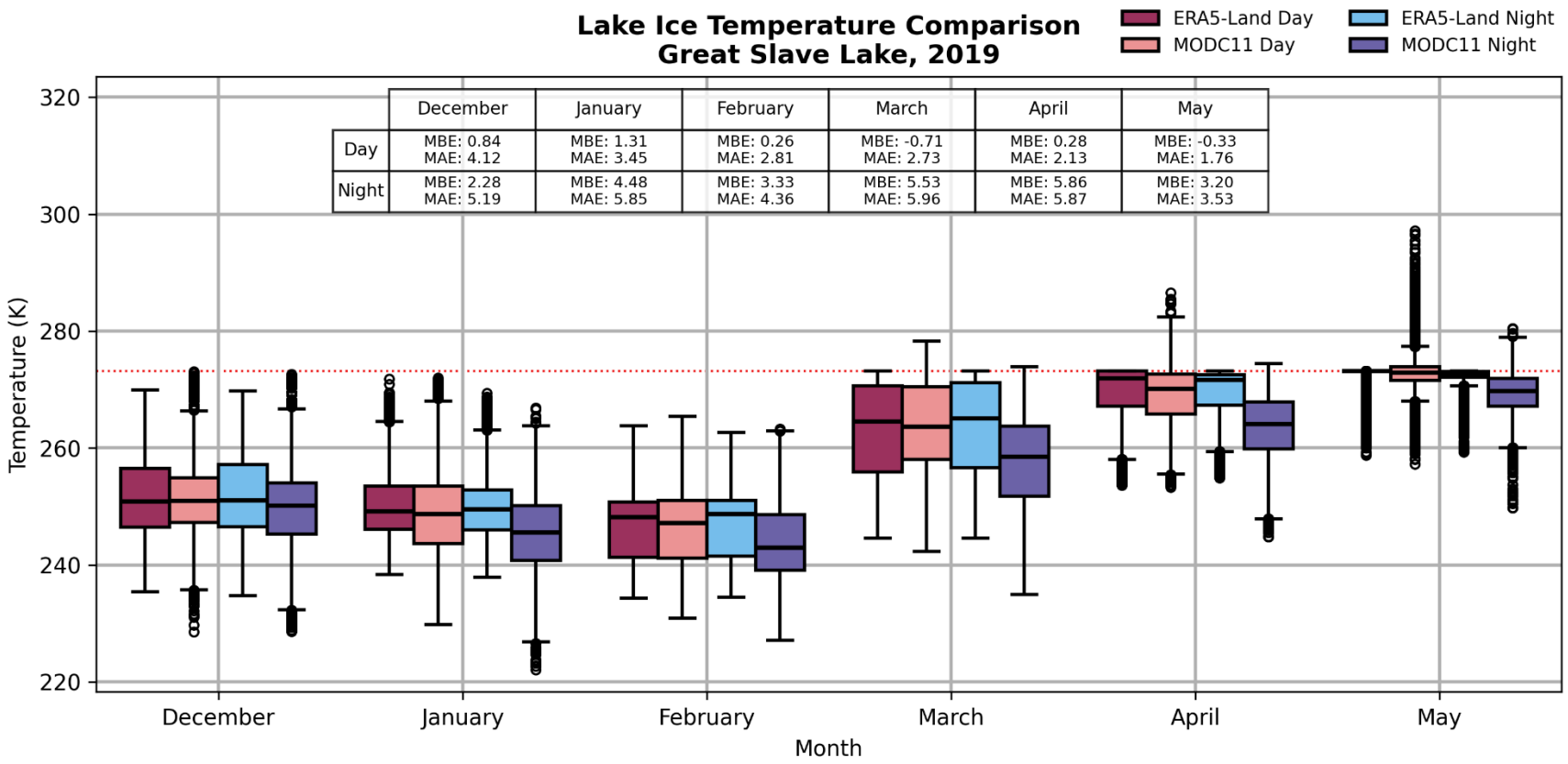


Figure C.2. 16: Boxplot of monthly lake ice surface temperatures during ice-on period of ERA5-Land and MODIS for Great Slave Lake, 2019

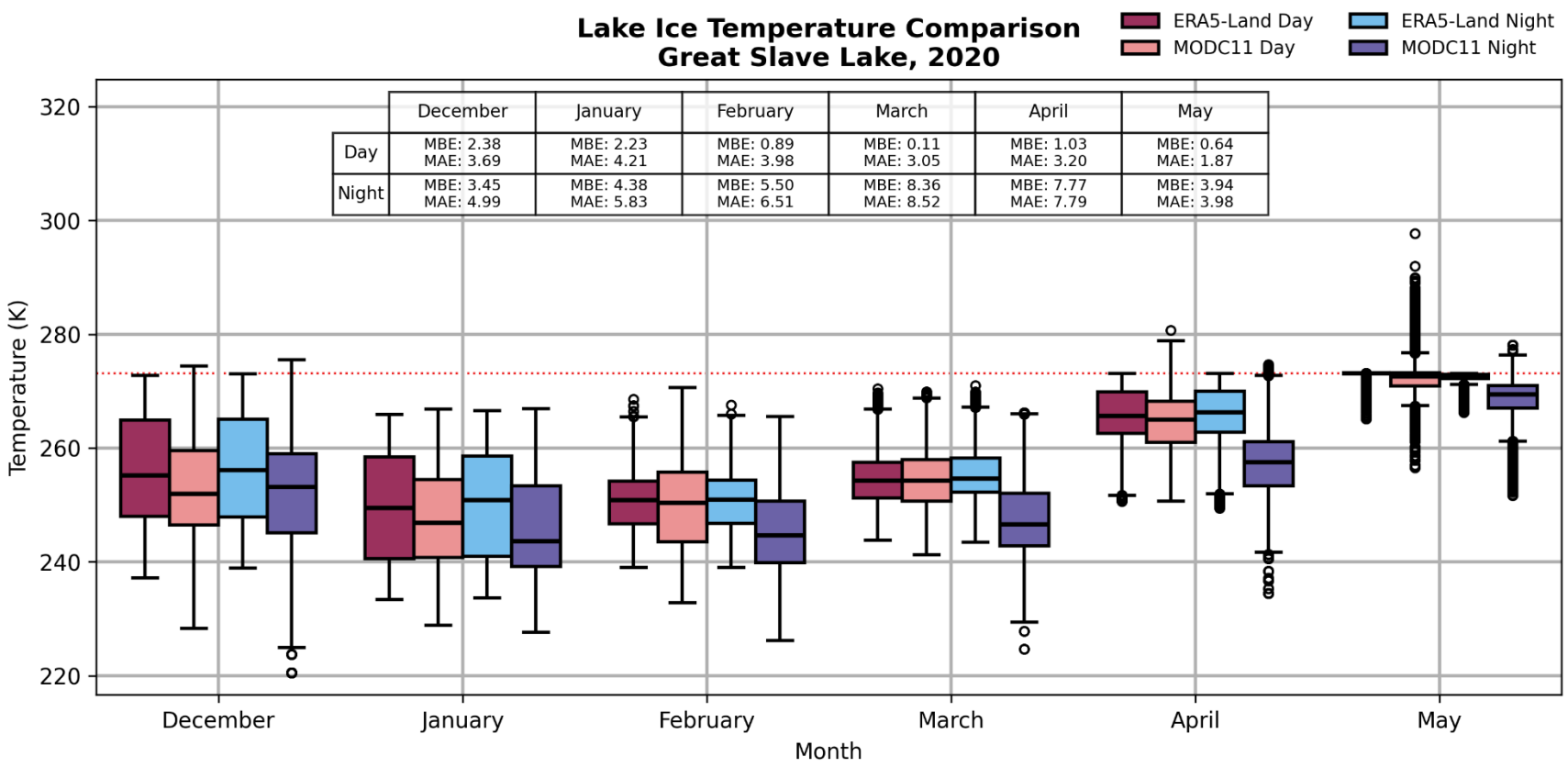


Figure C.2. 17: Boxplot of monthly lake ice surface temperatures during ice-on period of ERA5-Land and MODIS for Great Slave Lake, 2020

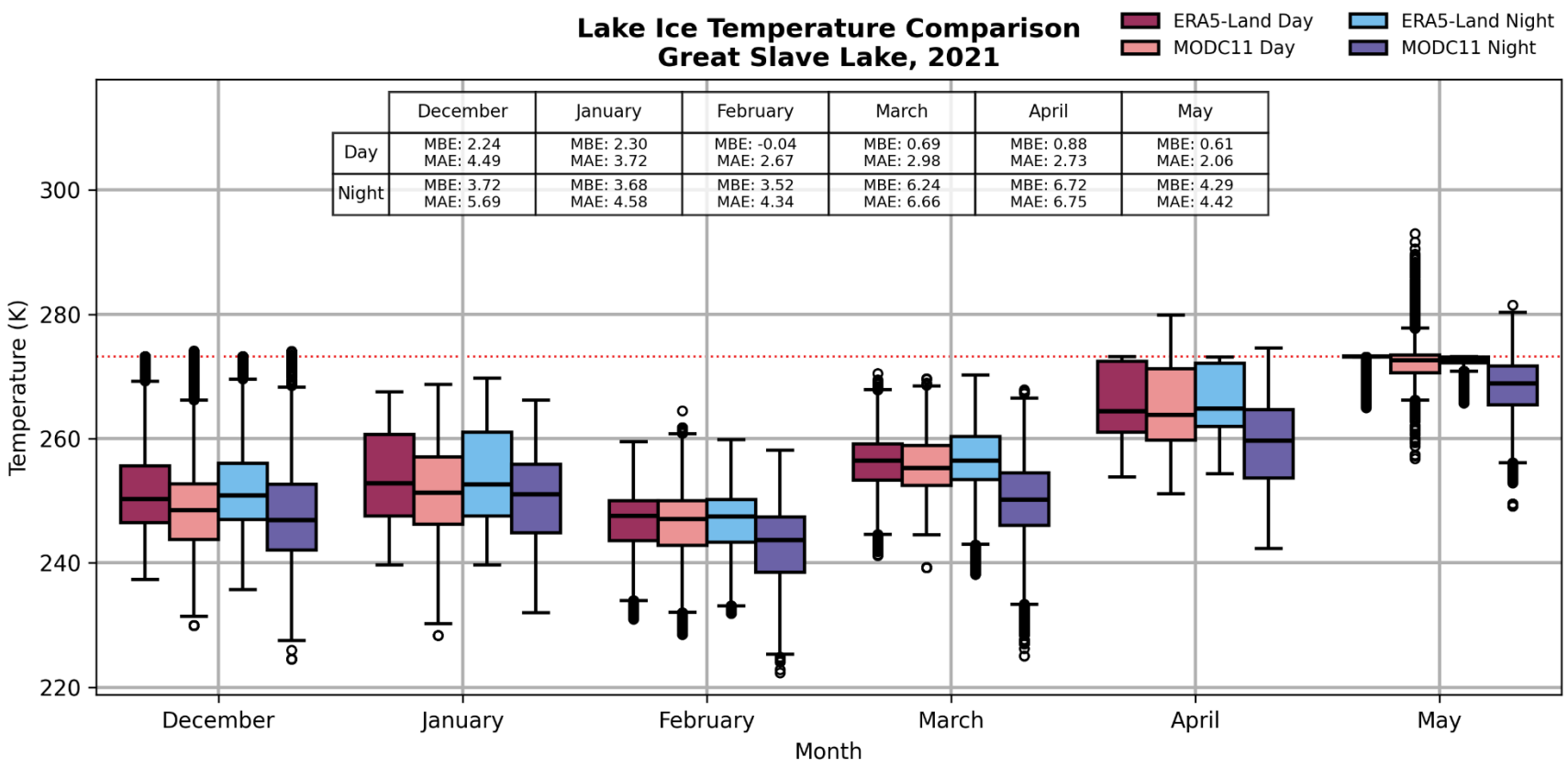


Figure C.2. 18: Boxplot of monthly lake ice surface temperatures during ice-on period of ERA5-Land and MODIS for Great Slave Lake, 2021

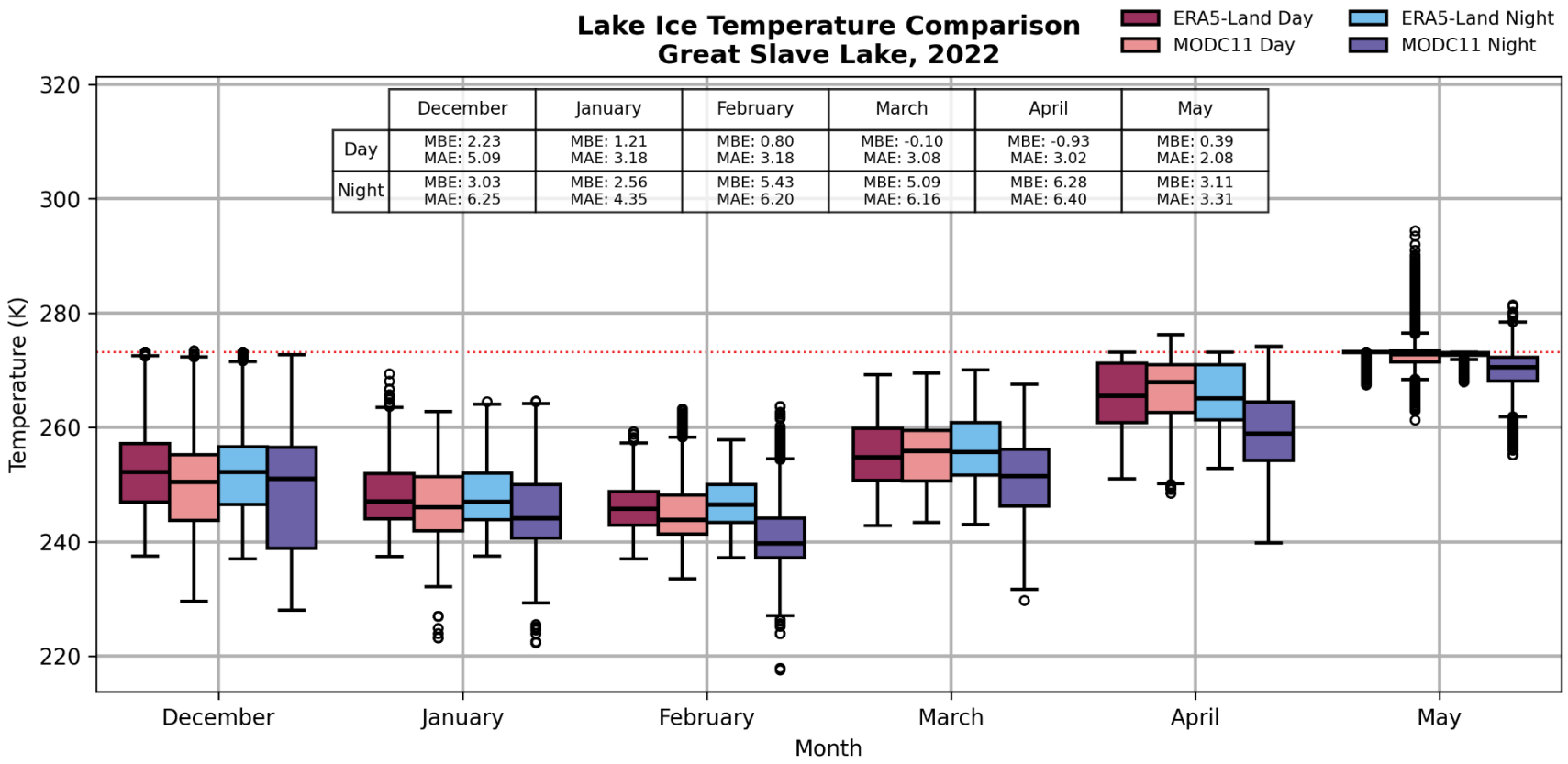


Figure C.2. 19: Boxplot of monthly lake ice surface temperatures during ice-on period of ERA5-Land and MODIS for Great Slave Lake, 2022

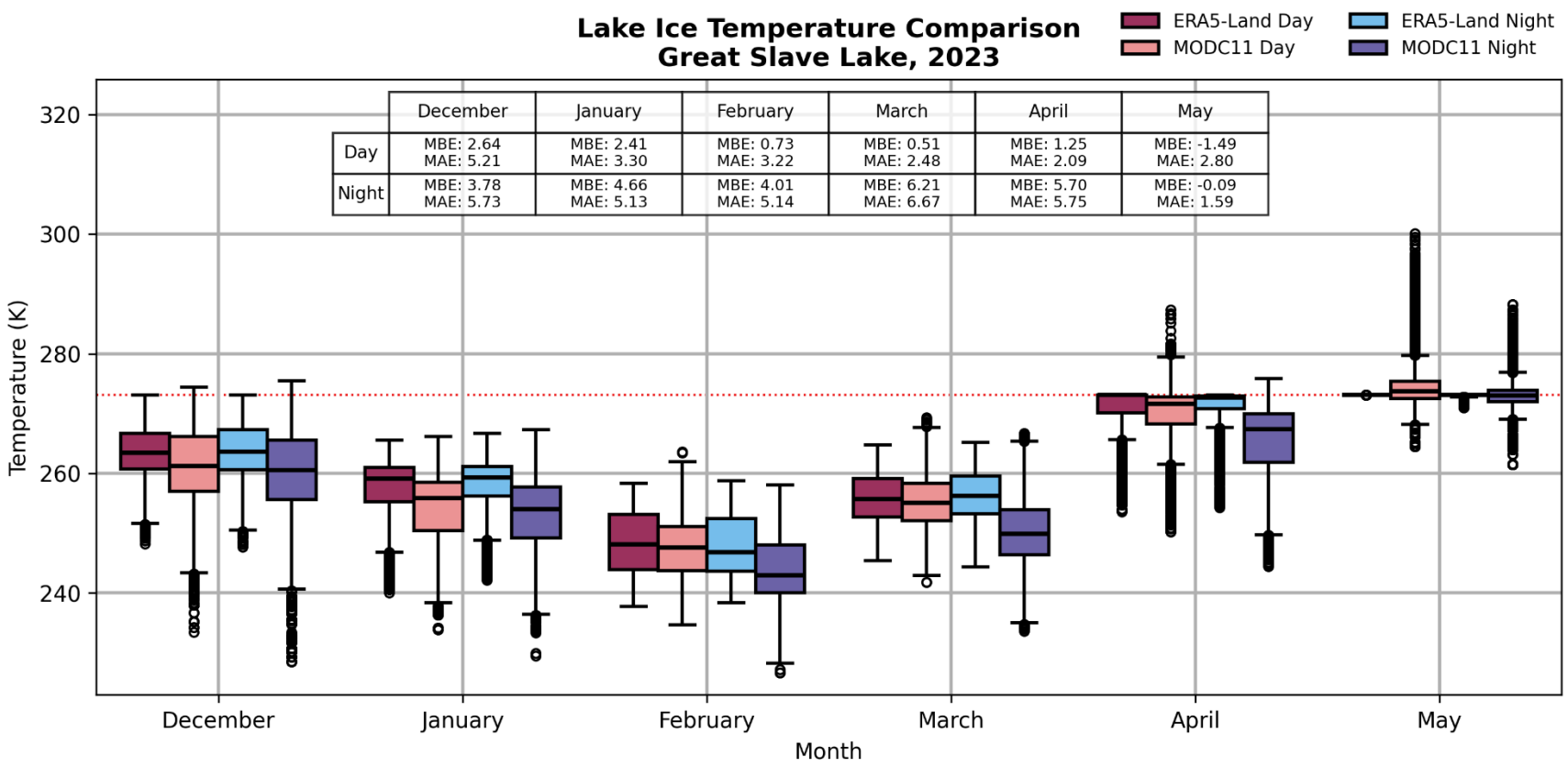


Figure C.2. 20: Boxplot of monthly lake ice surface temperatures during ice-on period of ERA5-Land and MODIS for Great Slave Lake, 2023

C.3 Lake Athabasca

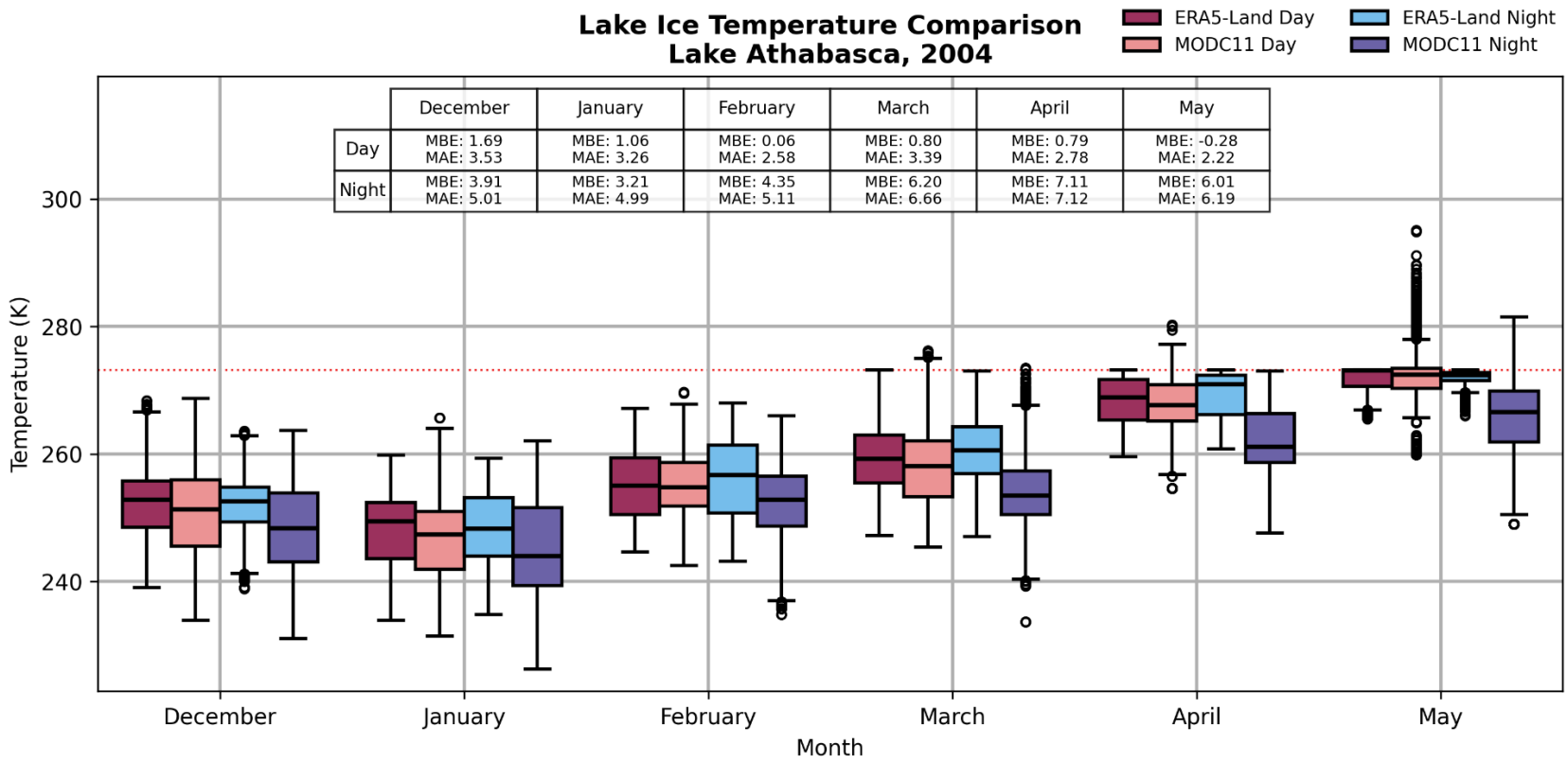


Figure C.3.1: Boxplot of monthly lake ice surface temperatures during ice-on period of ERA5-Land and MODIS for Lake Athabasca, 2004

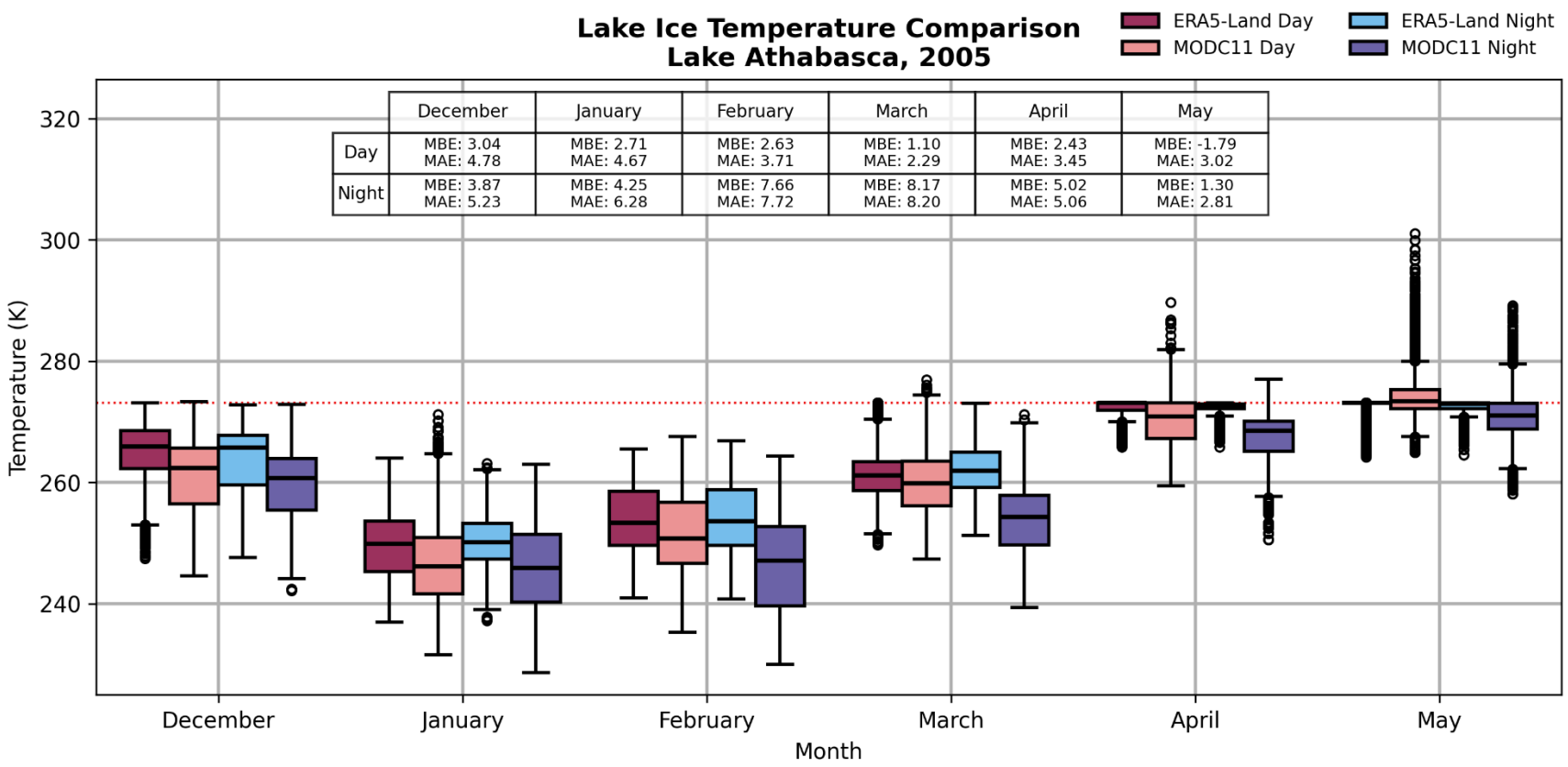


Figure C.3. 2: Boxplot of monthly lake ice surface temperatures during ice-on period of ERA5-Land and MODIS for Lake Athabasca, 2005

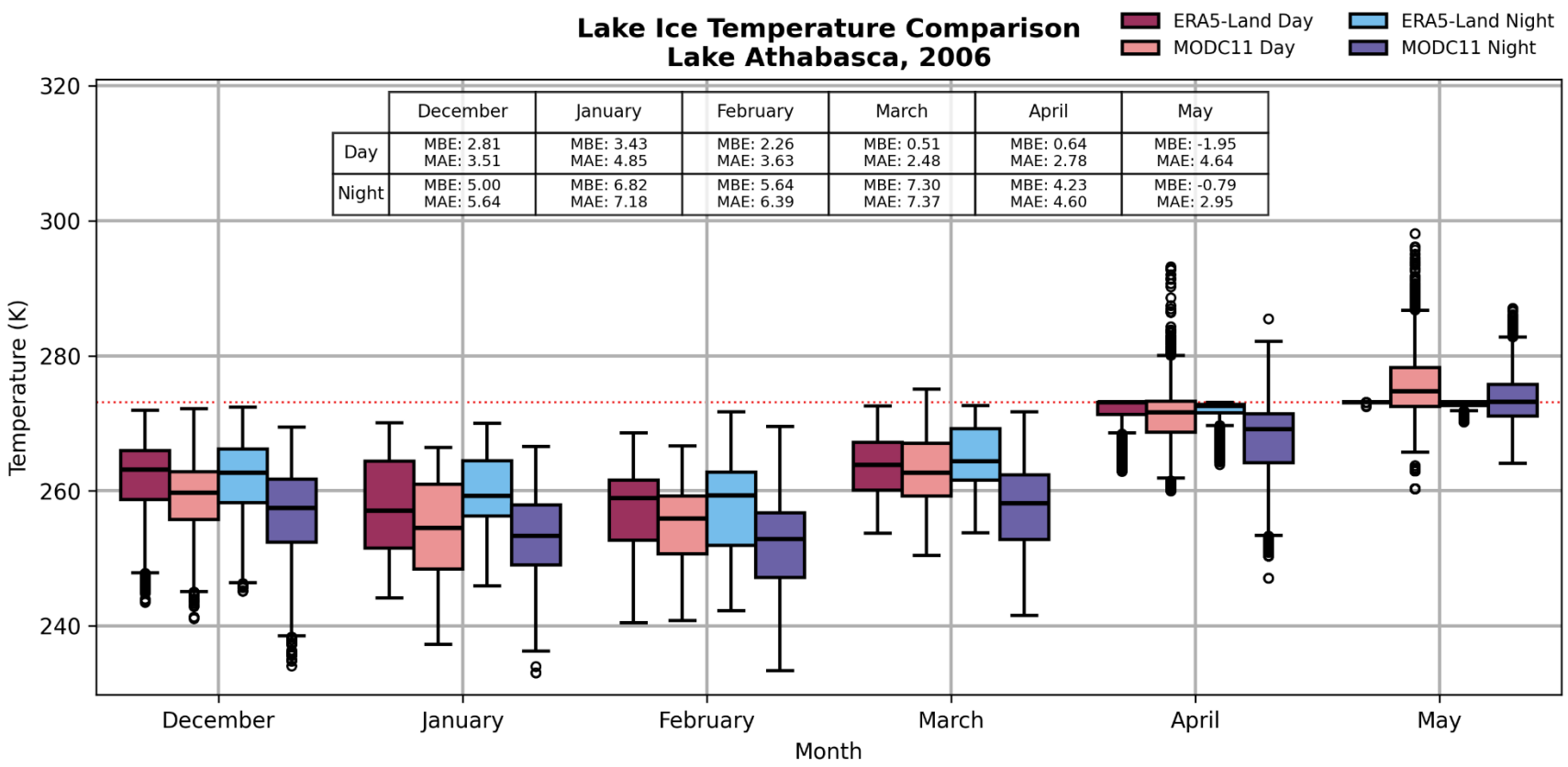


Figure C.3. 3: Boxplot of monthly lake ice surface temperatures during ice-on period of ERA5-Land and MODIS for Lake Athabasca, 2006

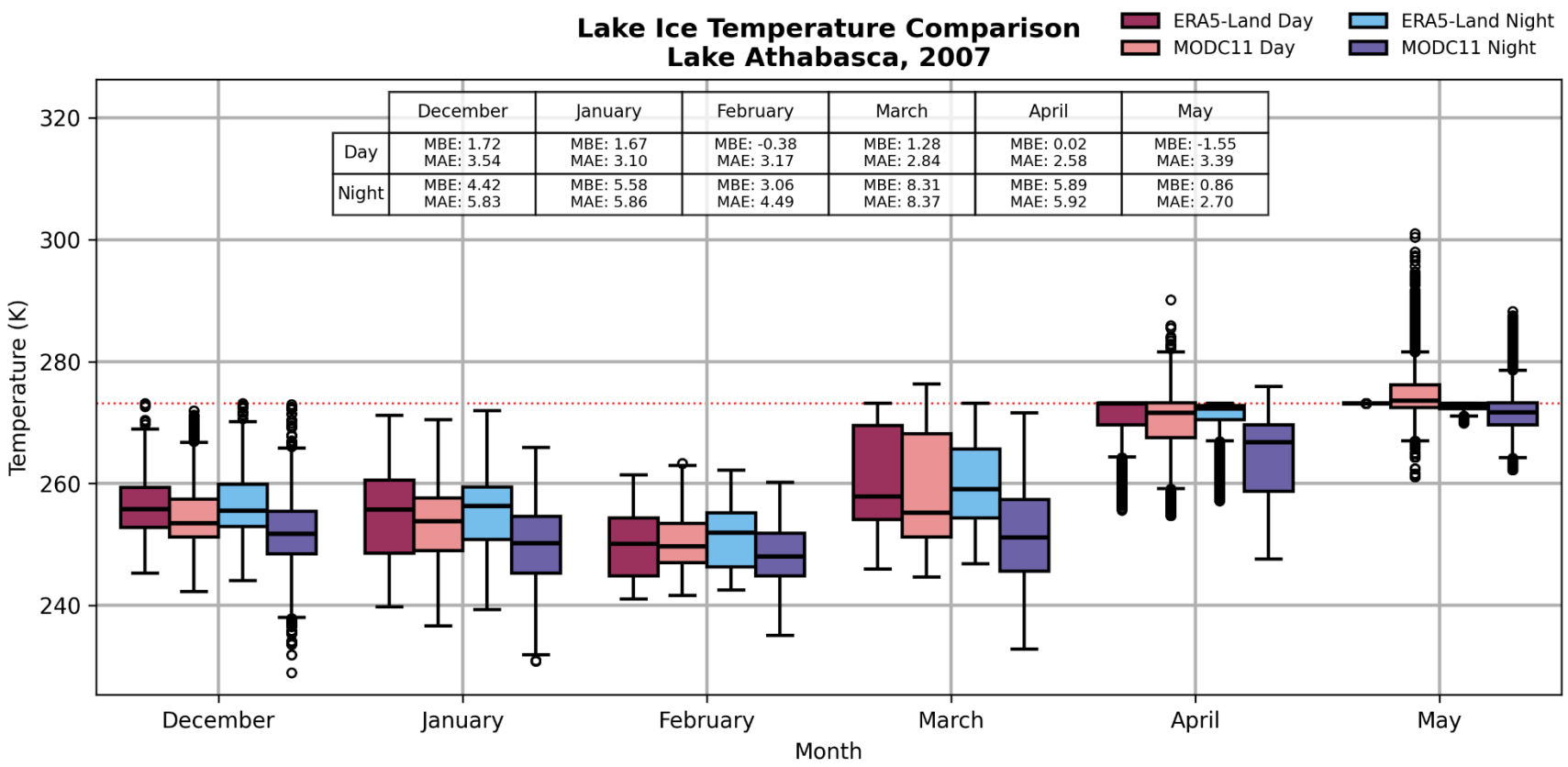


Figure C.3. 4: Boxplot of monthly lake ice surface temperatures during ice-on period of ERA5-Land and MODIS for Lake Athabasca, 2007

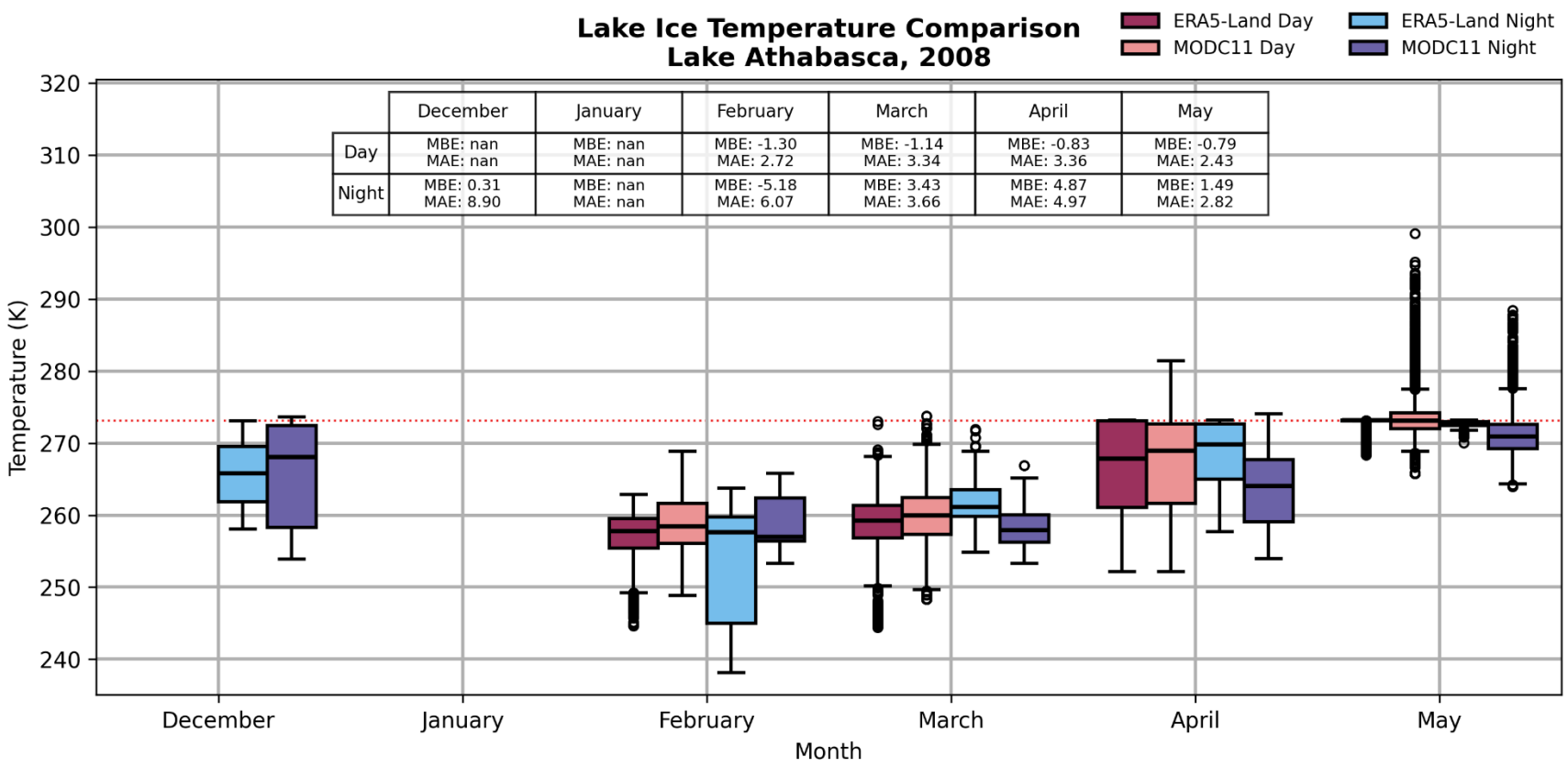


Figure C.3. 5: Boxplot of monthly lake ice surface temperatures during ice-on period of ERA5-Land and MODIS for Lake Athabasca, 2008

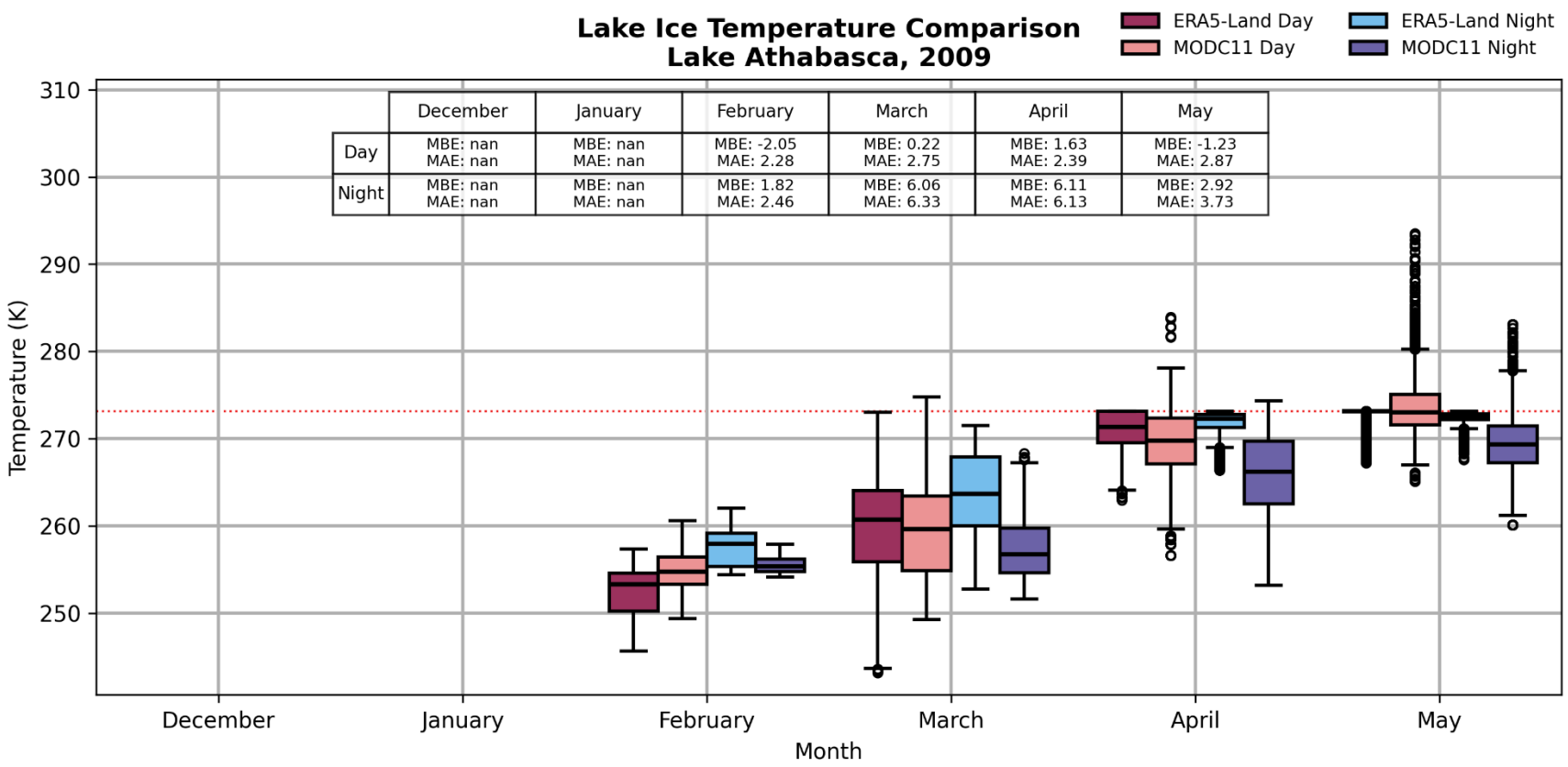


Figure C.3. 6: Boxplot of monthly lake ice surface temperatures during ice-on period of ERA5-Land and MODIS for Lake Athabasca, 2009

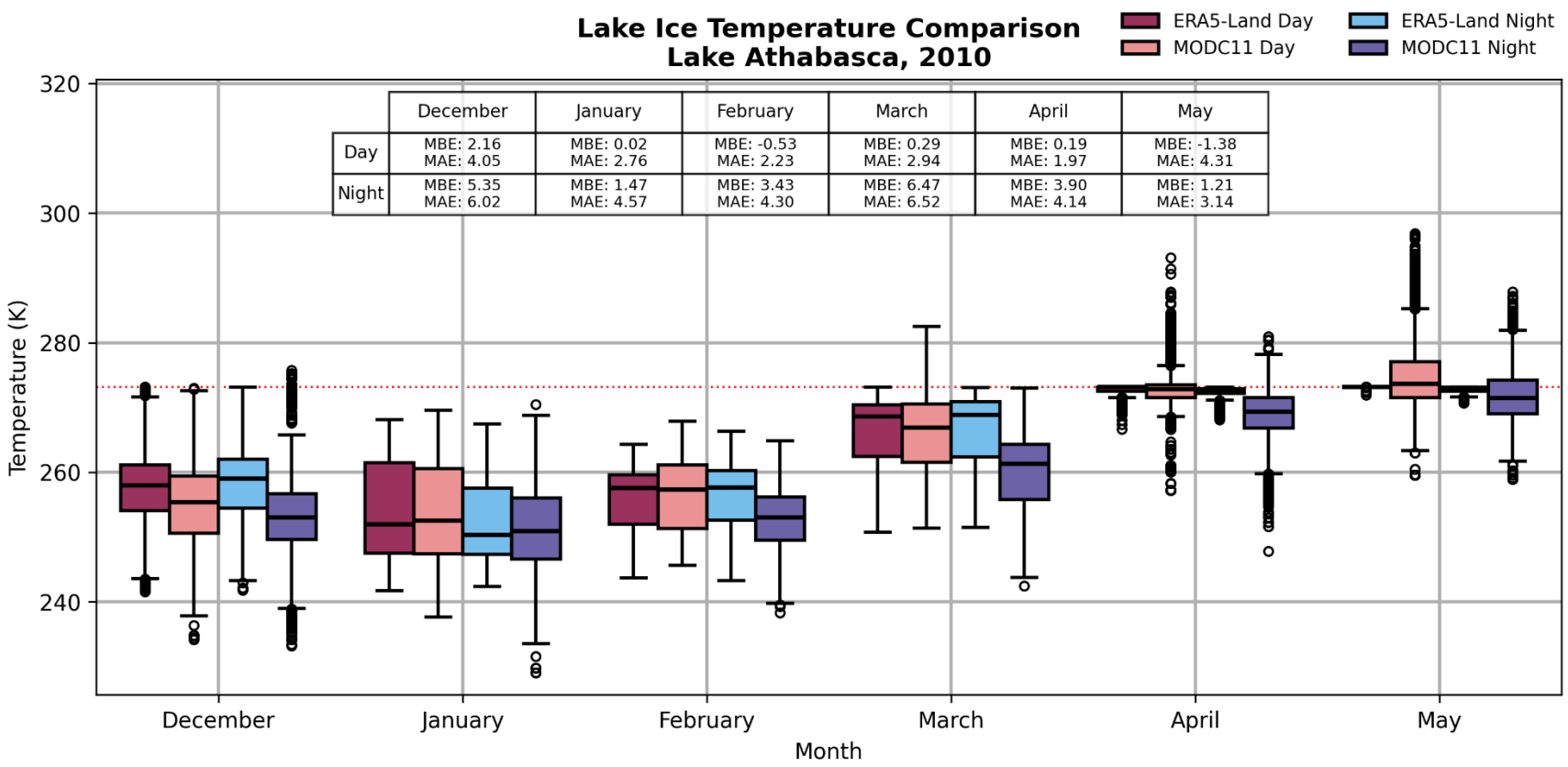


Figure C.3. 7: Boxplot of monthly lake ice surface temperatures during ice-on period of ERA5-Land and MODIS for Lake Athabasca, 2010

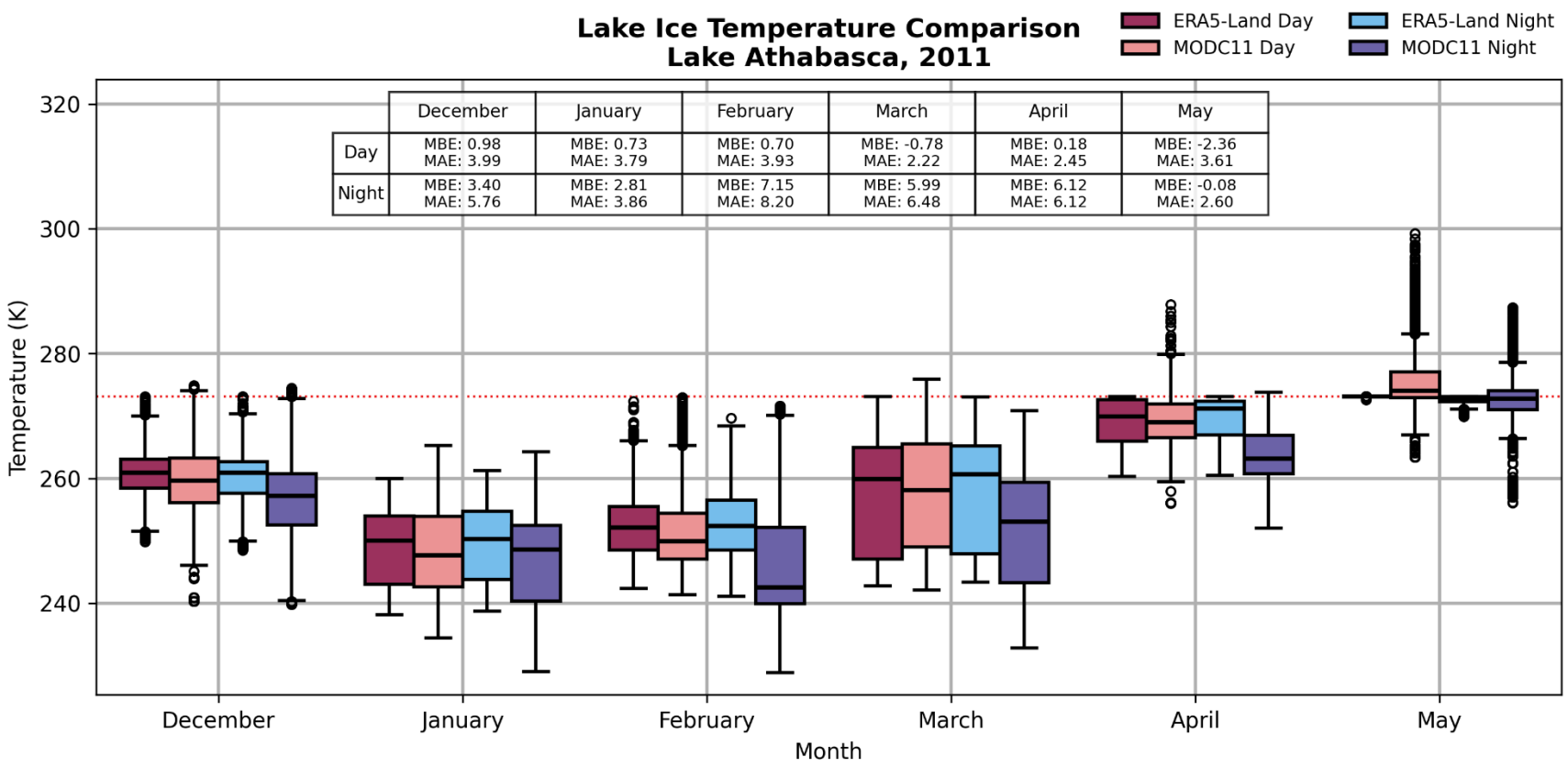


Figure C.3. 8: Boxplot of monthly lake ice surface temperatures during ice-on period of ERA5-Land and MODIS for Lake Athabasca, 2011

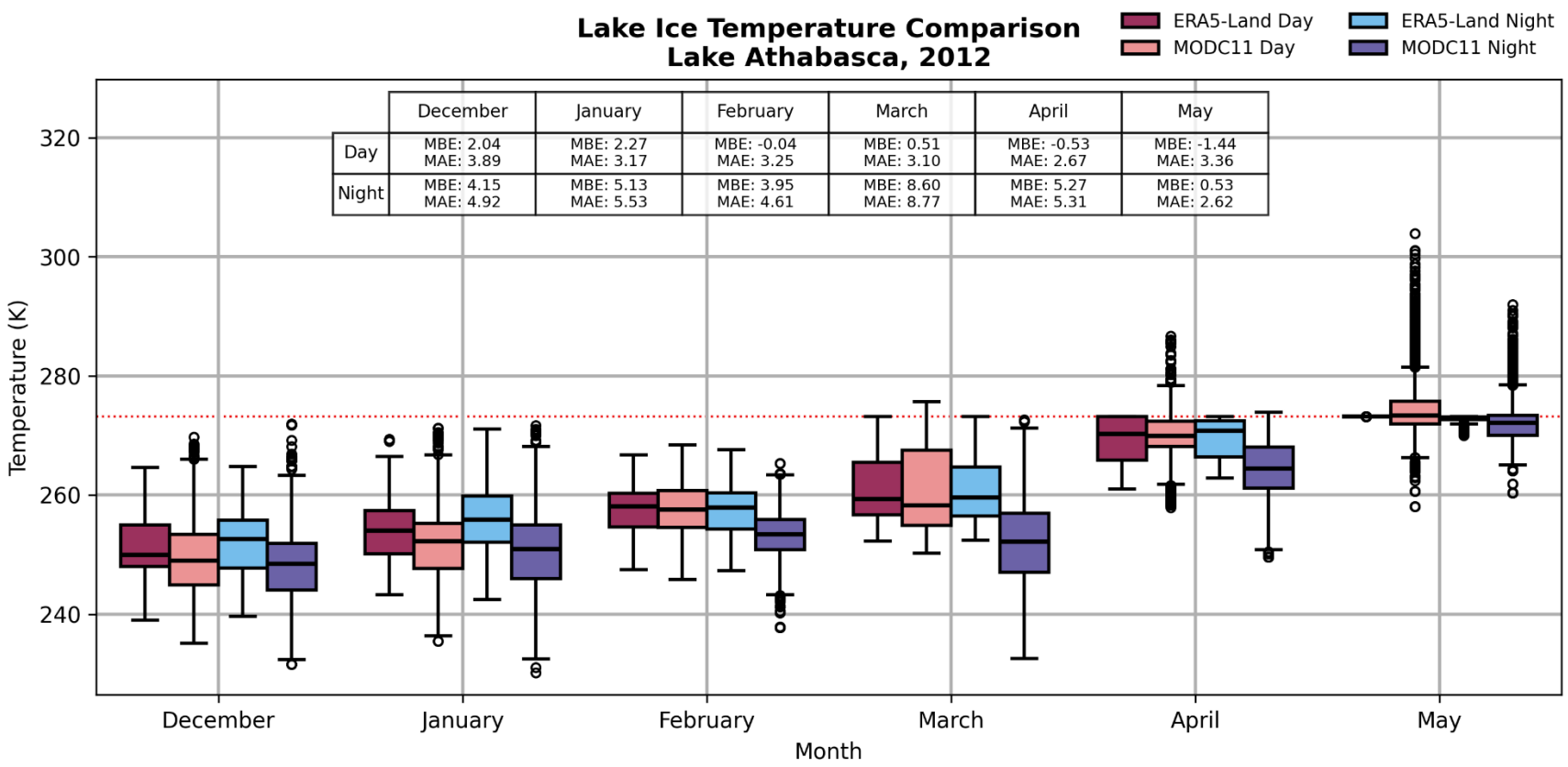


Figure C.3. 9: Boxplot of monthly lake ice surface temperatures during ice-on period of ERA5-Land and MODIS for Lake Athabasca, 2012

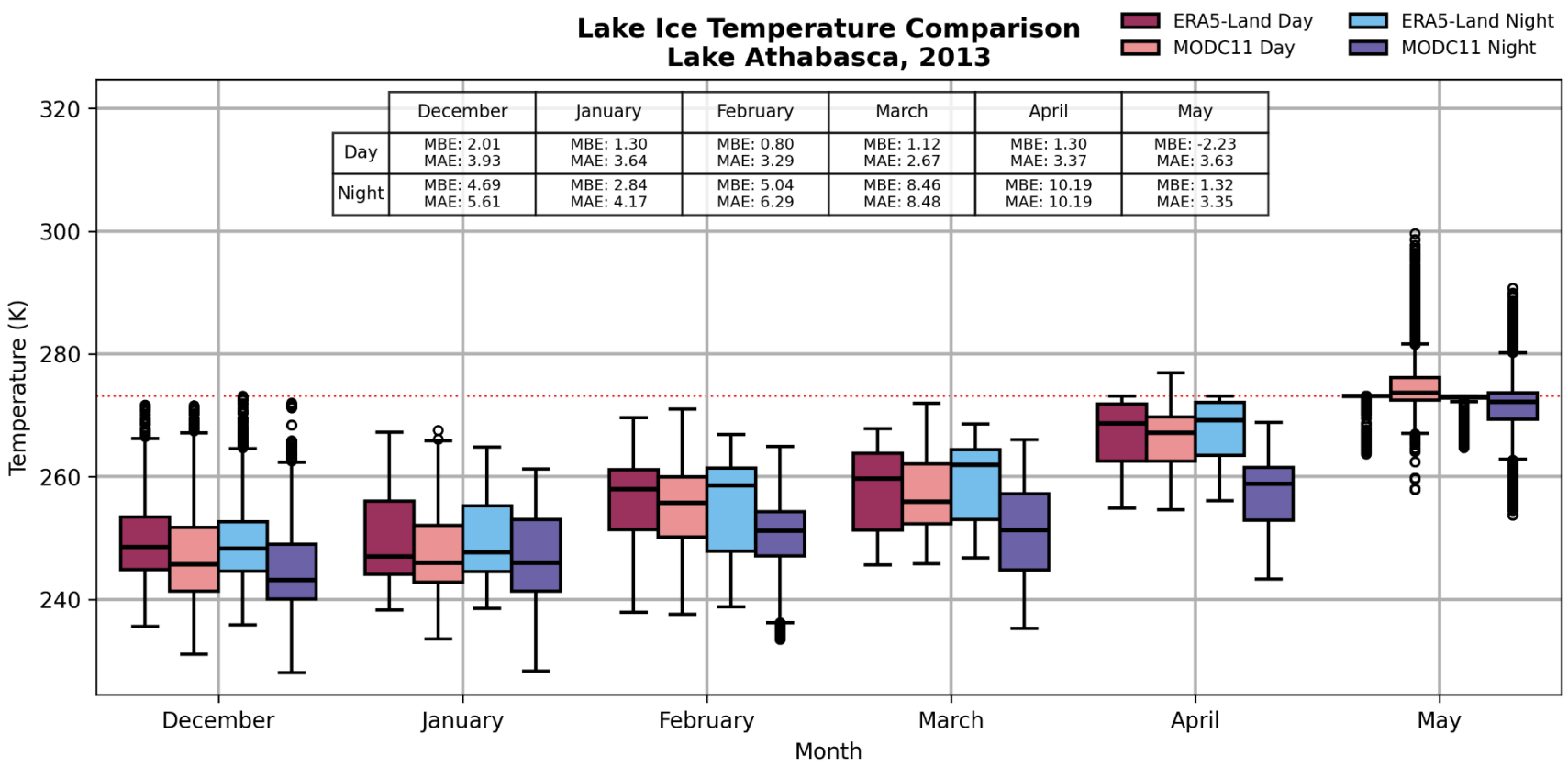


Figure C.3. 10: Boxplot of monthly lake ice surface temperatures during ice-on period of ERA5-Land and MODIS for Lake Athabasca, 2013

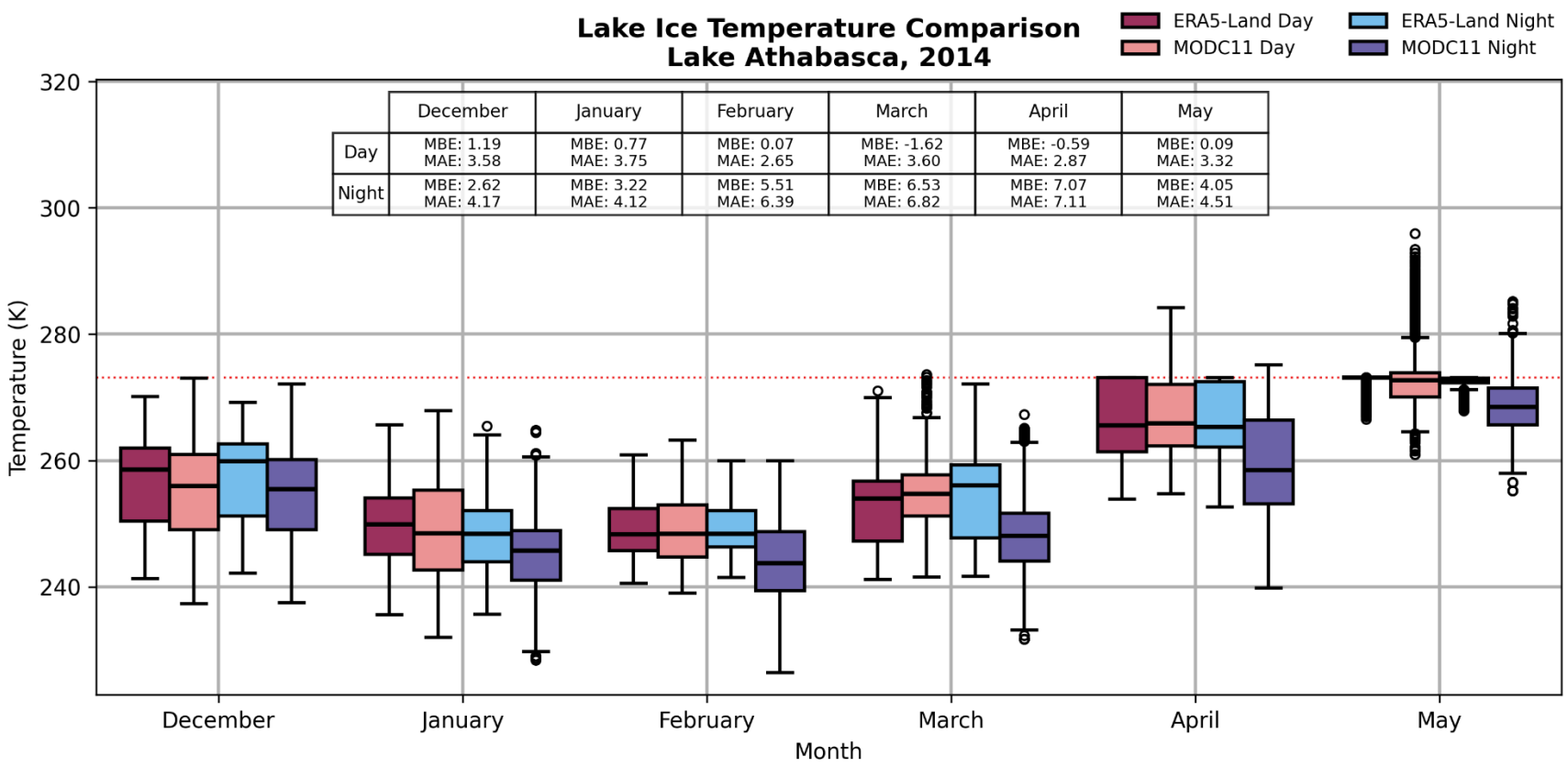


Figure C.3. 11: Boxplot of monthly lake ice surface temperatures during ice-on period of ERA5-Land and MODIS for Lake Athabasca, 2014

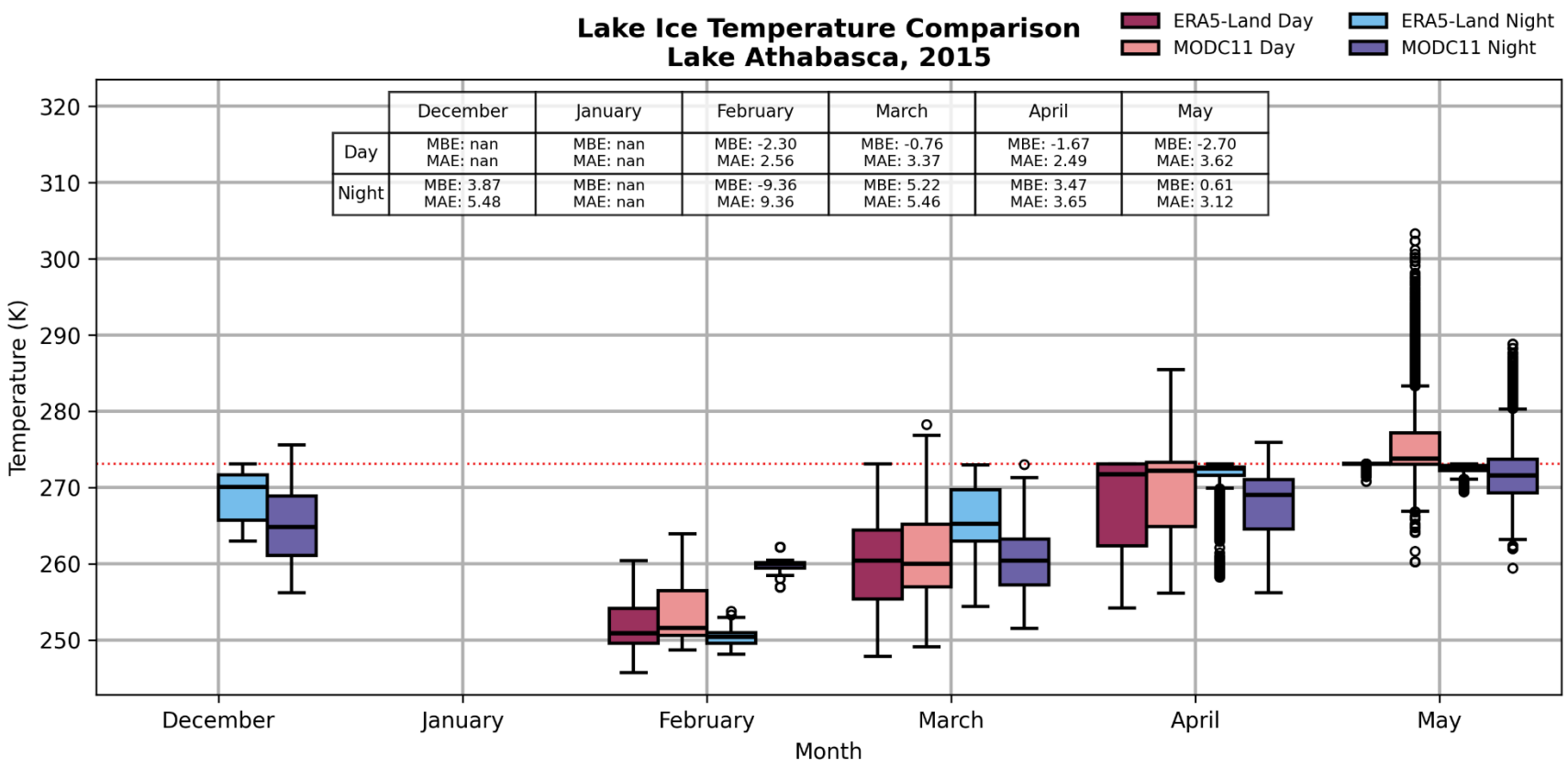


Figure C.3. 12: Boxplot of monthly lake ice surface temperatures during ice-on period of ERA5-Land and MODIS for Lake Athabasca, 2015

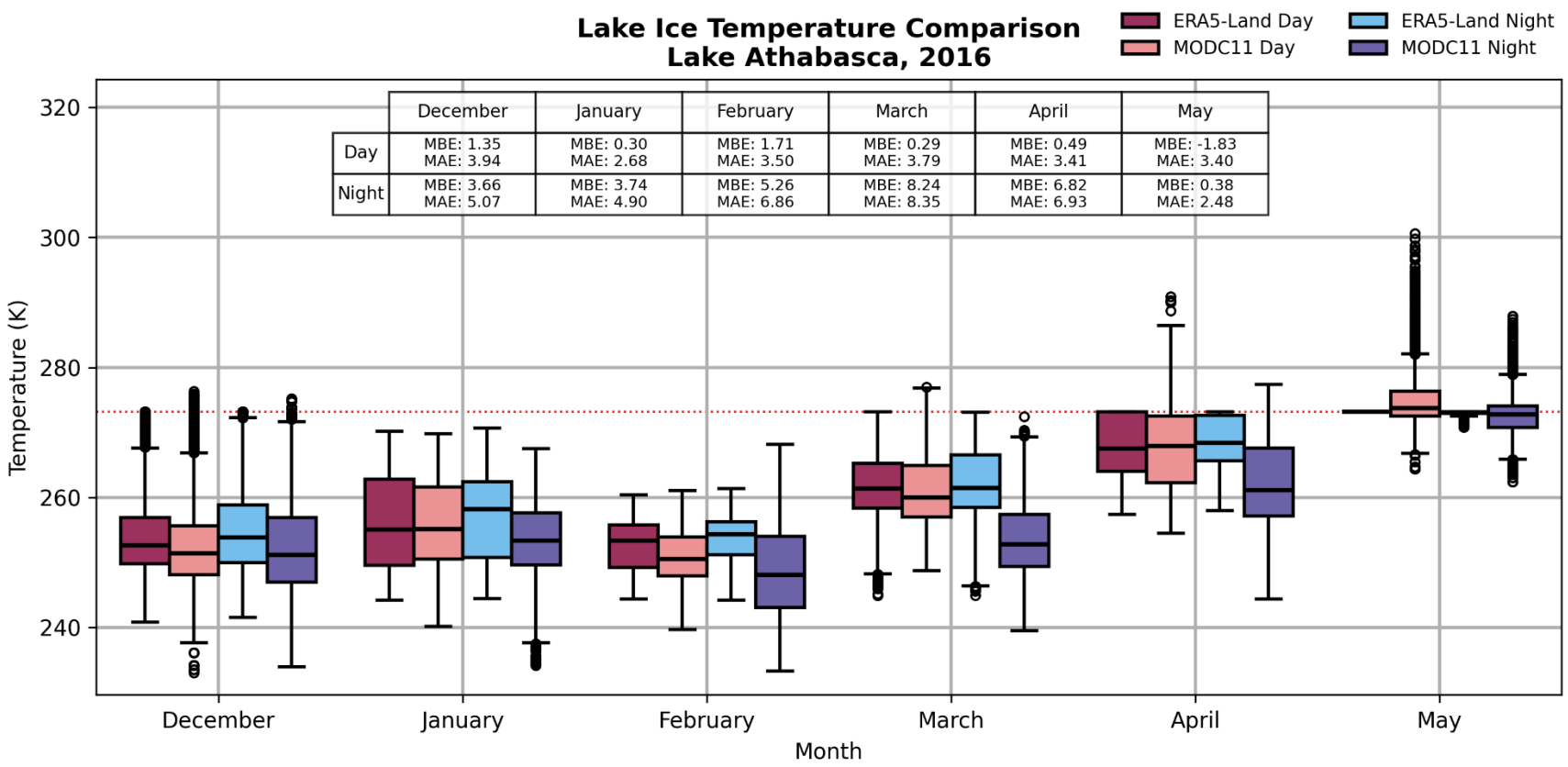


Figure C.3. 13: Boxplot of monthly lake ice surface temperatures during ice-on period of ERA5-Land and MODIS for Lake Athabasca, 2016

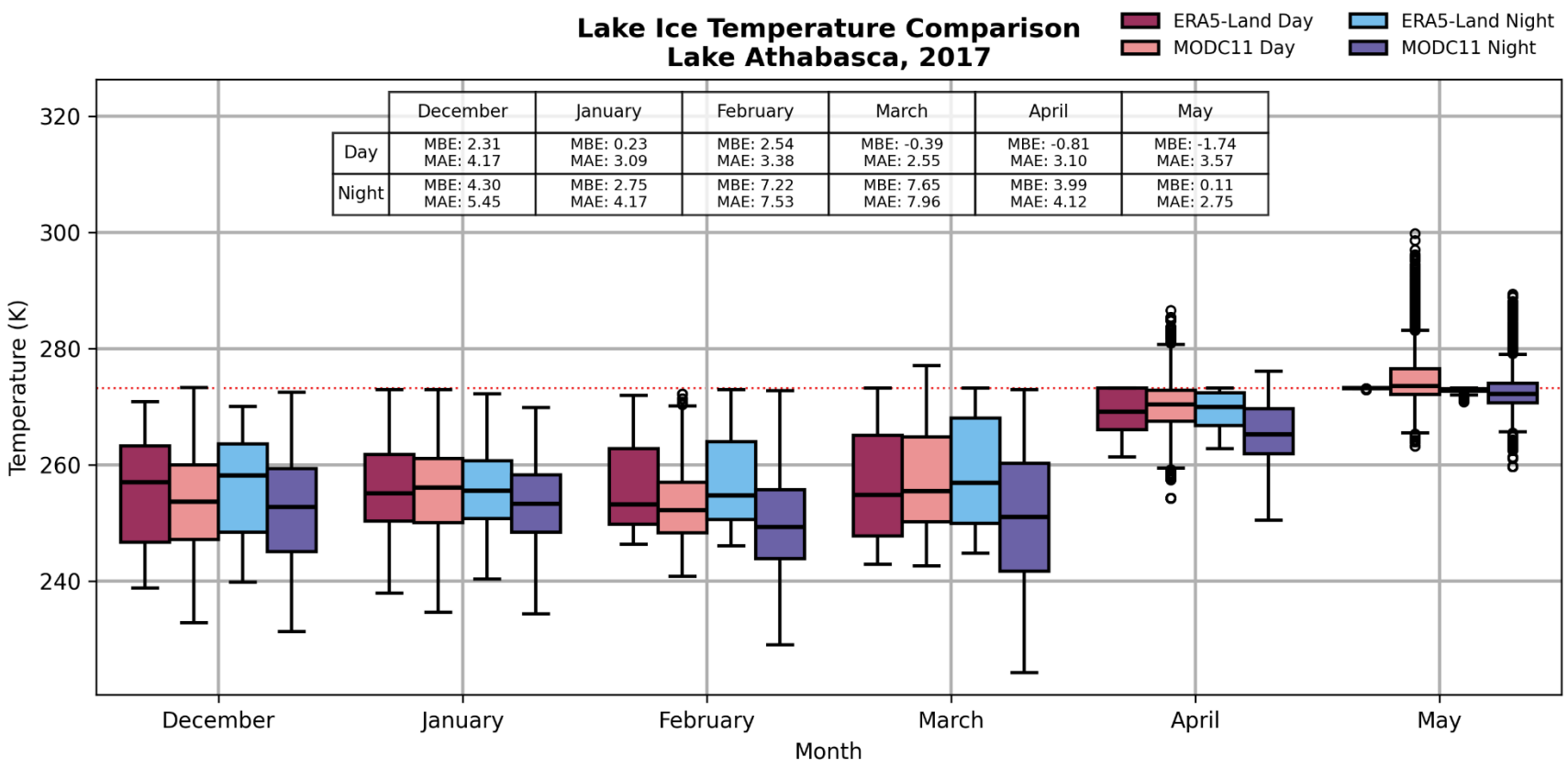


Figure C.3. 14: Boxplot of monthly lake ice surface temperatures during ice-on period of ERA5-Land and MODIS for Lake Athabasca, 2017

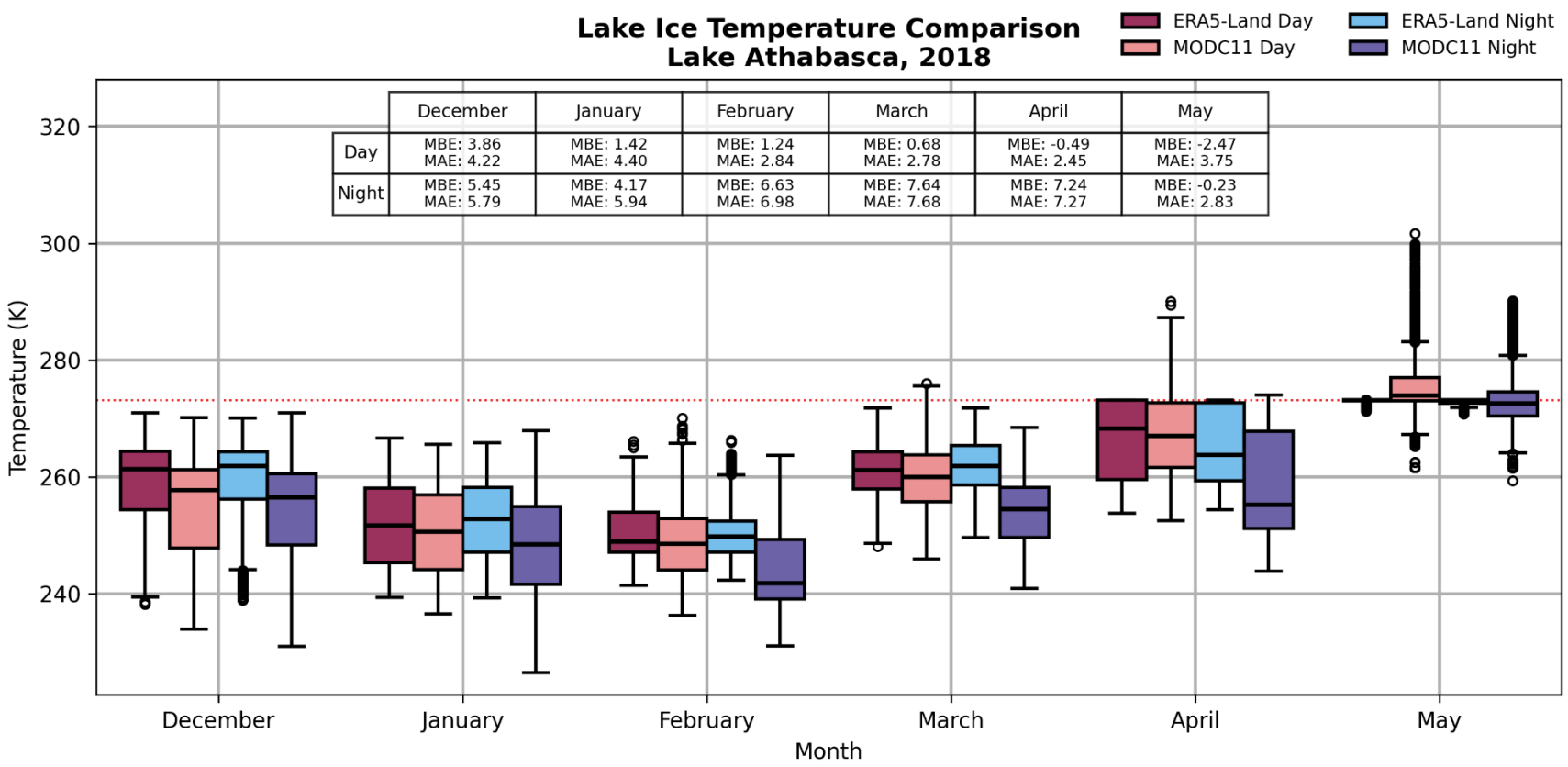


Figure C.3. 15: Boxplot of monthly lake ice surface temperatures during ice-on period of ERA5-Land and MODIS for Lake Athabasca, 2018

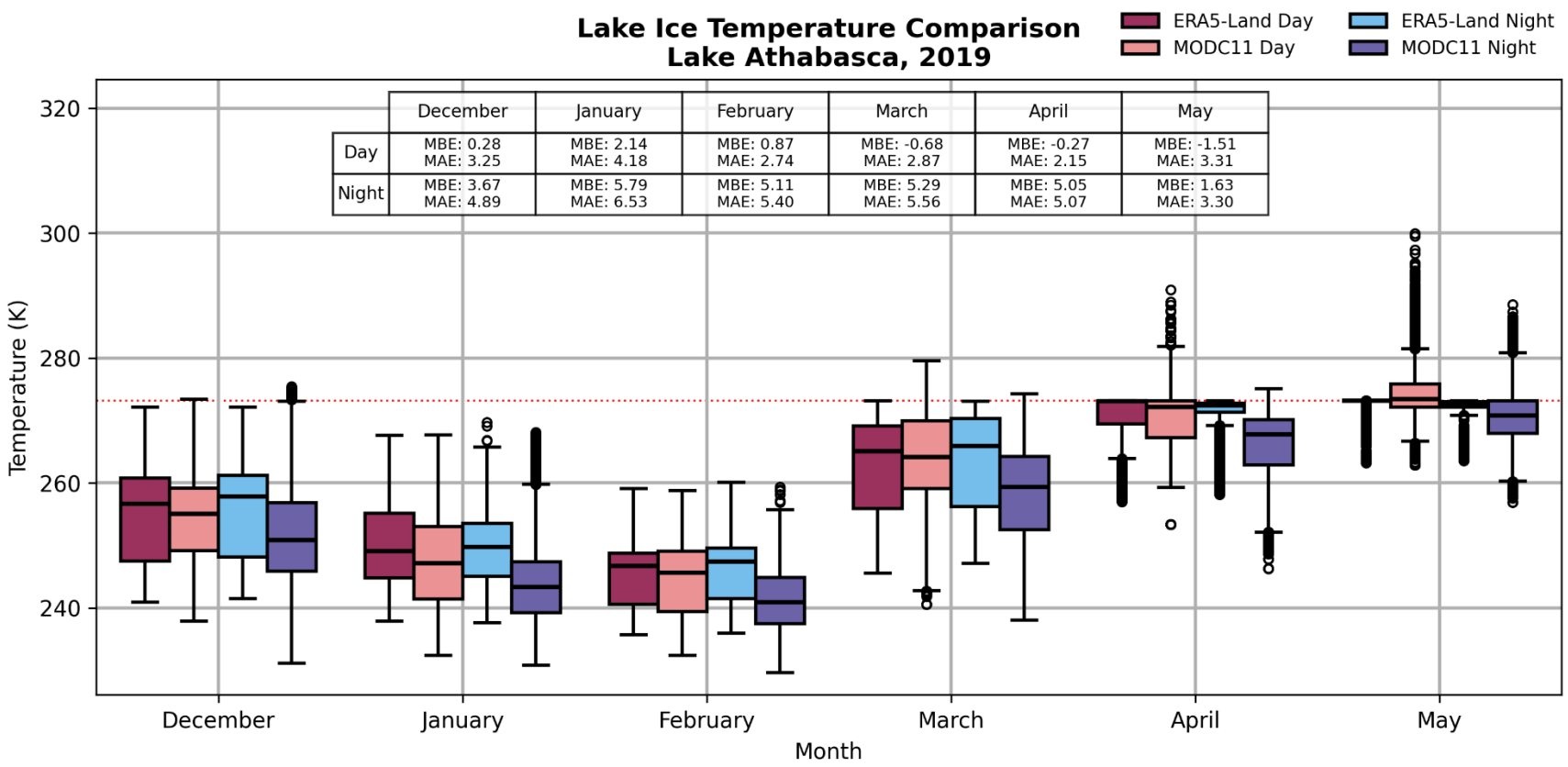


Figure C.3. 16: Boxplot of monthly lake ice surface temperatures during ice-on period of ERA5-Land and MODIS for Lake Athabasca, 2019

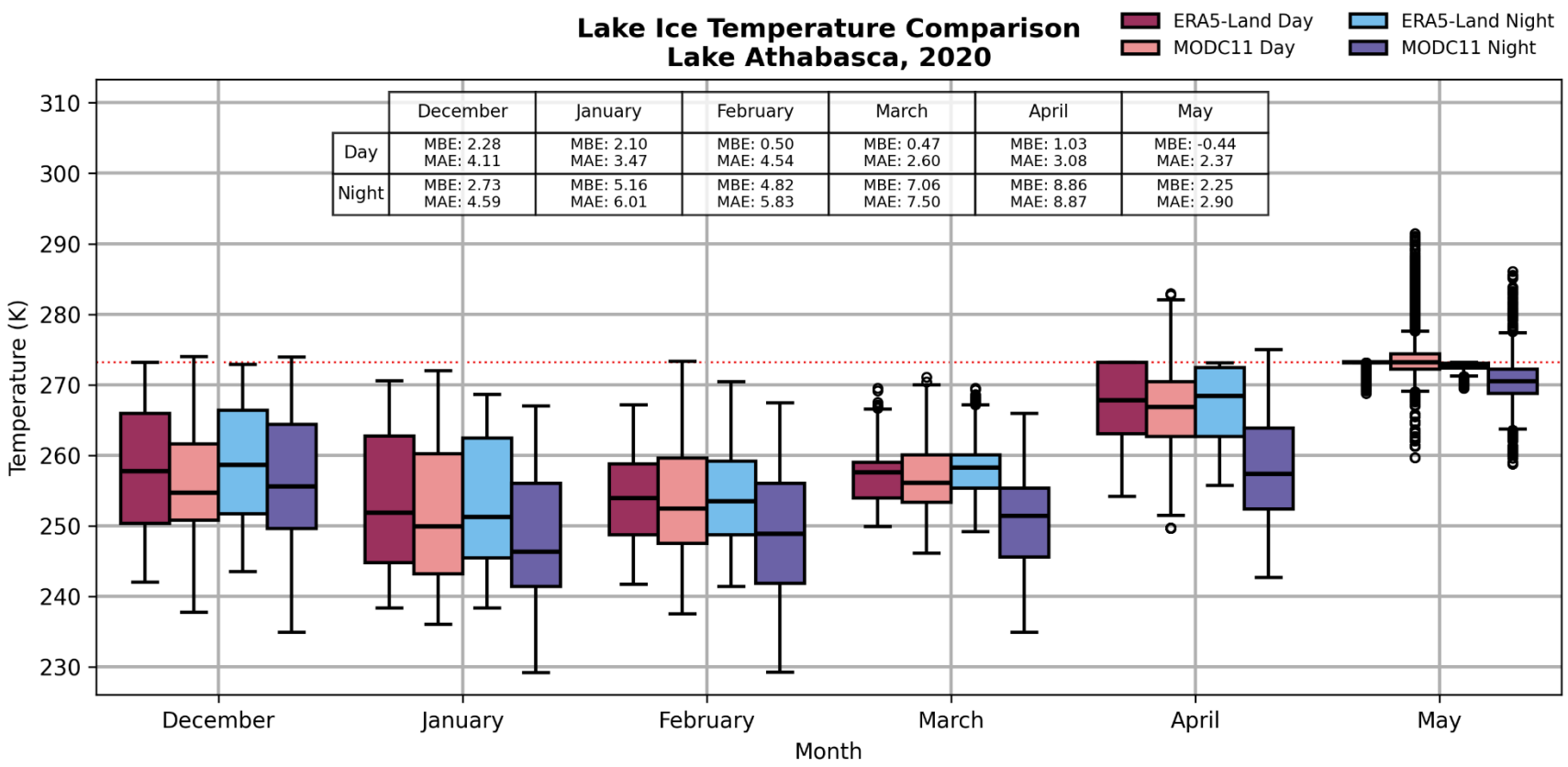


Figure C.3. 17: Boxplot of monthly lake ice surface temperatures during ice-on period of ERA5-Land and MODIS for Lake Athabasca, 2020

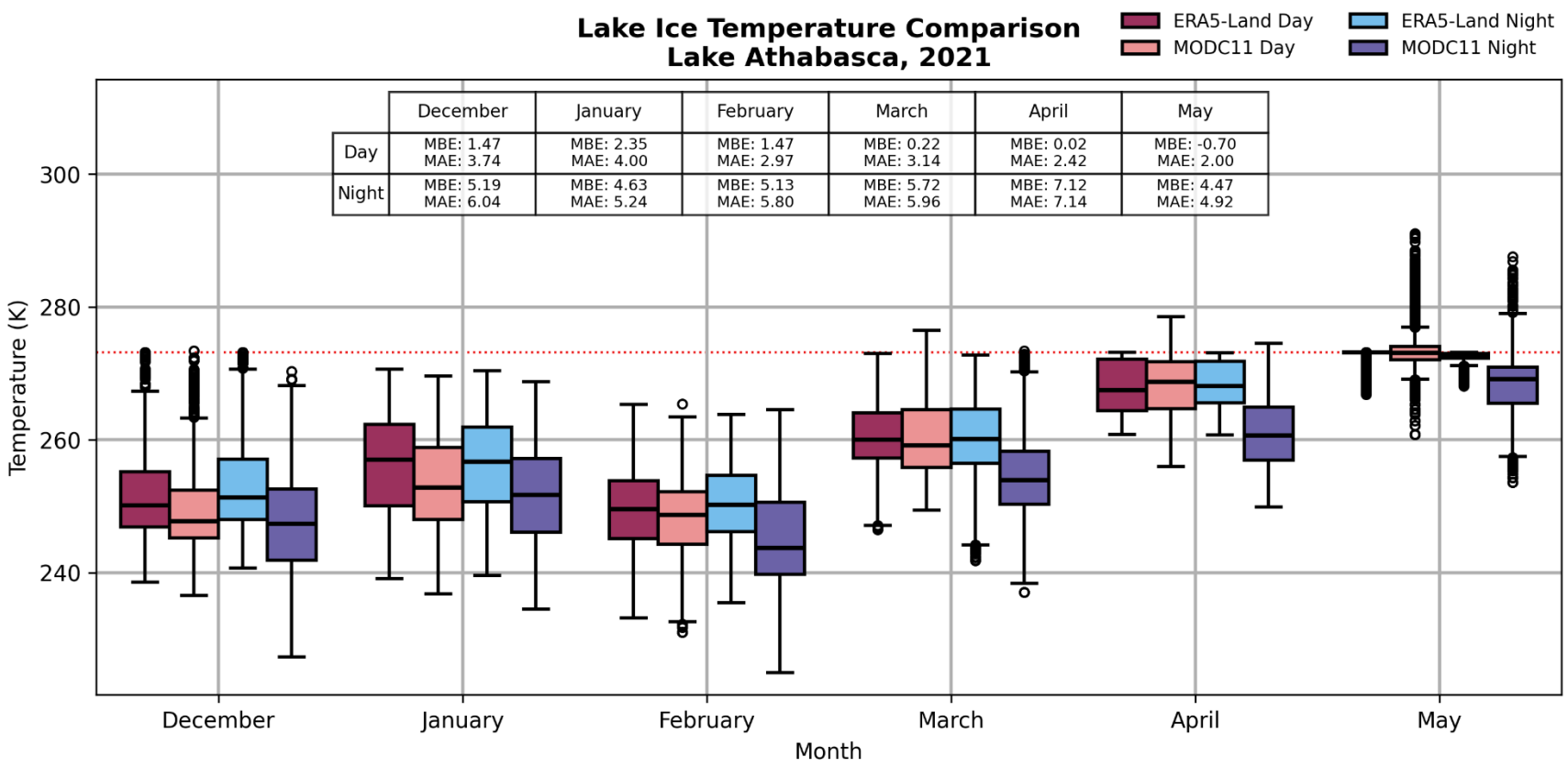


Figure C.3. 18: Boxplot of monthly lake ice surface temperatures during ice-on period of ERA5-Land and MODIS for Lake Athabasca, 2021

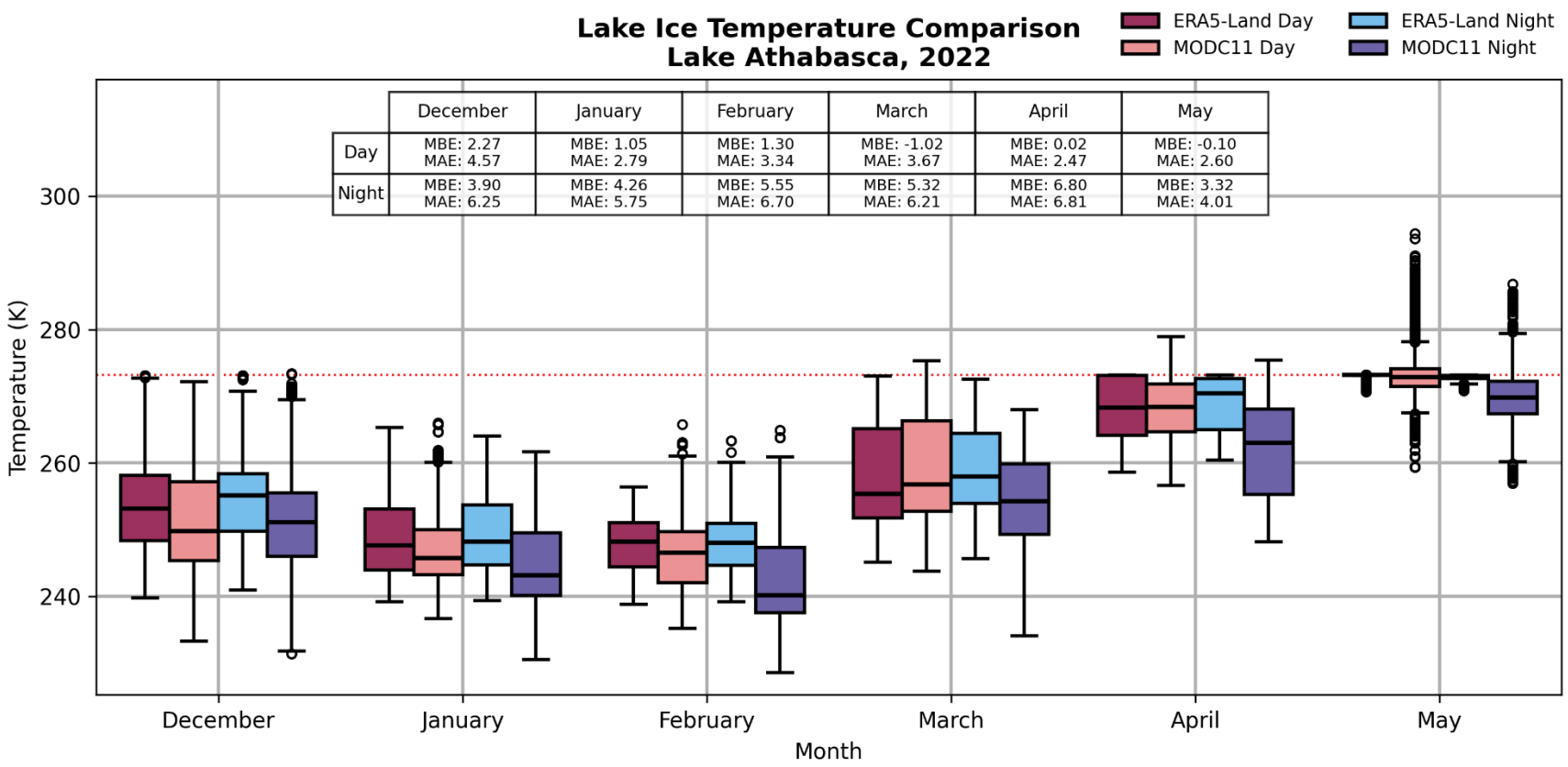


Figure C.3. 19: Boxplot of monthly lake ice surface temperatures during ice-on period of ERA5-Land and MODIS for Lake Athabasca, 2022

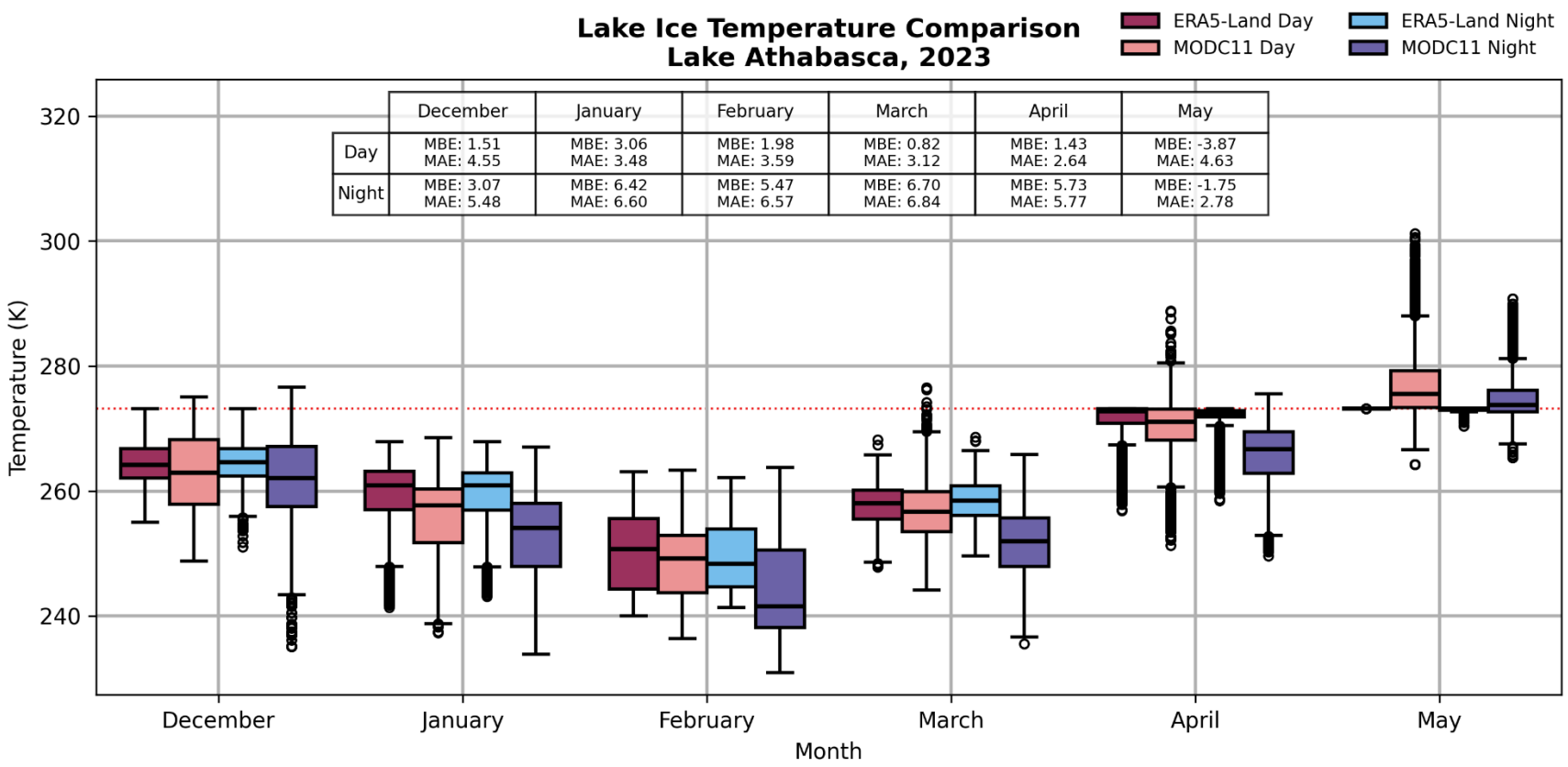


Figure C.3. 20: Boxplot of monthly lake ice surface temperatures during ice-on period of ERA5-Land and MODIS for Lake Athabasca, 2023

C.4 Lake Winnipeg

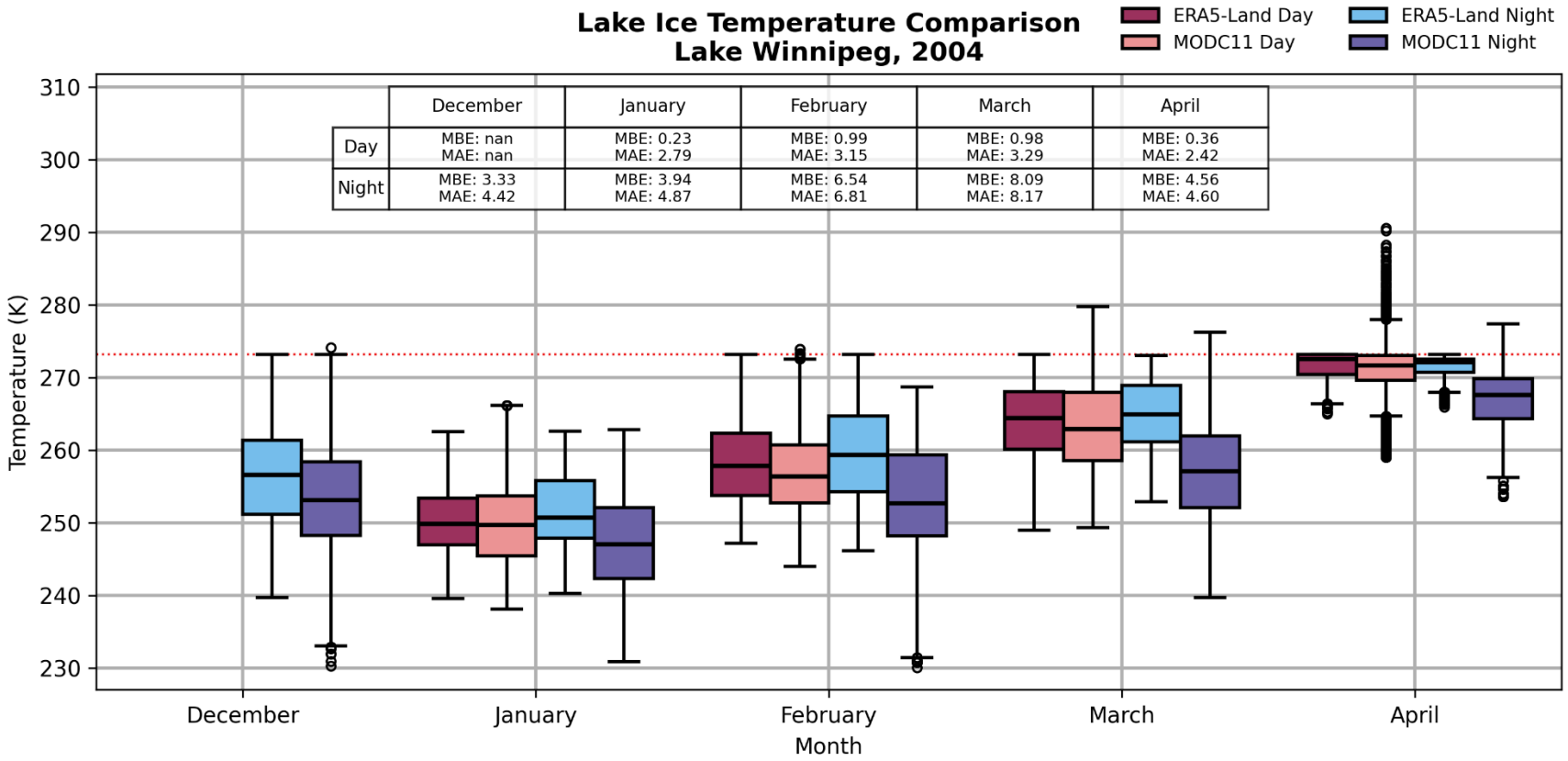


Figure C.4. 1: Boxplot of monthly lake ice surface temperatures during ice-on period of ERA5-Land and MODIS for Lake Winnipeg, 2004

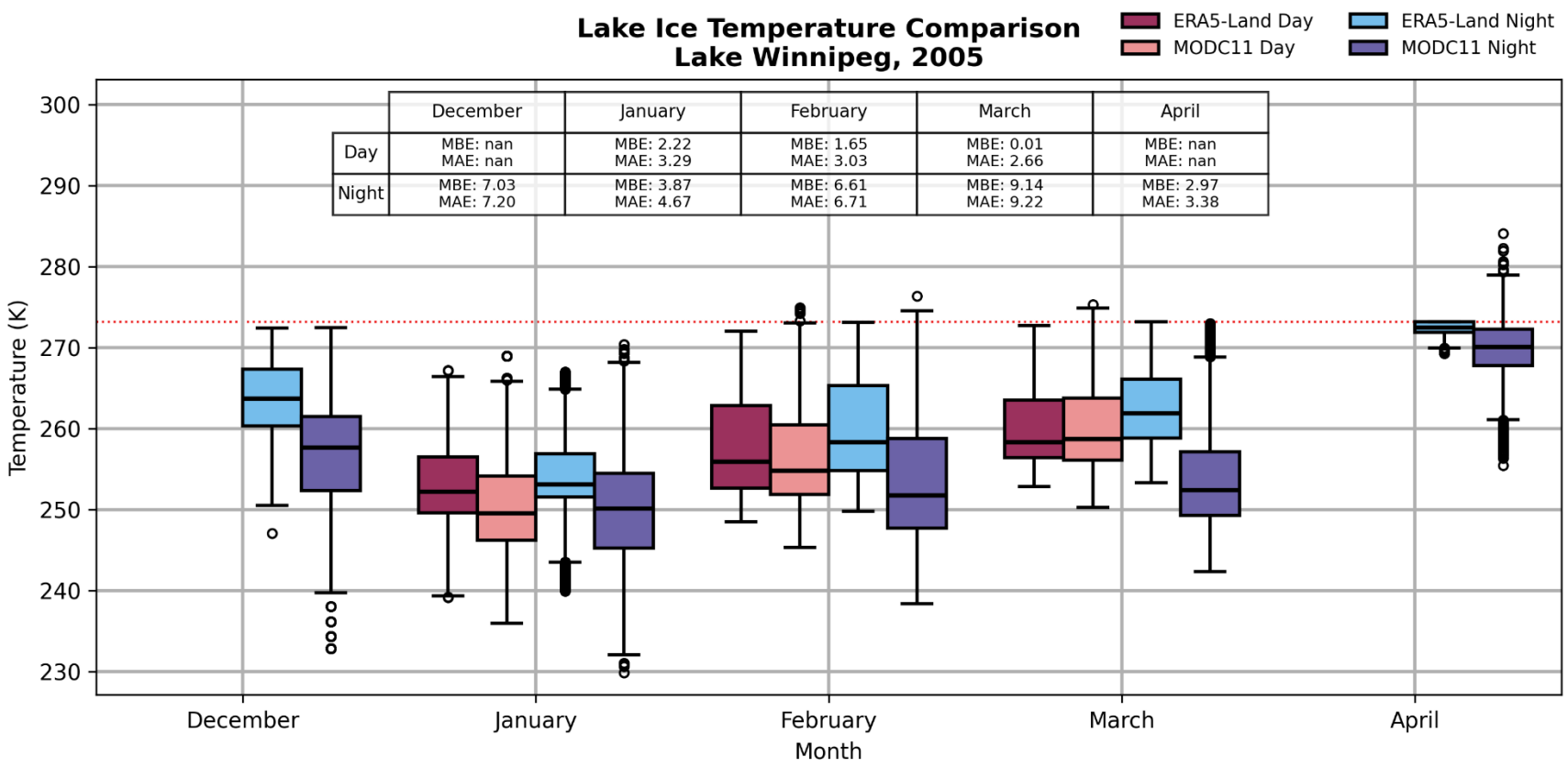


Figure C.4. 2: Boxplot of monthly lake ice surface temperatures during ice-on period of ERA5-Land and MODIS for Lake Winnipeg, 2005

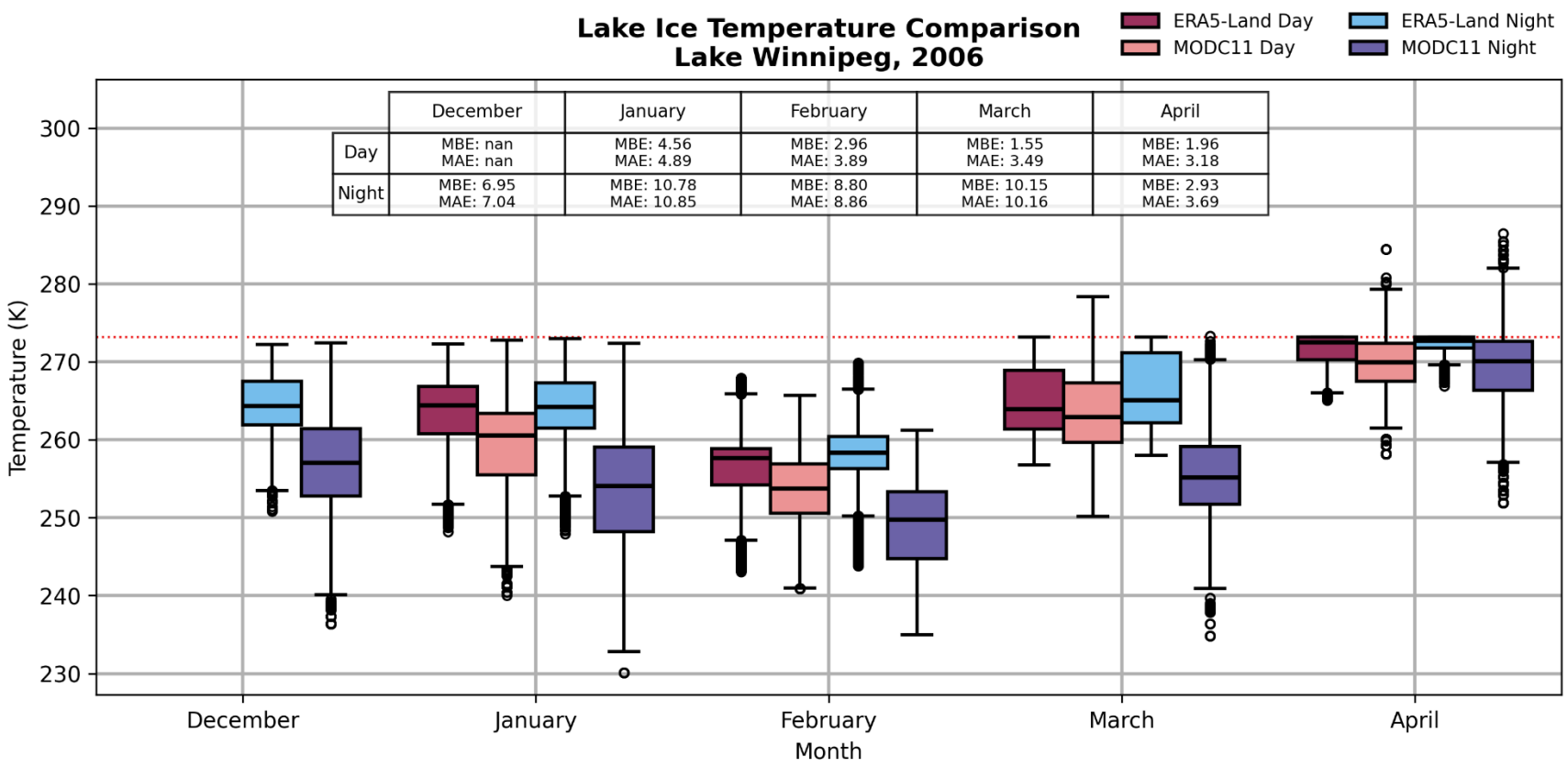


Figure C.4. 3: Boxplot of monthly lake ice surface temperatures during ice-on period of ERA5-Land and MODIS for Lake Winnipeg, 2006

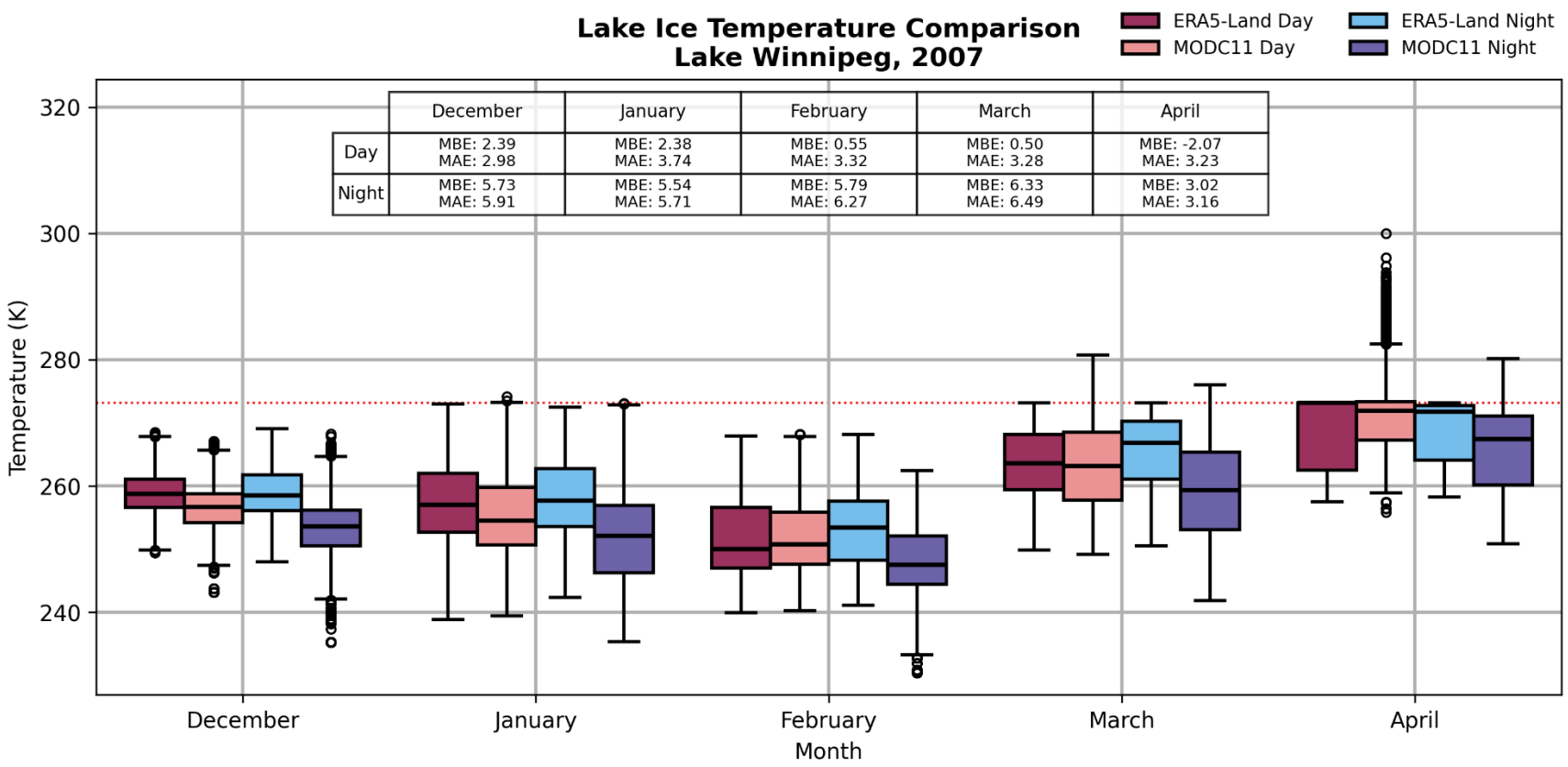


Figure C.4. 4: Boxplot of monthly lake ice surface temperatures during ice-on period of ERA5-Land and MODIS for Lake Winnipeg, 2007

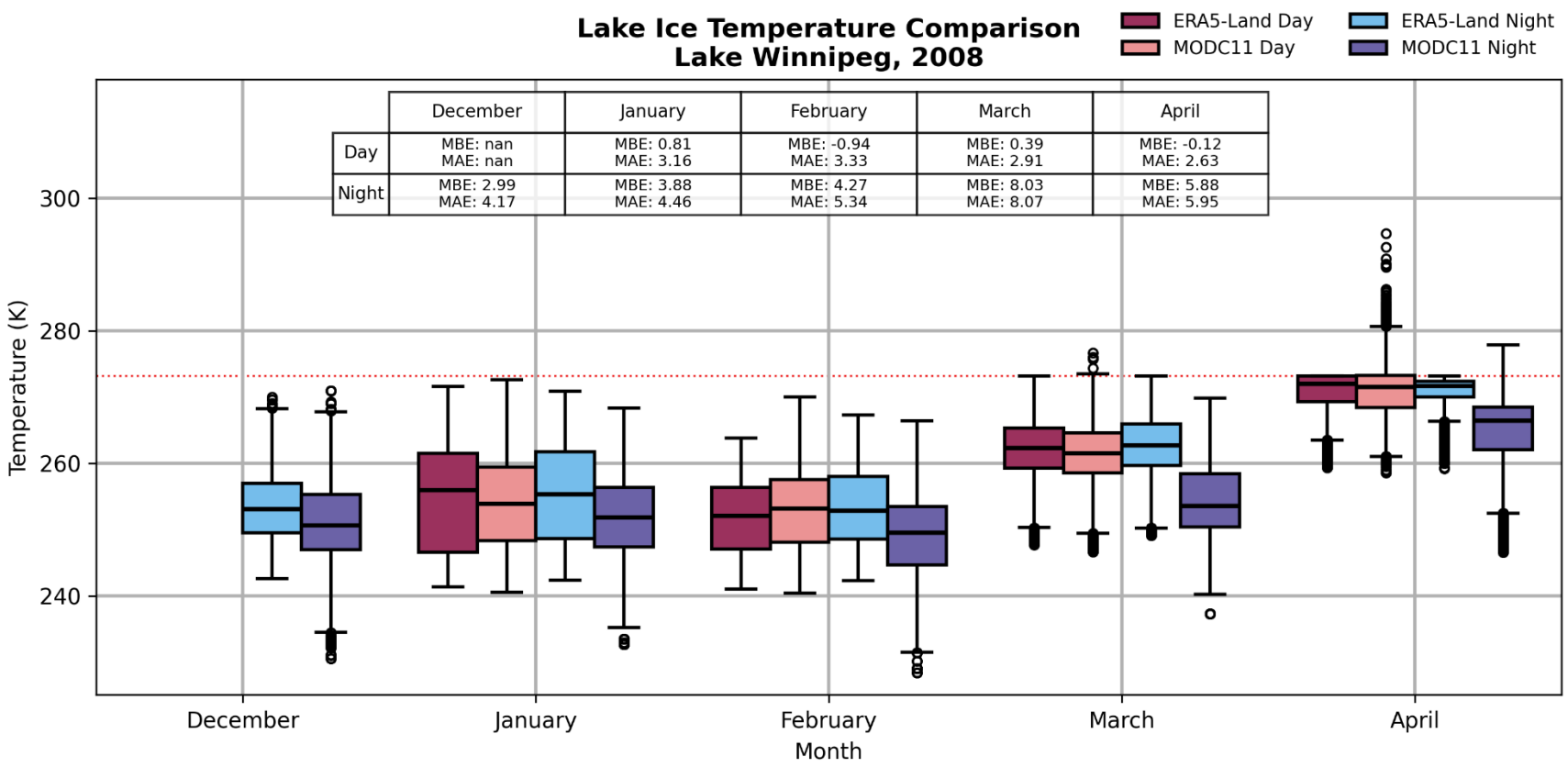


Figure C.4. 5: Boxplot of monthly lake ice surface temperatures during ice-on period of ERA5-Land and MODIS for Lake Winnipeg, 2008

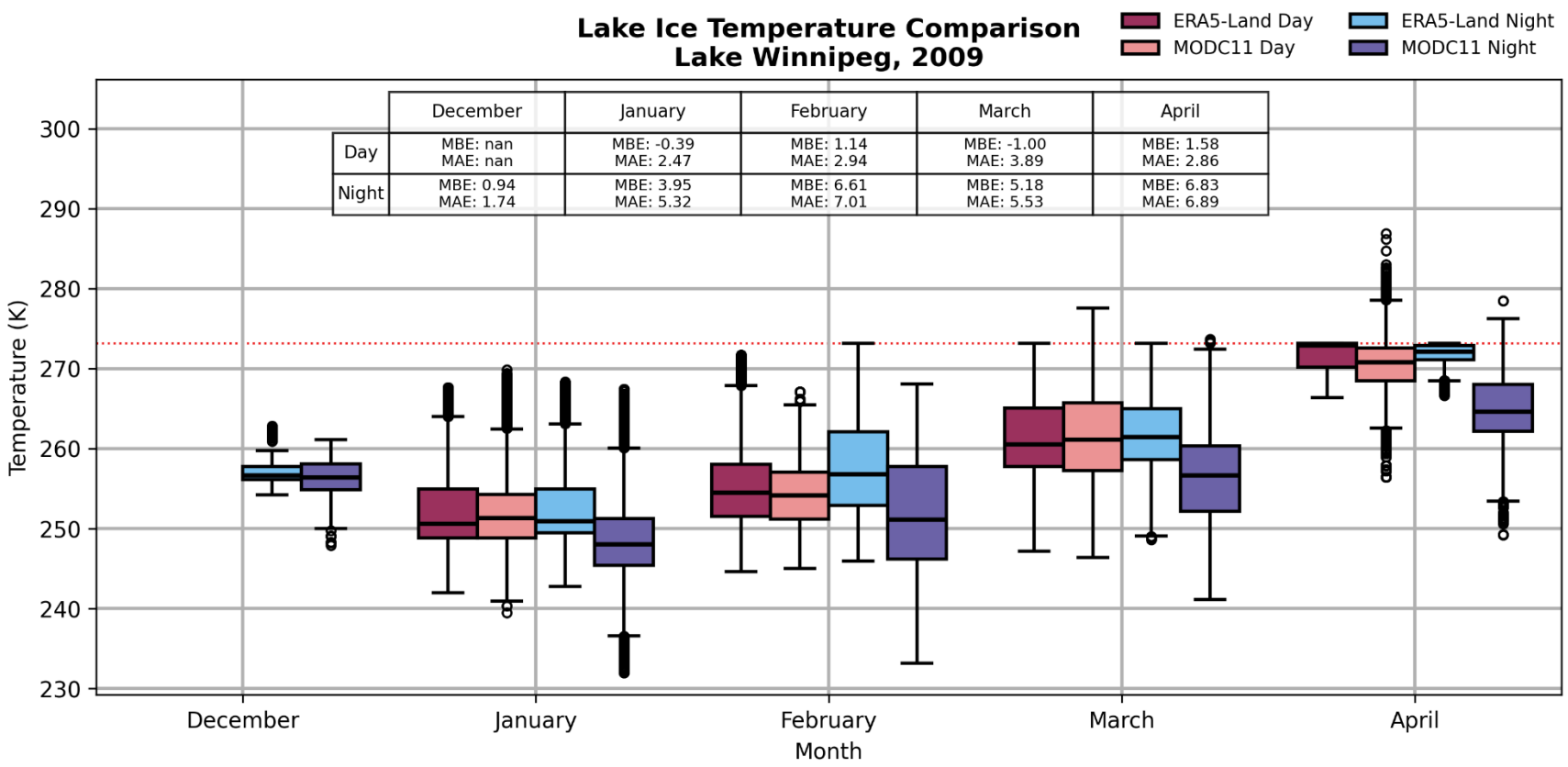


Figure C.4. 6: Boxplot of monthly lake ice surface temperatures during ice-on period of ERA5-Land and MODIS for Lake Winnipeg, 2009

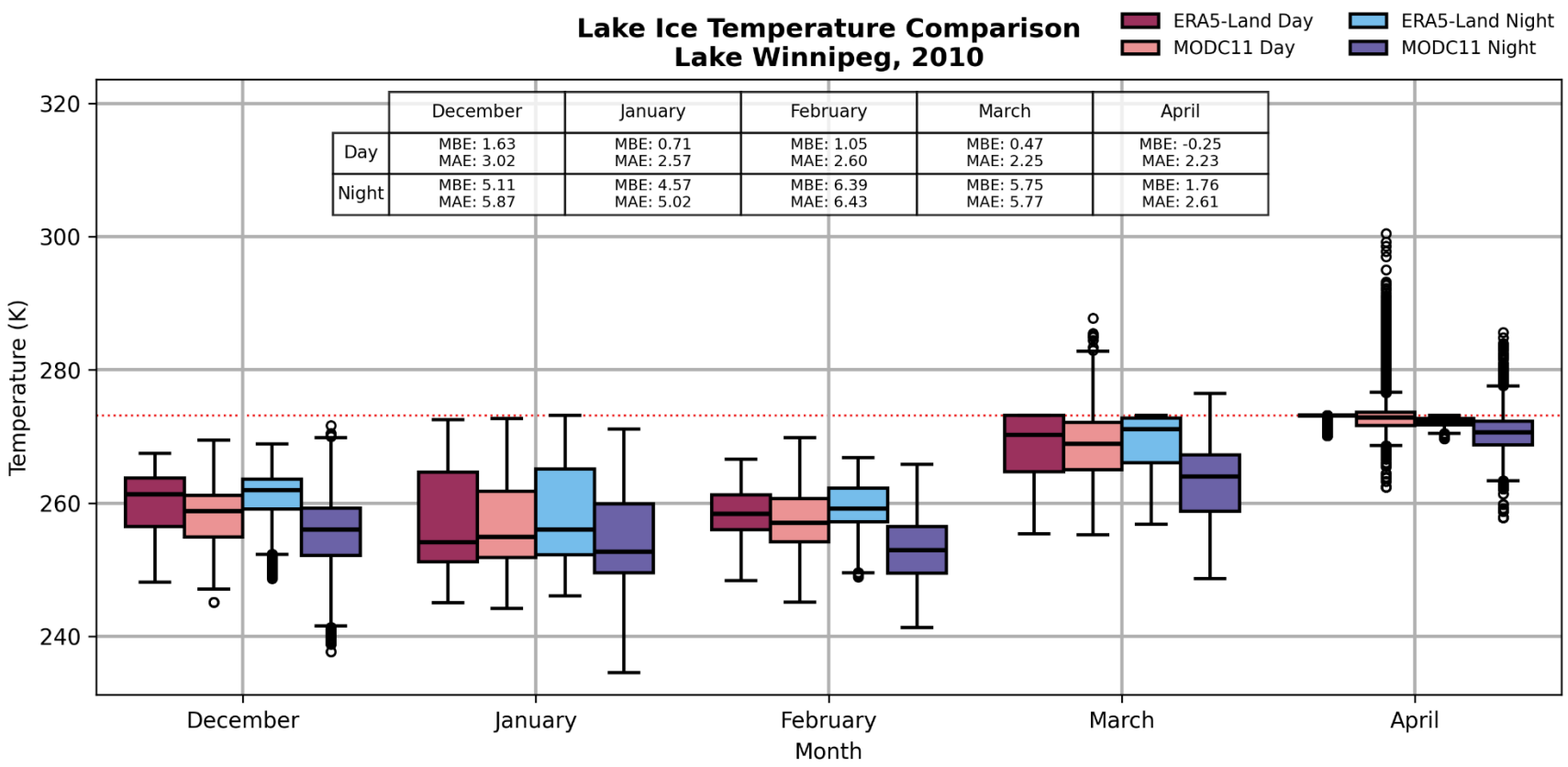


Figure C.4. 7: Boxplot of monthly lake ice surface temperatures during ice-on period of ERA5-Land and MODIS for Lake Winnipeg, 2010

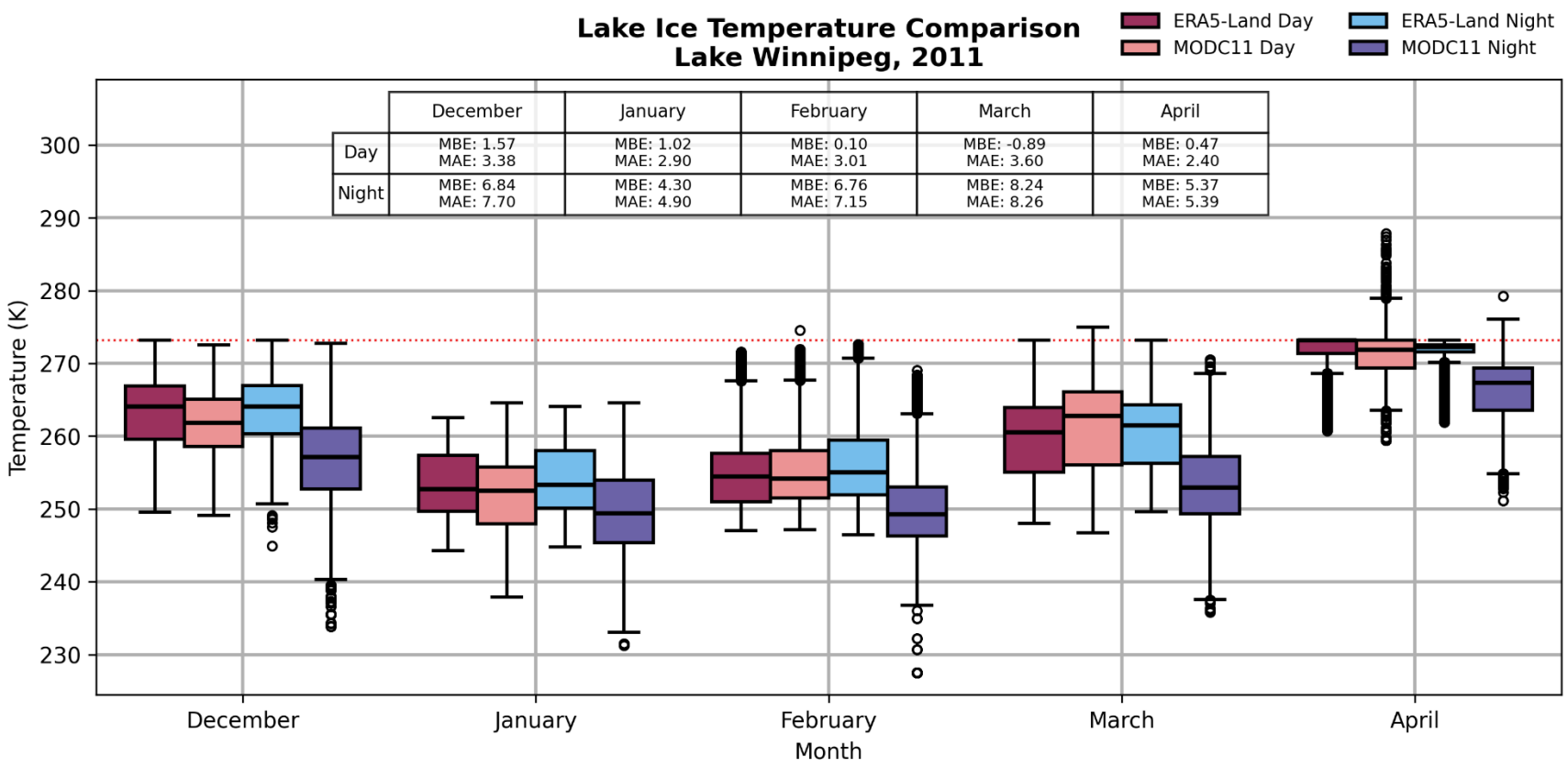


Figure C.4. 8: Boxplot of monthly lake ice surface temperatures during ice-on period of ERA5-Land and MODIS for Lake Winnipeg, 2011

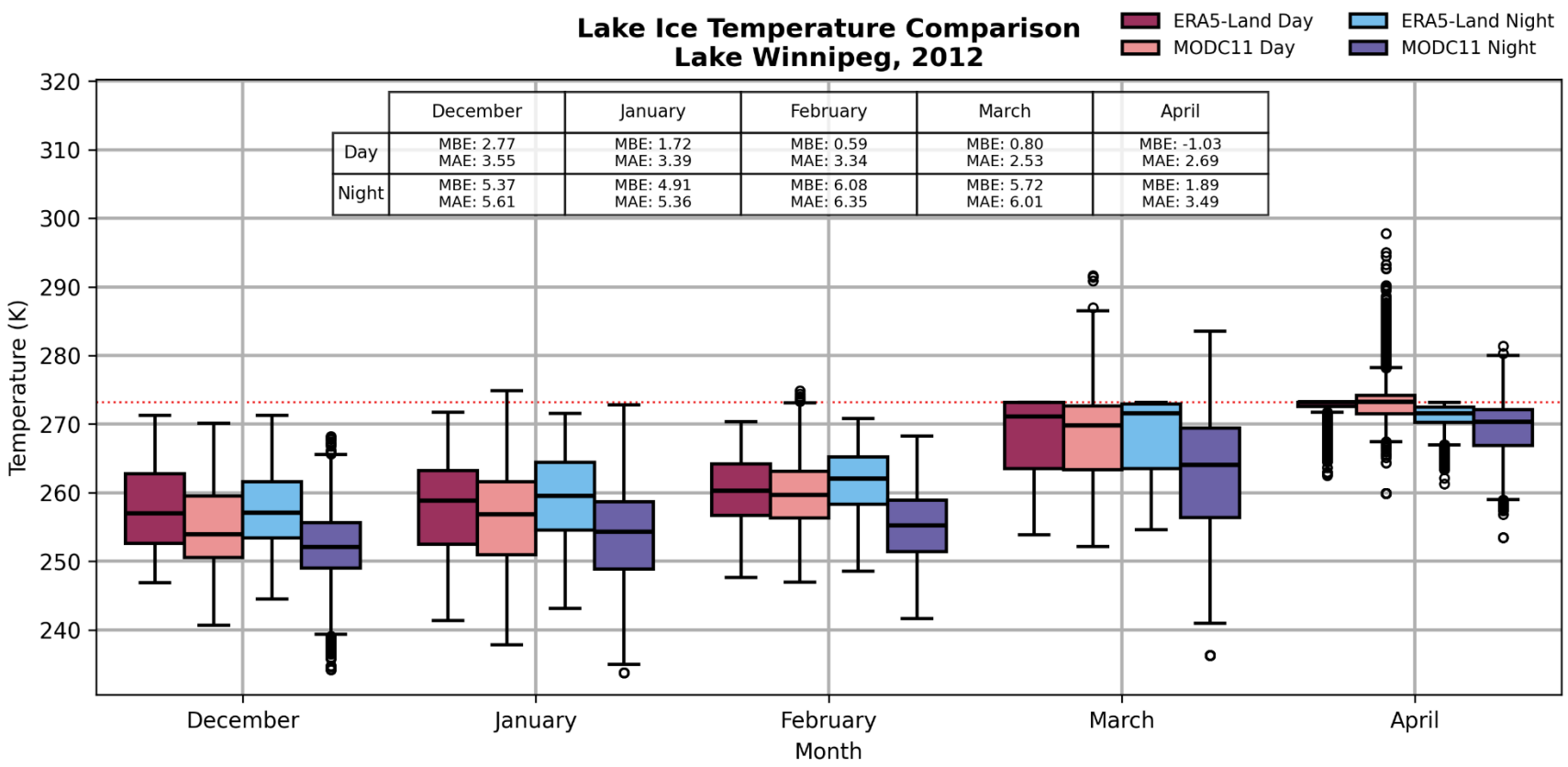


Figure C.4. 9: Boxplot of monthly lake ice surface temperatures during ice-on period of ERA5-Land and MODIS for Lake Winnipeg, 2012

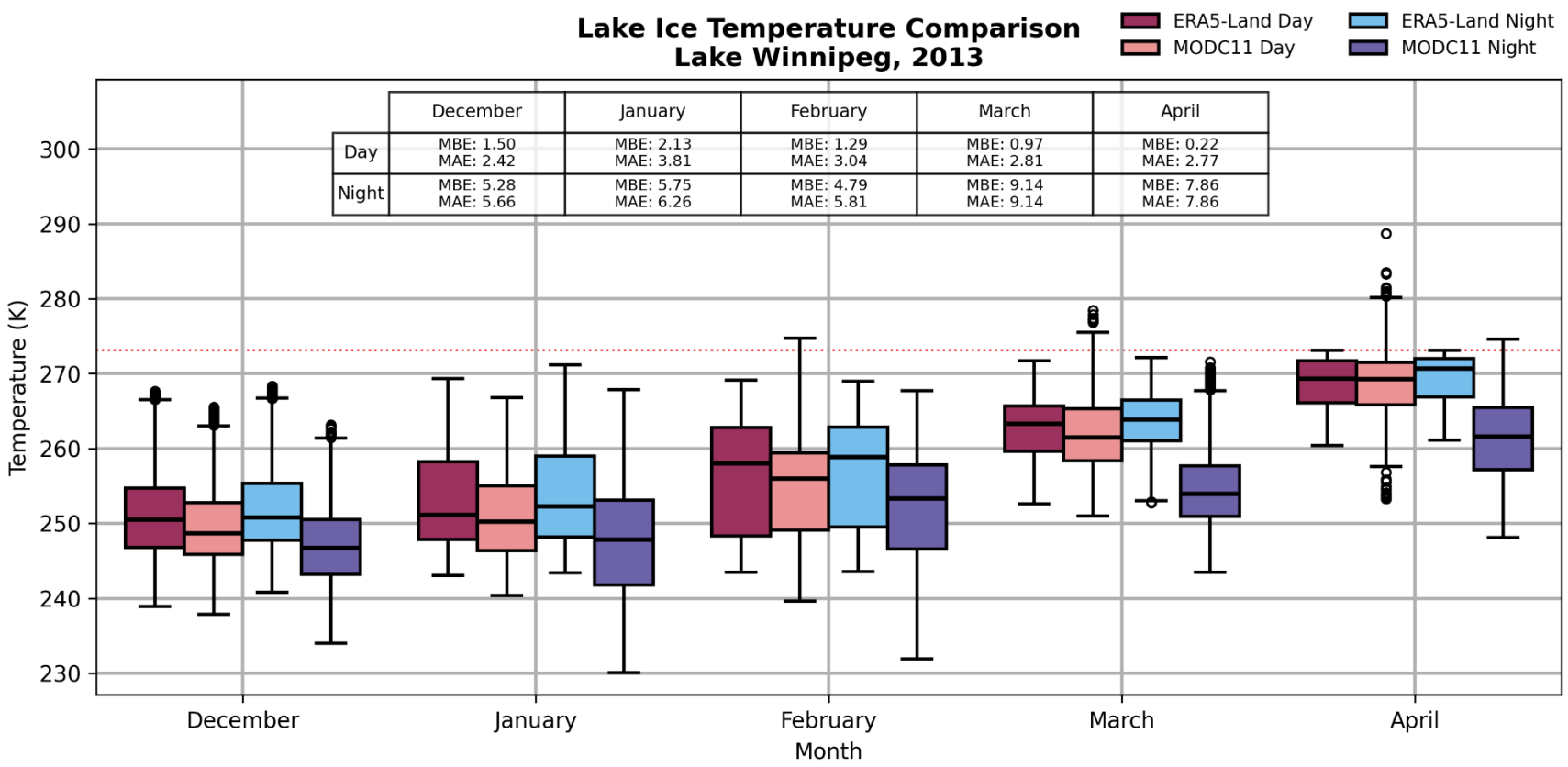


Figure C.4. 10: Boxplot of monthly lake ice surface temperatures during ice-on period of ERA5-Land and MODIS for Lake Winnipeg, 2013

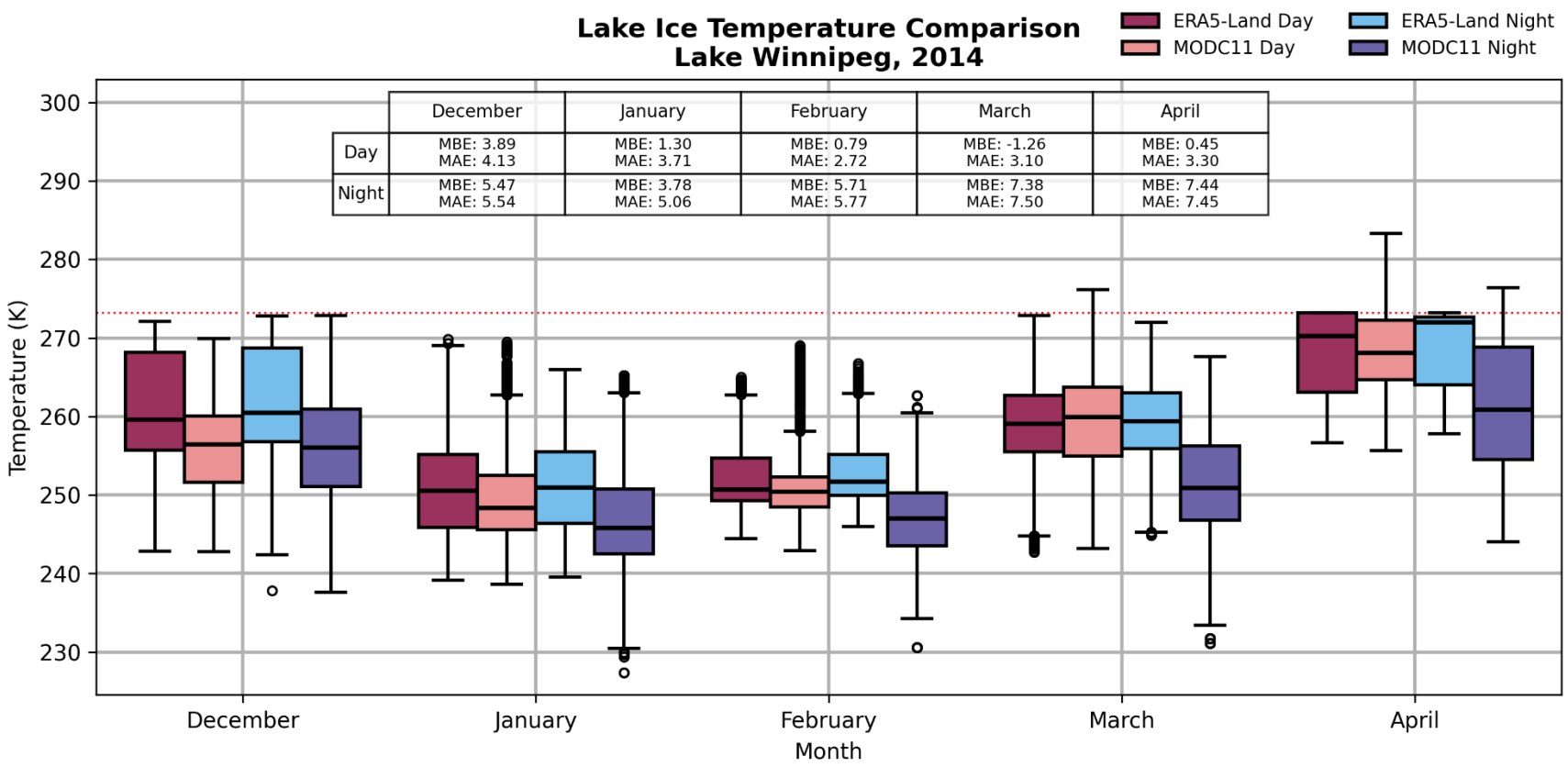


Figure C.4. 11: Boxplot of monthly lake ice surface temperatures during ice-on period of ERA5-Land and MODIS for Lake Winnipeg, 2014

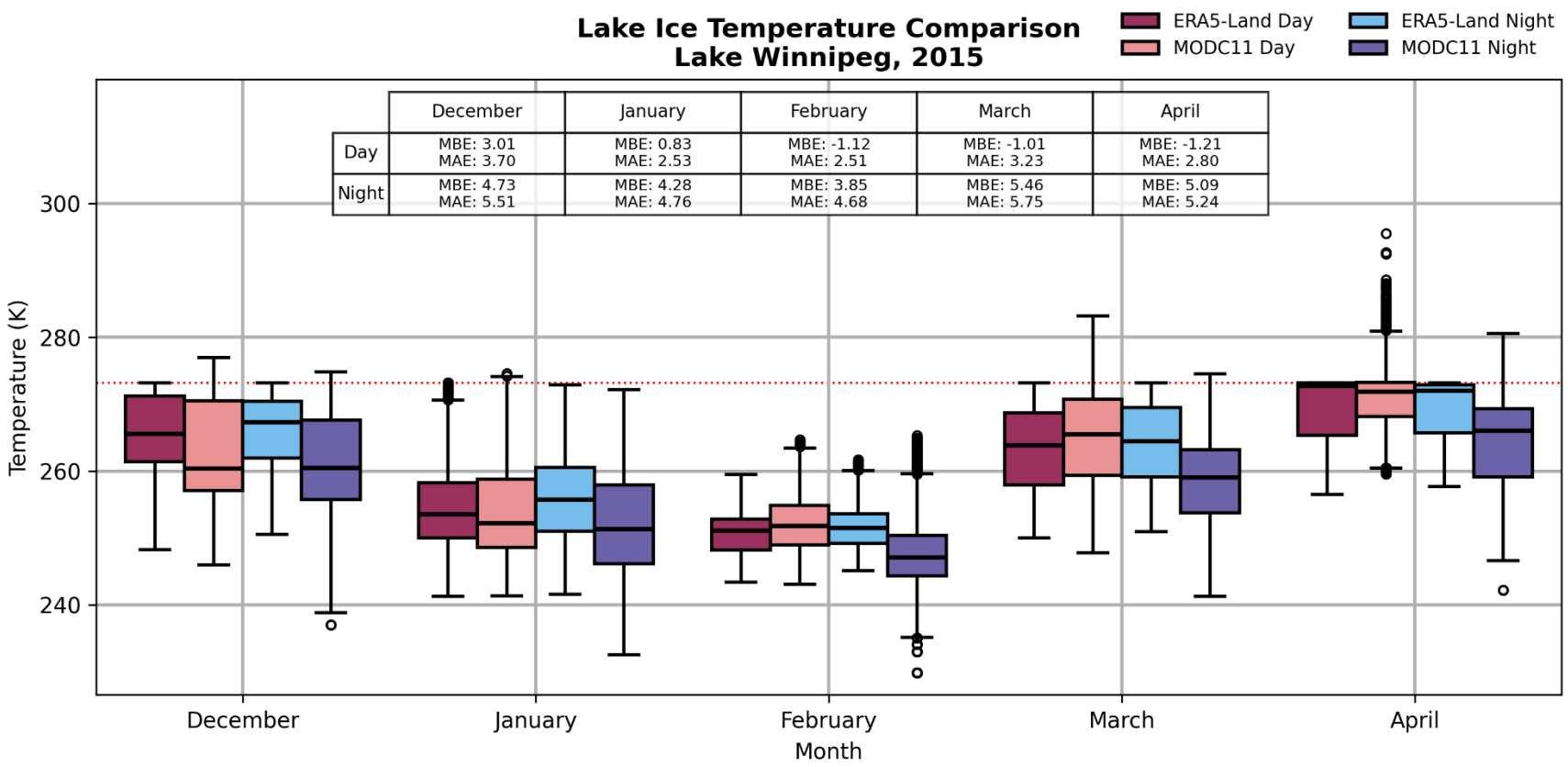


Figure C.4. 12: Boxplot of monthly lake ice surface temperatures during ice-on period of ERA5-Land and MODIS for Lake Winnipeg, 2015

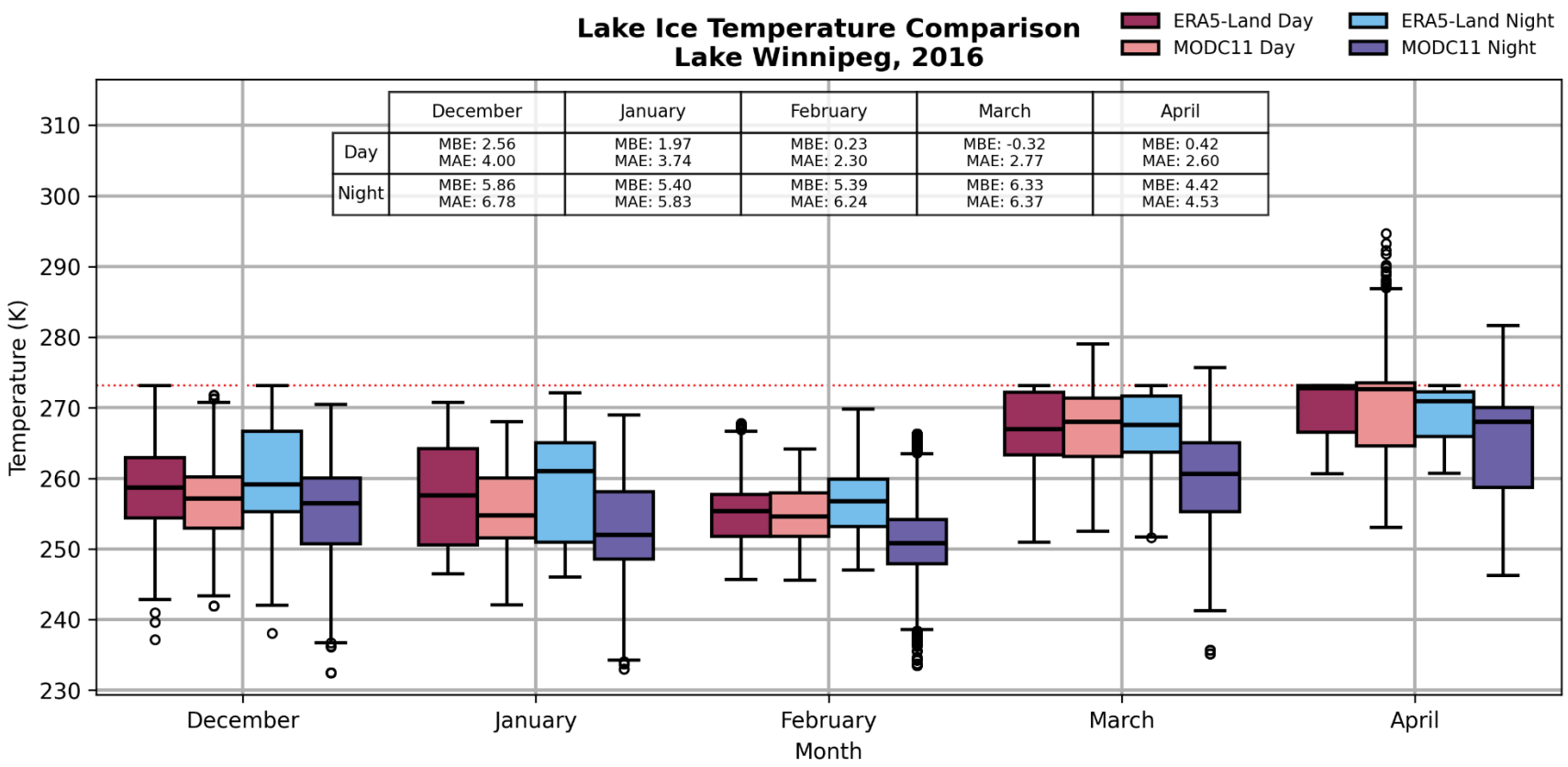


Figure C.4. 13: Boxplot of monthly lake ice surface temperatures during ice-on period of ERA5-Land and MODIS for Lake Winnipeg, 2016

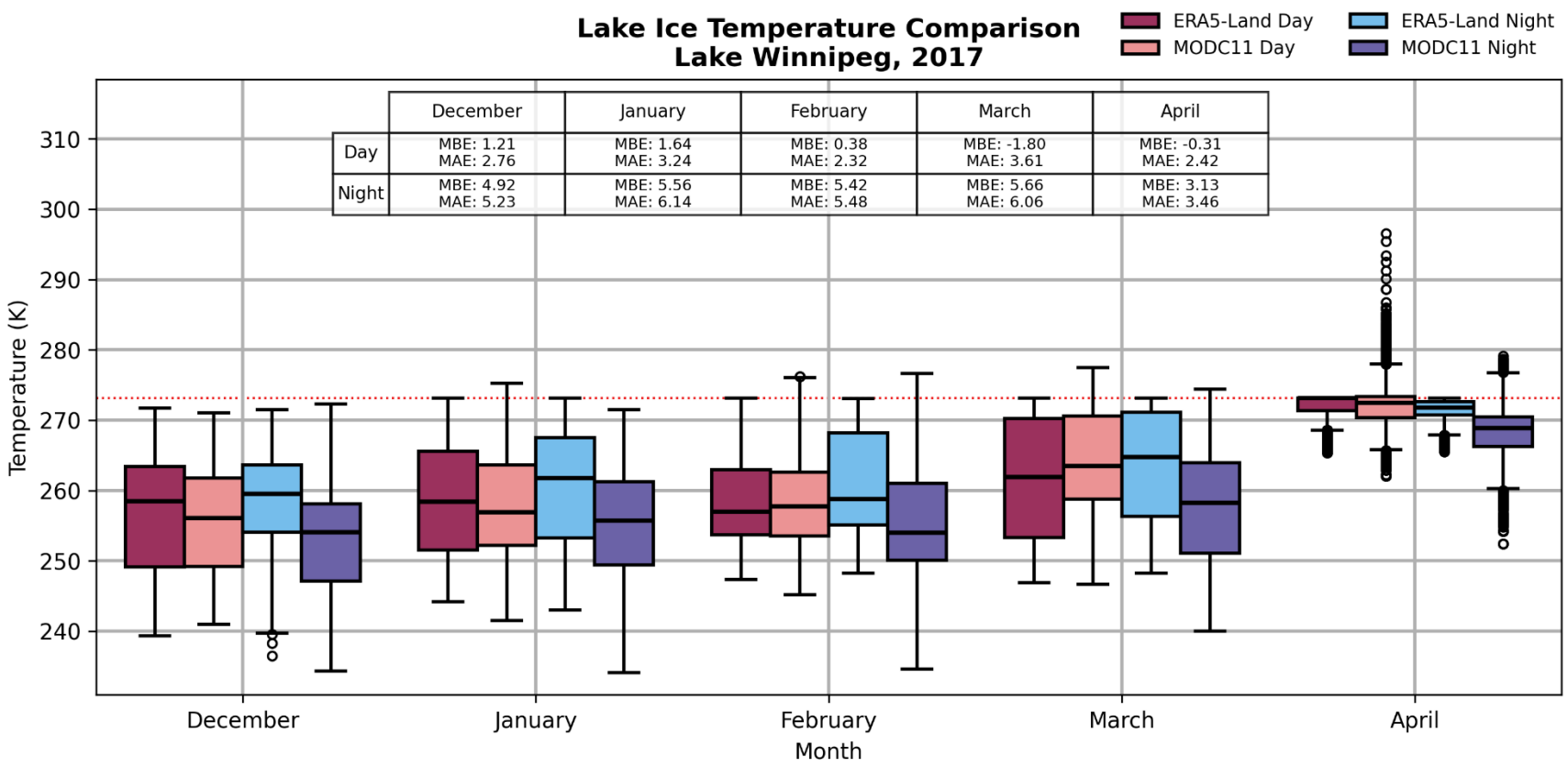


Figure C.4. 14: Boxplot of monthly lake ice surface temperatures during ice-on period of ERA5-Land and MODIS for Lake Winnipeg, 2017

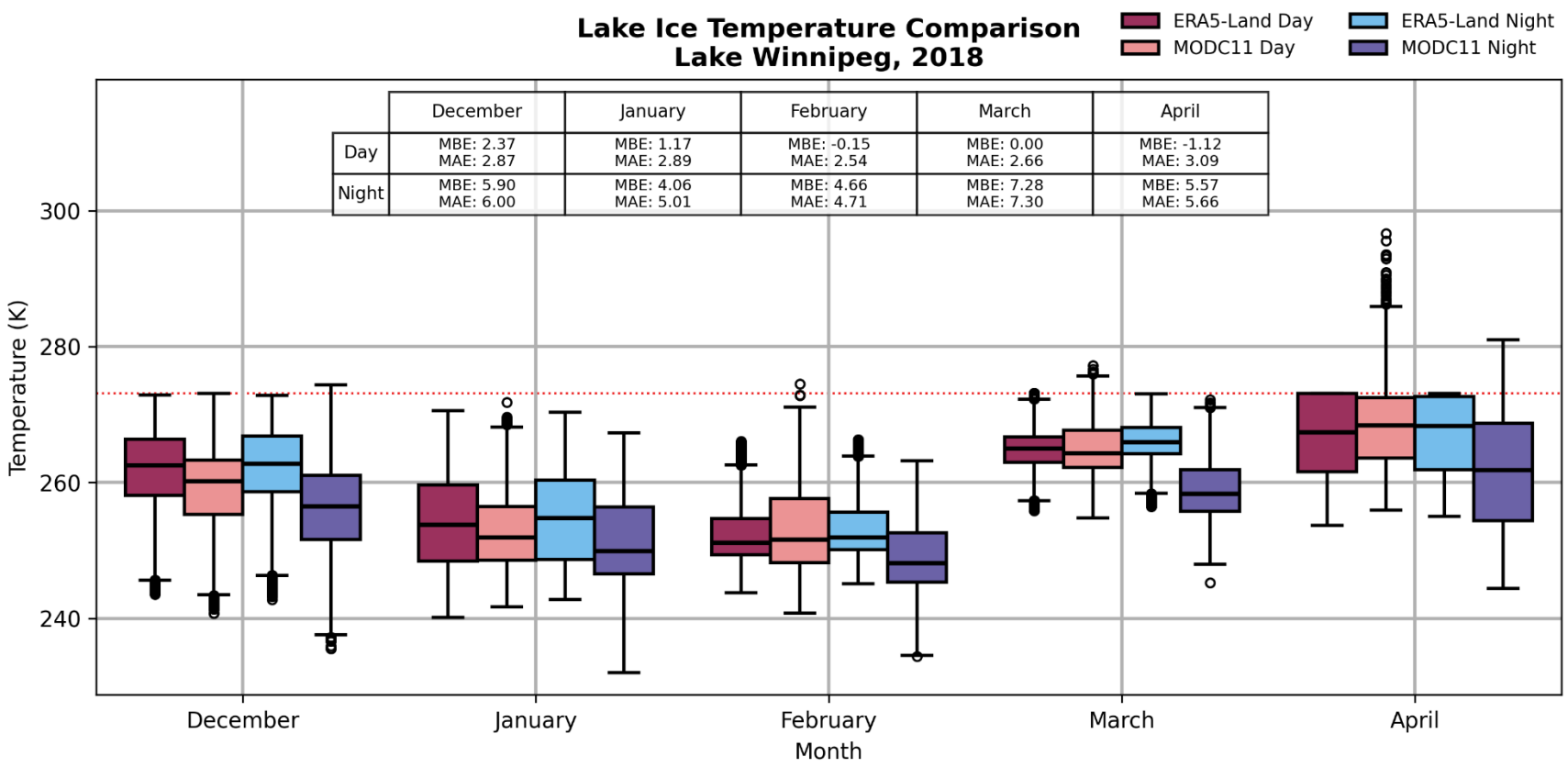


Figure C.4. 15: Boxplot of monthly lake ice surface temperatures during ice-on period of ERA5-Land and MODIS for Lake Winnipeg, 2018

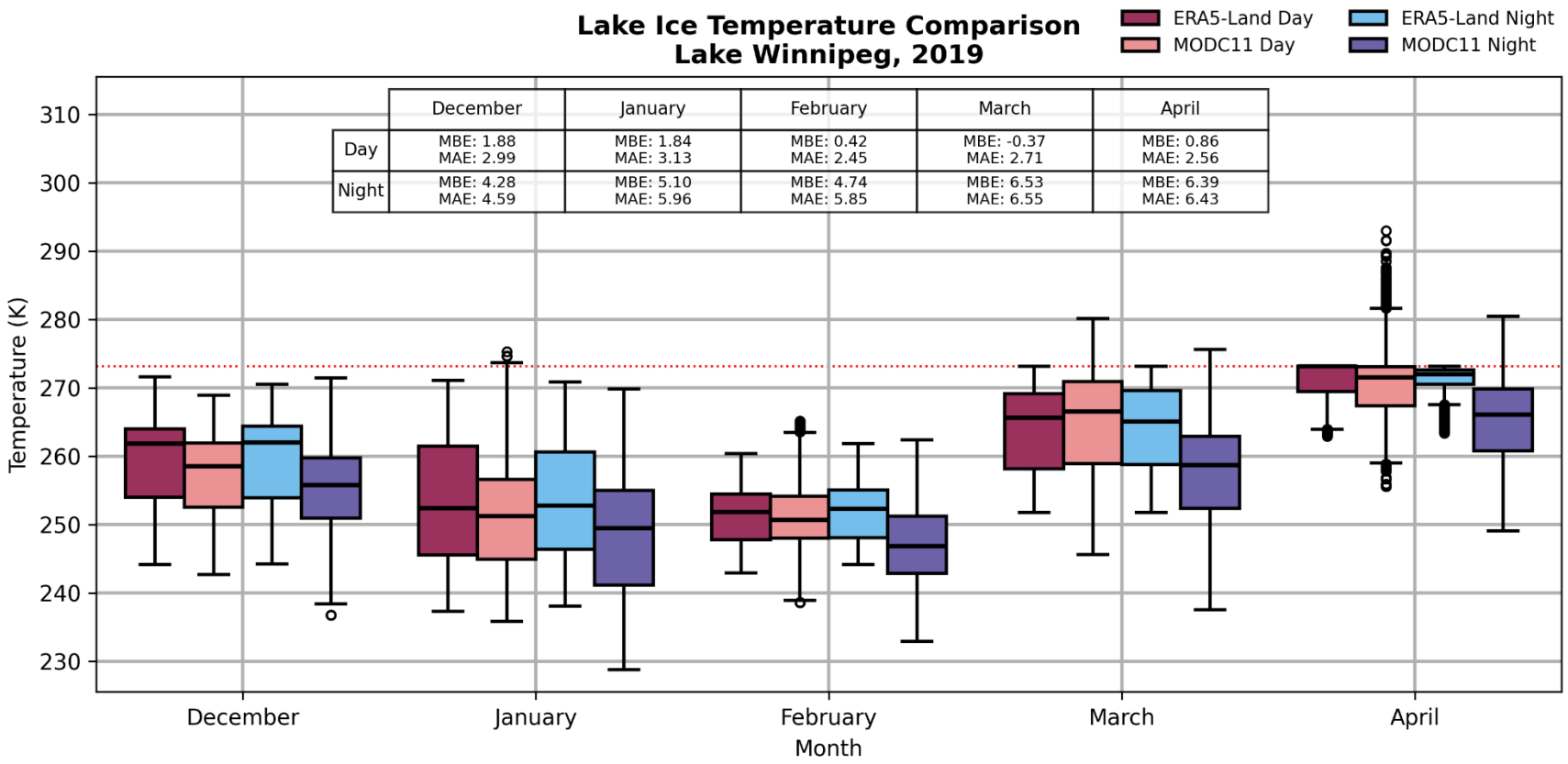


Figure C.4. 16: Boxplot of monthly lake ice surface temperatures during ice-on period of ERA5-Land and MODIS for Lake Winnipeg, 2019

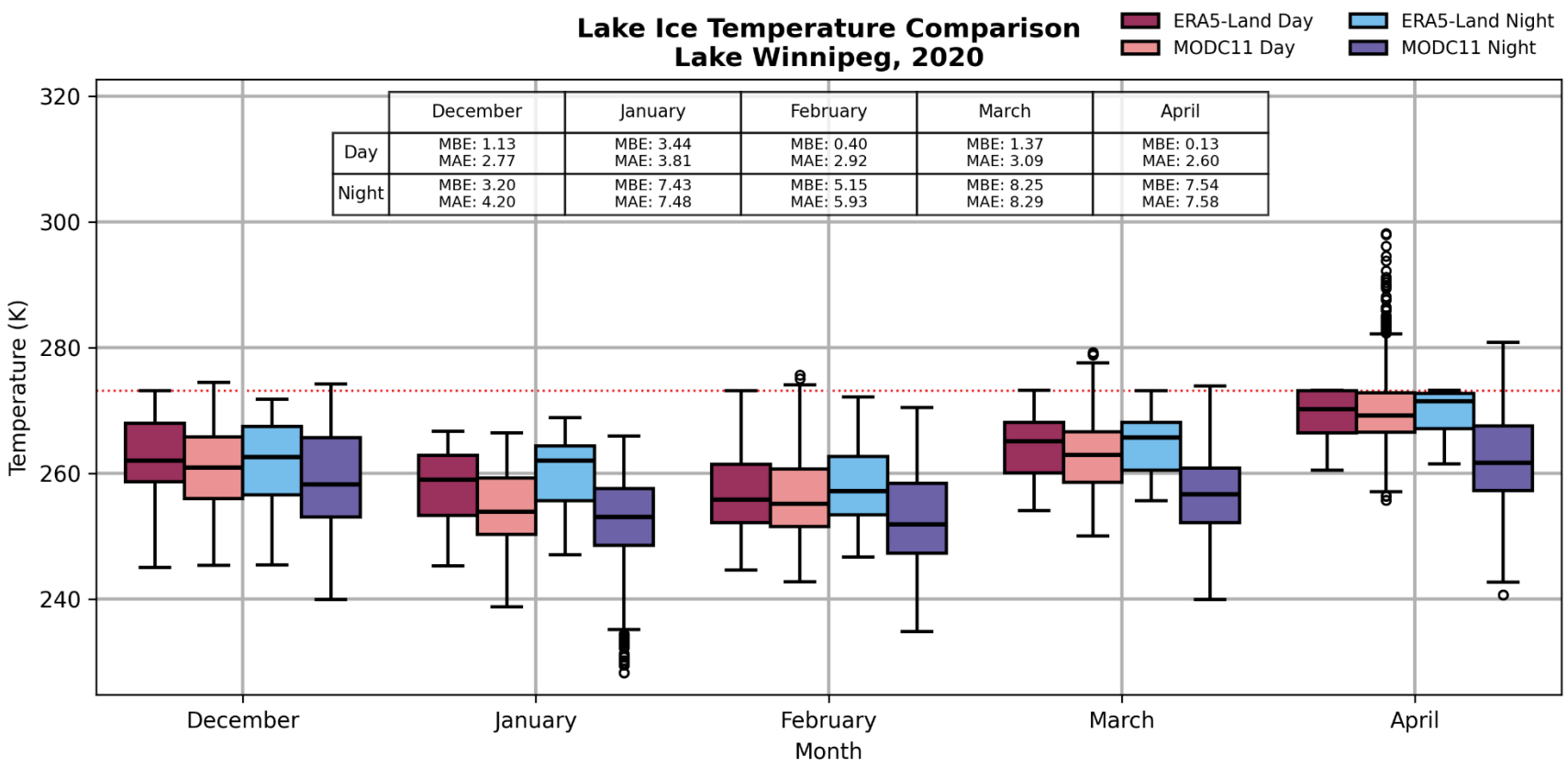


Figure C.4. 17: Boxplot of monthly lake ice surface temperatures during ice-on period of ERA5-Land and MODIS for Lake Winnipeg, 2020

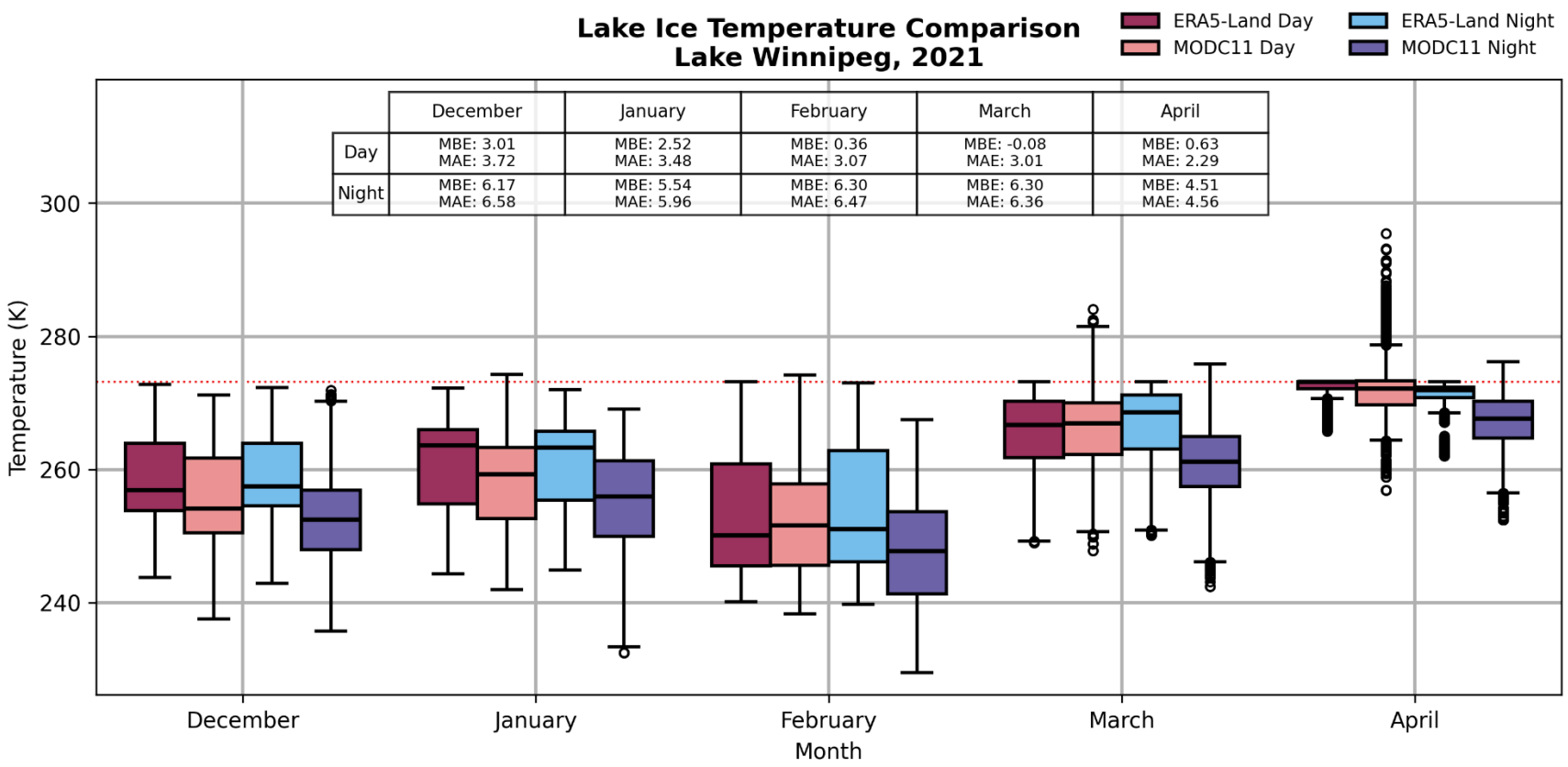


Figure C.4. 18: Boxplot of monthly lake ice surface temperatures during ice-on period of ERA5-Land and MODIS for Lake Winnipeg, 2021

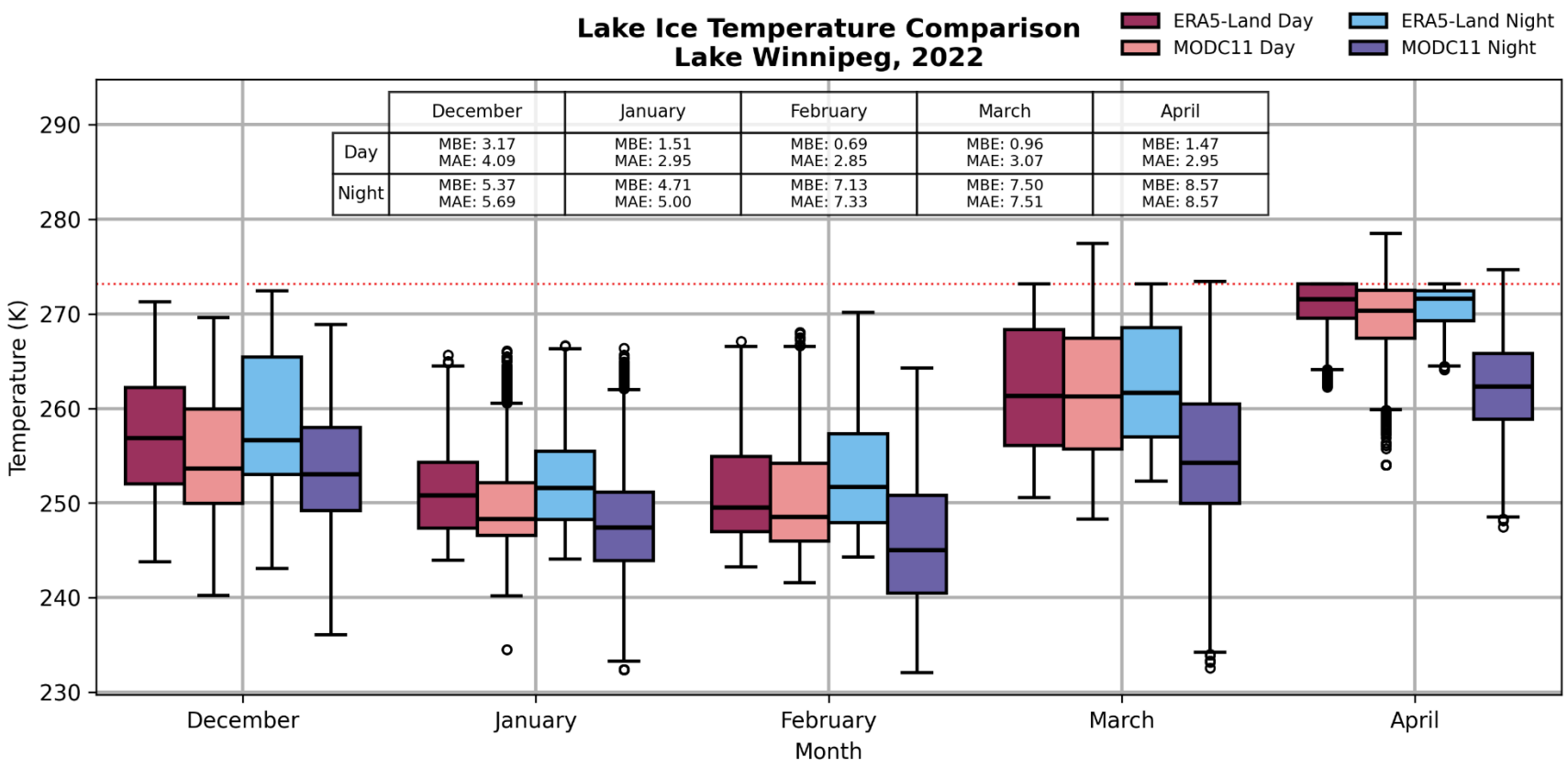


Figure C.4. 19: Boxplot of monthly lake ice surface temperatures during ice-on period of ERA5-Land and MODIS for Lake Winnipeg, 2022

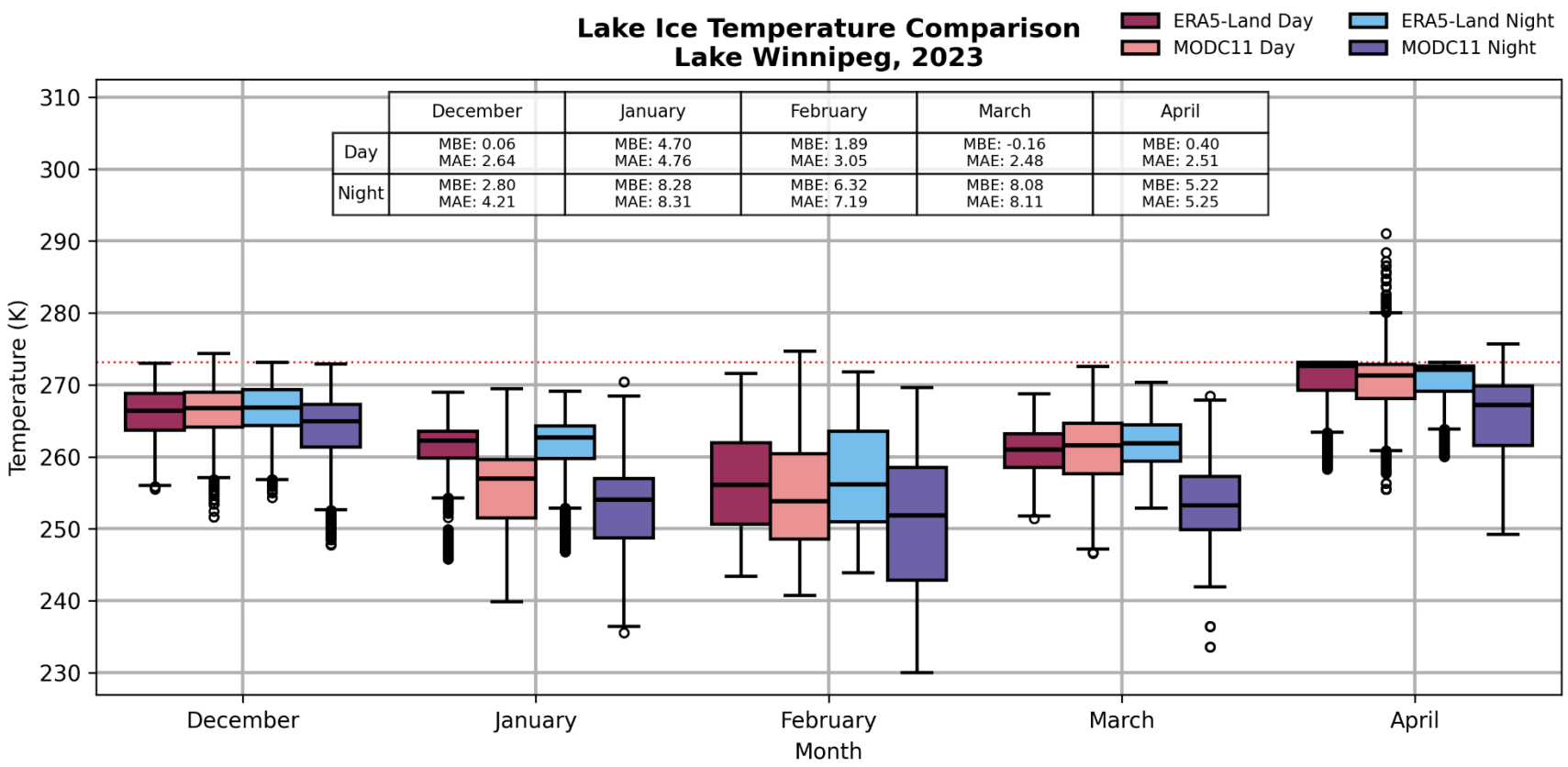


Figure C.4. 20: Boxplot of monthly lake ice surface temperatures during ice-on period of ERA5-Land and MODIS for Lake Winnipeg, 2023

C.5 Lake Superior

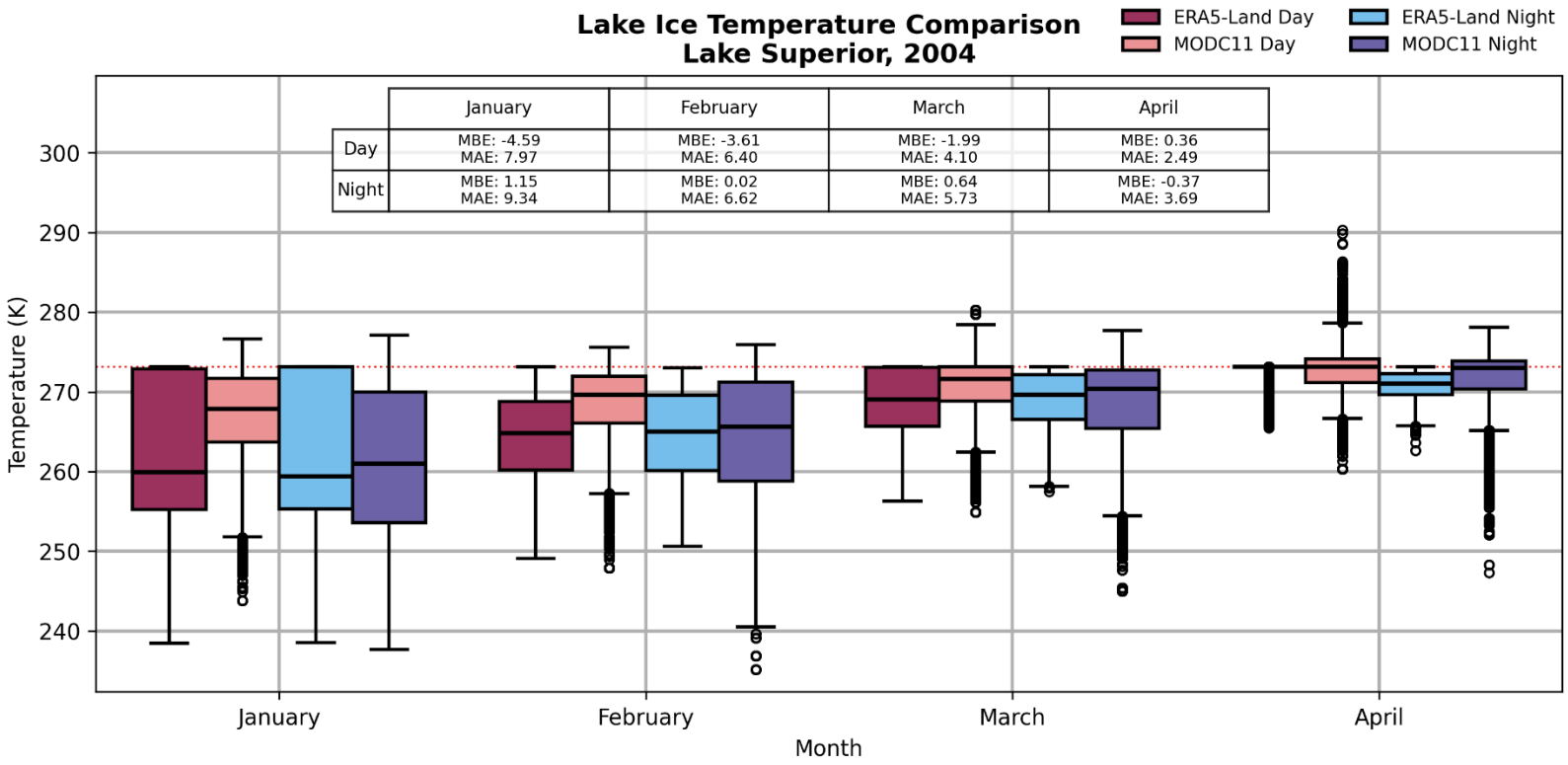


Figure C.5. 1: Boxplot of monthly lake ice surface temperatures during ice-on period of ERA5-Land and MODIS for Lake Superior, 2004

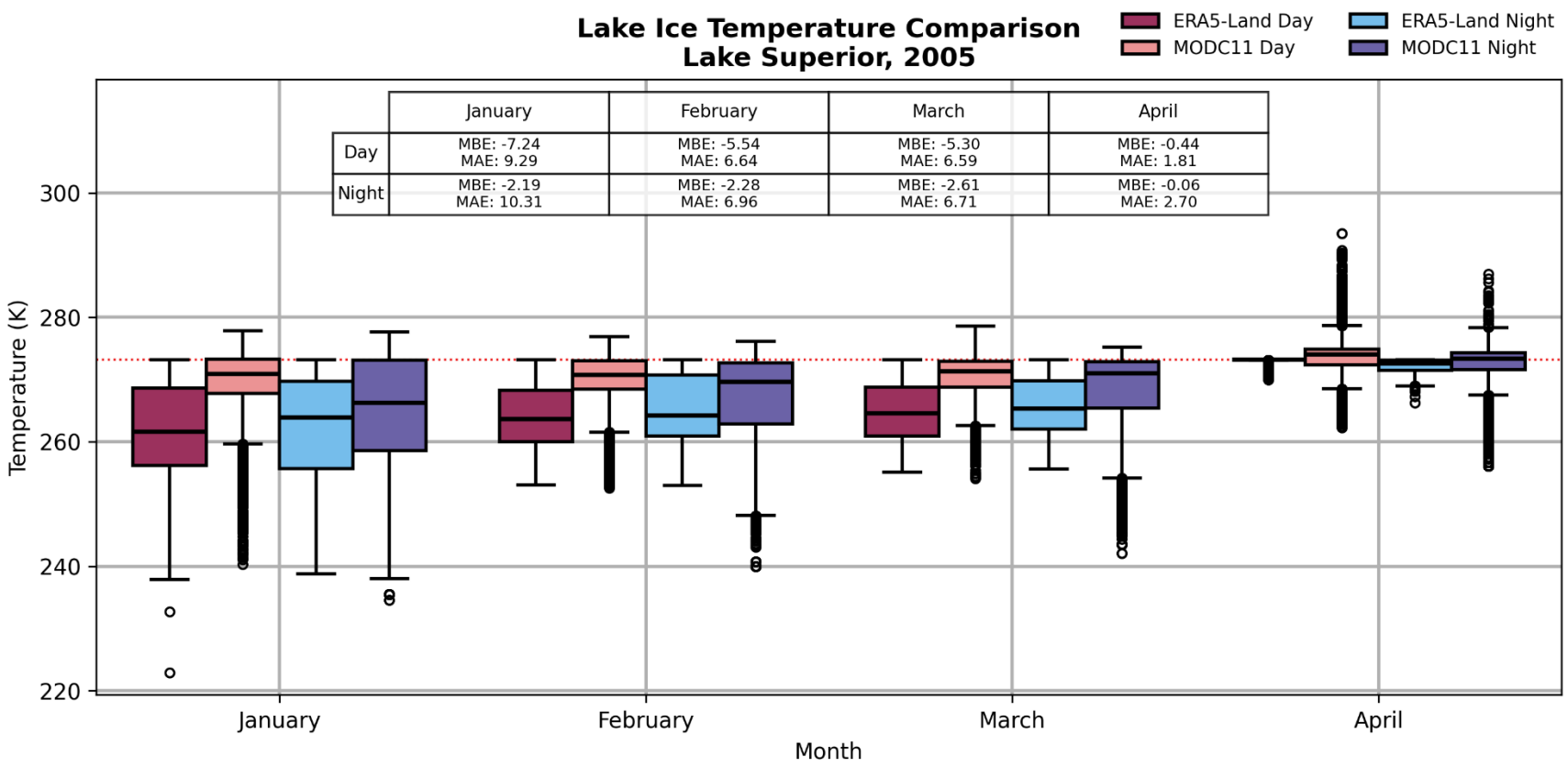


Figure C.5. 2: Boxplot of monthly lake ice surface temperatures during ice-on period of ERA5-Land and MODIS for Lake Superior, 2005

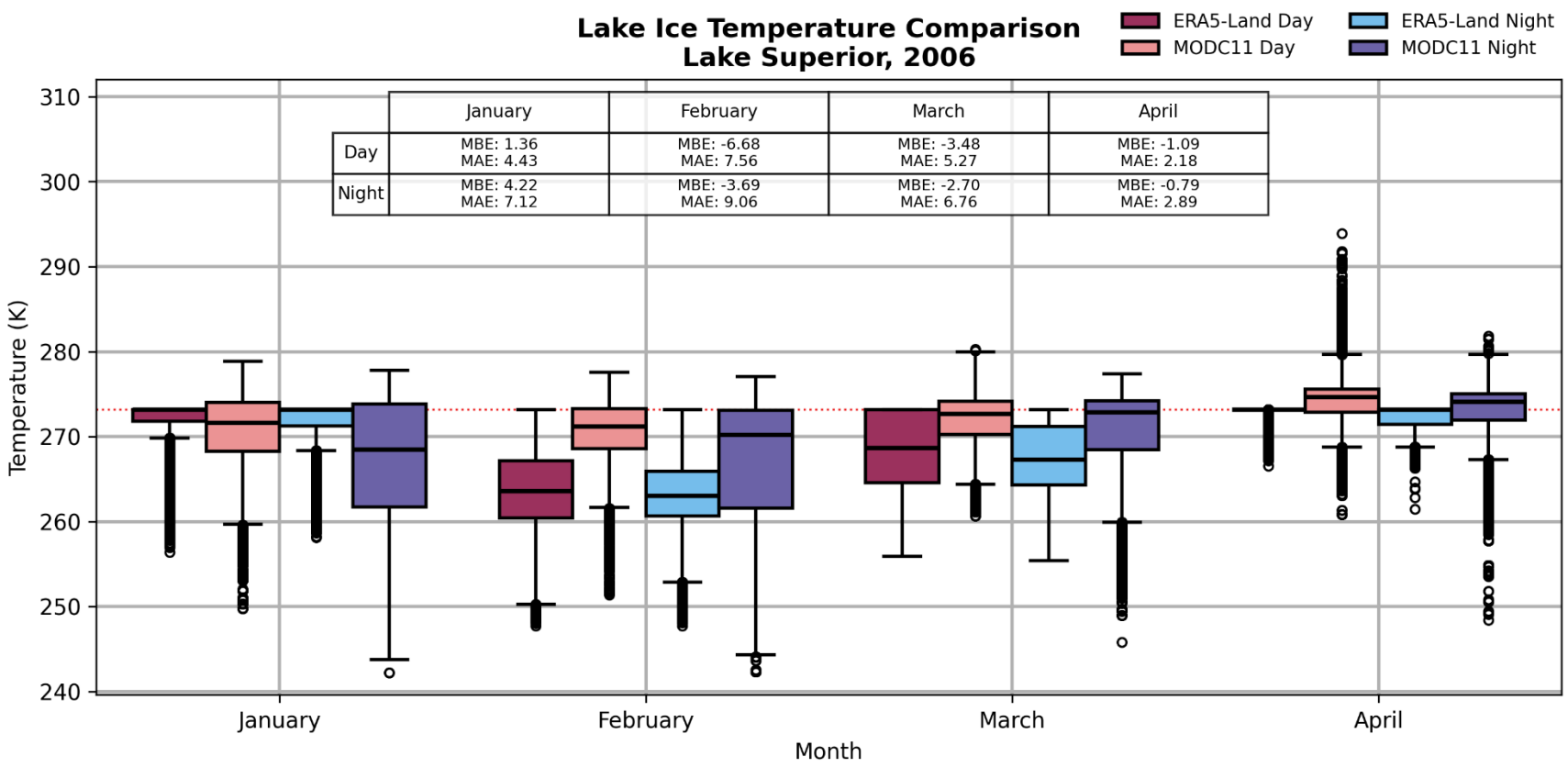


Figure C.5. 3: Boxplot of monthly lake ice surface temperatures during ice-on period of ERA5-Land and MODIS for Lake Superior, 2006

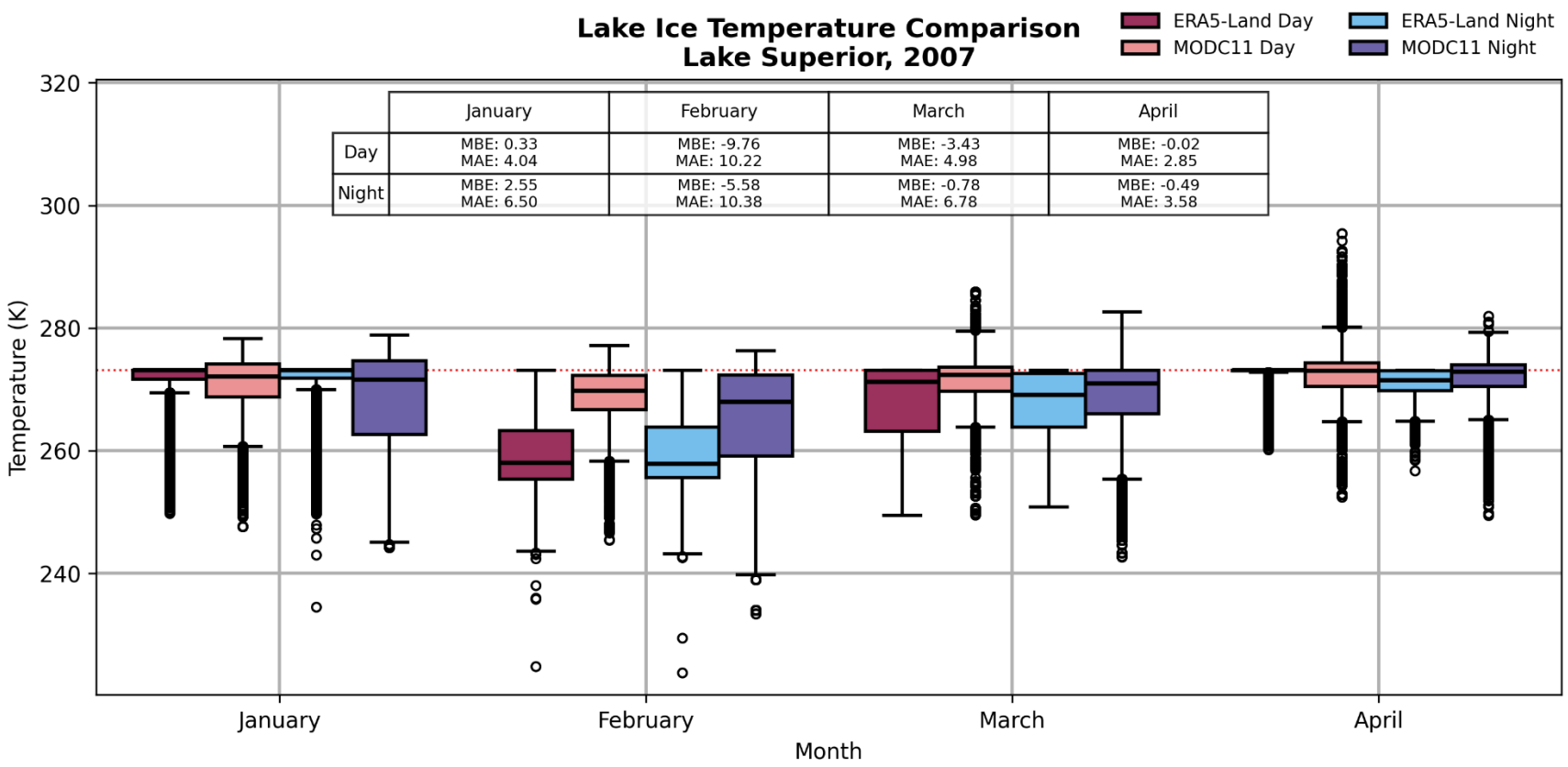


Figure C.5. 4: Boxplot of monthly lake ice surface temperatures during ice-on period of ERA5-Land and MODIS for Lake Superior, 2007

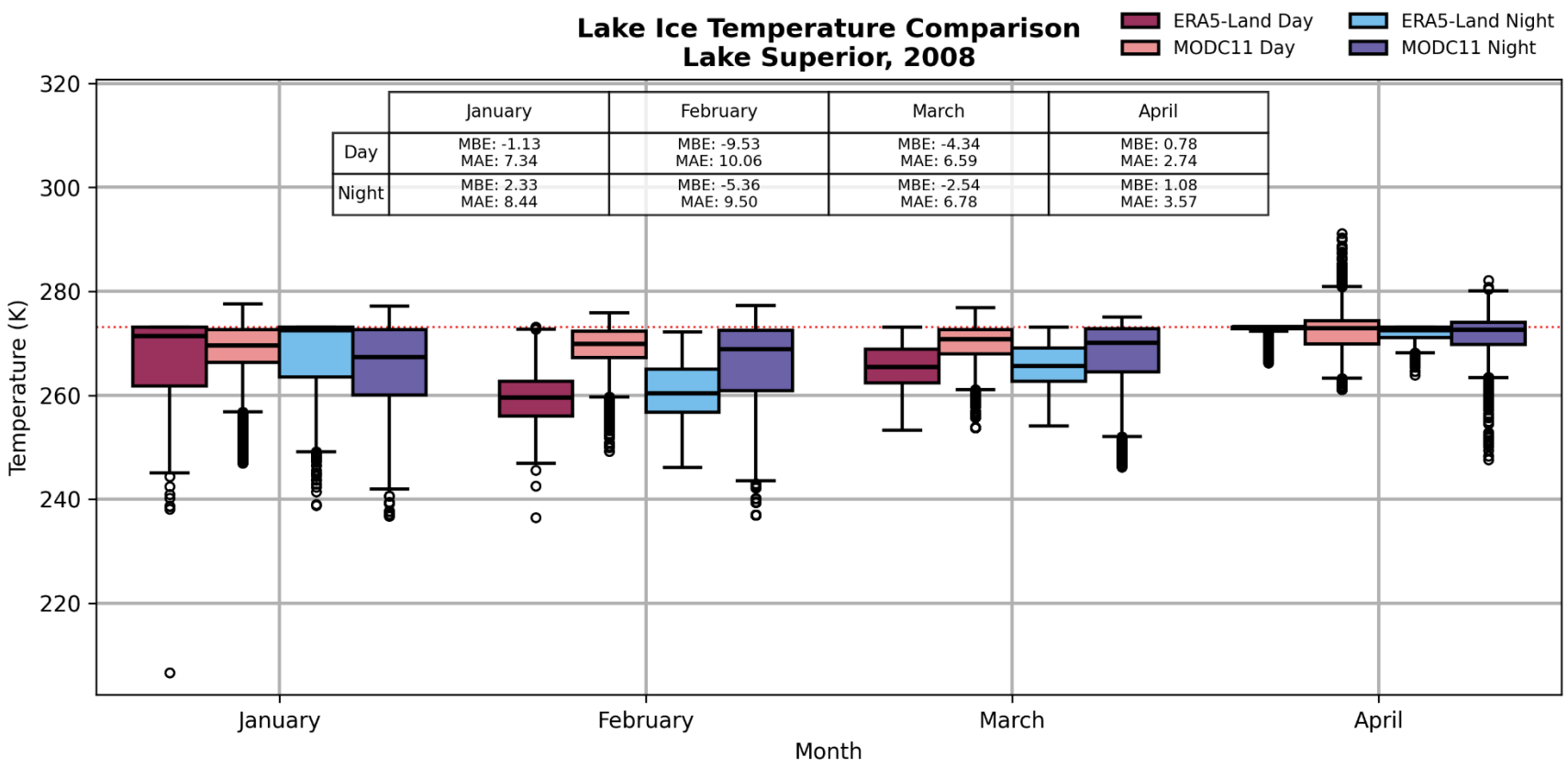


Figure C.5. 5: Boxplot of monthly lake ice surface temperatures during ice-on period of ERA5-Land and MODIS for Lake Superior, 2008

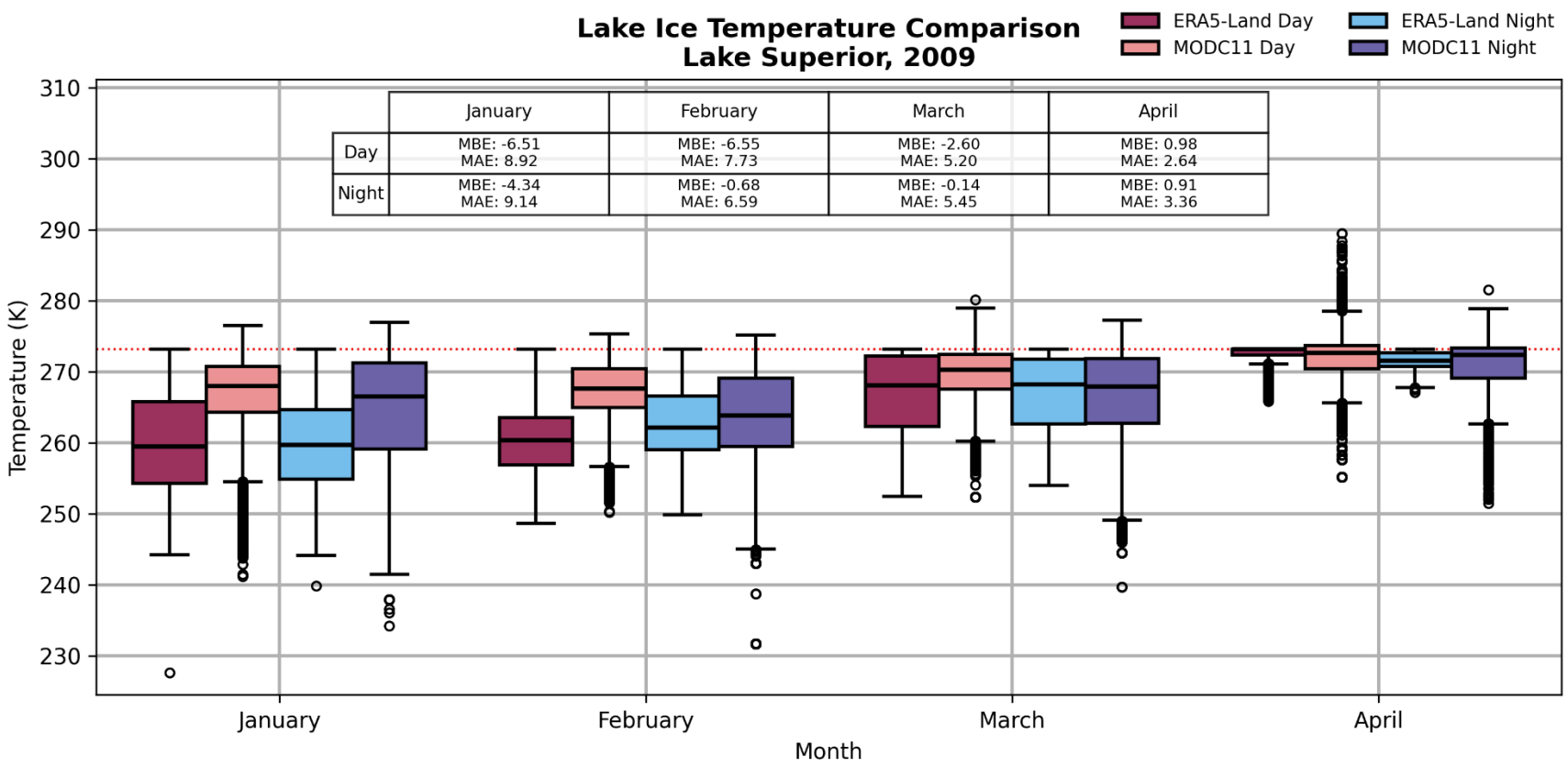


Figure C.5. 6: Boxplot of monthly lake ice surface temperatures during ice-on period of ERA5-Land and MODIS for Lake Superior, 2009

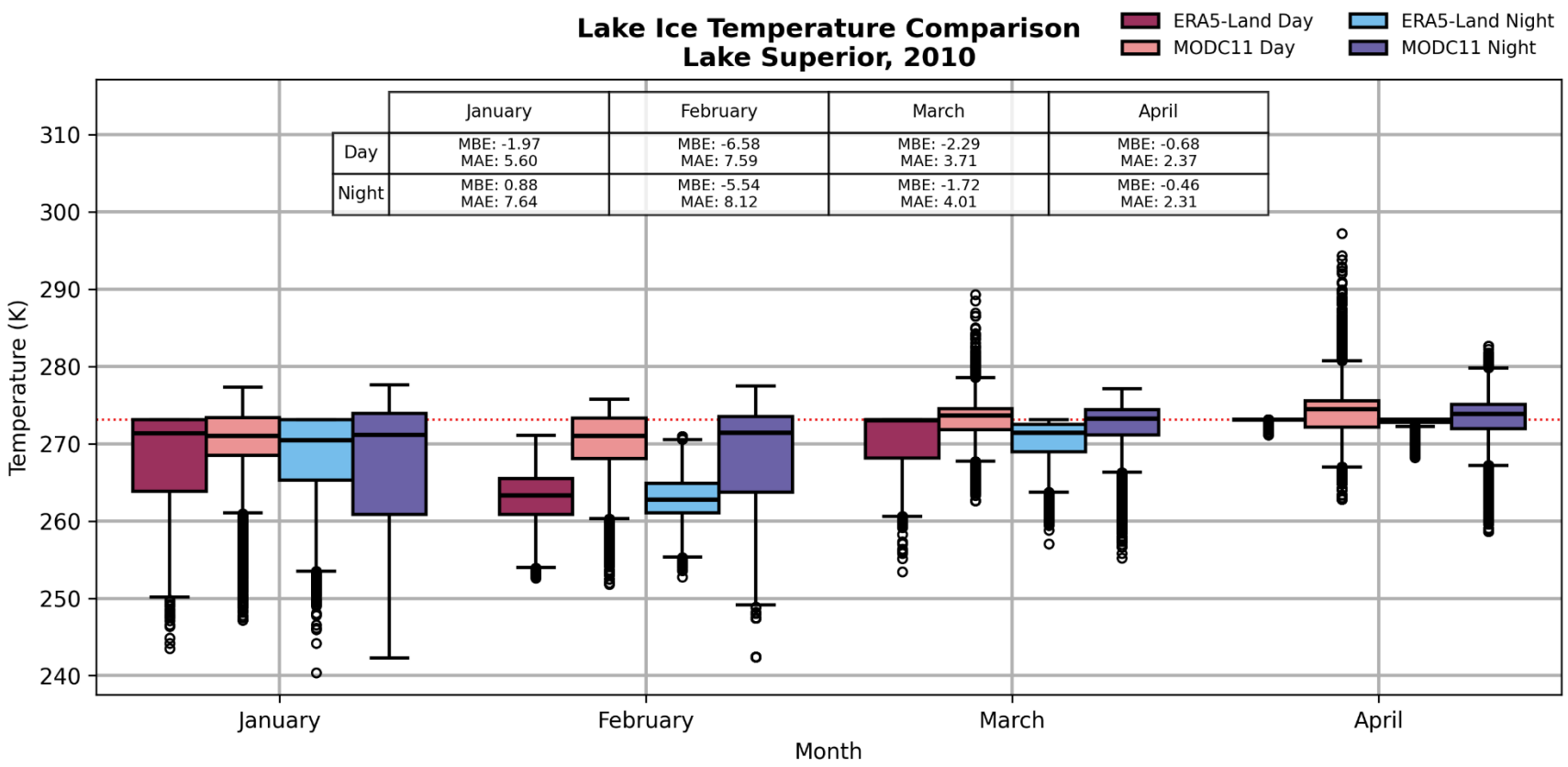


Figure C.5. 7: Boxplot of monthly lake ice surface temperatures during ice-on period of ERA5-Land and MODIS for Lake Superior, 2010

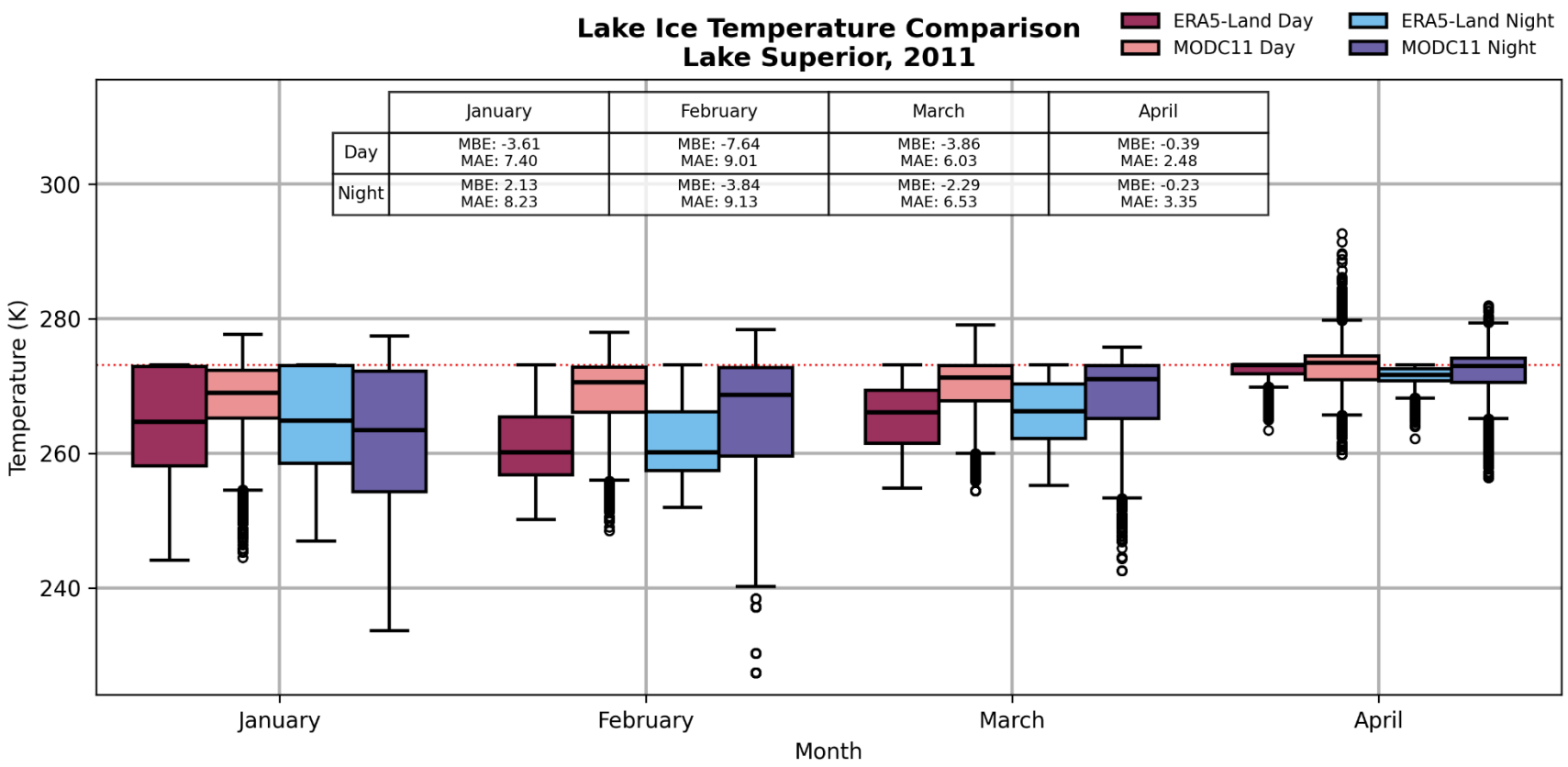


Figure C.5. 8: Boxplot of monthly lake ice surface temperatures during ice-on period of ERA5-Land and MODIS for Lake Superior, 2011

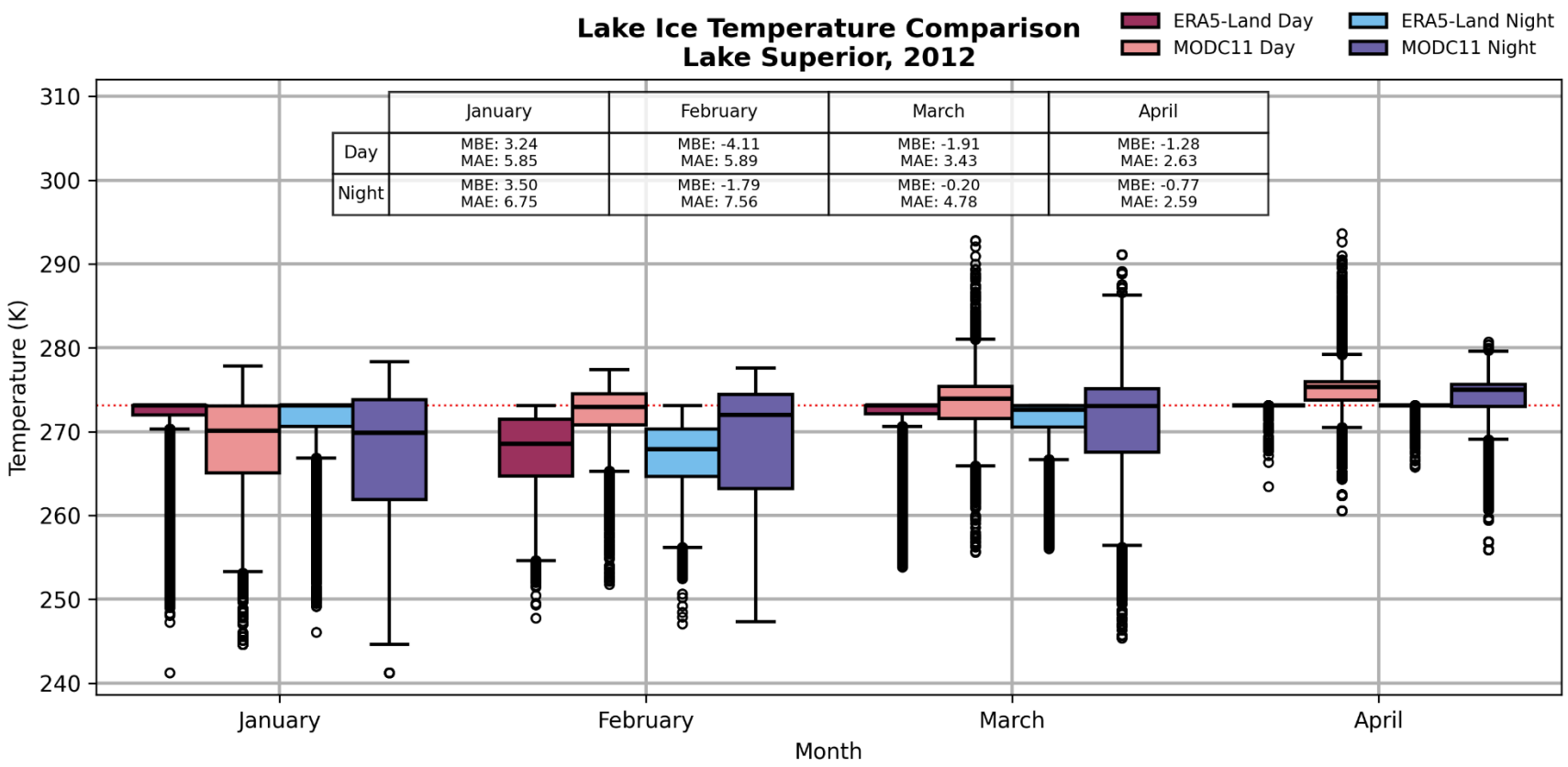


Figure C.5. 9: Boxplot of monthly lake ice surface temperatures during ice-on period of ERA5-Land and MODIS for Lake Superior, 2012

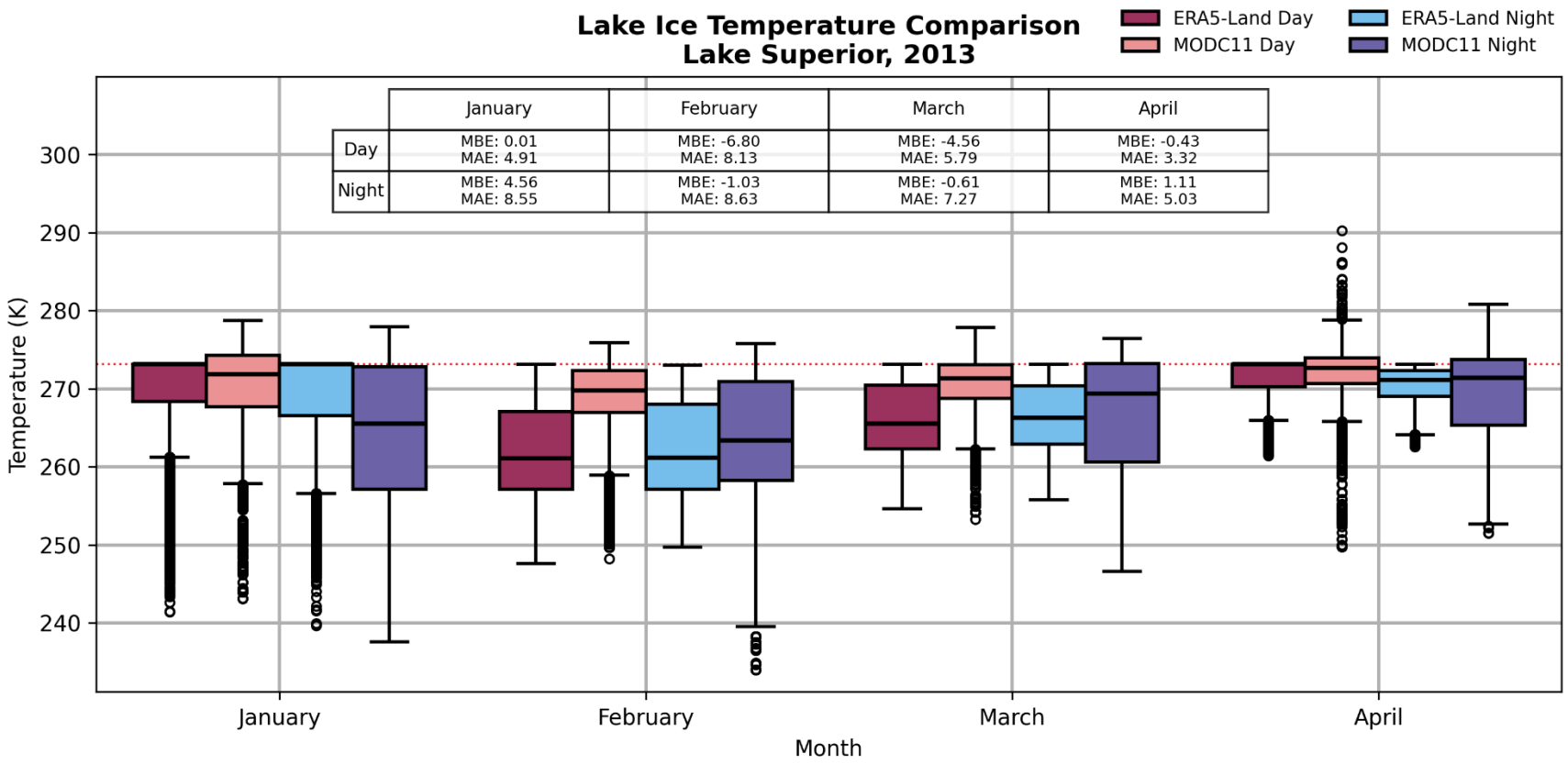


Figure C.5. 10: Boxplot of monthly lake ice surface temperatures during ice-on period of ERA5-Land and MODIS for Lake Superior, 2013

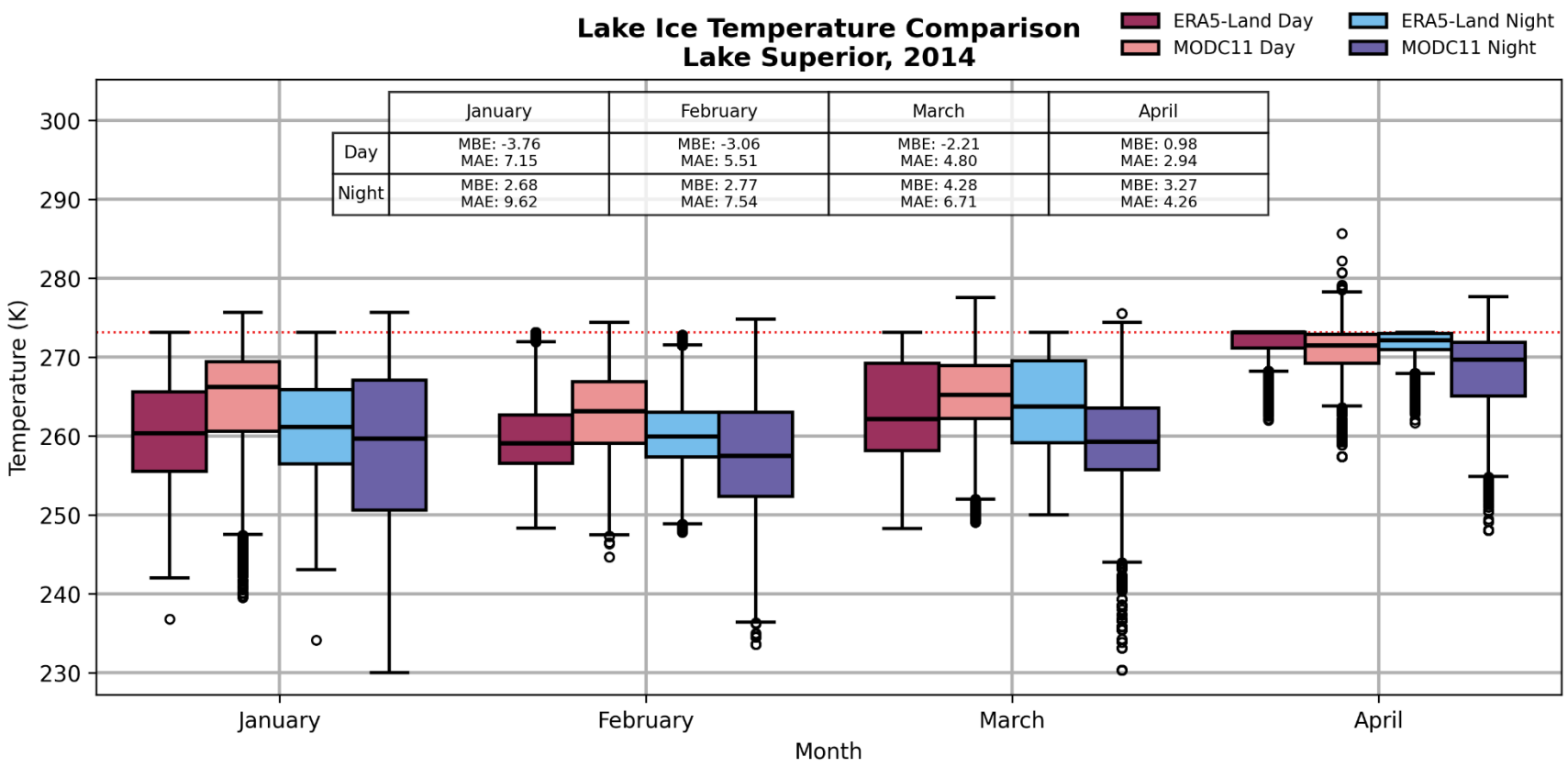


Figure C.5. 11: Boxplot of monthly lake ice surface temperatures during ice-on period of ERA5-Land and MODIS for Lake Superior, 2014

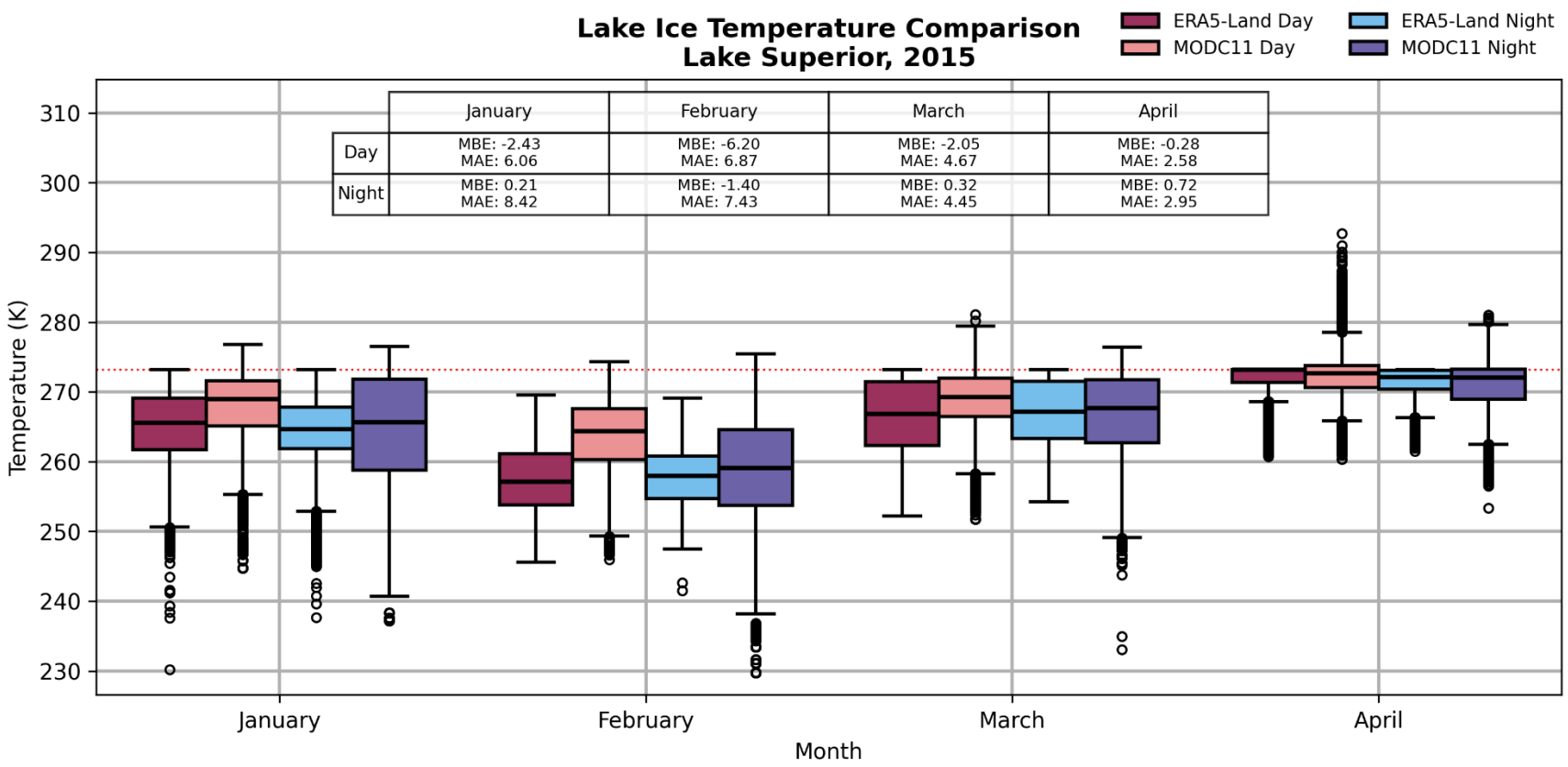


Figure C.5. 12: Boxplot of monthly lake ice surface temperatures during ice-on period of ERA5-Land and MODIS for Lake Superior, 2015

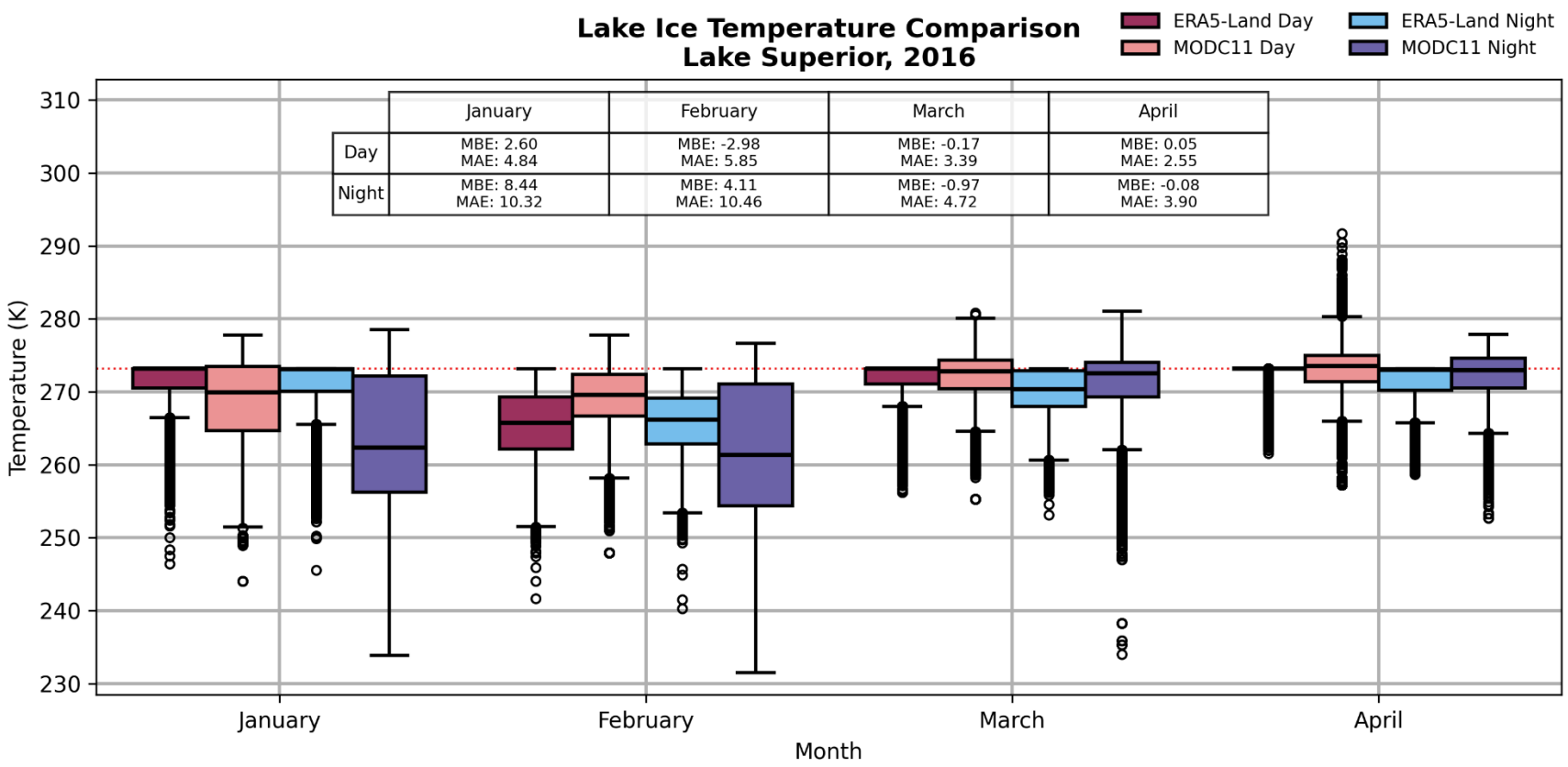


Figure C.5. 13: Boxplot of monthly lake ice surface temperatures during ice-on period of ERA5-Land and MODIS for Lake Superior, 2016

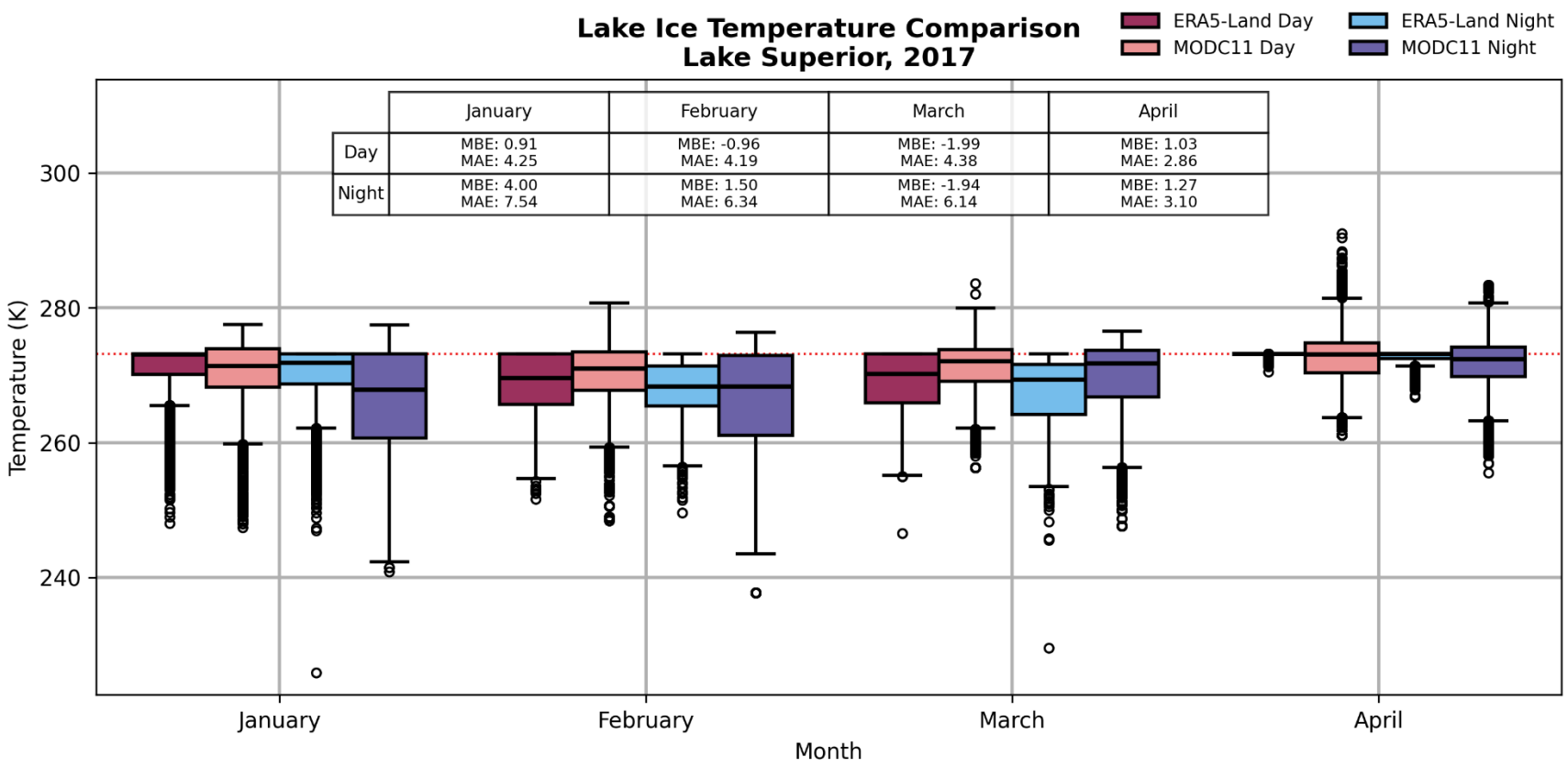


Figure C.5. 14: Boxplot of monthly lake ice surface temperatures during ice-on period of ERA5-Land and MODIS for Lake Superior, 2017

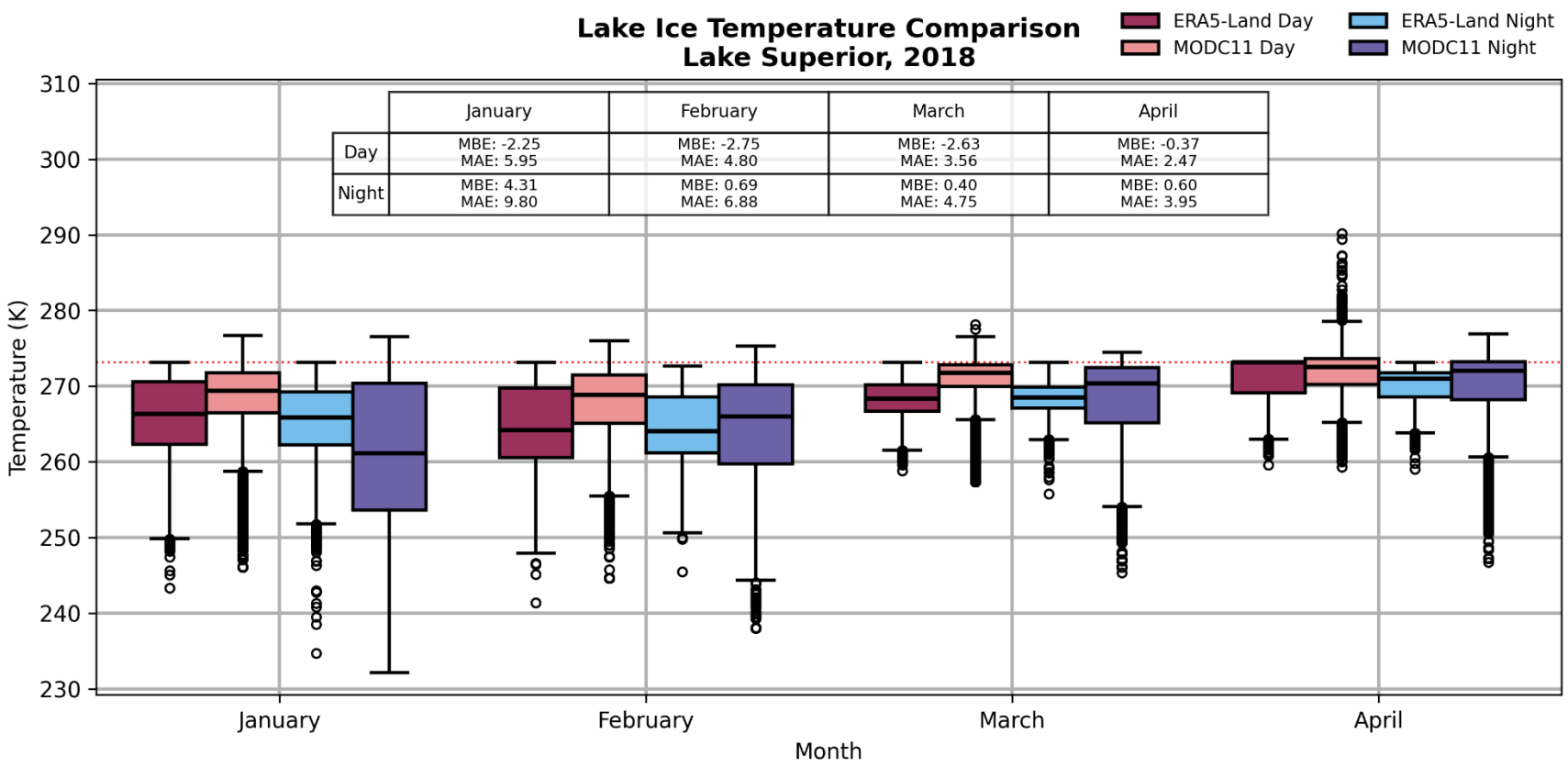


Figure C.5. 15: Boxplot of monthly lake ice surface temperatures during ice-on period of ERA5-Land and MODIS for Lake Superior, 2018

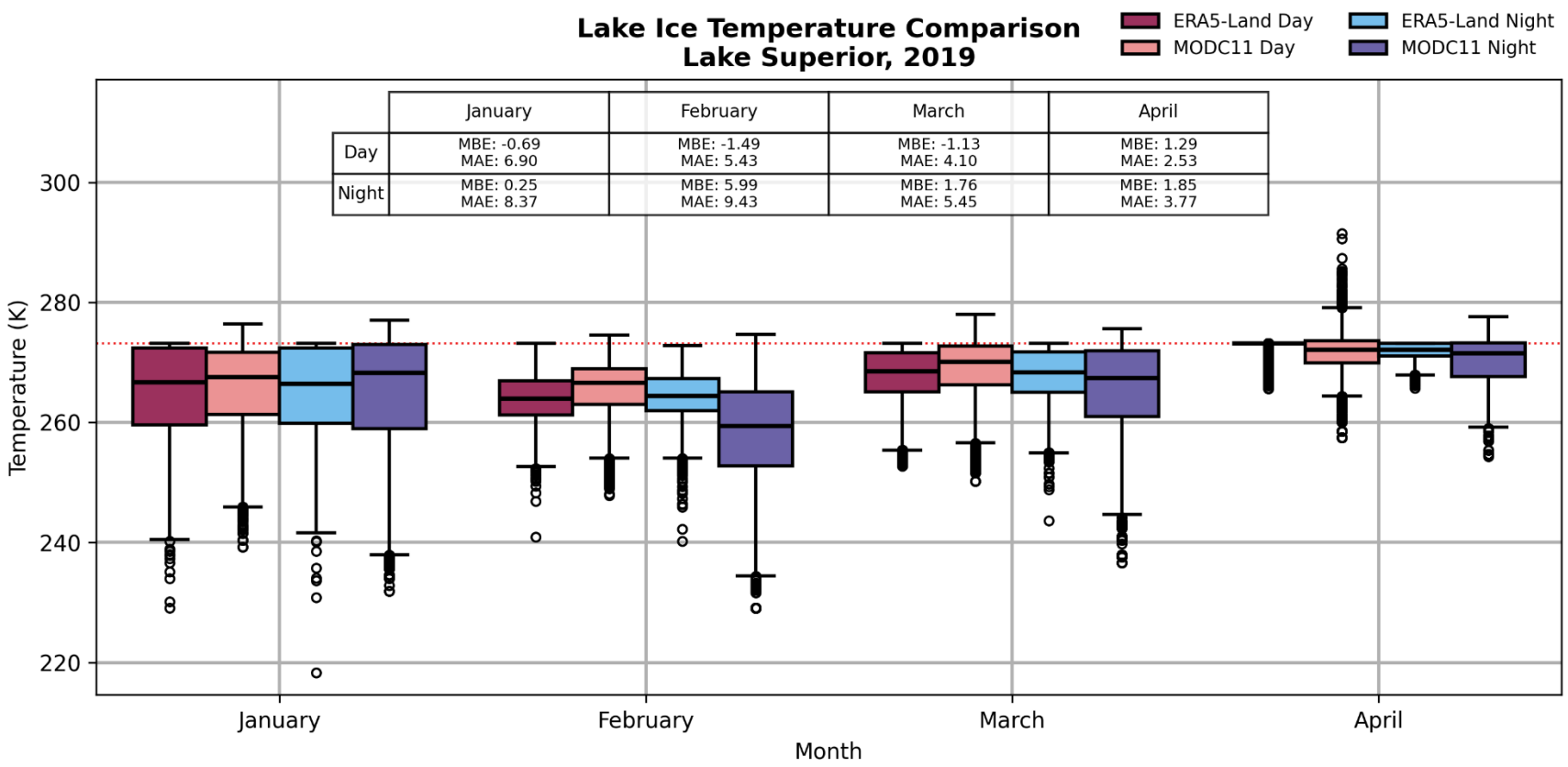


Figure C.5. 16: Boxplot of monthly lake ice surface temperatures during ice-on period of ERA5-Land and MODIS for Lake Superior, 2019

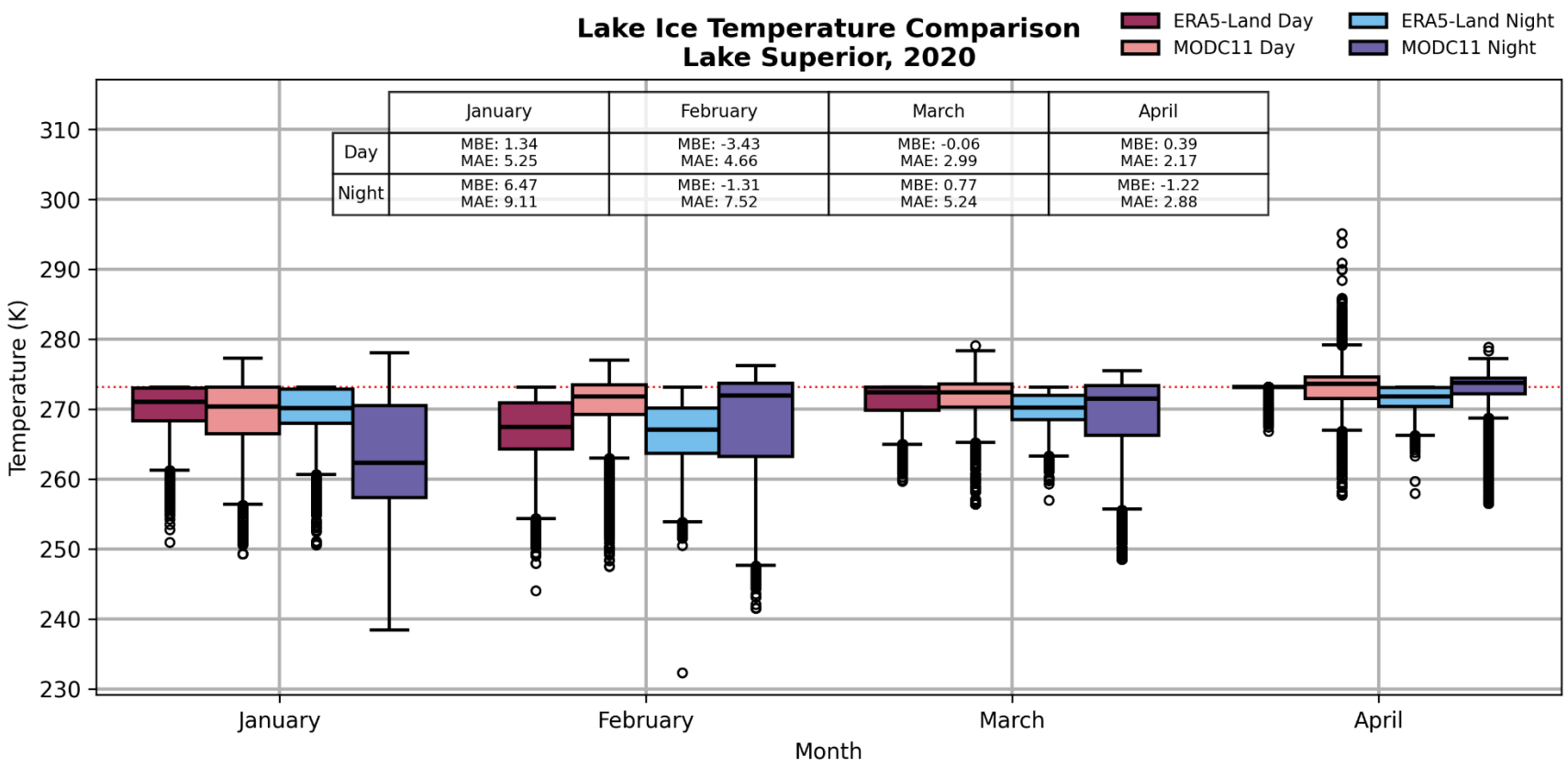


Figure C.5. 17: Boxplot of monthly lake ice surface temperatures during ice-on period of ERA5-Land and MODIS for Lake Superior, 2020

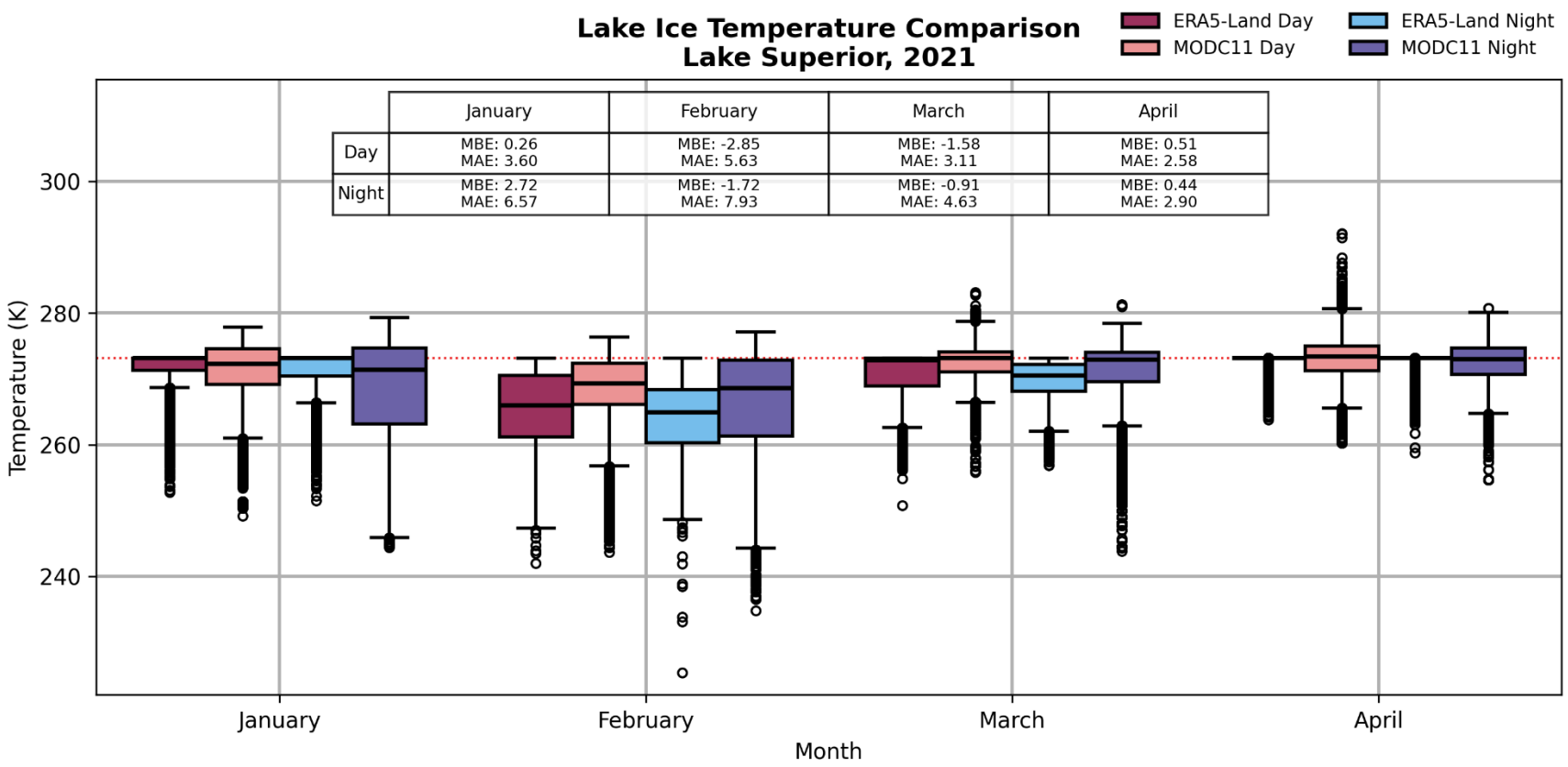


Figure C.5. 18: Boxplot of monthly lake ice surface temperatures during ice-on period of ERA5-Land and MODIS for Lake Superior, 2021

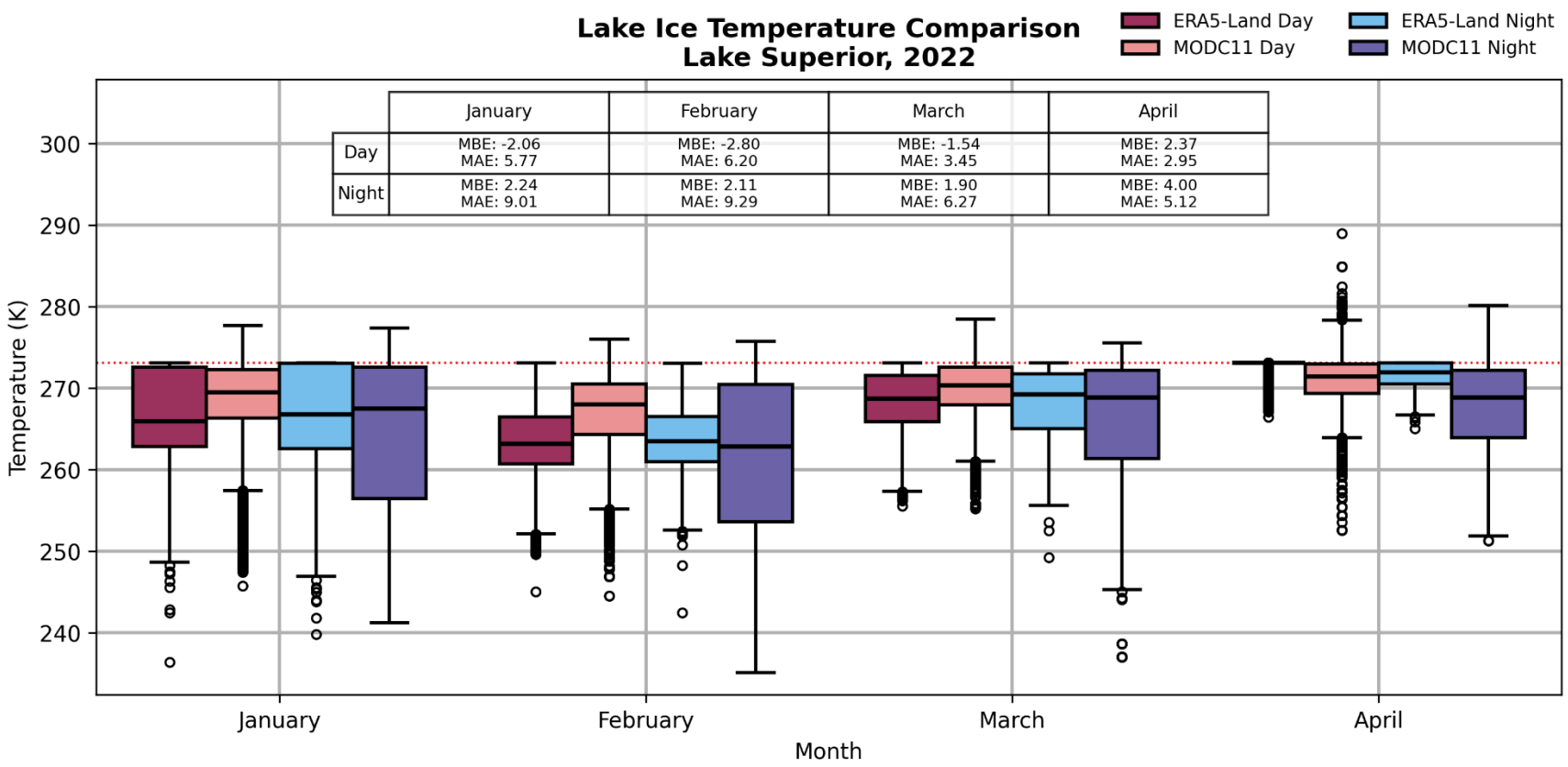


Figure C.5. 19: Boxplot of monthly lake ice surface temperatures during ice-on period of ERA5-Land and MODIS for Lake Superior, 2022

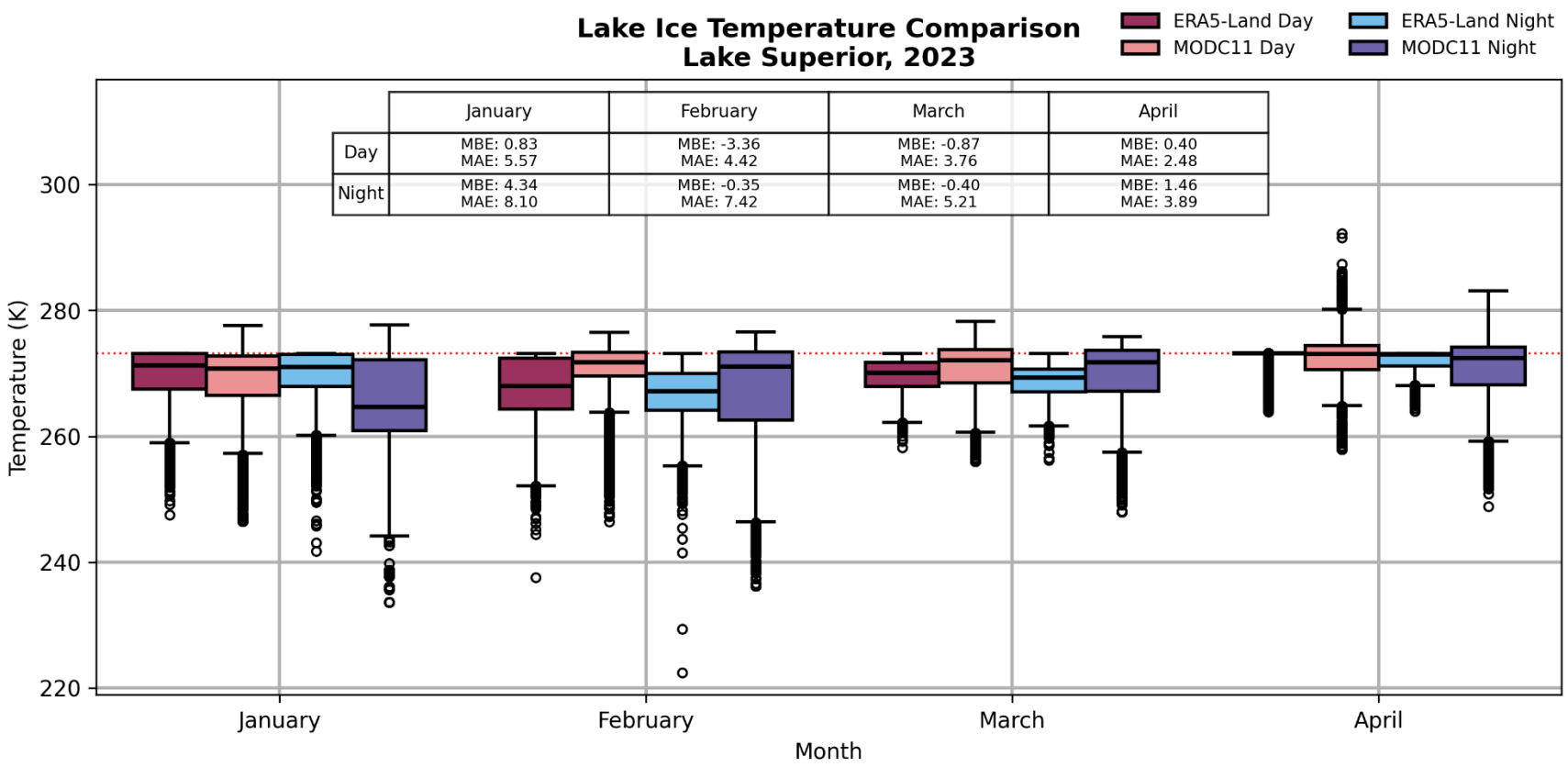


Figure C.5. 20: Boxplot of monthly lake ice surface temperatures during ice-on period of ERA5-Land and MODIS for Lake Superior, 2023

C.6 Lake Huron

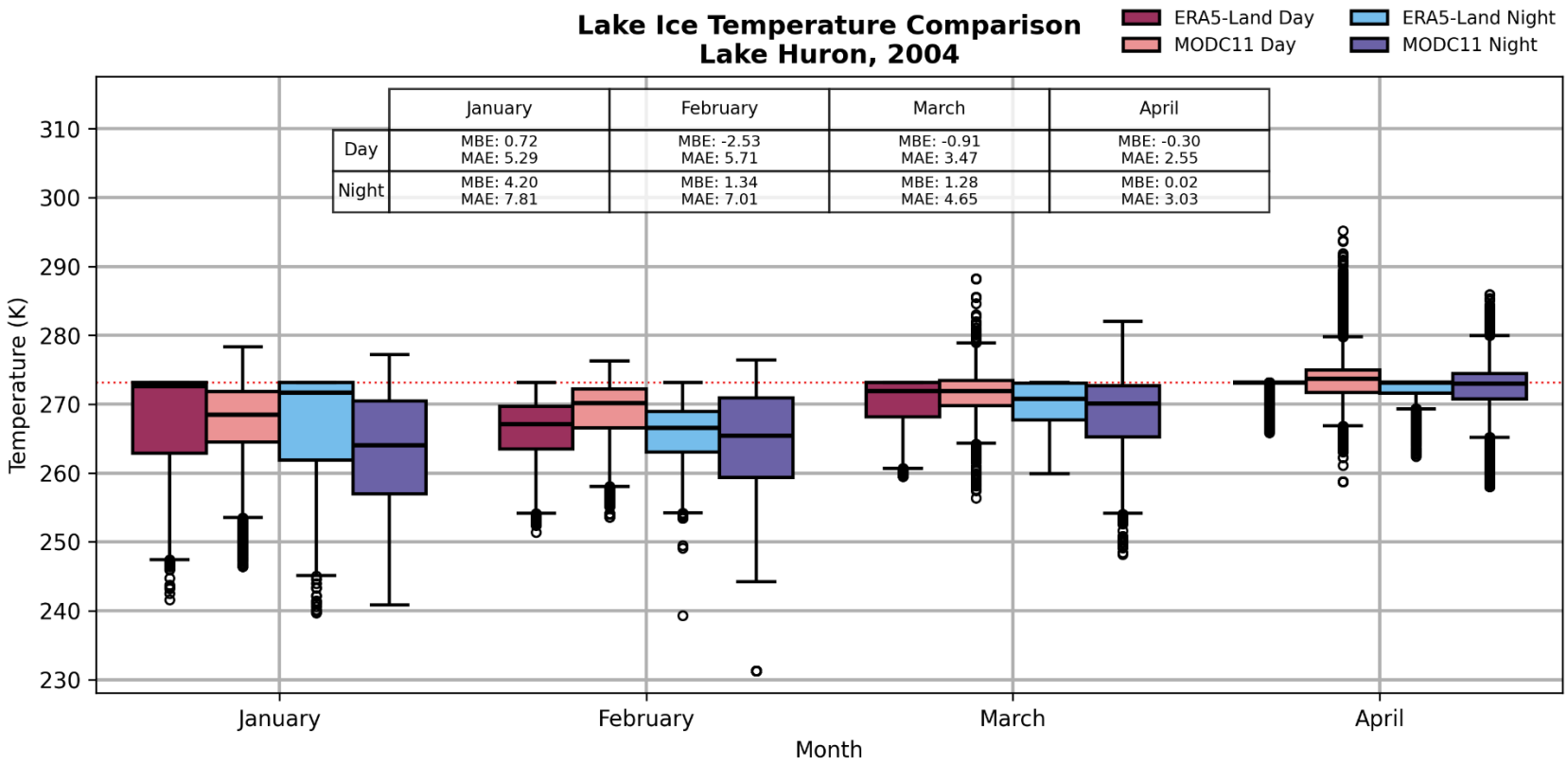


Figure C.6. 1: Boxplot of monthly lake ice surface temperatures during ice-on period of ERA5-Land and MODIS for Lake Huron, 2004

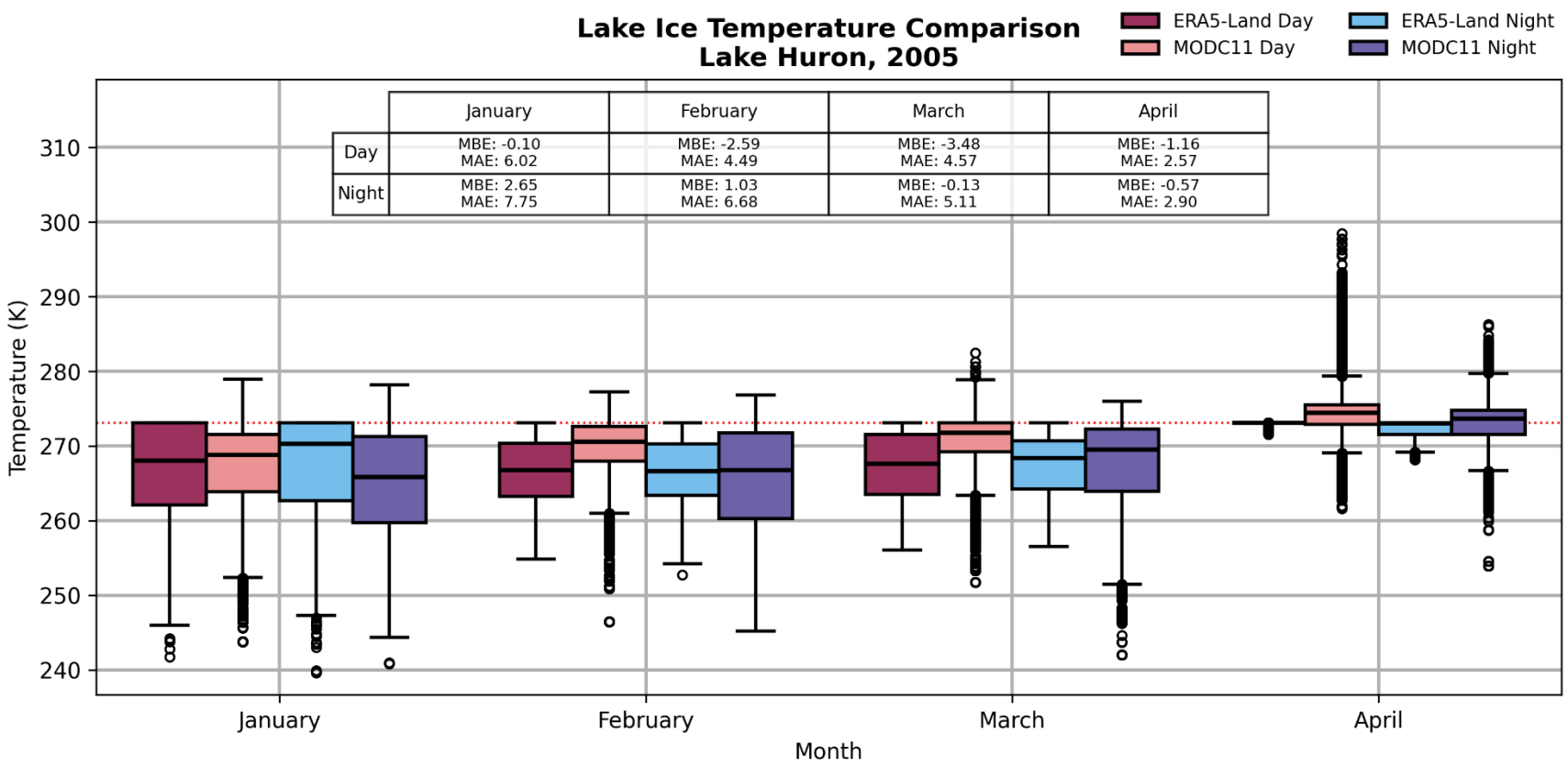


Figure C.6. 2: Boxplot of monthly lake ice surface temperatures during ice-on period of ERA5-Land and MODIS for Lake Huron, 2005

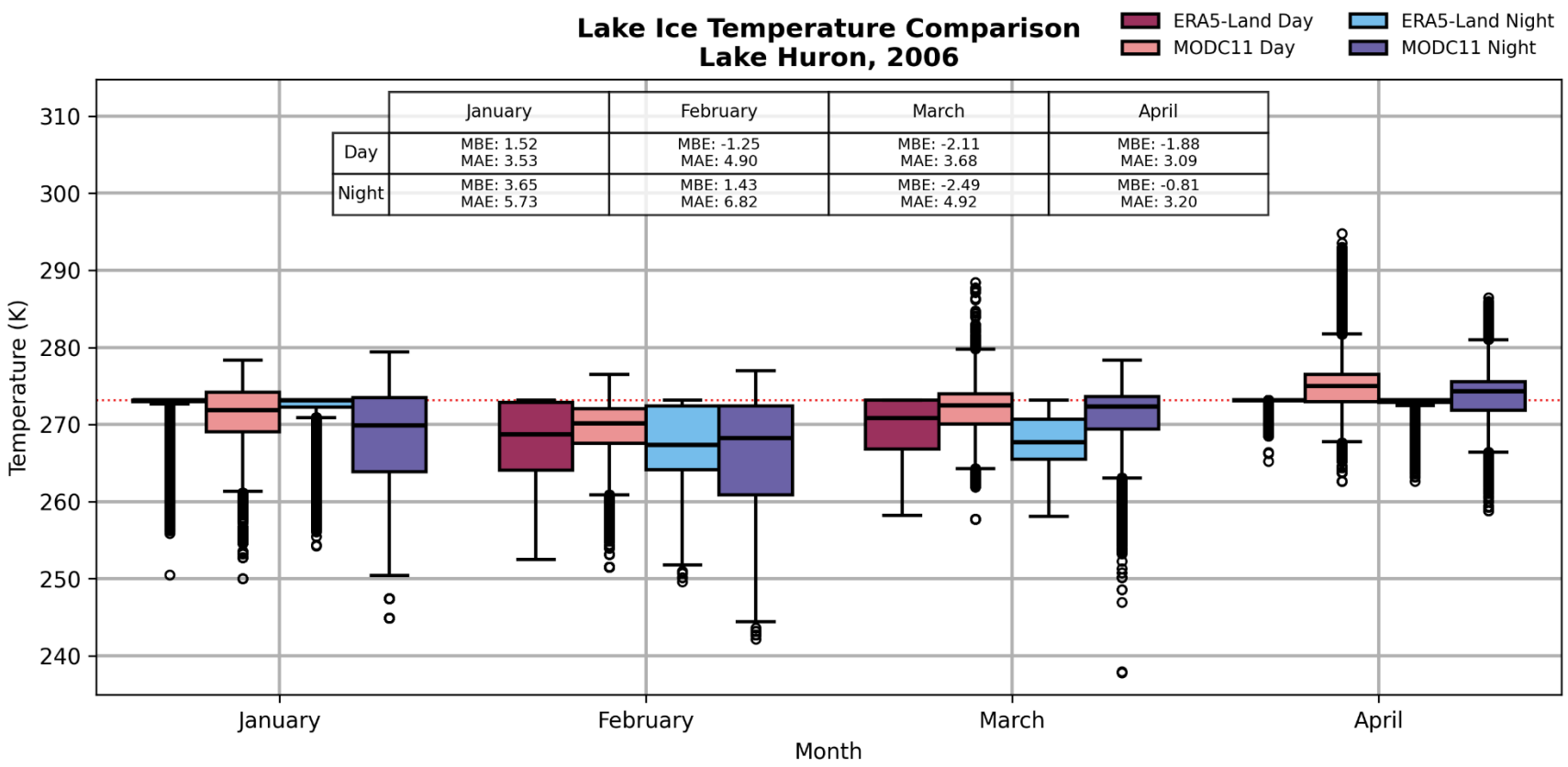


Figure C.6. 3: Boxplot of monthly lake ice surface temperatures during ice-on period of ERA5-Land and MODIS for Lake Huron, 2006

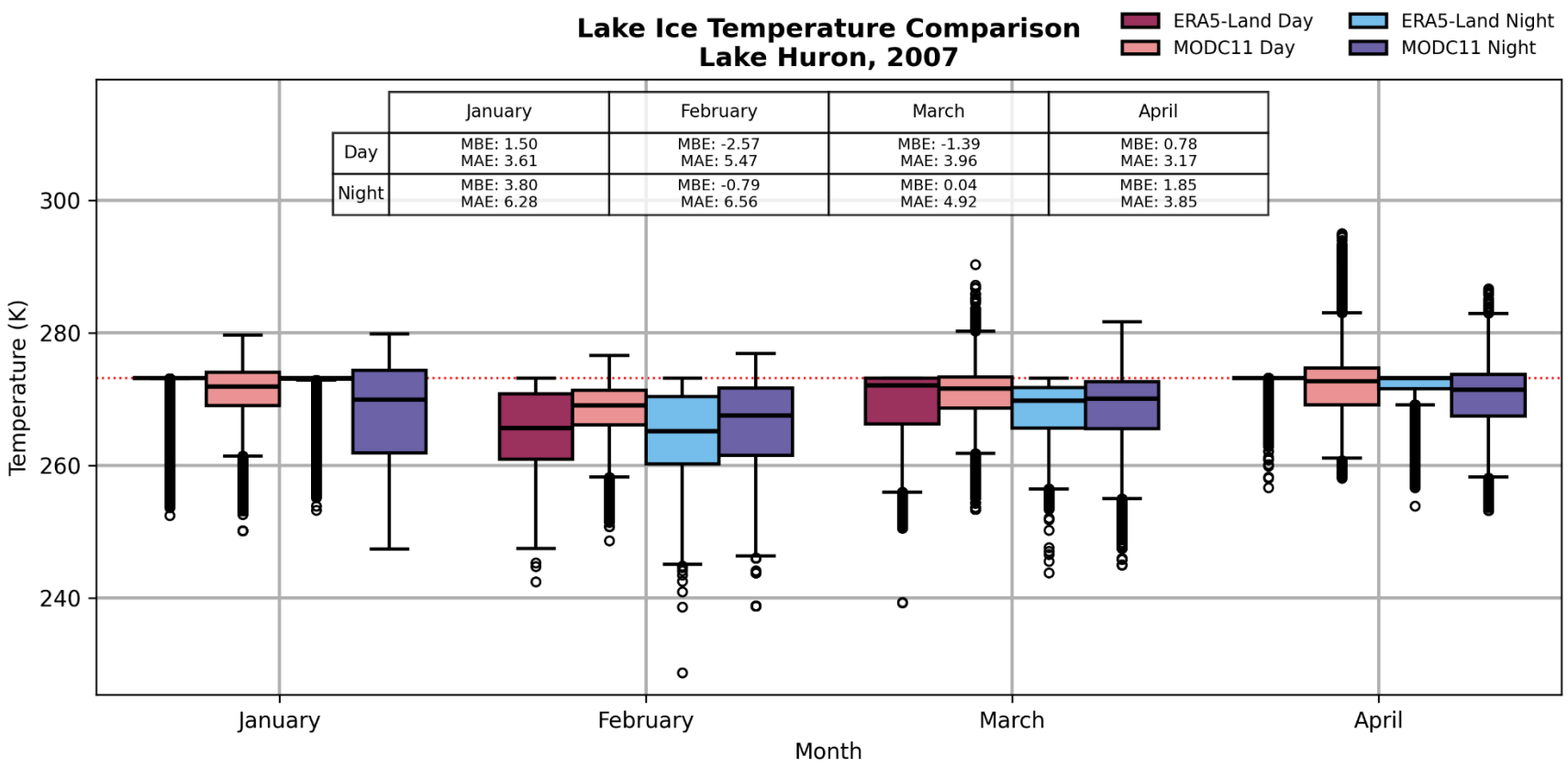


Figure C.6. 4: Boxplot of monthly lake ice surface temperatures during ice-on period of ERA5-Land and MODIS for Lake Huron, 2007

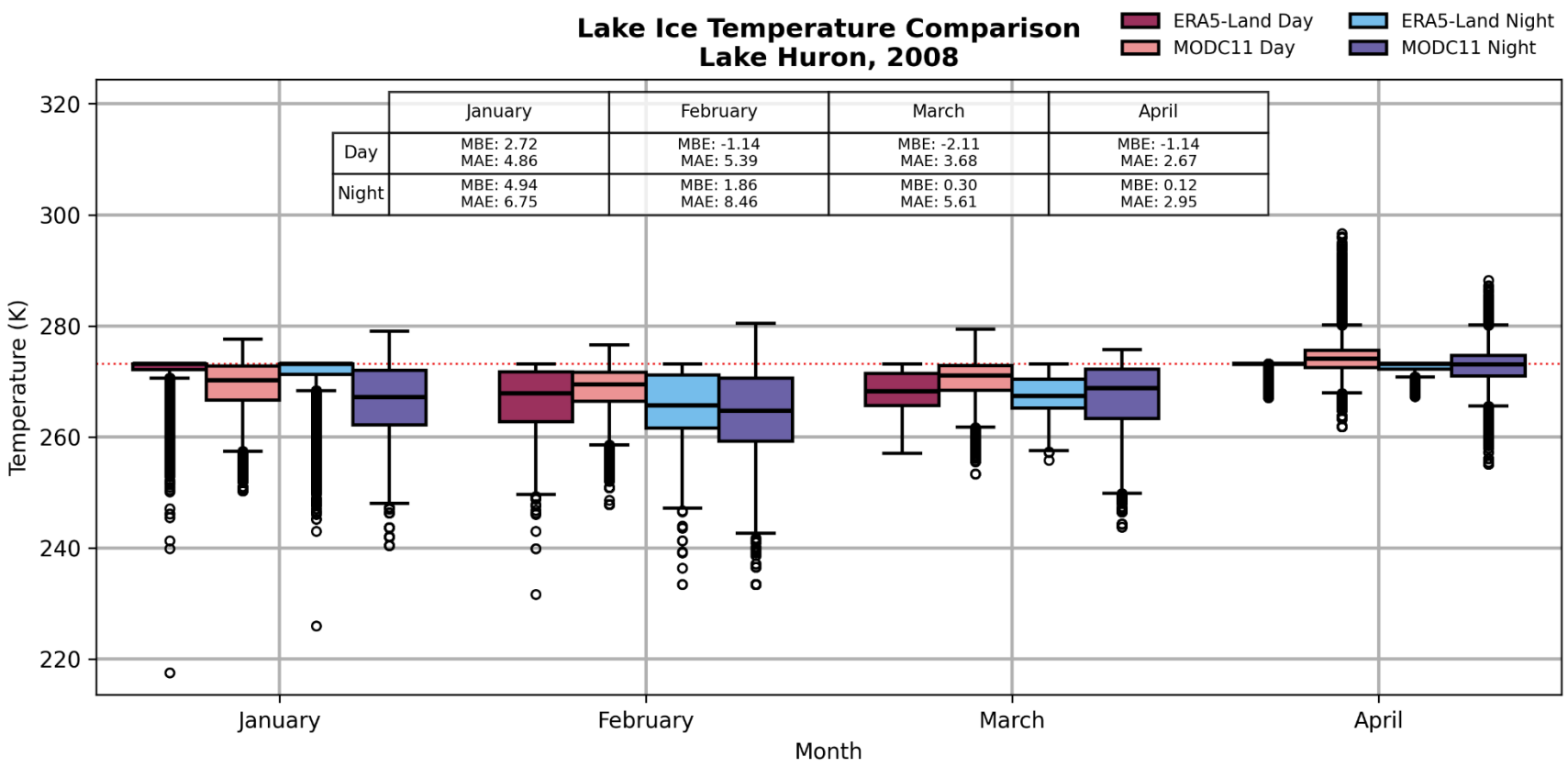


Figure C.6. 5: Boxplot of monthly lake ice surface temperatures during ice-on period of ERA5-Land and MODIS for Lake Huron, 2008

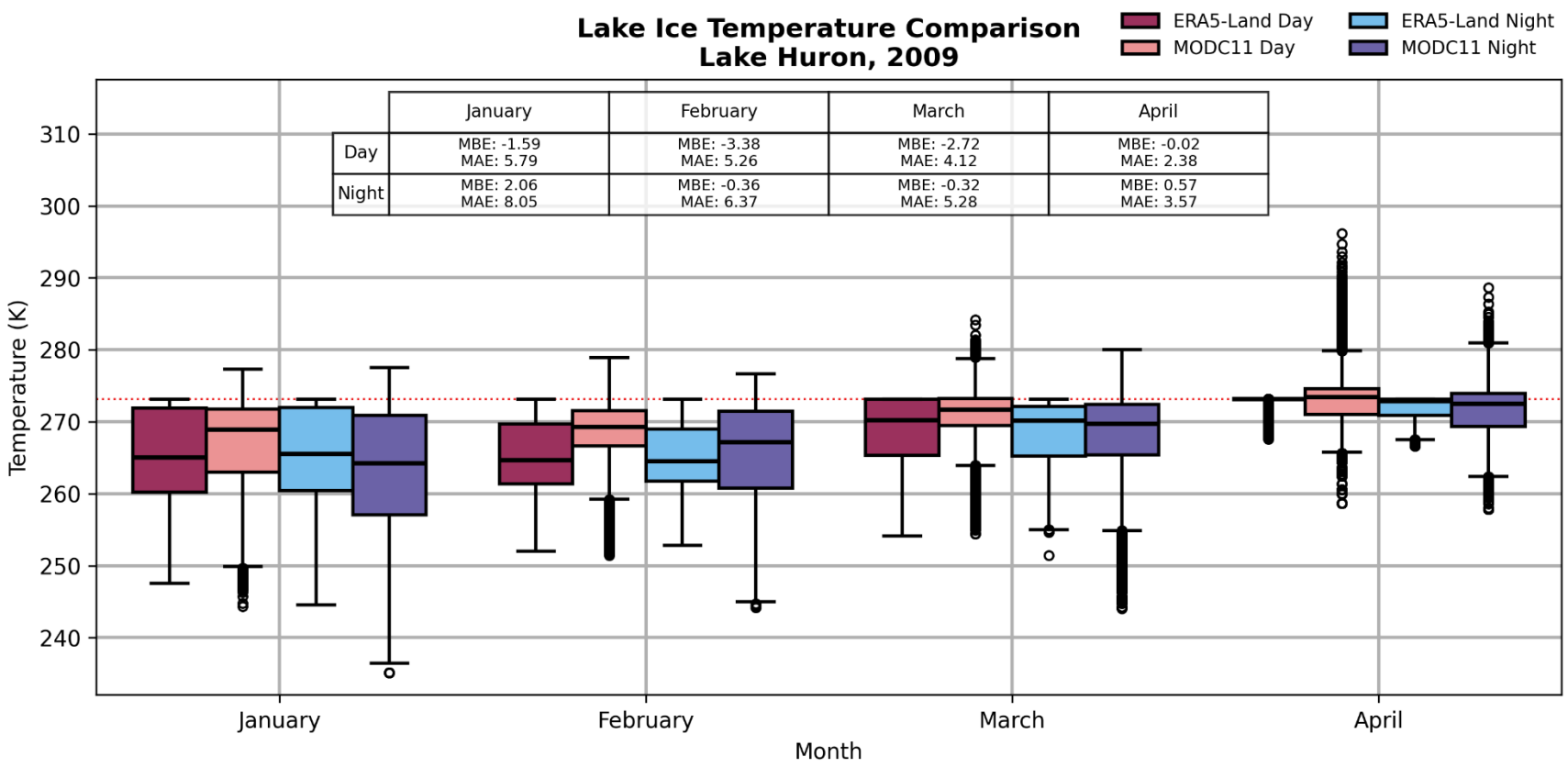


Figure C.6. 6: Boxplot of monthly lake ice surface temperatures during ice-on period of ERA5-Land and MODIS for Lake Huron, 2009

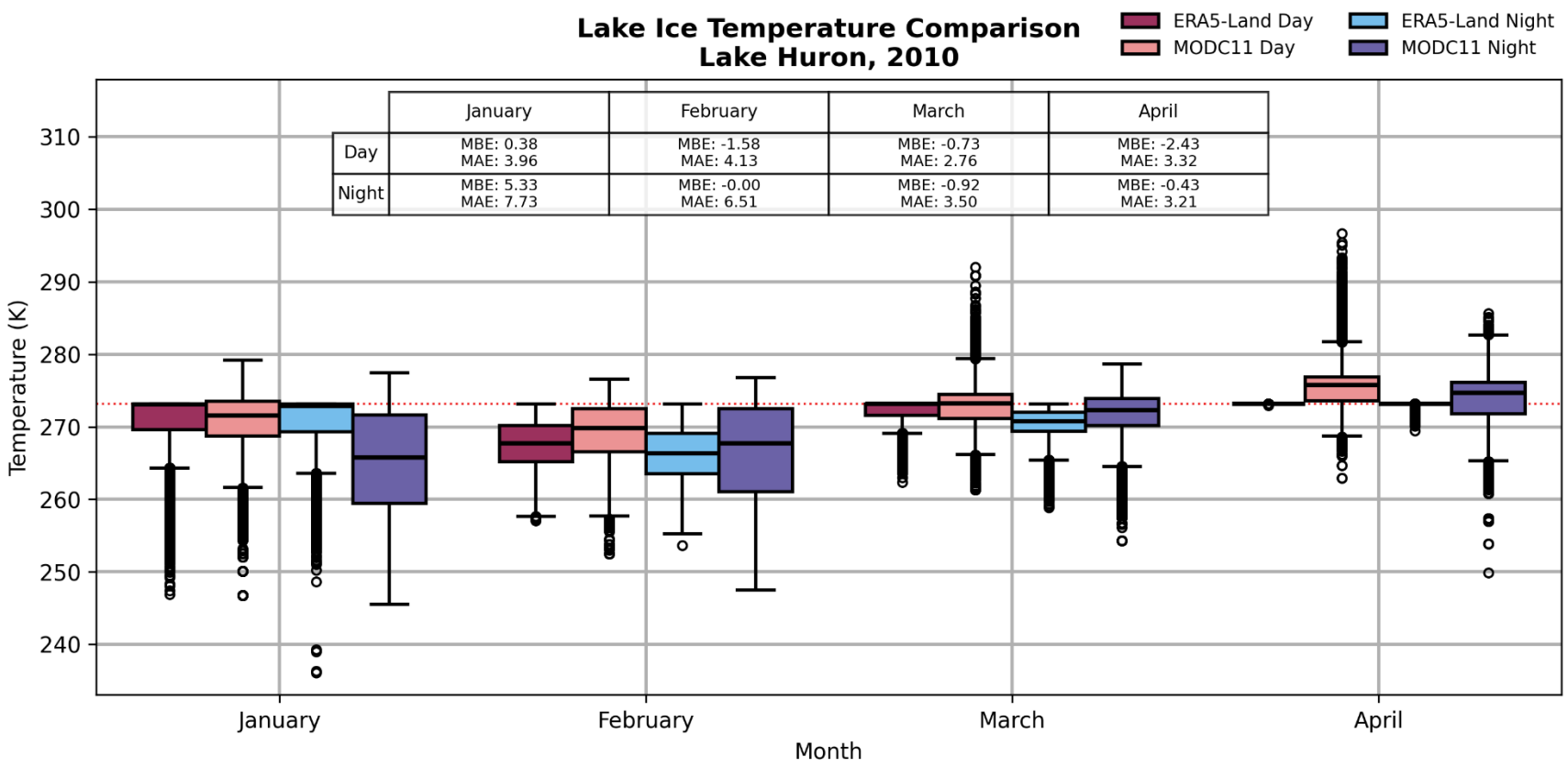


Figure C.6. 7: Boxplot of monthly lake ice surface temperatures during ice-on period of ERA5-Land and MODIS for Lake Huron, 2010

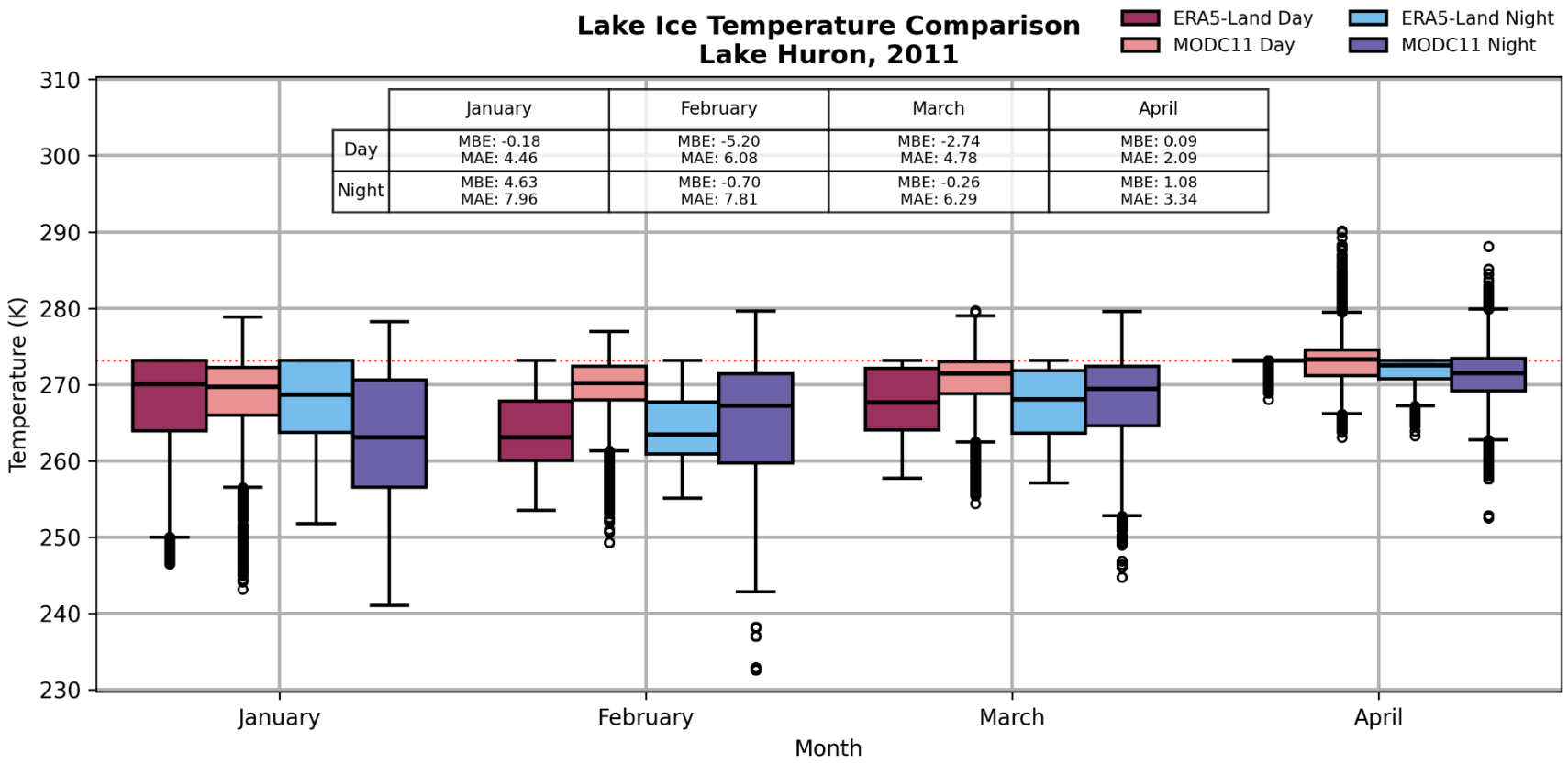


Figure C.6. 8: Boxplot of monthly lake ice surface temperatures during ice-on period of ERA5-Land and MODIS for Lake Huron, 2011

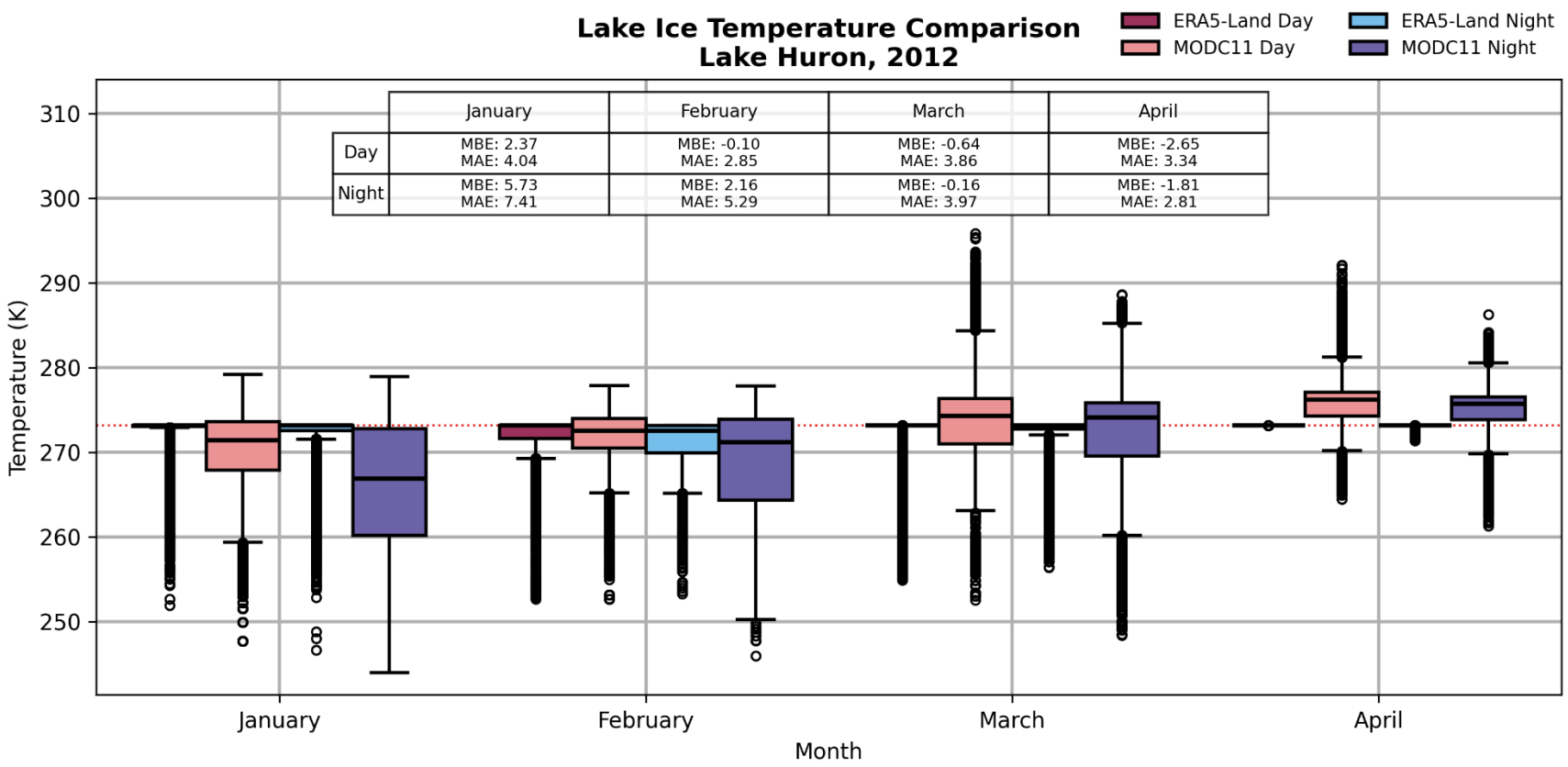


Figure C.6. 9: Boxplot of monthly lake ice surface temperatures during ice-on period of ERA5-Land and MODIS for Lake Huron, 2012

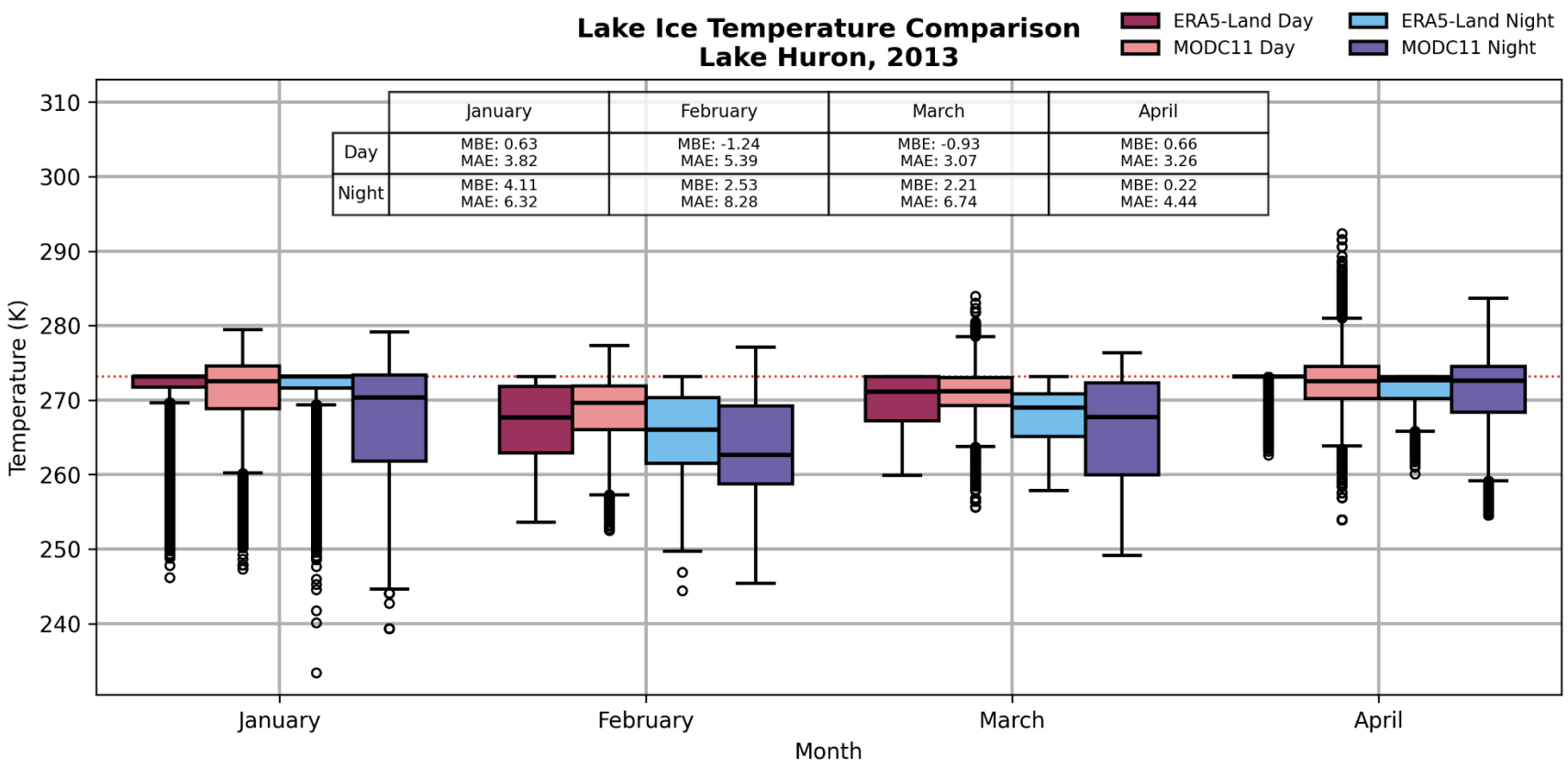


Figure C.6. 10: Boxplot of monthly lake ice surface temperatures during ice-on period of ERA5-Land and MODIS for Lake Huron, 2013

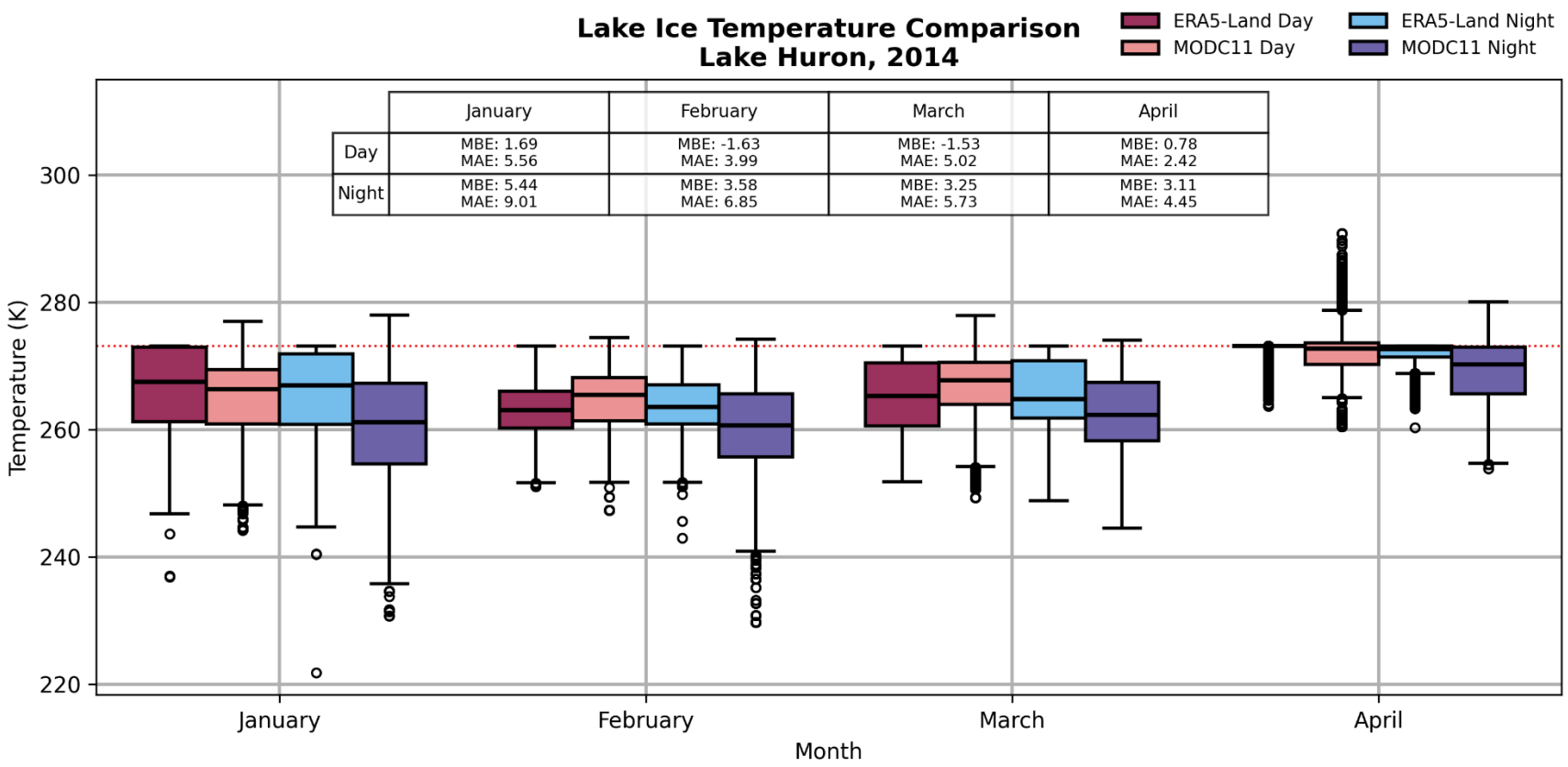


Figure C.6. 11: Boxplot of monthly lake ice surface temperatures during ice-on period of ERA5-Land and MODIS for Lake Huron, 2014

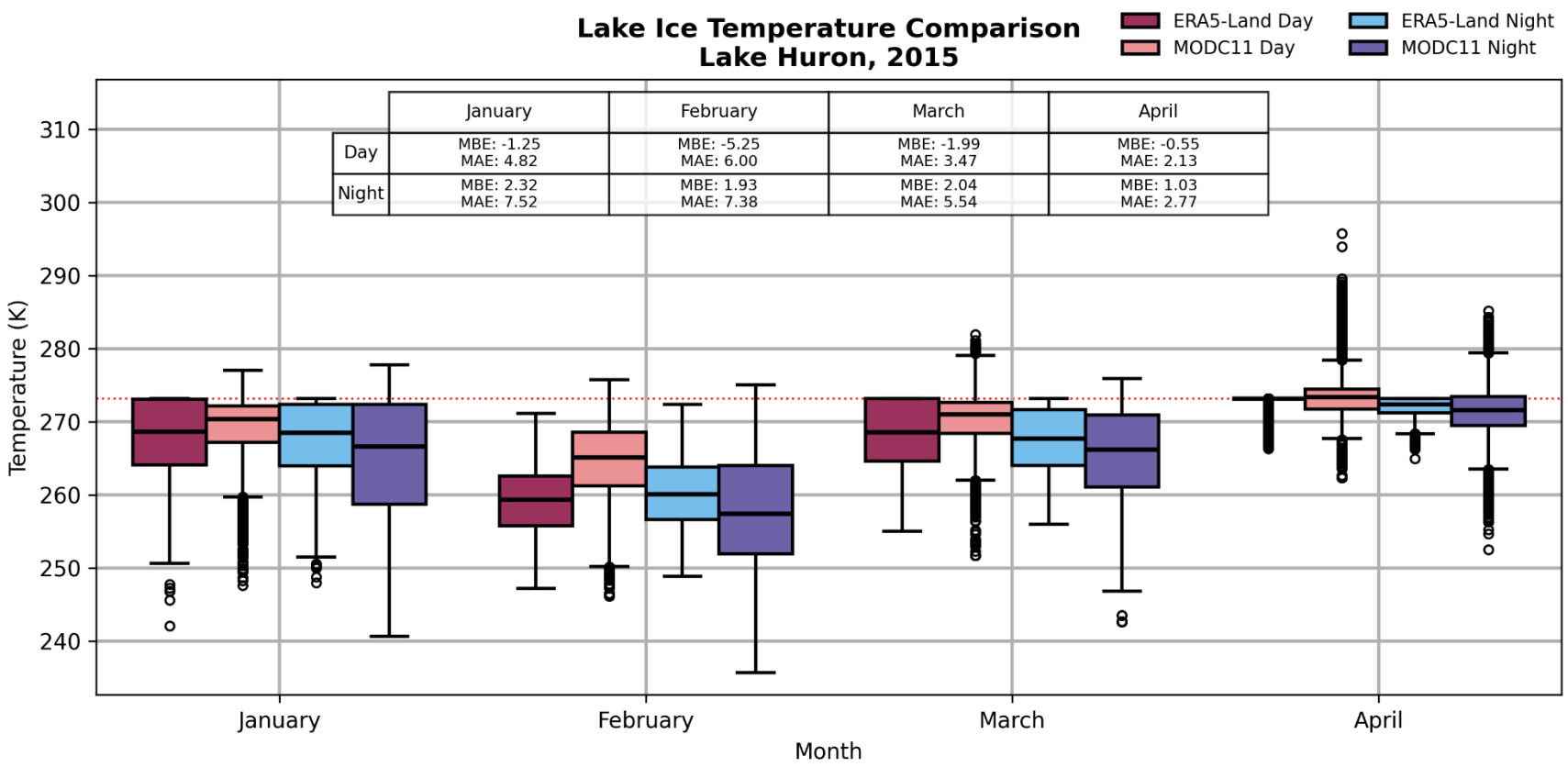


Figure C.6. 12: Boxplot of monthly lake ice surface temperatures during ice-on period of ERA5-Land and MODIS for Lake Huron, 2015

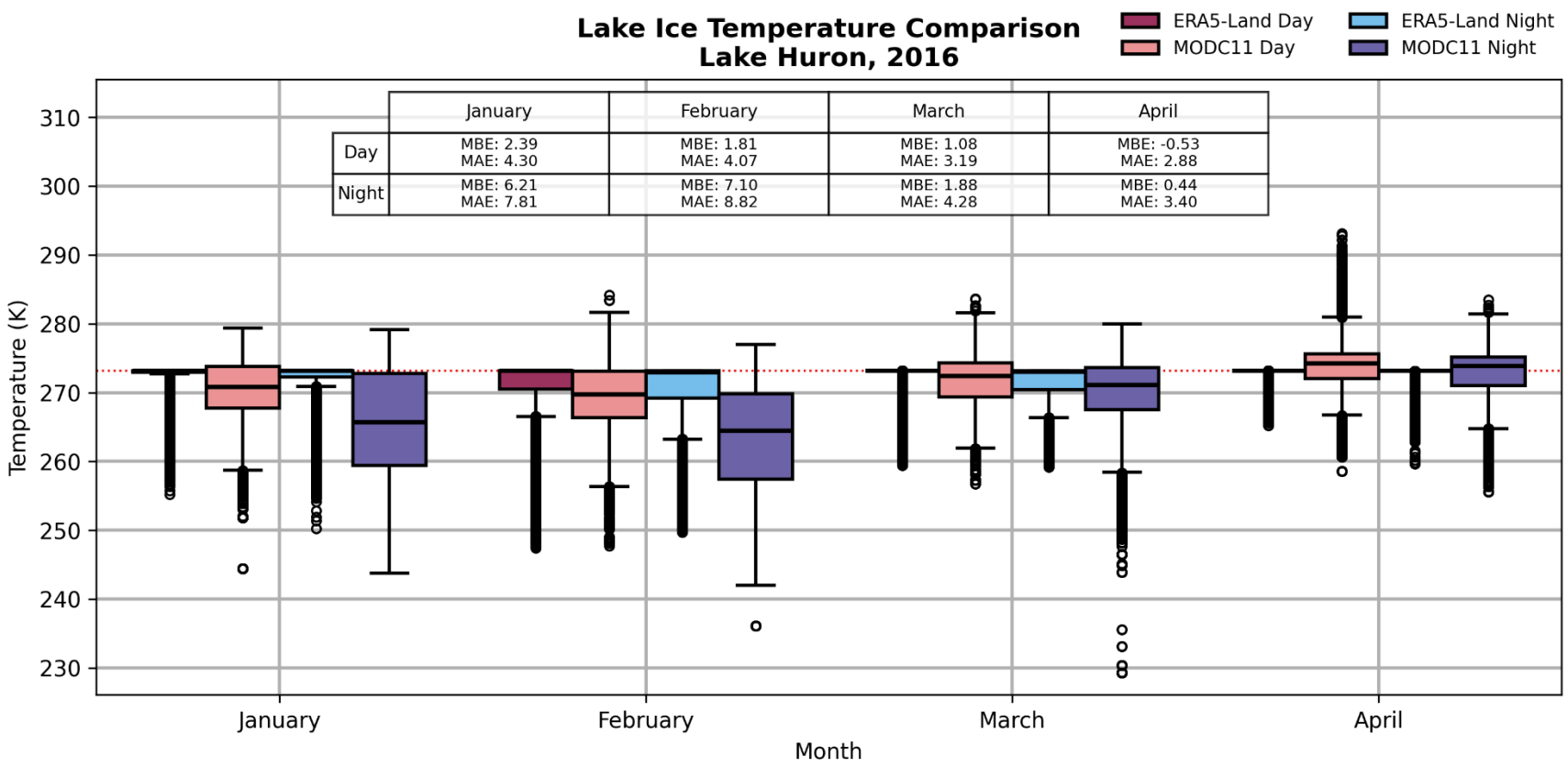


Figure C.6. 13: Boxplot of monthly lake ice surface temperatures during ice-on period of ERA5-Land and MODIS for Lake Huron, 2016

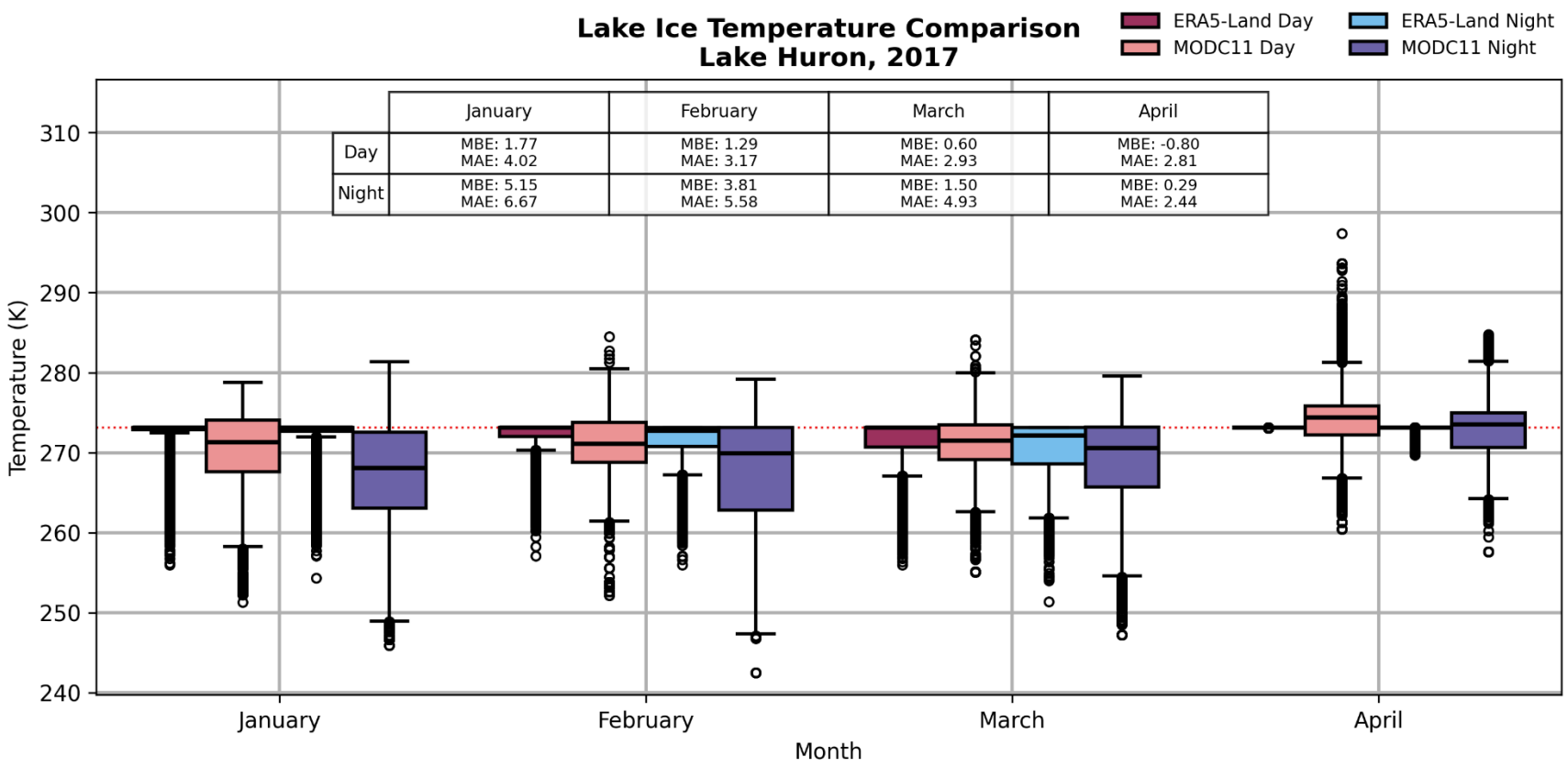


Figure C.6. 14: Boxplot of monthly lake ice surface temperatures during ice-on period of ERA5-Land and MODIS for Lake Huron, 2017

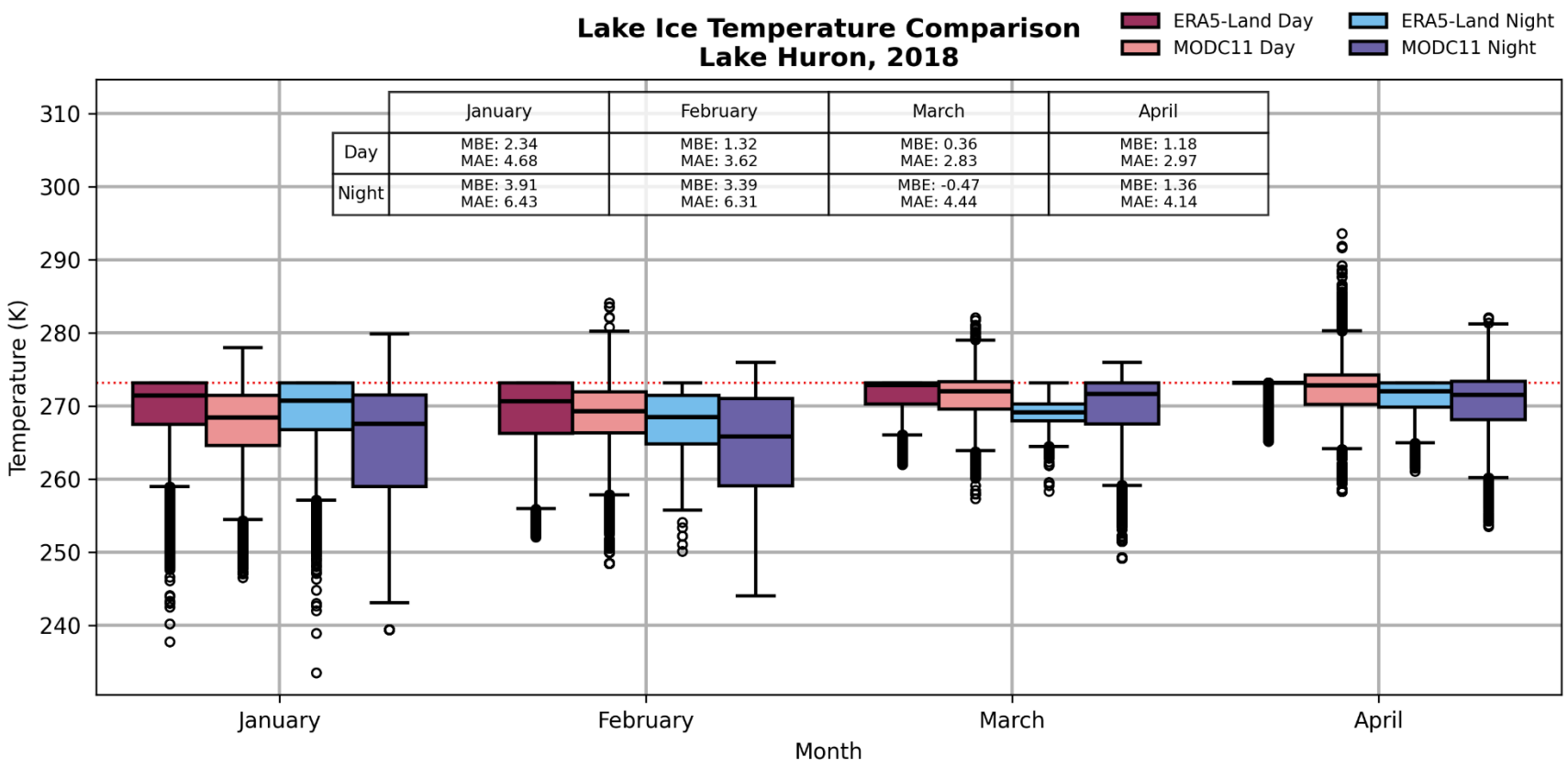


Figure C.6. 15: Boxplot of monthly lake ice surface temperatures during ice-on period of ERA5-Land and MODIS for Lake Huron, 2017

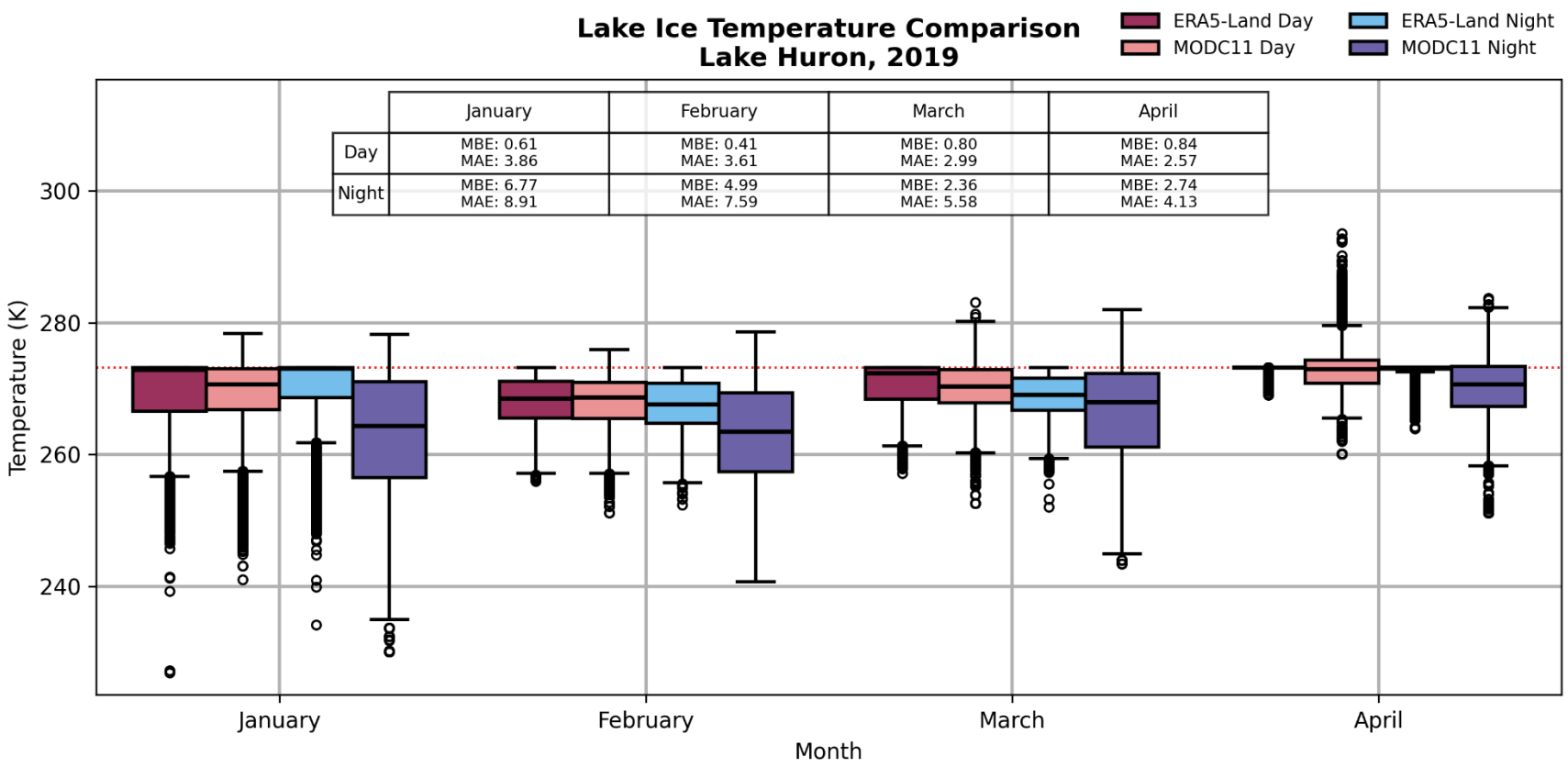


Figure C.6. 16: Boxplot of monthly lake ice surface temperatures during ice-on period of ERA5-Land and MODIS for Lake Huron, 2019

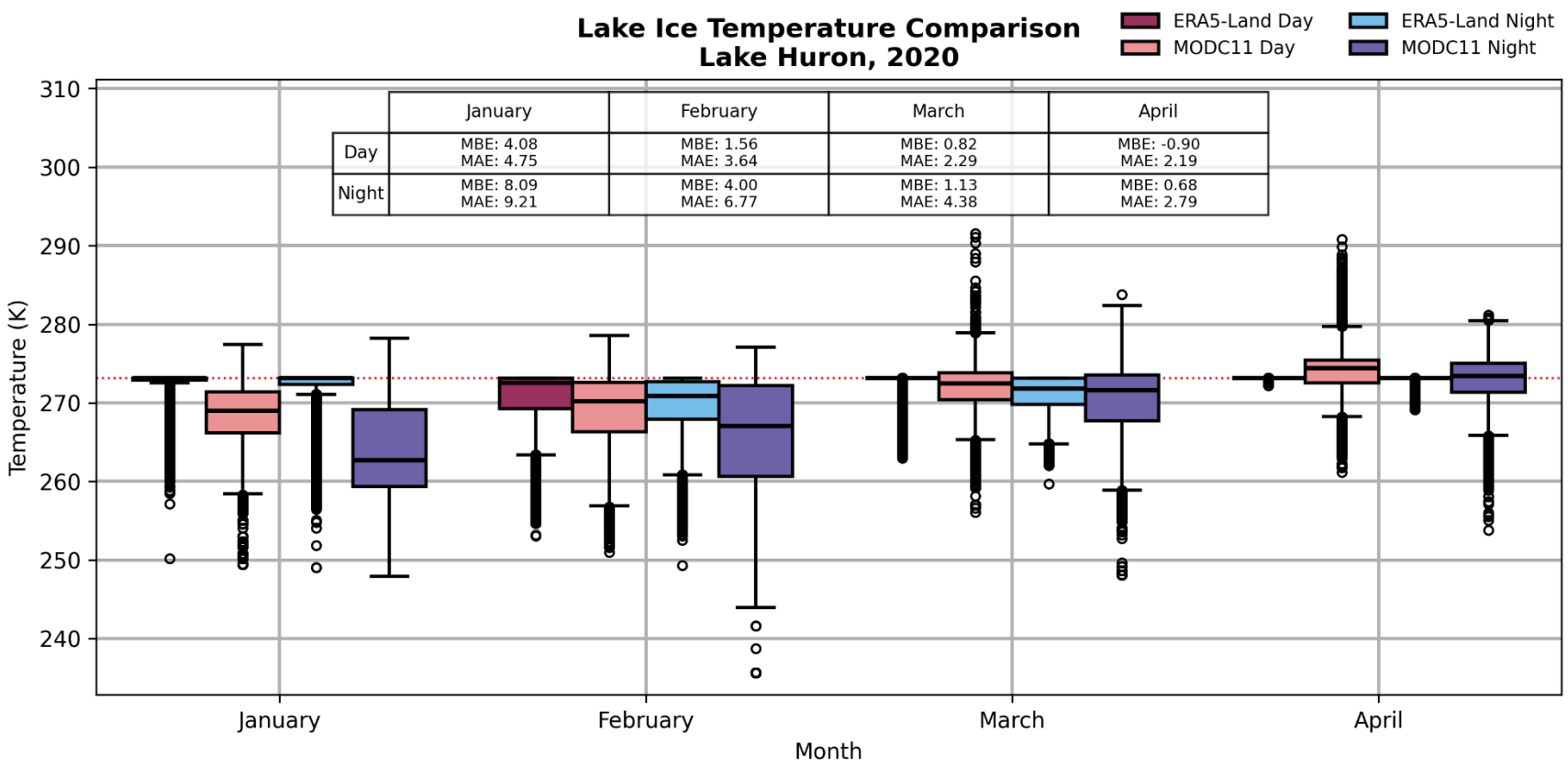


Figure C.6. 17: Boxplot of monthly lake ice surface temperatures during ice-on period of ERA5-Land and MODIS for Lake Huron, 2020

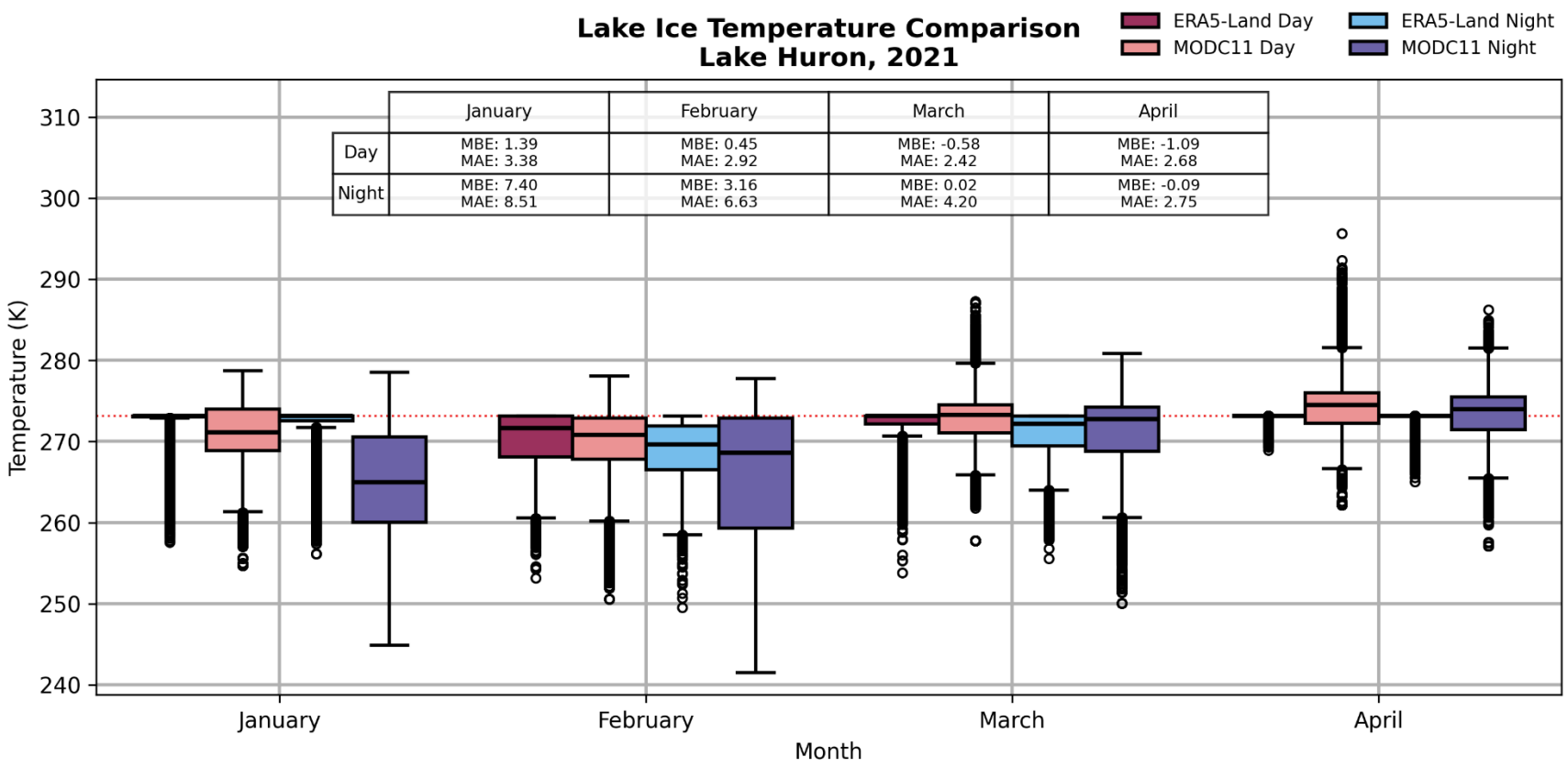


Figure C.6. 18: Boxplot of monthly lake ice surface temperatures during ice-on period of ERA5-Land and MODIS for Lake Huron, 2021

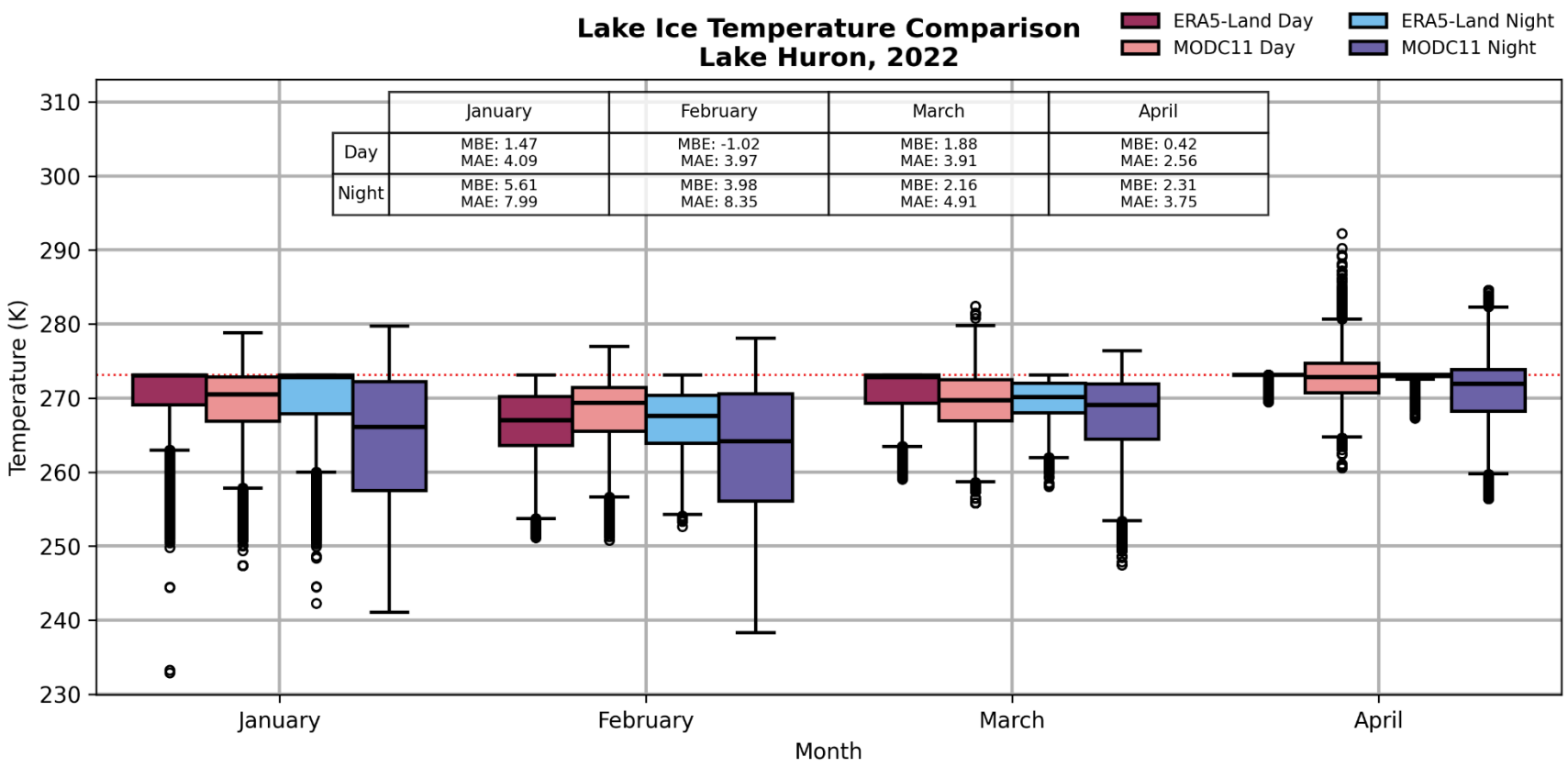


Figure C.6. 19: Boxplot of monthly lake ice surface temperatures during ice-on period of ERA5-Land and MODIS for Lake Huron, 2022

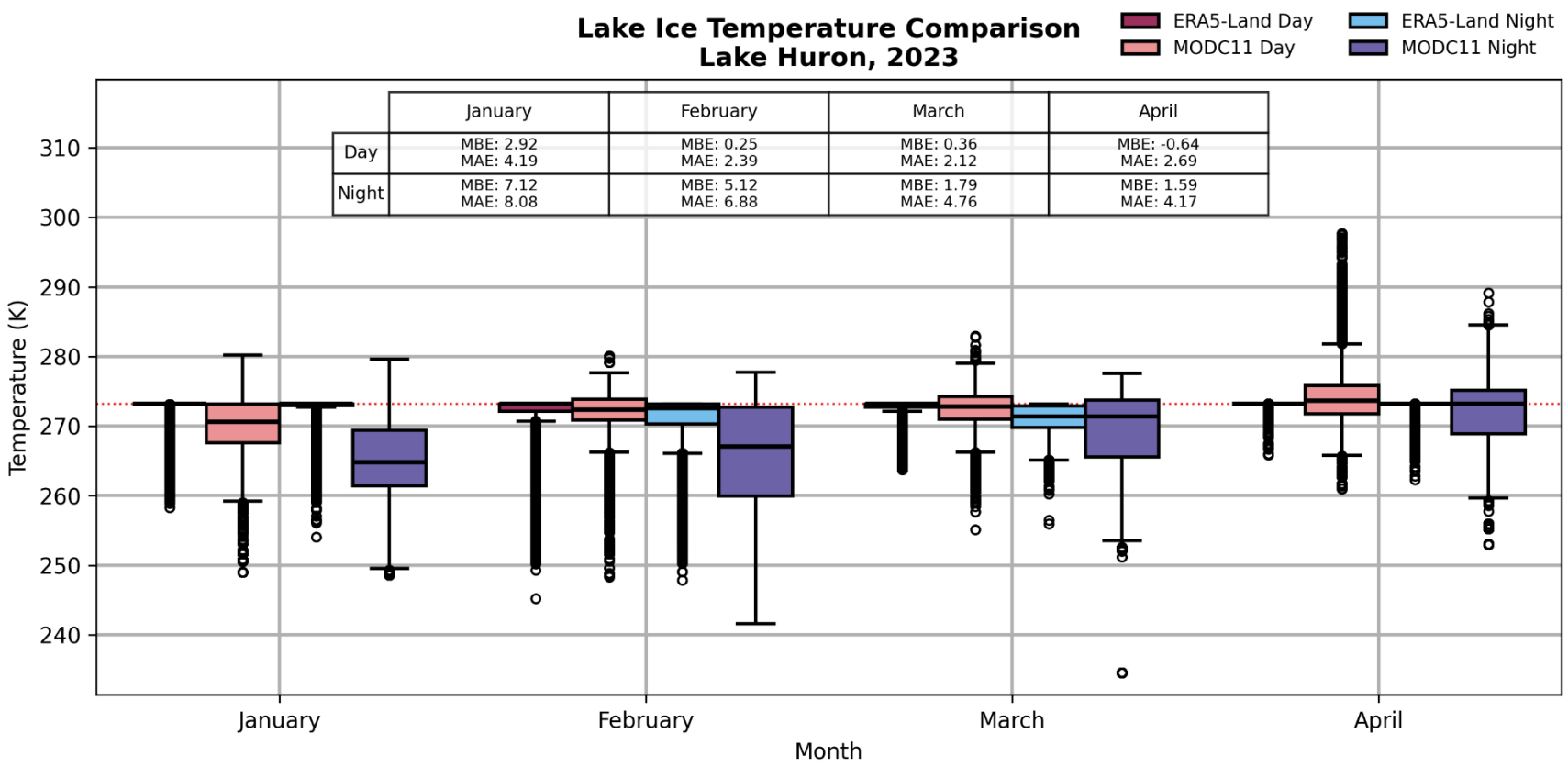


Figure C.6. 20: Boxplot of monthly lake ice surface temperatures during ice-on period of ERA5-Land and MODIS for Lake Huron, 2023

C.7 Lake Erie

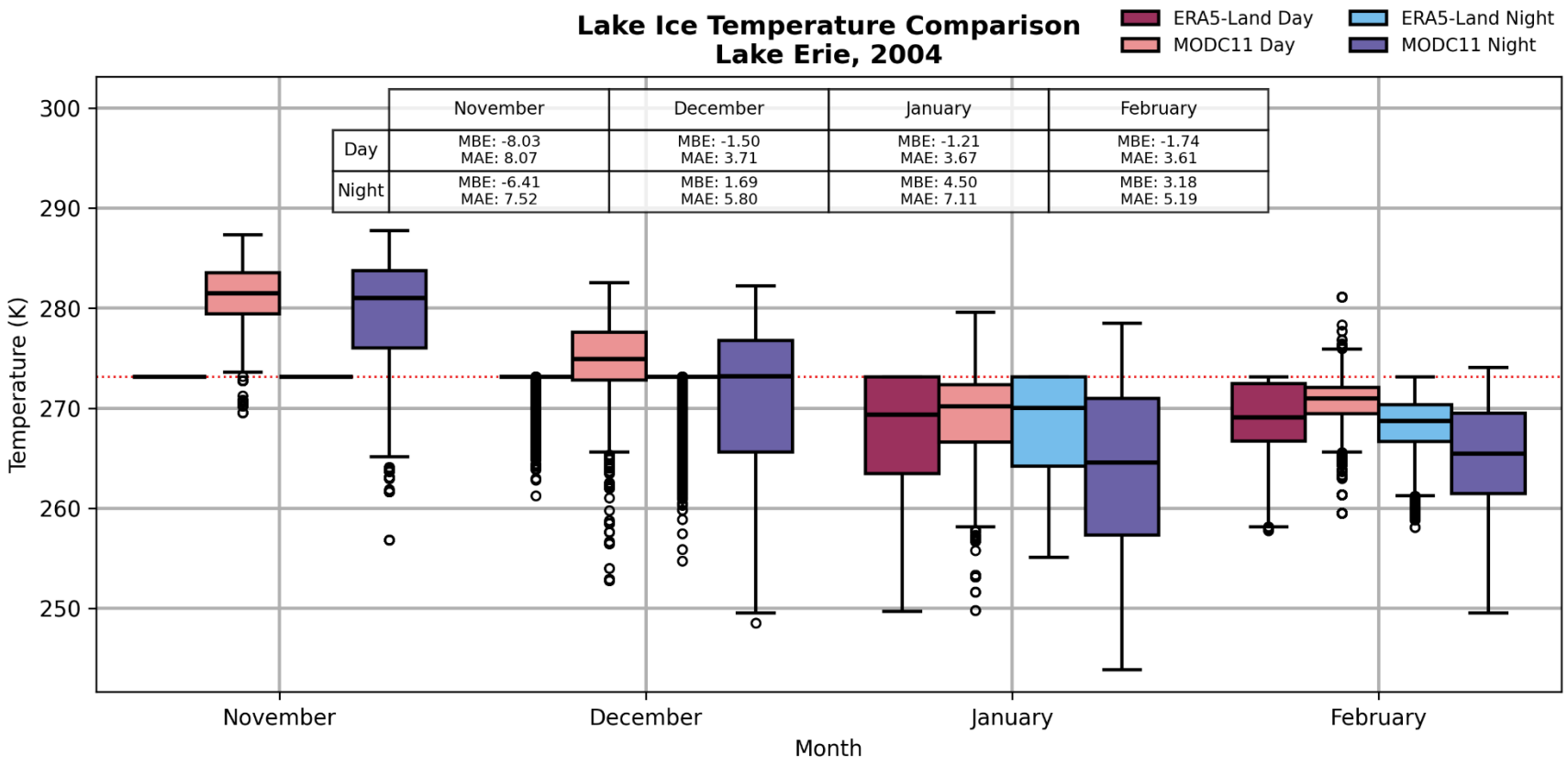


Figure C.7. 1: Boxplot of monthly lake ice surface temperatures during ice-on period of ERA5-Land and MODIS for Lake Erie, 2004

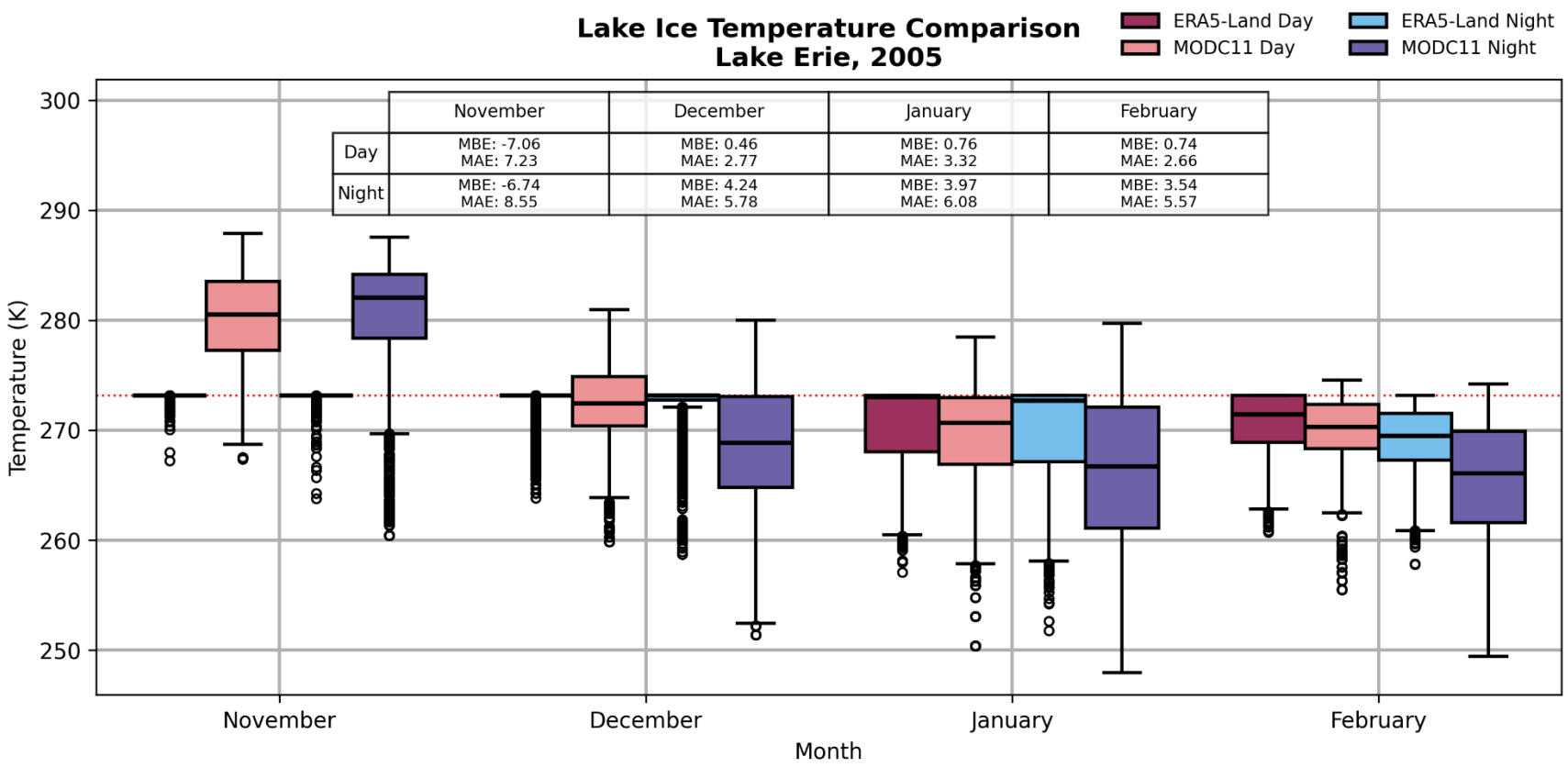


Figure C.7. 2: Boxplot of monthly lake ice surface temperatures during ice-on period of ERA5-Land and MODIS for Lake Erie, 2005

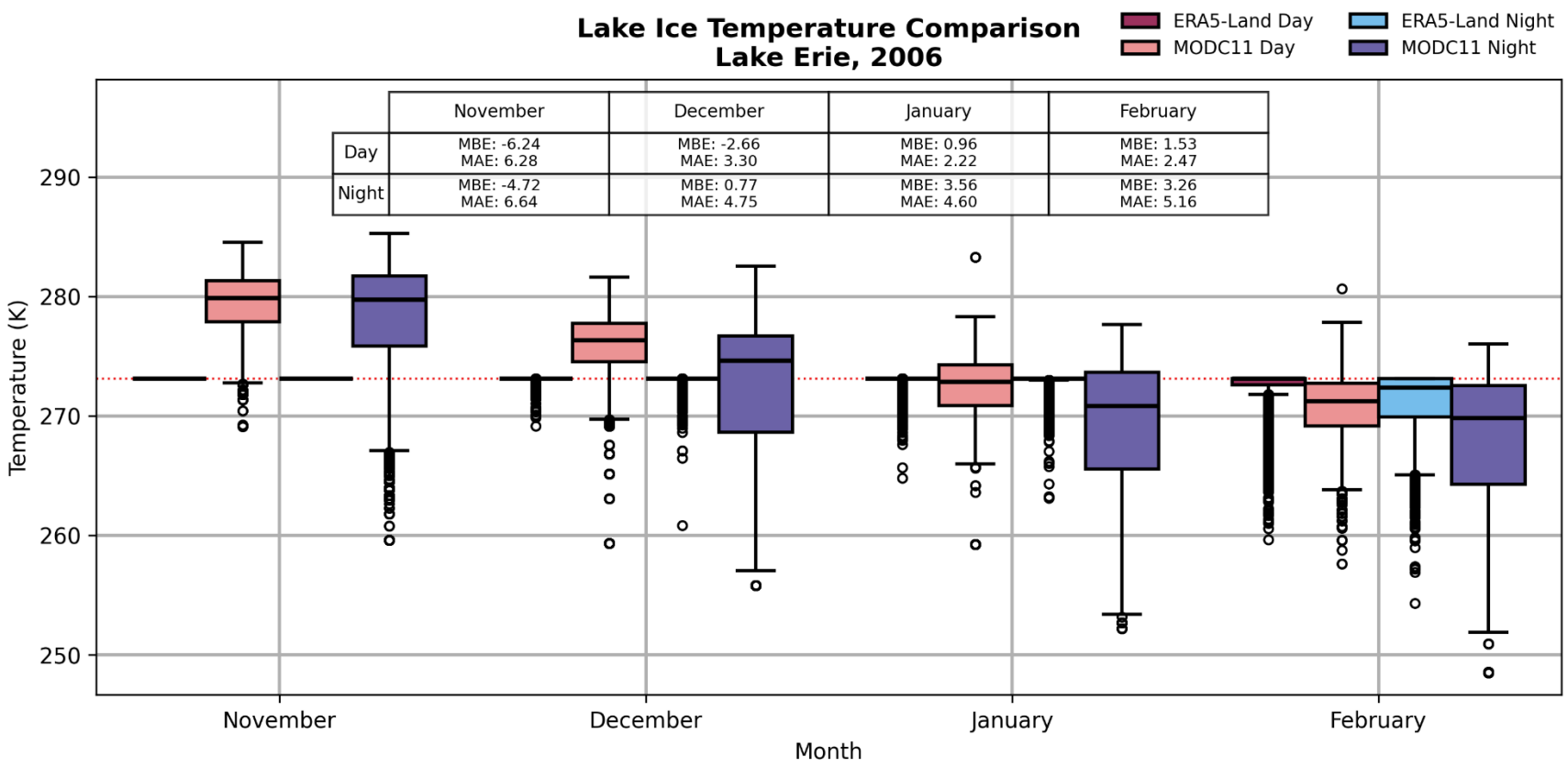


Figure C.7. 3: Boxplot of monthly lake ice surface temperatures during ice-on period of ERA5-Land and MODIS for Lake Erie, 2006

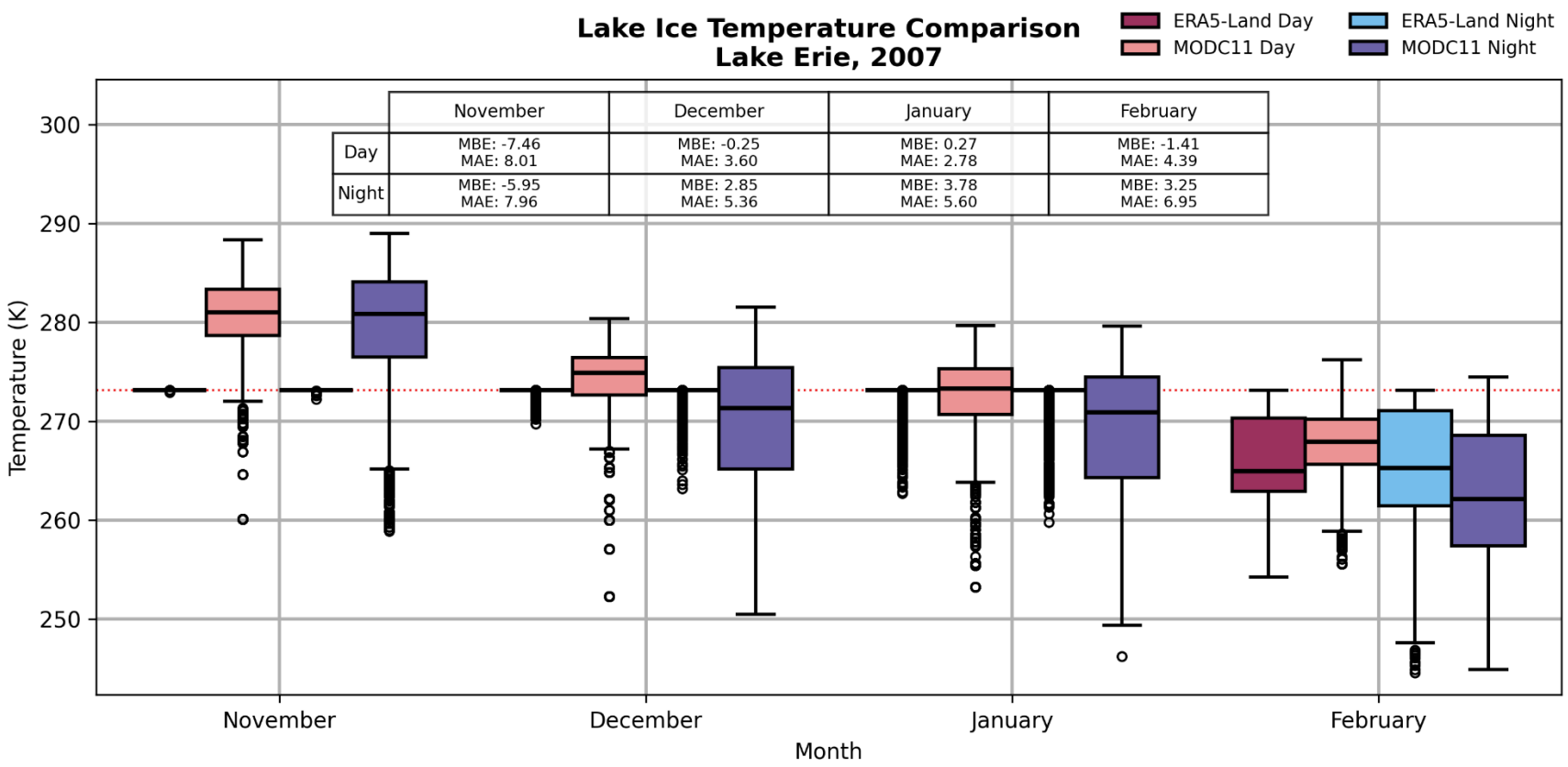


Figure C.7. 4: Boxplot of monthly lake ice surface temperatures during ice-on period of ERA5-Land and MODIS for Lake Erie, 2007

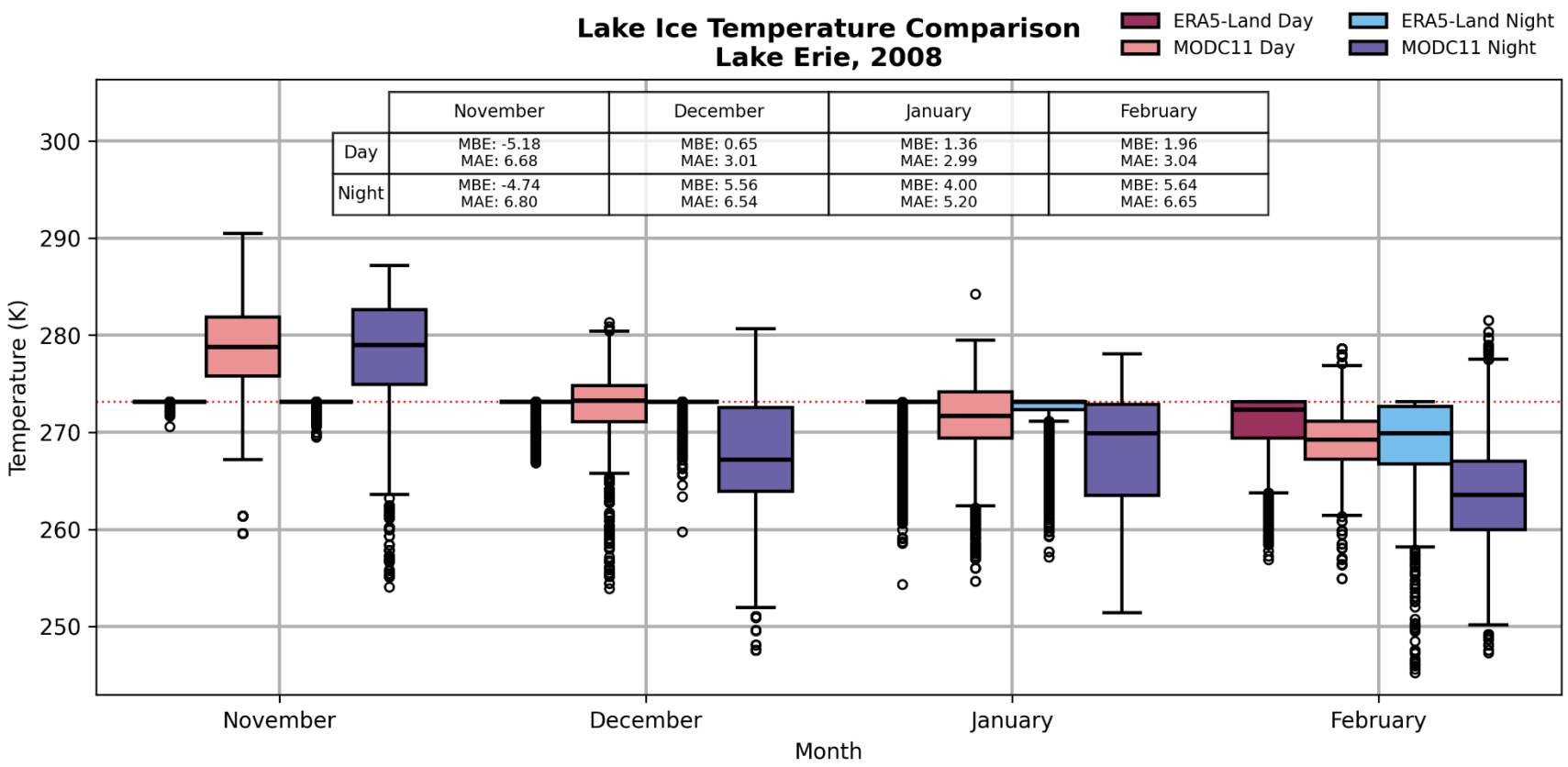


Figure C.7. 5: Boxplot of monthly lake ice surface temperatures during ice-on period of ERA5-Land and MODIS for Lake Erie, 2008

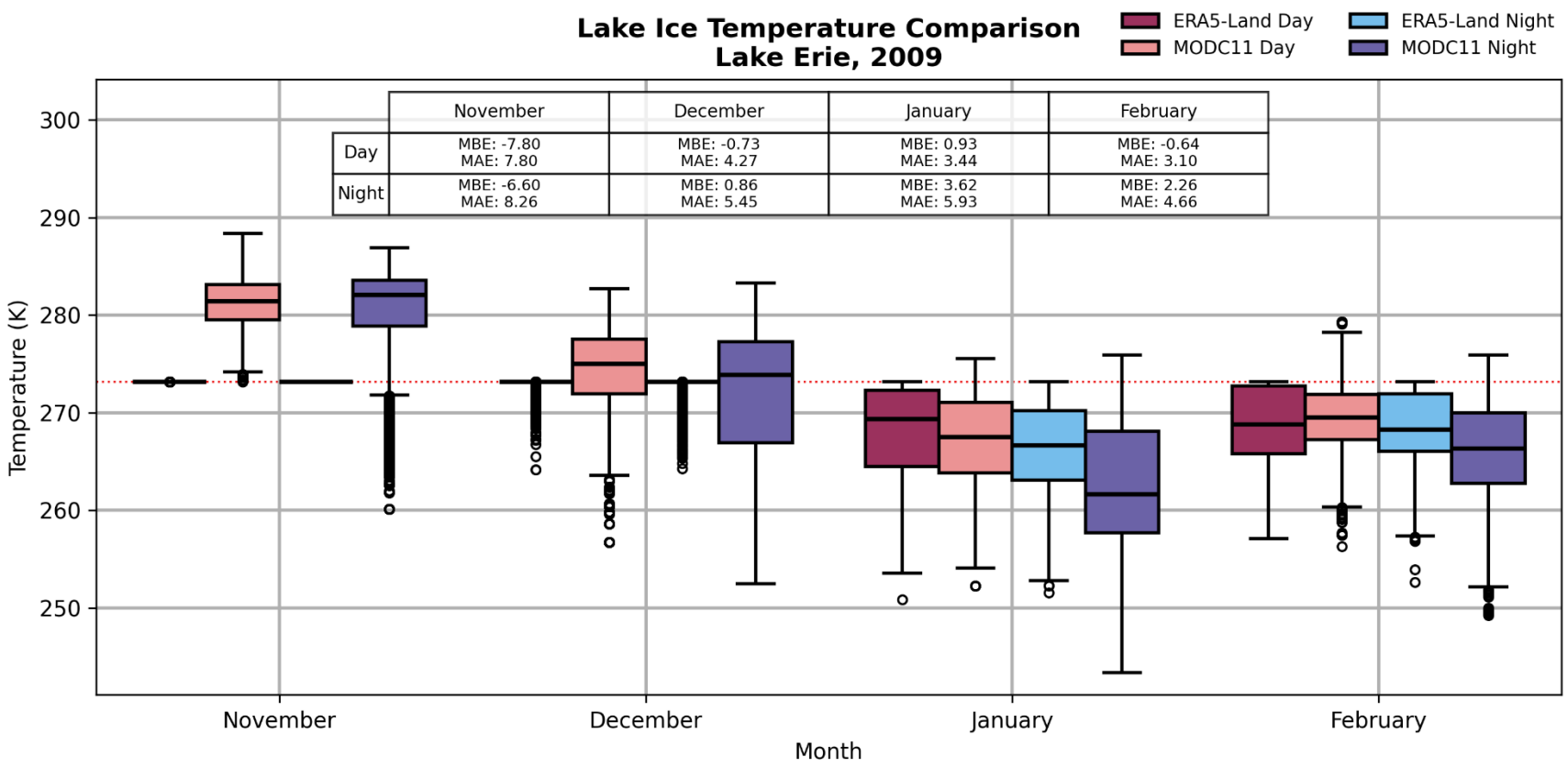


Figure C.7. 6: Boxplot of monthly lake ice surface temperatures during ice-on period of ERA5-Land and MODIS for Lake Erie, 2009

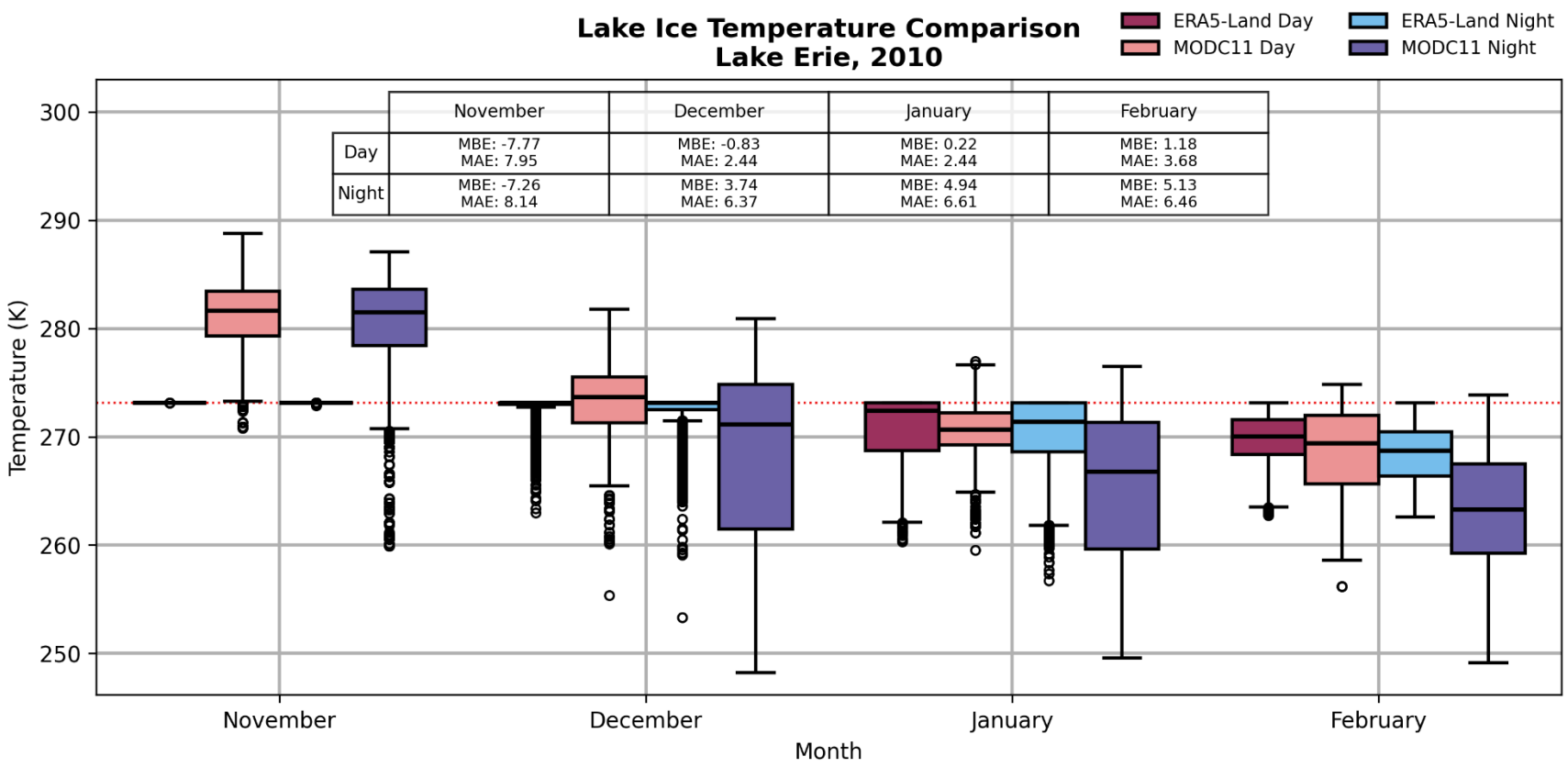


Figure C.7. 7: Boxplot of monthly lake ice surface temperatures during ice-on period of ERA5-Land and MODIS for Lake Erie, 2010

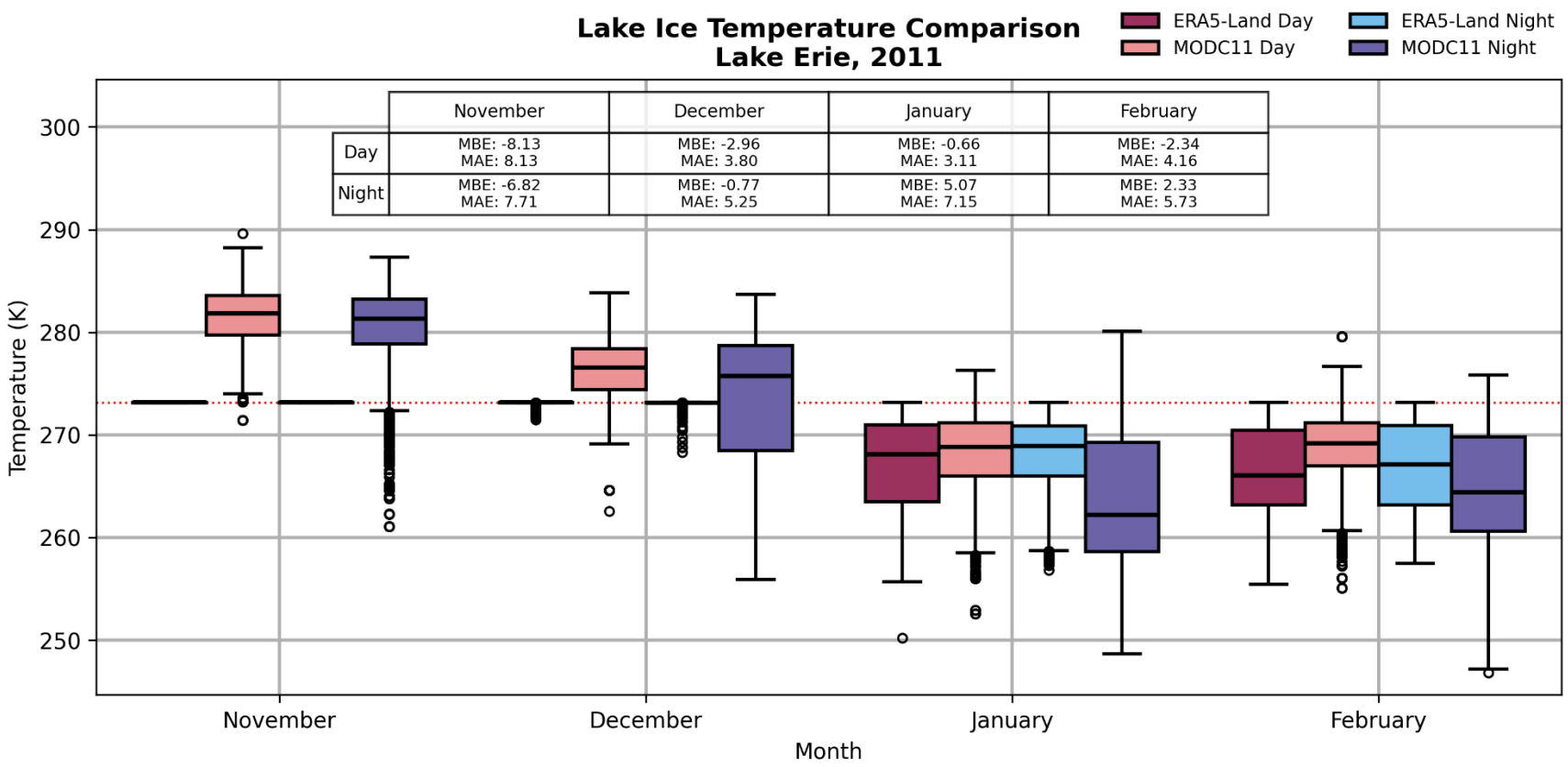


Figure C.7. 8: Boxplot of monthly lake ice surface temperatures during ice-on period of ERA5-Land and MODIS for Lake Erie, 2011

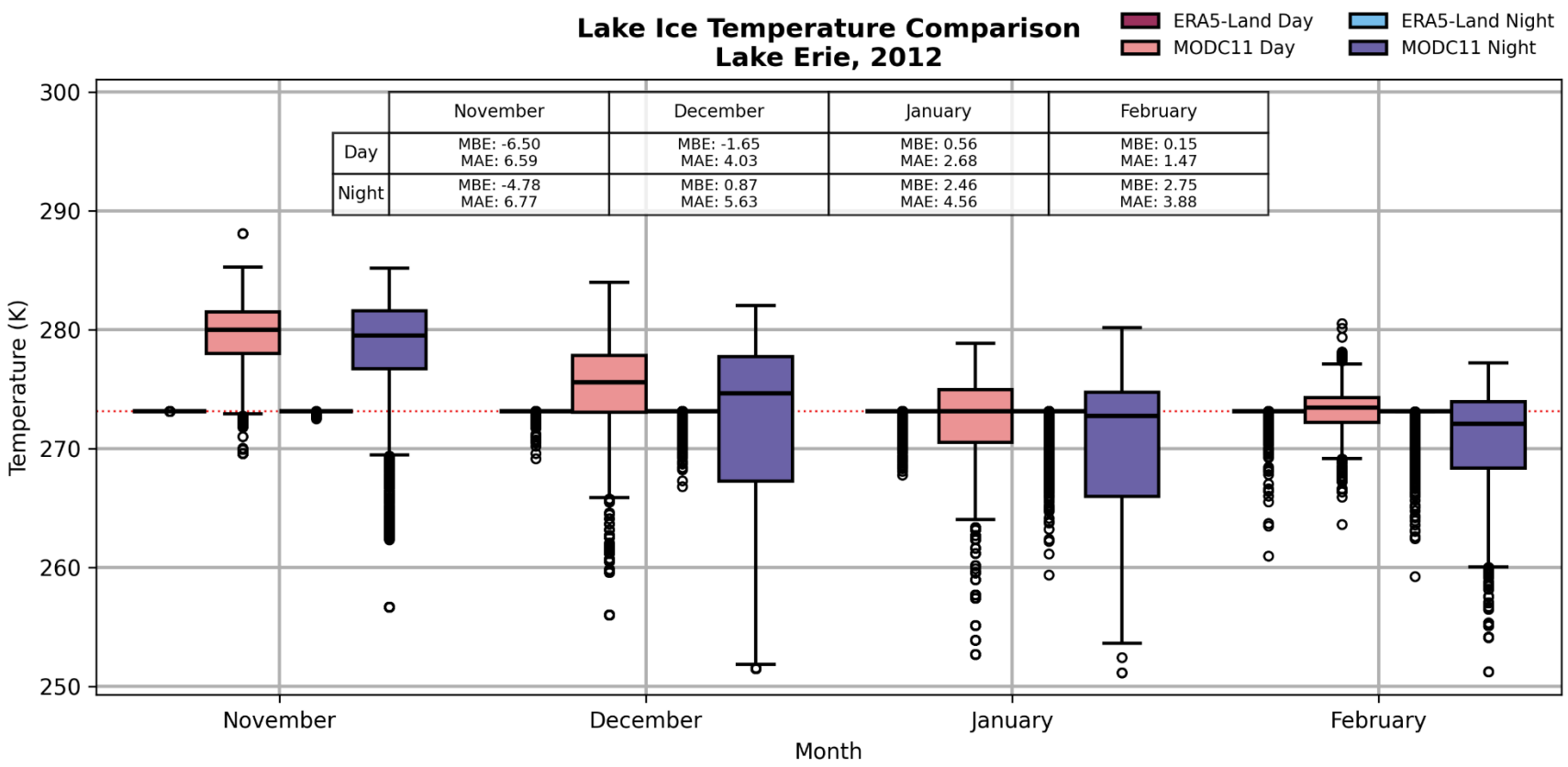


Figure C.7. 9: Boxplot of monthly lake ice surface temperatures during ice-on period of ERA5-Land and MODIS for Lake Erie, 2012

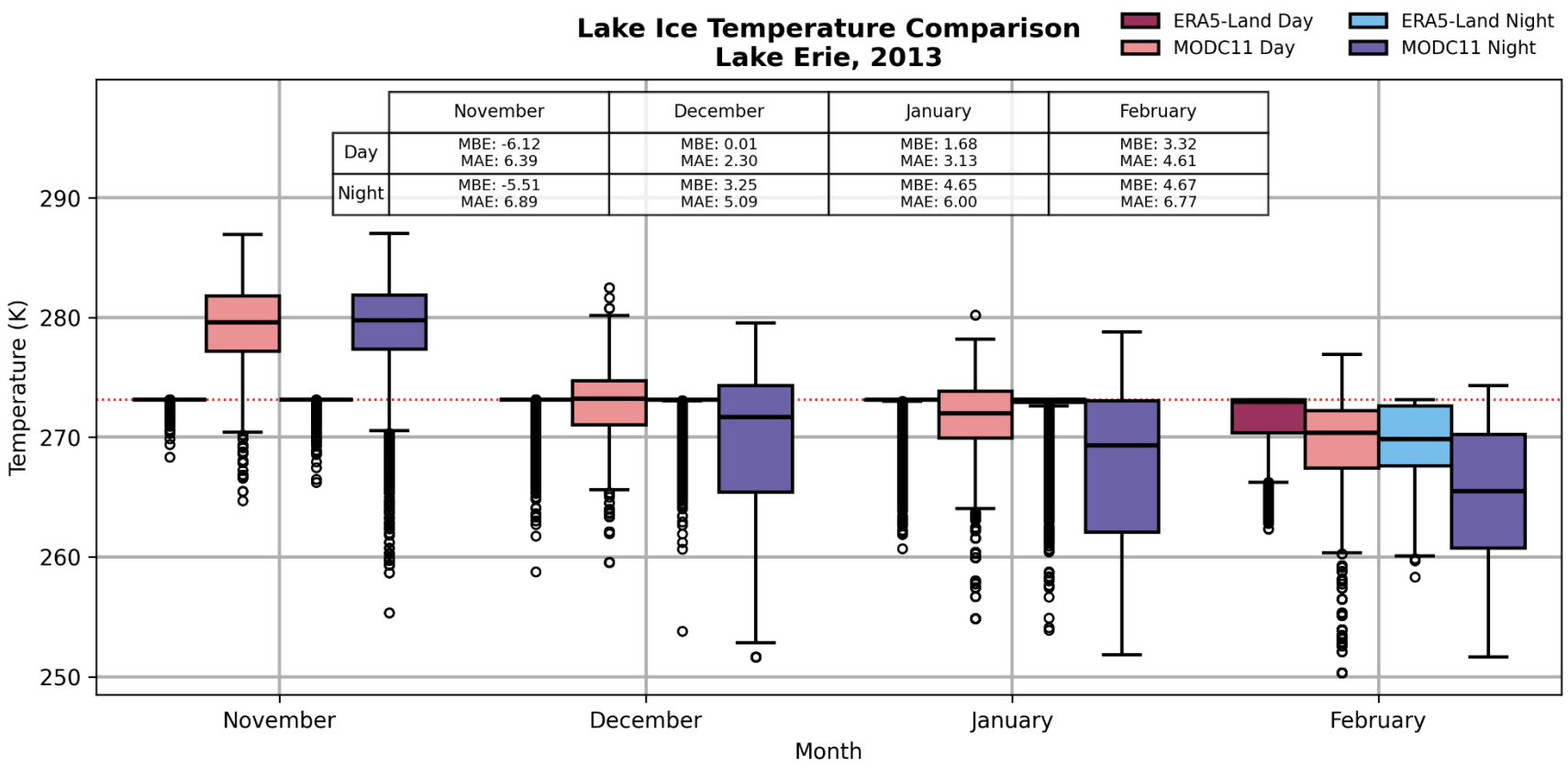


Figure C.7. 10: Boxplot of monthly lake ice surface temperatures during ice-on period of ERA5-Land and MODIS for Lake Erie, 2013

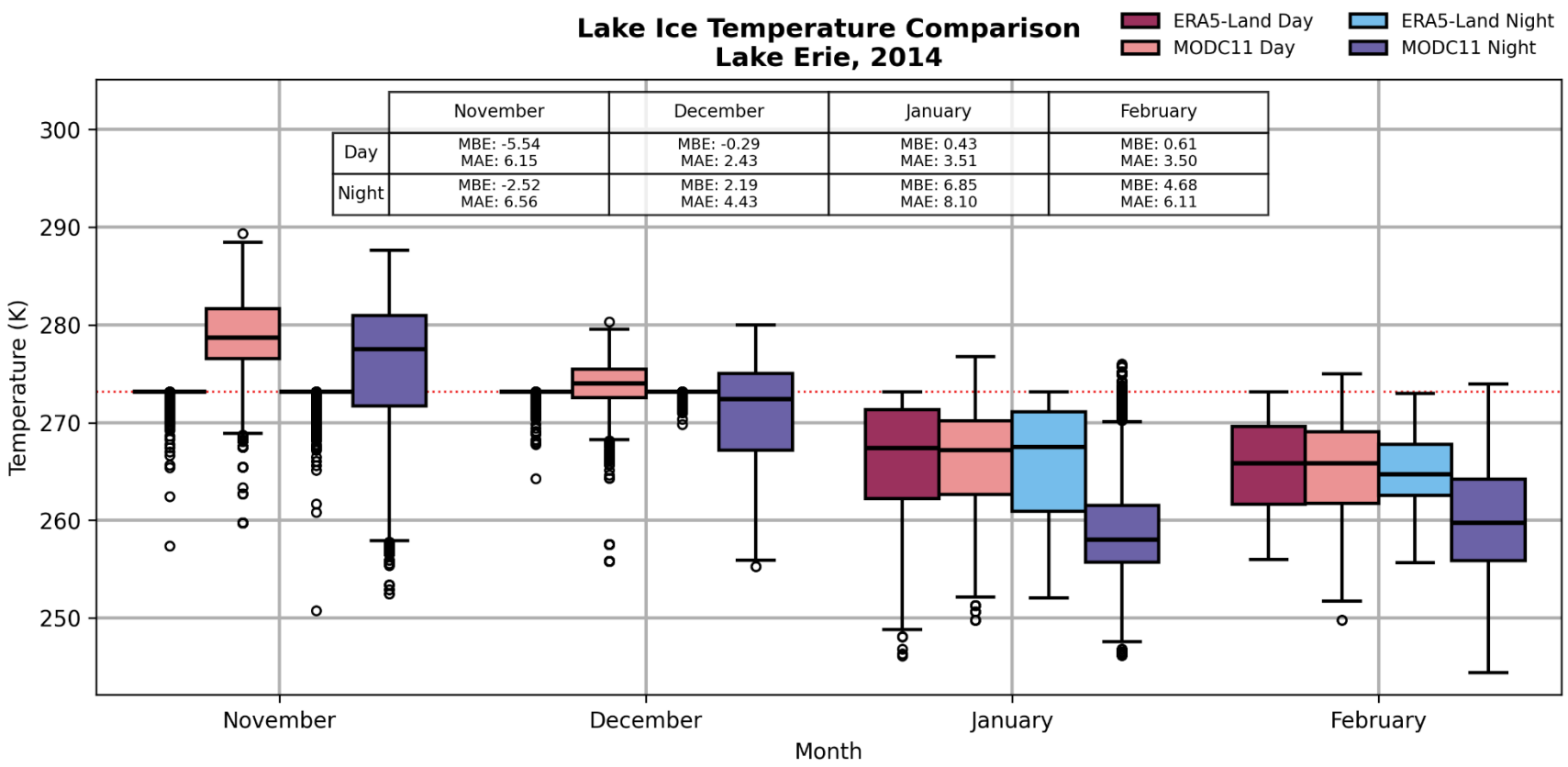


Figure C.7. 11: Boxplot of monthly lake ice surface temperatures during ice-on period of ERA5-Land and MODIS for Lake Erie, 2014

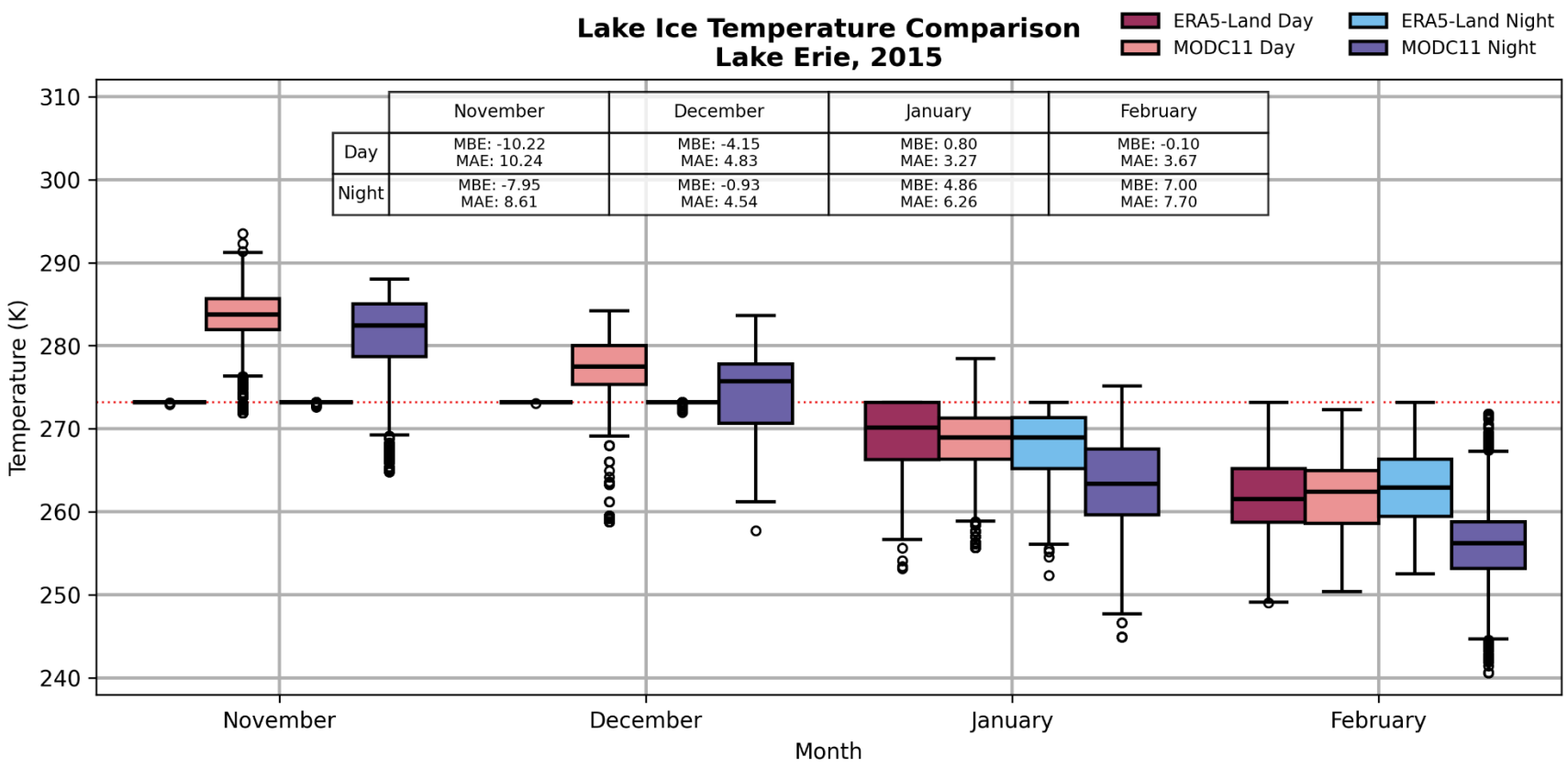


Figure C.7. 12: Boxplot of monthly lake ice surface temperatures during ice-on period of ERA5-Land and MODIS for Lake Erie, 2015

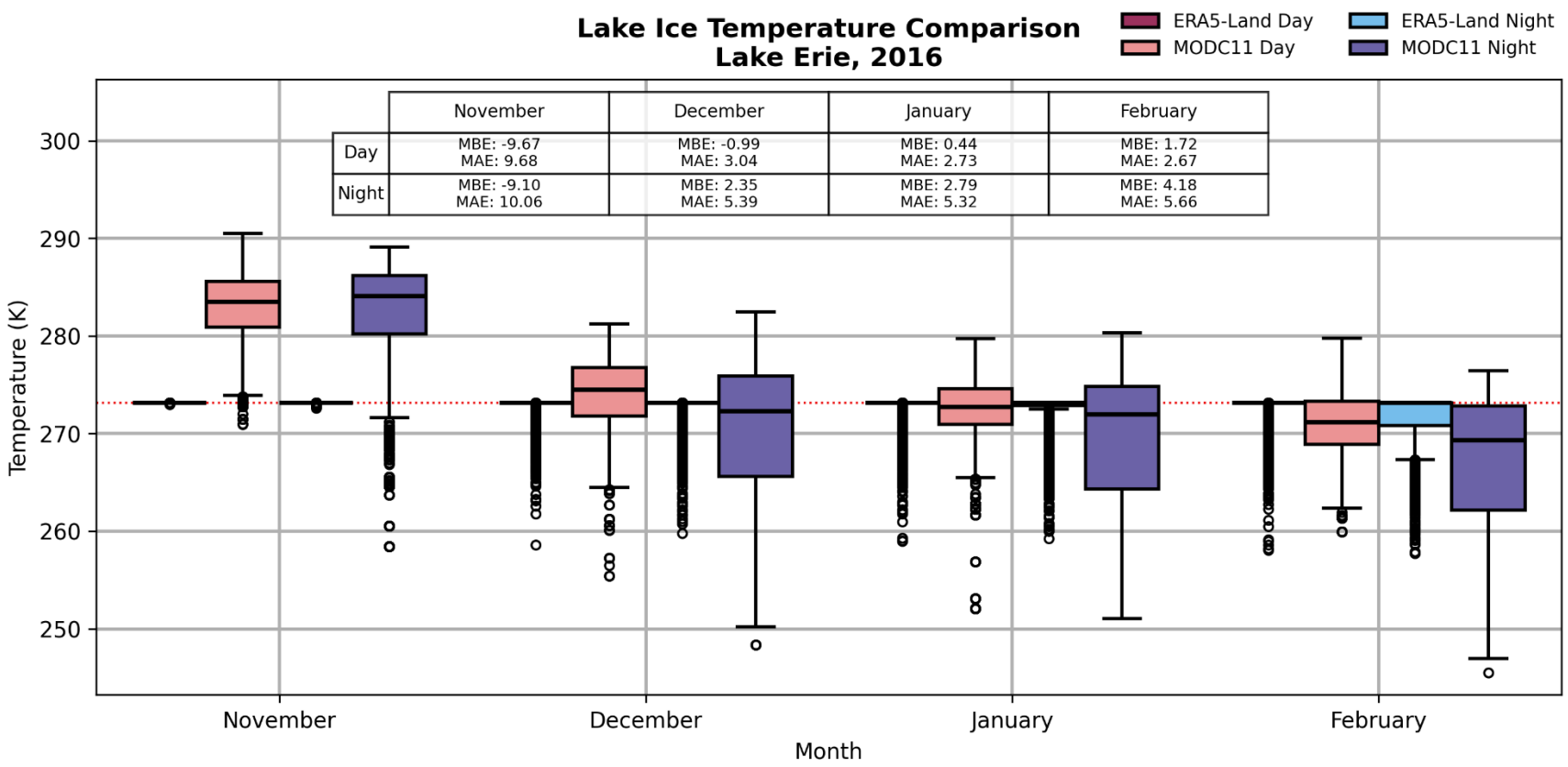


Figure C.7. 13: Boxplot of monthly lake ice surface temperatures during ice-on period of ERA5-Land and MODIS for Lake Erie, 2016

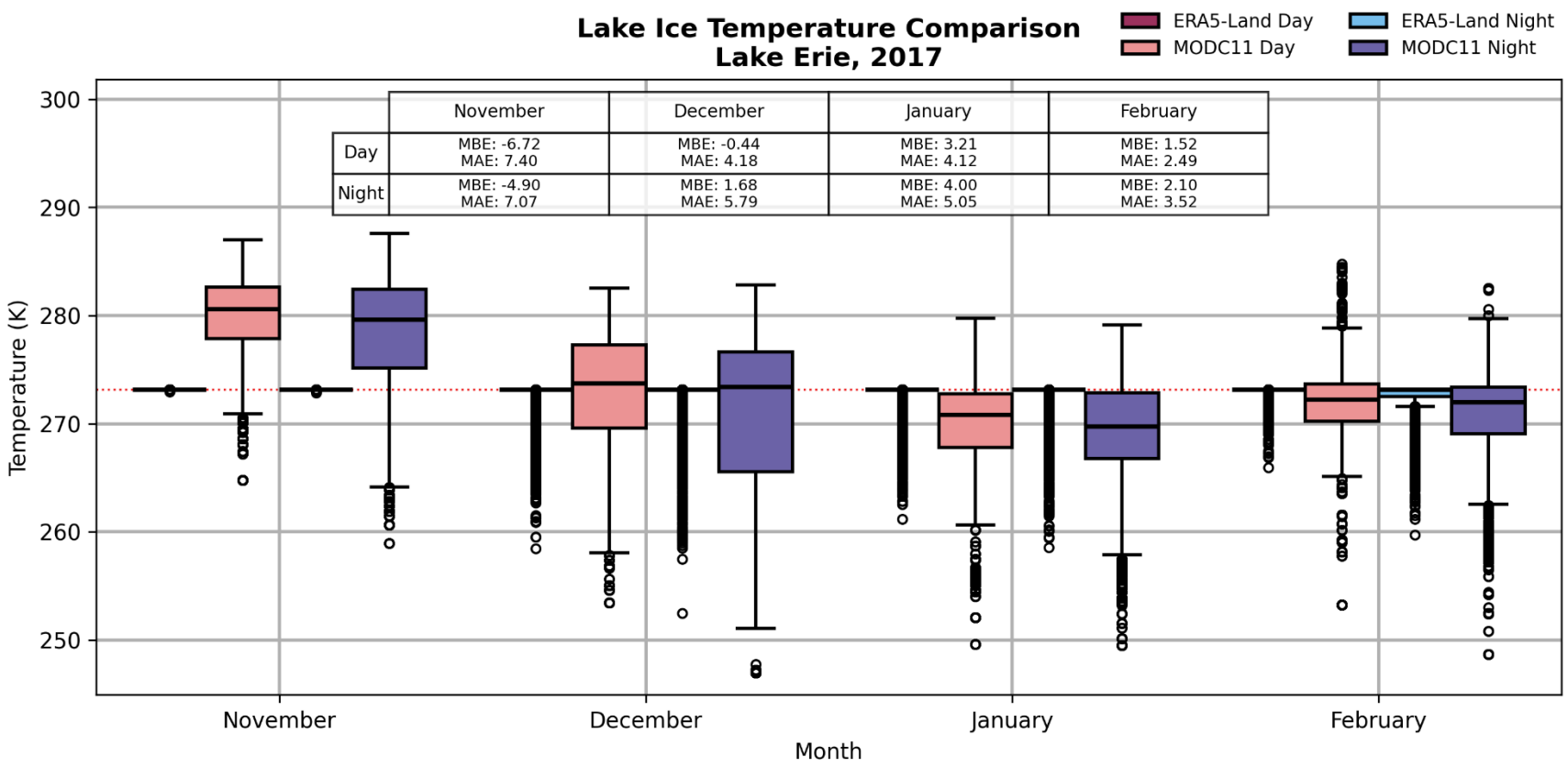


Figure C.7. 14: Boxplot of monthly lake ice surface temperatures during ice-on period of ERA5-Land and MODIS for Lake Erie, 2017

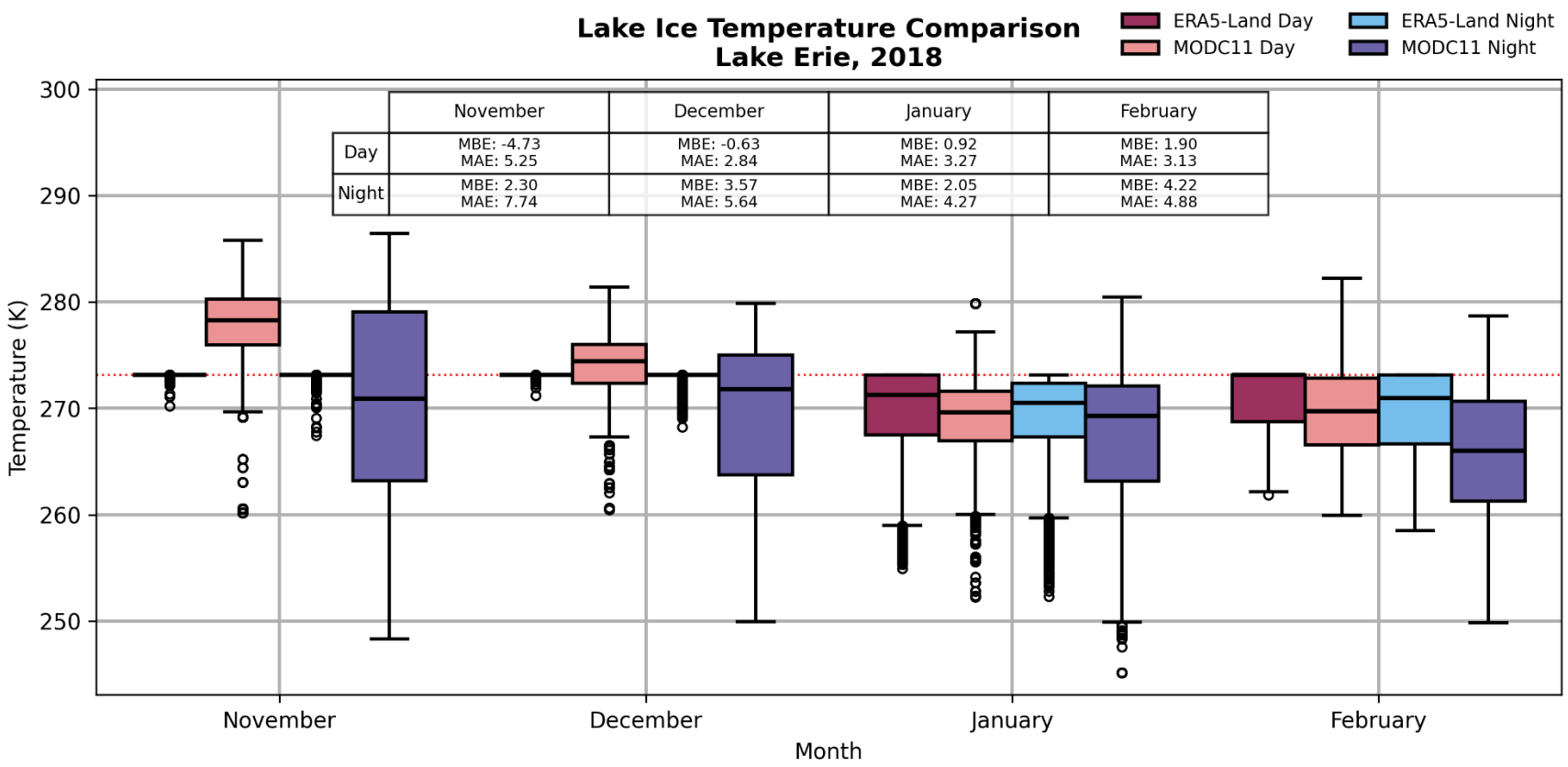


Figure C.7. 15: Boxplot of monthly lake ice surface temperatures during ice-on period of ERA5-Land and MODIS for Lake Erie, 2018

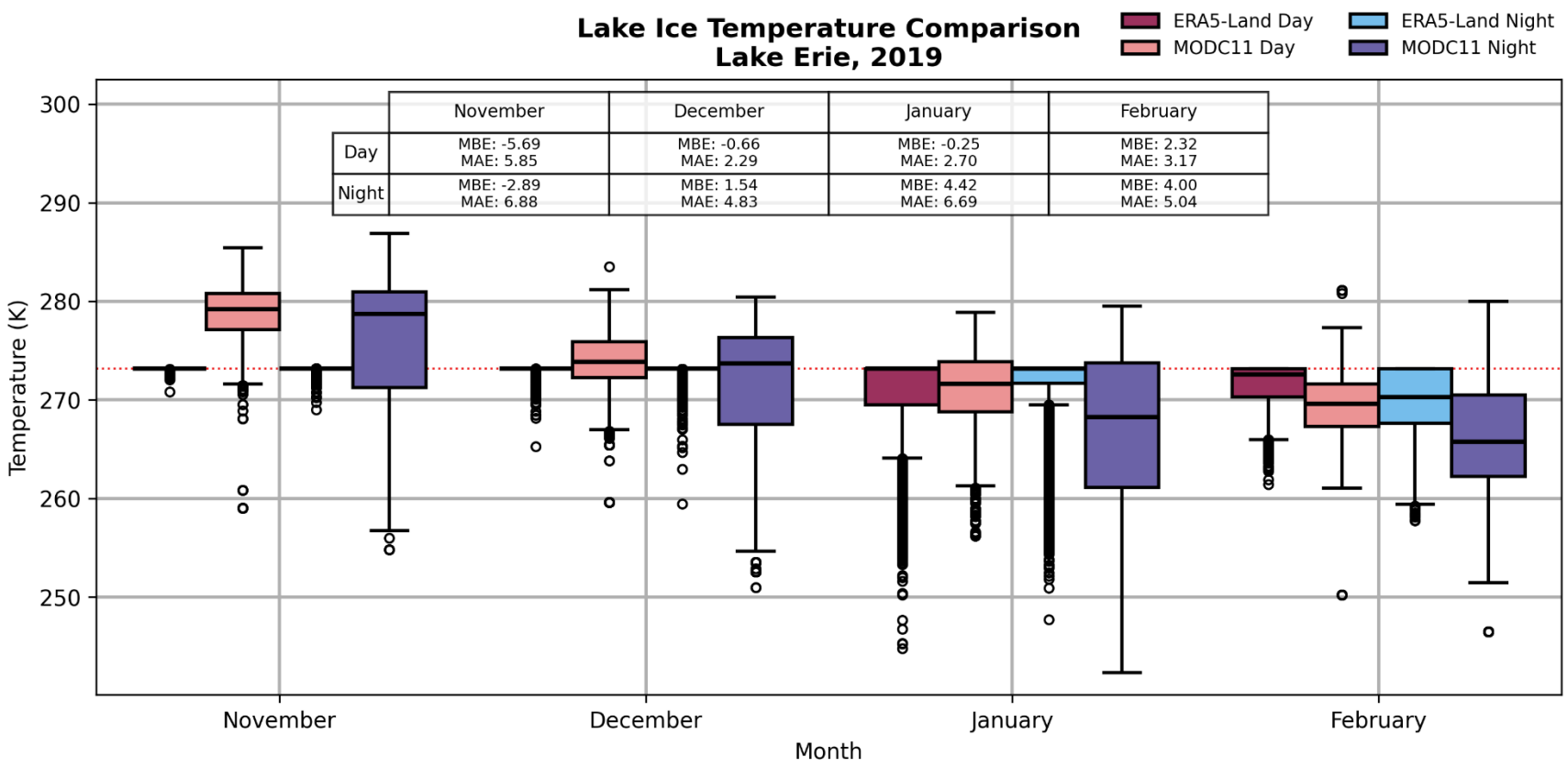


Figure C.7. 16: Boxplot of monthly lake ice surface temperatures during ice-on period of ERA5-Land and MODIS for Lake Erie, 2019

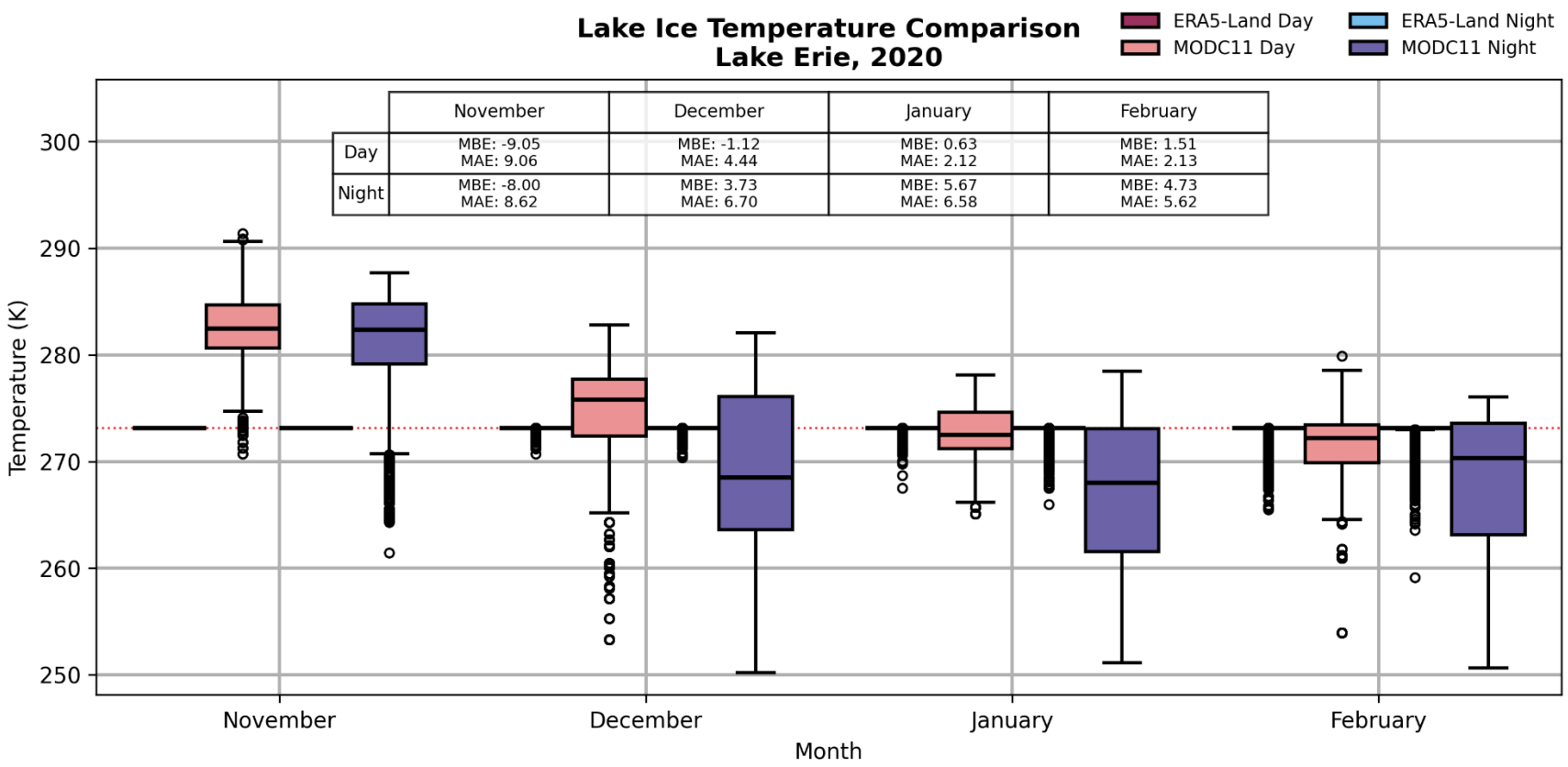


Figure C.7. 17: Boxplot of monthly lake ice surface temperatures during ice-on period of ERA5-Land and MODIS for Lake Erie, 2020

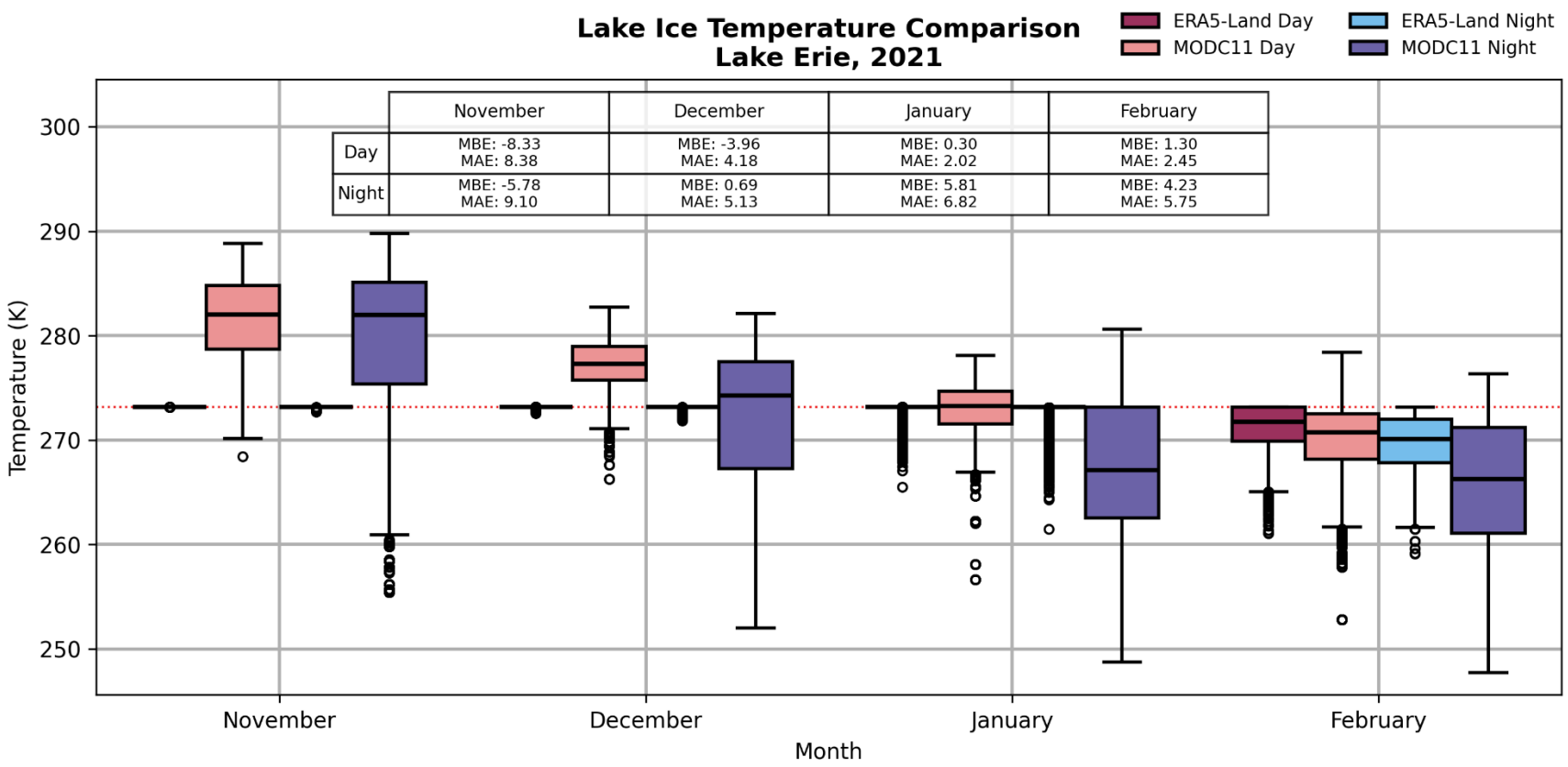


Figure C.7. 18: Boxplot of monthly lake ice surface temperatures during ice-on period of ERA5-Land and MODIS for Lake Erie, 2021

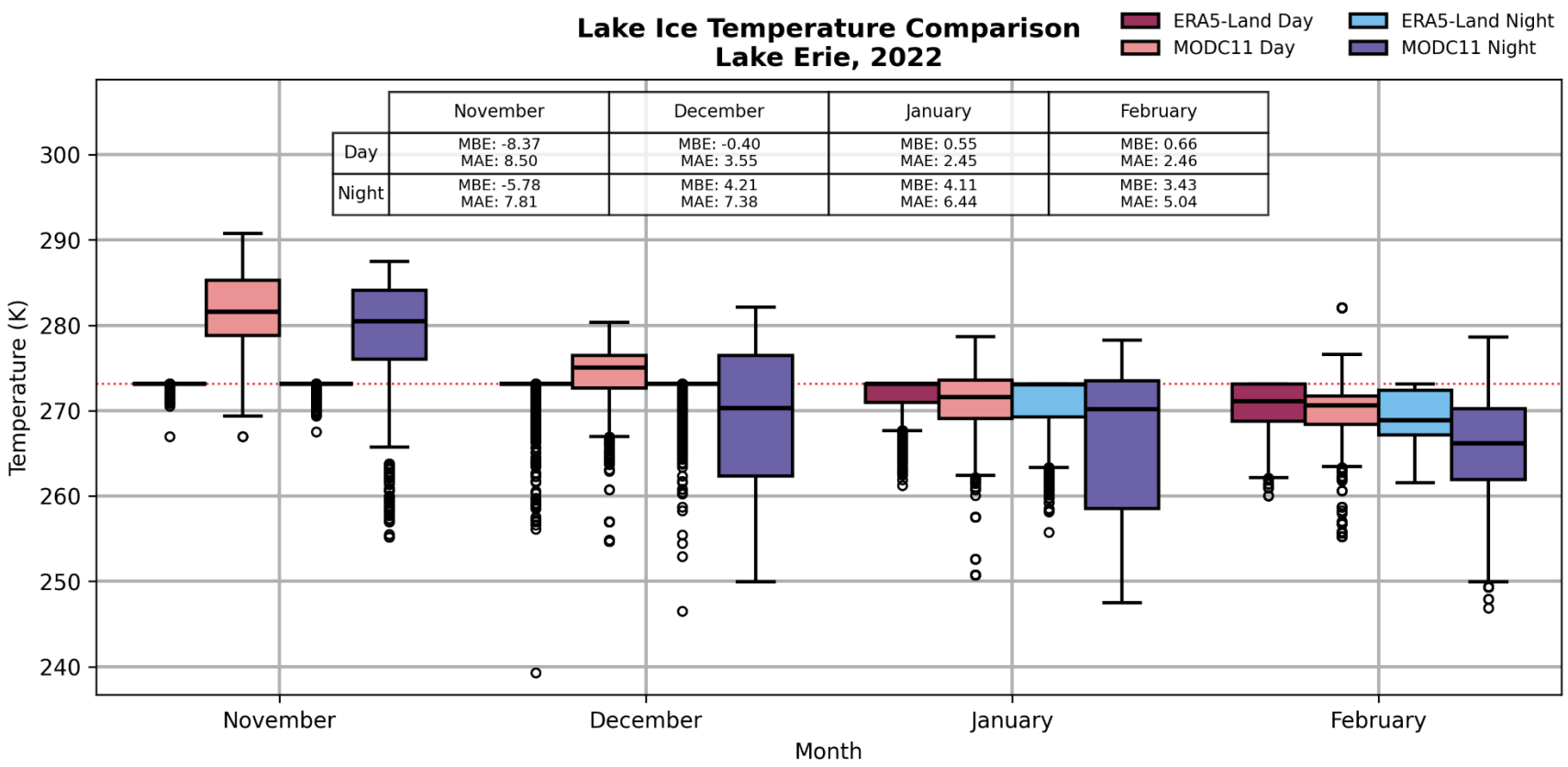


Figure C.7. 19: Boxplot of monthly lake ice surface temperatures during ice-on period of ERA5-Land and MODIS for Lake Erie, 2022

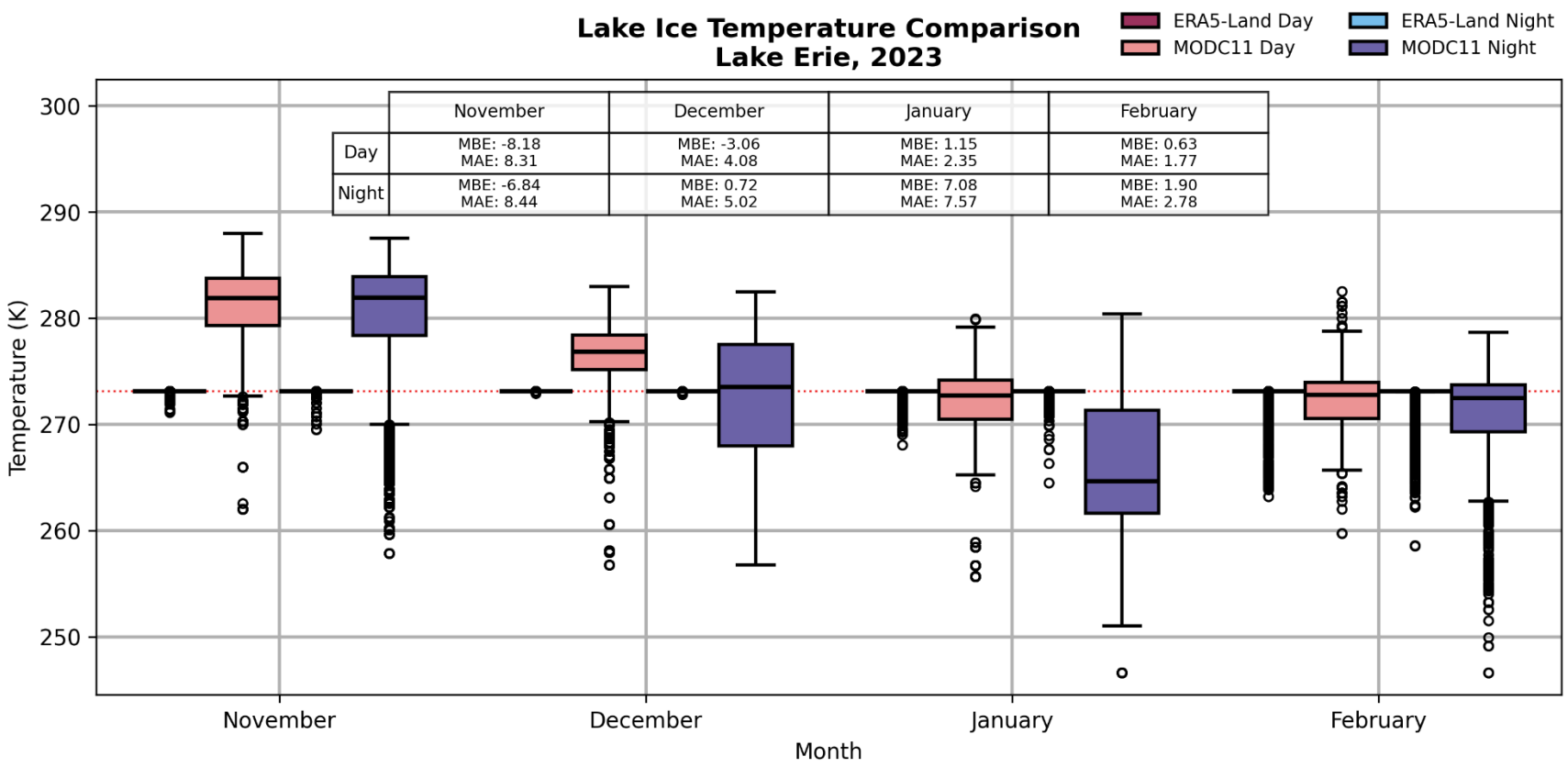


Figure C.7. 20: Boxplot of monthly lake ice surface temperatures during ice-on period of ERA5-Land and MODIS for Lake Erie, 2023